The Role of the Fibrinolytic System and Fibrin in Fracture Healing

By

Nicholas Anthony Mignemi

Dissertation

Submitted to the Faculty of the

Graduate School of Vanderbilt University

in partial fulfillment of the requirements

for the degree of

DOCTOR OF PHILOSOPHY

in

Pathology

May, 2015

Nashville, Tennessee

Approved:

Jonathan G. Schoenecker M.D. Ph.D.

David Gailani M.D.

Joey V, Barnett Ph.D.

Justin M. Cates M.D. Ph.D.

Herbert S. Schwartz M.D.

Dedication

This dissertation is dedicated to family and friends who supported me through out my years of educations. I am truly grateful for their love and support.

Acknowledgements

I would like to thank the Musculoskeletal Transplant Foundation, the Caitlin Lovejoy fund, Dr. Bill Sales, Mrs. Sally A. Schoenecker, and Dr. Perry L. Schoenecker for their generous contributions and support. I would also like to thank my committee for their hours of work in developing me into the scientist. Lastly, I would like thank my mentor who continues to inspire me to ask the right questions in life.

Table of Contents

7. Methylglyoxal Modifies Plasminogen Binding and Activation

8. Future Direction

9. Clinical Implications

List of Tables

List of Figures

List of Abbreviations

Wild Type = WT

Tissue plasminogen activator = tPA

Urokinase plasminogen activator = uPA

Single chain urokinase plasminogen activator = ScuPA

Two chain urokinase plasminogen activator = TcuPA

Serpin protease inhibitor = Serpin

Reactive center loop = RCL

Plasminogen activator inhibitor = PAI

Thrombin activatable fibrinolysis inhibitor = TAFI

Vascular endothelial growth factor = VEGF

Vascular endothelial growth factor receptor = VEGFR

Micro-computed Tomgraphy = µ-CT

Days Post Fracture = DPF

Two Dimensional = 2D

Three Dimensional = 3D

Fibrinogen deficient mice = Fbg -/-

Polar moment of inertia = pMOI

Plasminogen deficient mice = Plg -/-

Heterotopic ossification = HO

Standard error of the mean = SEM

Antisense oligonucleotide = ASO

Plasminogen deficient mouse treated with fibrinogen antisense oligonucleotide = Plg -/- Fbg ^{Low}

Transforming growth factor beta = TGFβ

Enzyme-linked immunosorbent assay = ELISA

Duschenne's Muscular Dystrophy = DMD

Inferior vena cava = IVC

Ethylenediaminetetraacetic acid = EDTA

Volume of interest = VOI

Tissue mineral density = TMD

Hematoxilyin and Eosin = H&E

Milligram hydroxyapatite divided by cubic centimeter = mgHA/cm^3

Ethyl Alcohol = ETOH

Horseradish peroxides = HRP

Tris buffered saline = TBS

Type 2 diabetes mellitus = DM2

Reactive oxidative species = ROS

ε-Aminocraproic acid = εACA

Phe-Arg-chloromethylketone = FFR-CK

H-D-Phe-Pro-Arg-chloromethylketone = FPR-CK

Phenylmethylsulfonyl fluoride = PMSF

Absorbance = OD

Relative fluorescent units = RFU

Calcium = Ci

Phosphate = Pi

Pyrophosphate = PPi

Tartrate resistant alkaline phosphate 5b = Tracp-5b

Osteoprotegerin = OPG

CHAPTER 1

Prevalence and Impact of Impaired Fracture Healing

The Cost of Impaired Fracture Healing

Over 16 million fractures are treated in the United States annually (1). Of these, between 2.5% and 10% of patients suffer from impaired fracture healing with resultant pain and loss of function (2-4). In addition to substantial morbidity, these complications impose a significant cost burden on the health care system (1). It is estimated that it costs $32,500 more to treat a patient with impaired fracture healing than one with normal fracture healing (5). Given the number of fractures that occur each year, the treatment of impaired fracture healing costs the United State of America's health care system between 13-52 billion dollars annually (Figure 1). Thus, there are considerable ongoing efforts to develop novel methods of fracture fixation and/or application of bone-inducing biological agents to stimulate fracture healing and prevent nonunion.

Nonunion can occur following any fracture, however investigations have shown they are more commonly associated with patients with obesity, diabetes, smoking and advanced age. (1-5). Given the increasing incidence of most of these associated comorbid conditions it is likely that the frequency of nonunion will increase. There are three main types of nonunion: hypertrophic, atrophic, and oligotrophic (Figure 2). The treatment strategy for nonunion is primarily based on their classification but generally involve removal of fibrocartliangous tissue opposing the two ends of the fracture, improving fixation and in the case of atrophic and oligotrophic nonunion supplement with

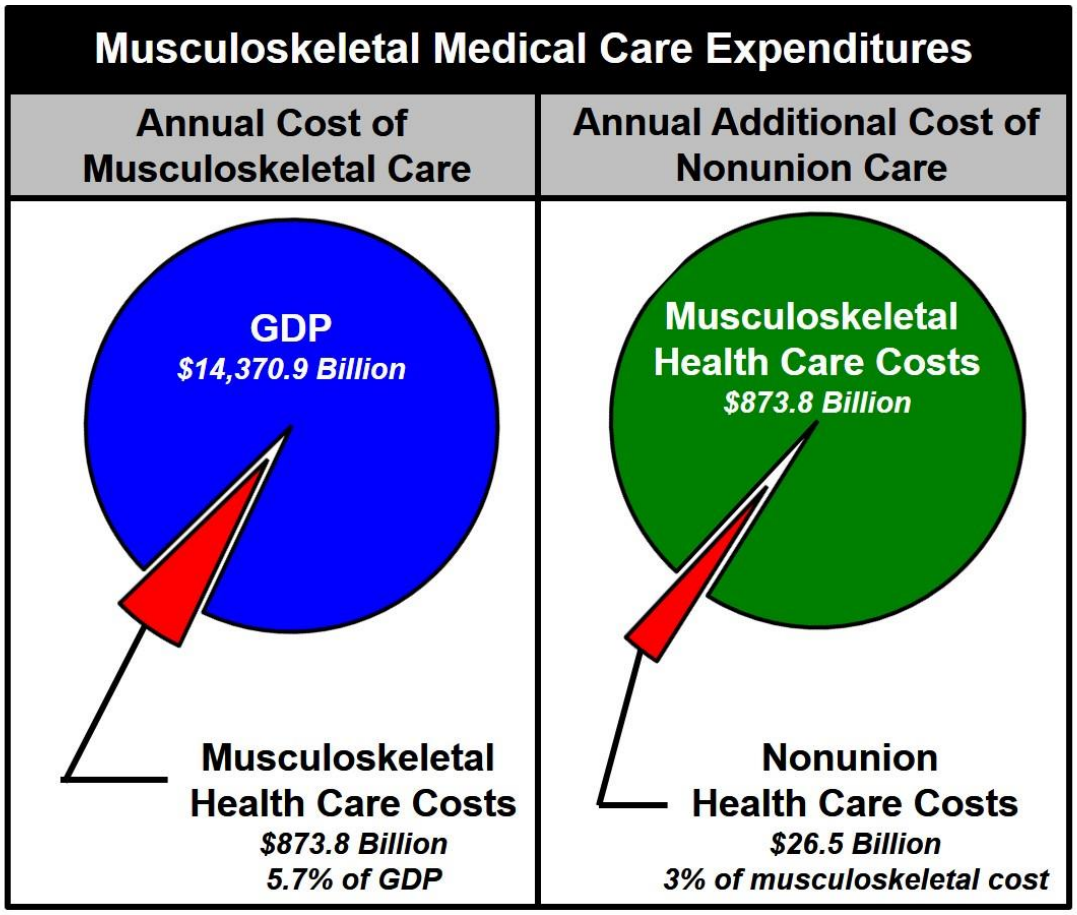

Figure 1: Economic burden of musculoskeletal care and cost of treating impaired fracture healing (nonunion) in the United States of America. Data represent averages from 2009- 2011 and assumes a 5% rate of nonunion.

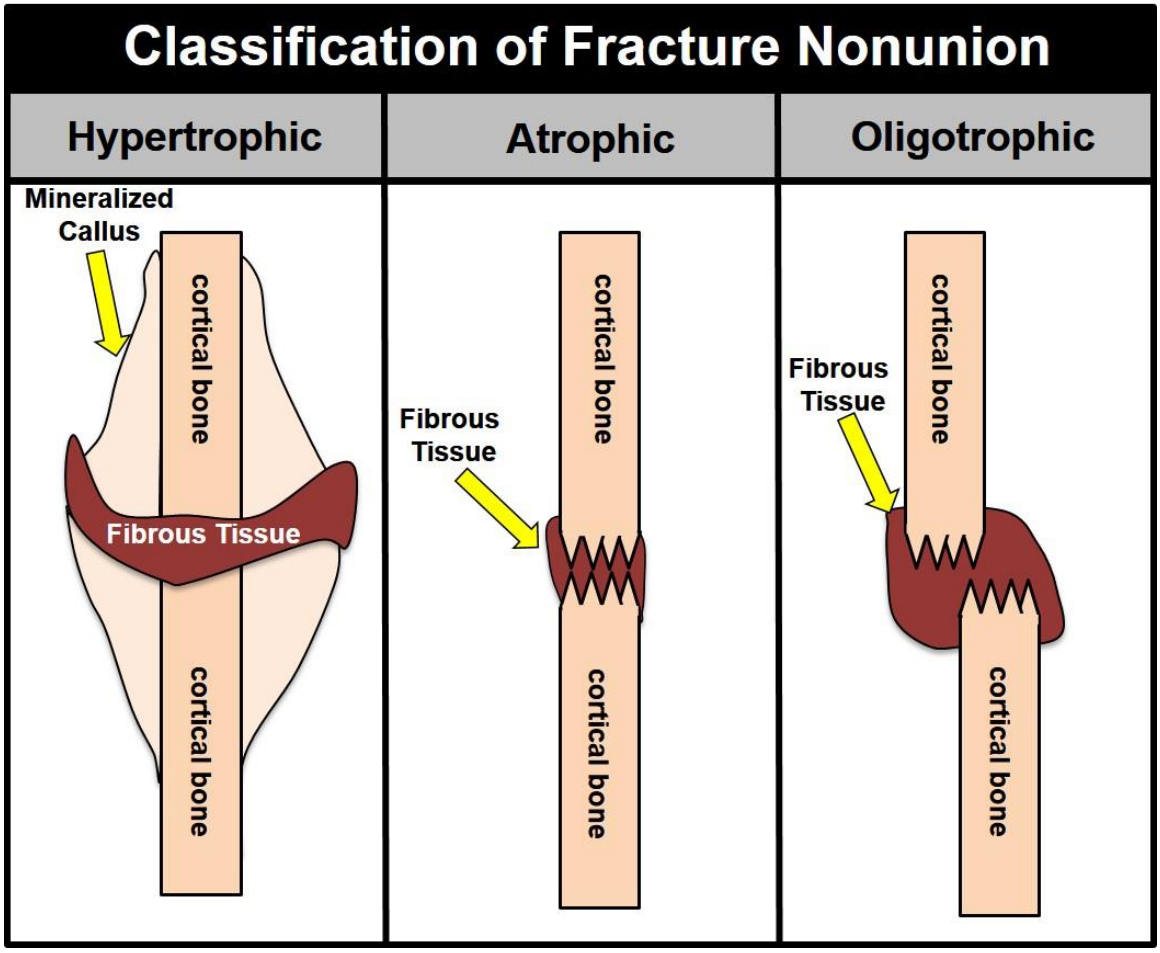

Figure 2: Classification of fracture nonunion

osteoconductive growth factors such as BMP and/or autologous bone graft. While these treatments certainly improve impaired facture healing, they do not address the cause of the nonunion.

The overall goal of my work is to investigate mechanisms by which fractures fail to properly heal. Given that dysfunction of the coagulation system leading to accumulation of the coagulation matrix protein fibrin occurs in most comorbid conditions associated with fracture nonunion, the specific hypothesis of my thesis is that this matrix protein, and the system responsible for its clearance, fibrinolysis, play a central theme in fracture repair. In order to advance the treatment of patients with impaired fracture healing, I will evaluate new procedures and pharmacological approaches to achieve this aim.

References

1. Gunnar B. J. Andersson M, PhD, Bouchard J, Kevin J. Bozic M, MBA, Robert M. Campbell J, MD, Miriam G. Cisternas M, Adolfo Correa M, MPH, PhD, Felicia Cosman M, Janet D. Cragan M, MPH, Kristen D'Andrea B, Doernberg N, et al. *United States Bone and Joint Initiative: The Burden of Musculoskeletal Diseases in the United States, Second Edition.* Park Ridge, Ill.: American Academy of Orthopaedic Surgeons; 2011.

2. Einhorn TA. Enhancement of fracture-healing. *The Journal of bone and joint surgery American volume.* 1995;77(6):940-56.

3. Ebraheim NA, Martin A, Sochacki KR, and Liu J. Nonunion of distal femoral fractures: a systematic review. *Orthop Surg.* 2013;5(1):46-50.

4. Robinson CM, Court-Brown CM, McQueen MM, and Wakefield AE. Estimating the risk of nonunion following nonoperative treatment of a clavicular fracture. *The Journal of bone and joint surgery American volume.* 2004;86-A(7):1359-65.

5. Antonova E, Le TK, Burge R, and Mershon J. Tibia shaft fractures: costly burden of nonunions. *BMC musculoskeletal disorders.* 2013;14(42.

CHAPTER 2

Bone Formation and Repair

Types of Bone Formation

There are two biologically distinct processes that form bone: intramembranous bone formation and endochondral bone formation. Intramembranous bone formation, also referred to as primary bone formation, is the direct formation of bone from membranous tissue and does not involve a cartilaginous intermediate phase. Intramembranous bone formation begins with condensation of mesenchymal progenitor cells in a vascular rich microenvironment (Figure 1A). These progenitor cells then differentiate into osteoblasts and begin to produce type 1 collagen which mineralizes to form new bone (Figure 1) (3). While intramembranous bone formation occurs during development, it only accounts for a small percentage of total skeletal formation primarily the: clavicle, scapula and craniofacial bones (4). Further intramembranous bone formation is responsible for appositional growth of long bones (5).

Endochondral formation accounts for a majority of bone formation in our bodies during development. The process of endochondral bone formation begins with the proliferation and condensation of mesenchymal progenitor cells in the approximate shape of the developing bone (Figure 2A). These cells differentiate into chondrocytes and deposit an avascular cartilaginous matrix predominantly composed of type 2 collagen and proteoglycans (6). As the chondrocytes mature they become hypertrophic in the diaphysis

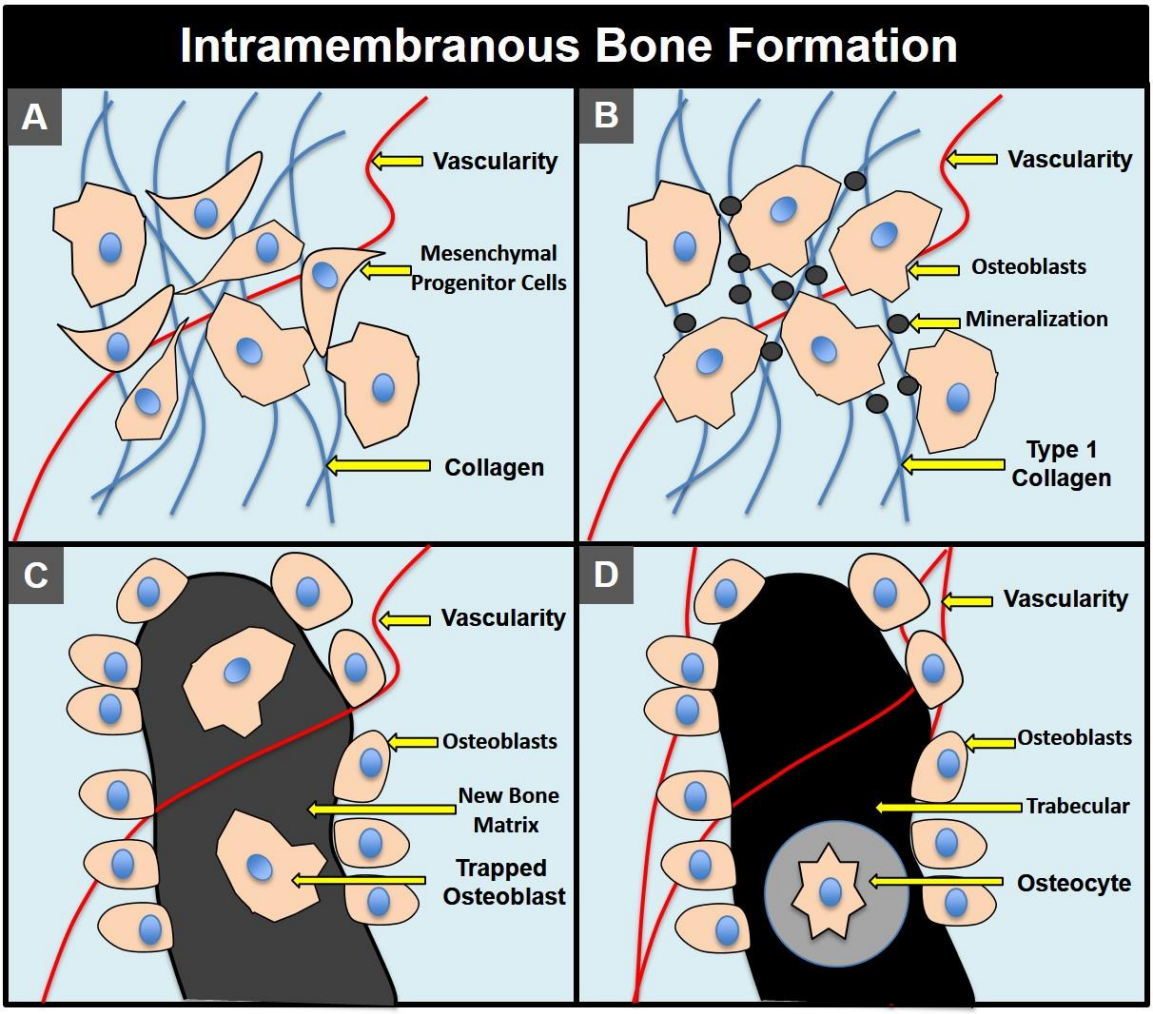

Figure 1: Intramembranous Bone Formation. **A)** Condensation of mesenchymal progenitor cells in close proximity to vasculature (red). **B)** Mesenchymal stem cells have differentiated into osteoblasts begun to mineralize (black circles) the type 1 collagen. **C)** Osteoblasts continue to lay down new bone and mostly line bone spicules however, some have become trapped within the mineralized matrix. **D)** Osteoblasts line the bone adding to its size and trapped osteoblasts has differentiated into osteocytes.

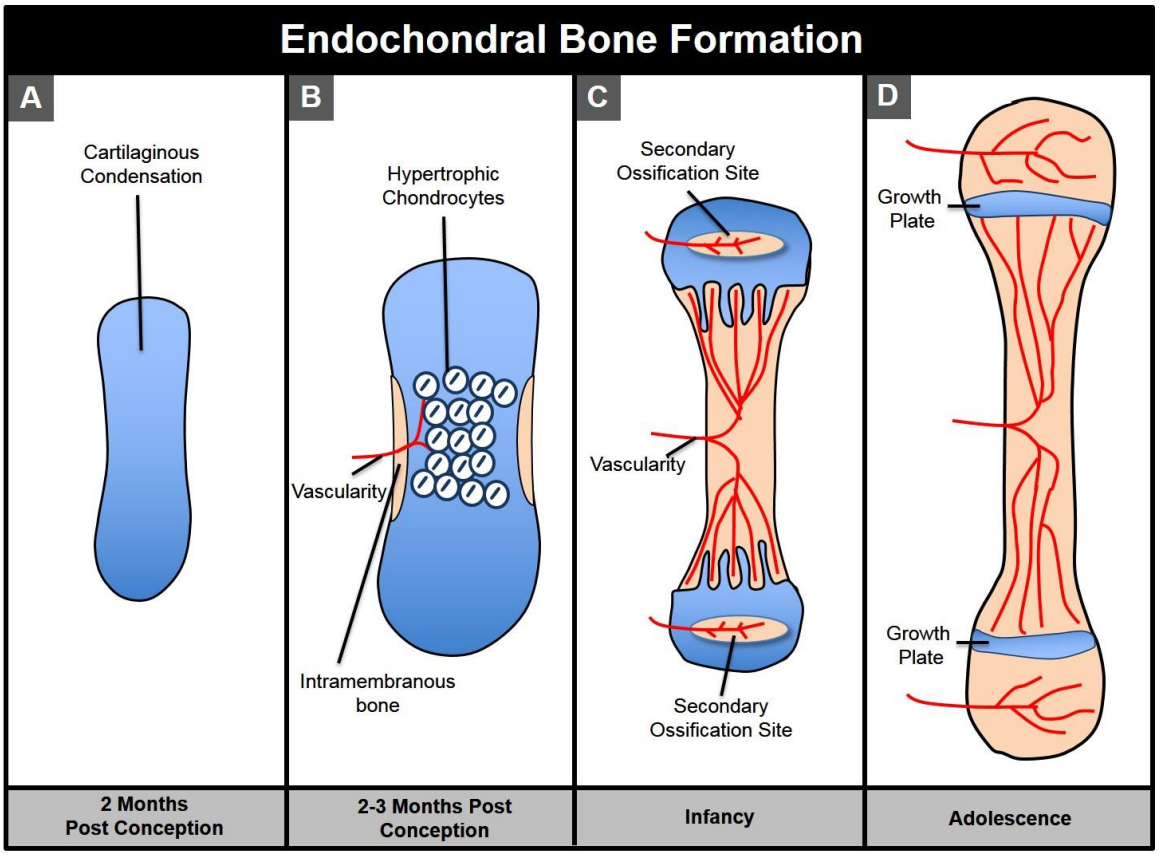

Figure 2: Endochondral Bone Formation. **A)** Condensation of mesenchymal progenitor cells that different into chondrocytes **B)** Intramembranous bone formation occurs at the mid-shaft of the newly forming bone. Chondrocytes adjacent to the newly forming bone become hypertrophic recruiting new vascularity. **C)** New bone is formed proximal and distal to the mid-shaft. At the same time vascularity is recruited to the utmost proximal and distal ends of the bone forming the secondary ossification sites. **D)** The Growth plate is well established at the proximal and distal ends of the bone allowing for longitudinal growth of the bone.

of the bone (Figure 2B). During hypertrophy, the intracellular volume of the chondrocytes increases, the chromatin condenses, and they secrete type X collagen and alkaline phosphatase into the extracellular environment (7, 8). Type X collagen serves as a nucleation site for hydroxyapatite formation resulting in the calcification of the extracellular matrix (8, 9). At the same time that the central chondrocytes undergo hypertrophy, the first mineralized bone forms through intramembranous ossification at the mid-shaft of the newly forming bone (Figure 2C). CD31-positive endothelial cells and osteoblast precursor cells then invade the region of hypertrophic chondrocytes and the deposition of osteoid which is mineralized to from trabecular bone forming the primary spongiosum (5, 10). New bone is then formed from the mid-shaft of the bone, advancing both proximally and distally eventually forming the growth plates (physis) (Figure 2D). Simultaneously occurring along with the establishment of physis, the secondary ossification sites develop in the proximal and distal ends of the bone, creating proximal and distal epiphyses.

The growth plate is composed of chondrocytes in various states of differentiation and is responsible for longitudinal bone growth (5). The resting zone of the growth plate contains quiescent chondrocytes which survive through diffusion of oxygen and nutrients supplied by epiphyseal vessels. Just below the resting zone, rows of chondrocytes stacked ina rouleaux proliferate away from the resting zone. The final subdivision of the growth plate consists of hypertrophic chondrocytes in an environment of low oxygen tension directly adjacent to vascularized new bone (11). These hypertrophic chondrocytes are invaded by an advancing front of new bone formation containing endothelial cells, osteoblasts and osteoclasts. (12) (Figure 3). The interactions of the hypertrophic chondrocytes and new bone formation results in longitudinal bone growth.

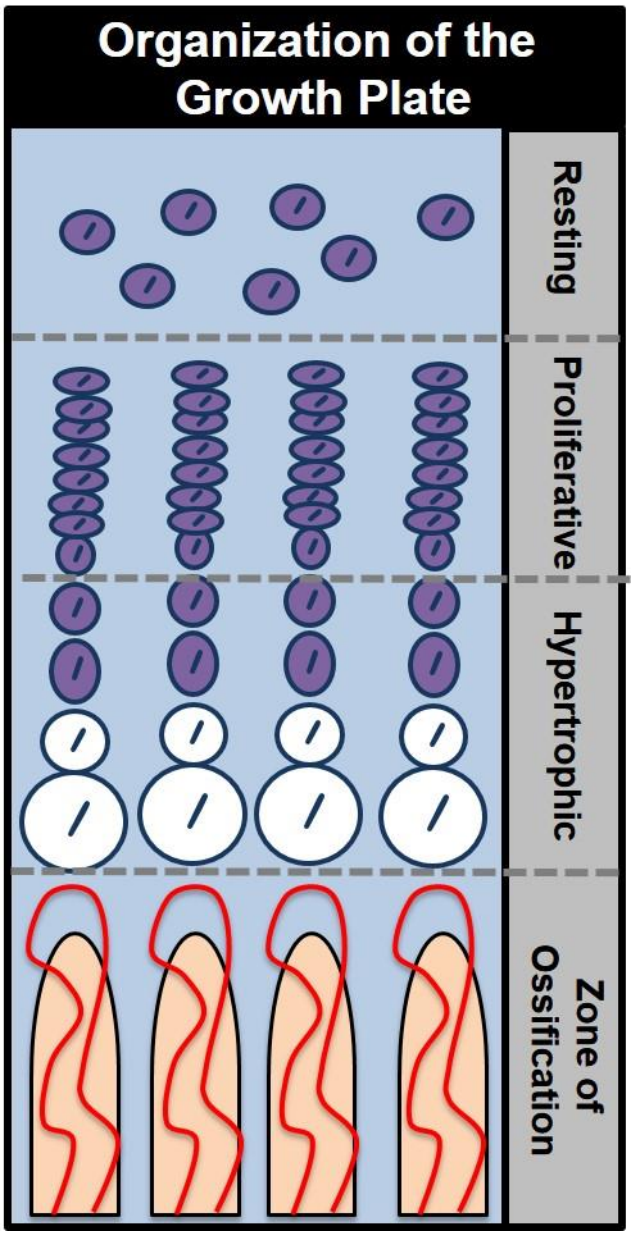

Figure 3: Organization of the growth plate. Longitudinal growth is achieved through the coordinated expansion of the growth plate and invasion of newly forming bone. The growth plate is composed of chondrocytes in the resting zone, proliferative zone, and hypertrophic zone that gets replaced by an advancing front of bone formation.

Biology of fracture repair

Fracture occurs when there is a break in the continuity of the mineralized bone. Bone heals through the formation of a fracture callus, which replicates intramembranous and endochondral bone formation during development, rather than the scarring process that occurs mostly in soft tissues. Healing through a callus rather than a scar is critically important in bone biology because of the biomechanical forces which bone must withstand to support our body. As such, repaired bone must maintain the biomechanical competency of the previous uninjured bone.

Fracture healing occurs in a series of overlapping, precisely coordinated phases using the same biological process employed by the body during development and growth; intramembranous bone formation and endochondral bone formation(13) (Figure 4). The first phase in the reparative process is the inflammatory phase. Upon fracture, the vessels contained within the bone and surrounding muscle become disrupted, resulting in the formation of a fracture hematoma containing extravagated red blood cells, platelets, and growth factors held together within a fibrin matrix (Figure 5). As healing progresses, neutrophils, monocytes, and macrophages invade the injured area to remove the hematoma. Simultaneously, there is a massive proliferation of mesenchymal progenitor cells that begin to define the shape of the fracture callus. These cells likely emanate from both the surrounding muscle and intact periosteum adjacent to the fracture site (14-17) (Figure 6). Five days post-fracture, intramembranous bone forms proximal and distal to the fracture site, through direct extension of blood vessels and osteoblasts. At this time chondrocytes appear within the fracture callus (Figure 7). Ten days post-fracture, the mesenchymal progenitors have differentiated into chondrocytes, forming a large soft tissue callus centrally located over the fracture site (Figure 8). At this time, the first evidence of endochondral bone

formation becomes apparent with new bone forming at the periphery of the fracture callus as the outer most chondrocytes undergo hypertrophy, mineralization and replacement by newly forming bone (Figure 8). Fourteen days post fracture, a large hard tissue callus containing newly formed bone is evident proximal and distal to the fracture site as the soft tissue callus is replaced by the invading new bone (Figure 9). New woven bone continues to replace the soft tissue callus towards the fracture site until about three weeks post fracture when the new bone being formed proximal and distal to the fracture site is united in an ossified union (Figure 10). Following union of new bone over the fracture site, the fracture callus begins to remodel back to the position and shape of the original cortical bone. The process of remodeling can continue for up to a year after the injury as new bone is resorbed and deposited in accordance with biomechanical forces experienced at the previous site of injury (Figure 10) (18).

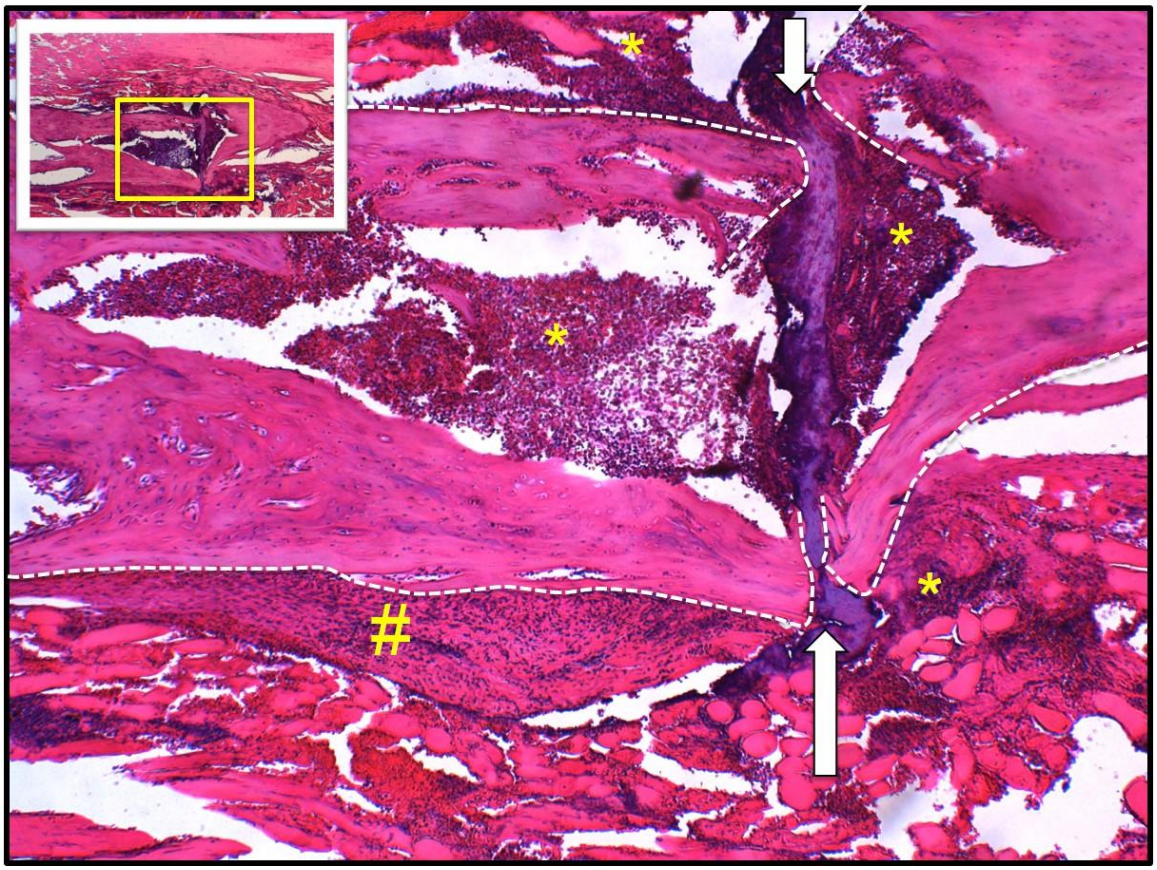

Figure 5: Histological examination of a fractured femur 1 day post fracture. Hematoxylin and eosin staining of a fracture mouse femur 1 day post fracture reveals the presence of extravascular blood cells (yellow Asterisk) and fibrinnous matrix, (yellow Sharp) adjacent to the fracture (White arrows). Yellow box in the inset image denotes approximate location of image and the white dotted line denotes the boarder of the cortical bone.

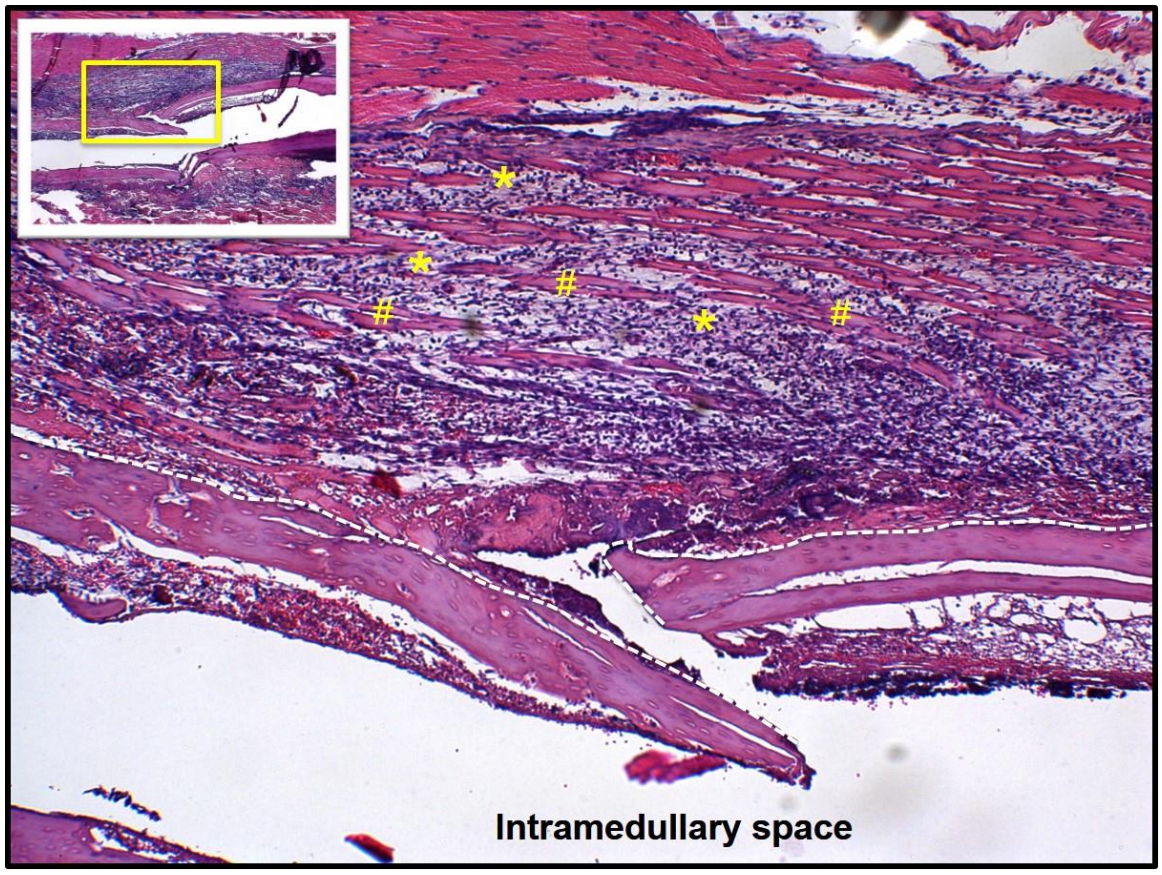

Figure 6: Histological examination of a fractured femur 3 days post fracture. Hematoxylin and eosin staining of a fracture mouse femur 3 days post fracture reveals myofibroblastic like cells (Yellow asterisk) interposed with damaged skeletal muscle (yellow sharps). Yellow box in the inset image denotes approximate location of image and the white dotted line denotes cortical bone.

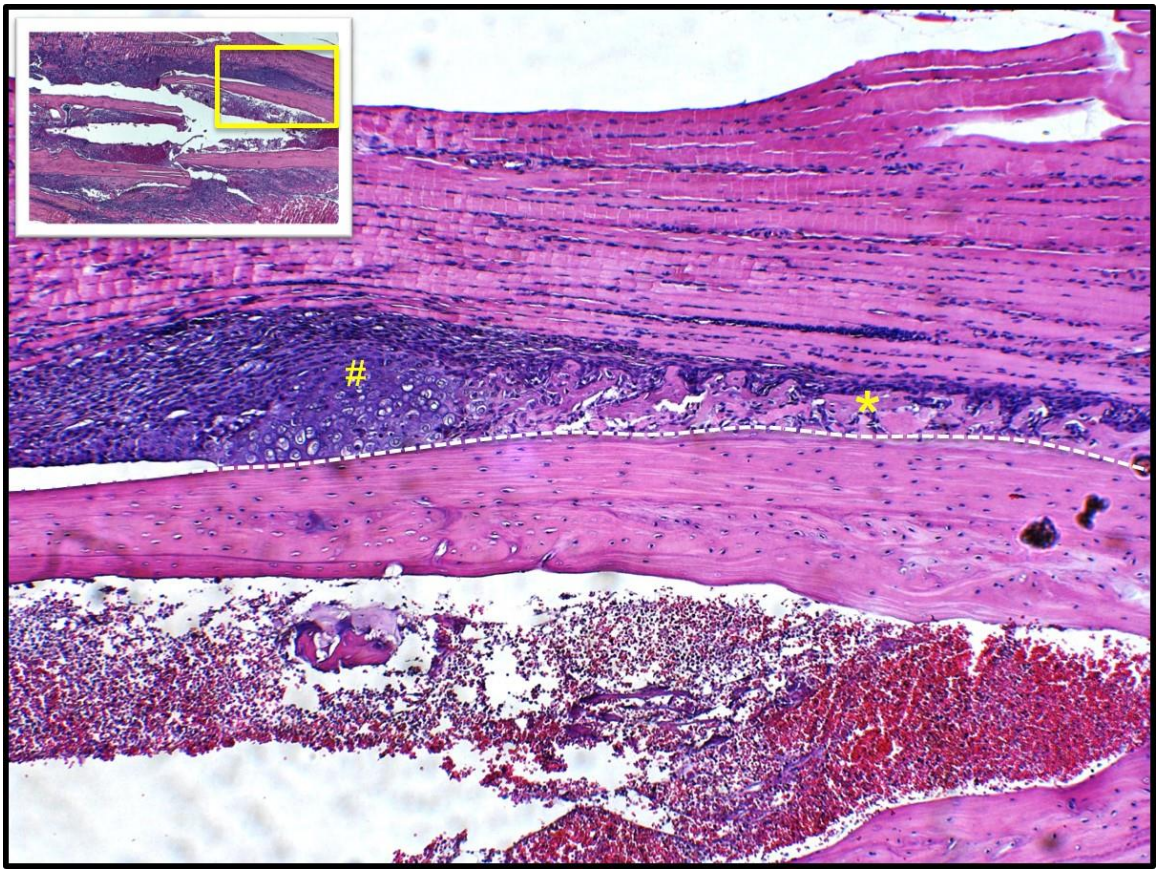

Figure 7: Histological examination of a fractured femur 5 days post fracture. Hematoxylin and Eosin staining of a fracture mouse femur 5 days post fracture reveals the presence intramembranous bone formation (yellow asterisk) and the new forming chondrocytes (yellow sharp). Yellow box in the inset image denotes approximate location of image and the white dotted line denotes the boarder of the cortical bone.

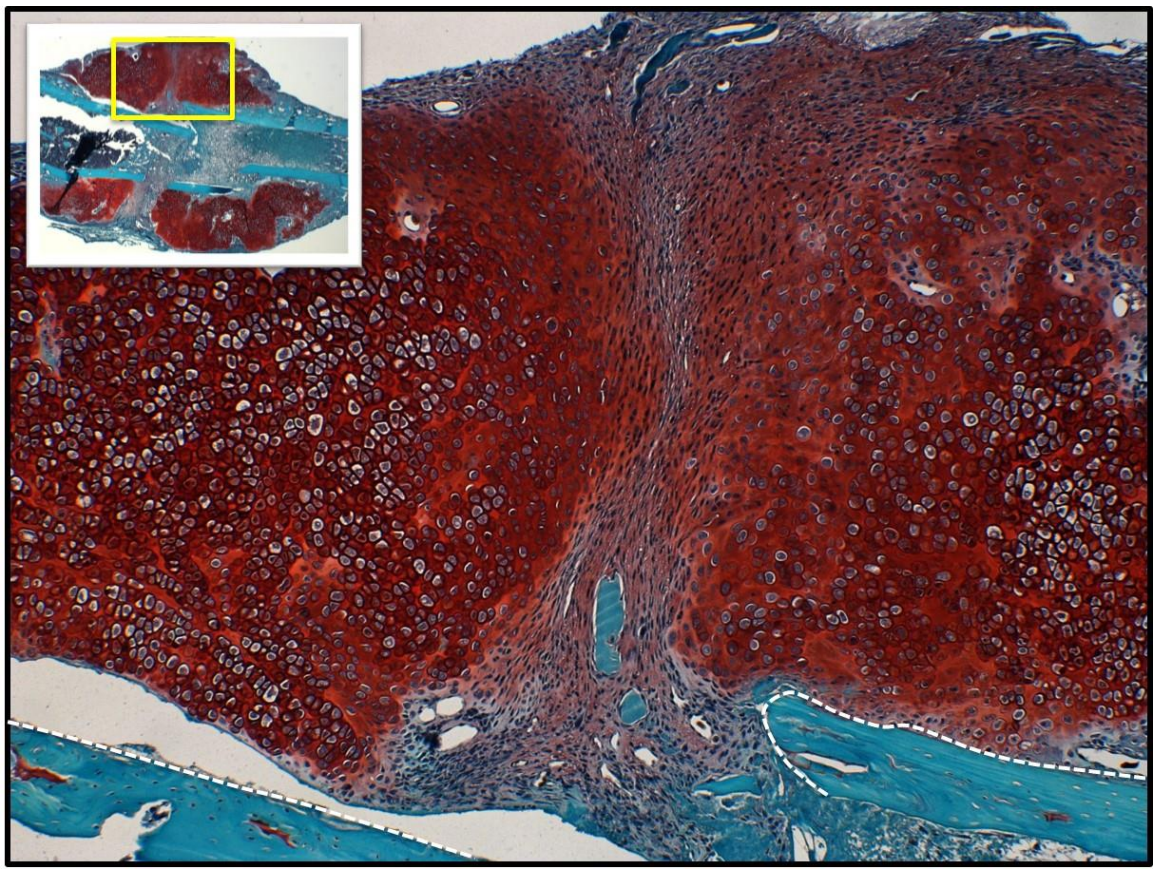

Figure 8: Histological examination of a fractured femur 10 days post fracture. Safranin-o staining staining of a fractured mouse femur 10 days post fracture reveals the soft tissue callus containing chondrocytes (red staining). Yellow box in the inset image denotes approximate location of image and the white dotted line denotes the border of the cortical bone.

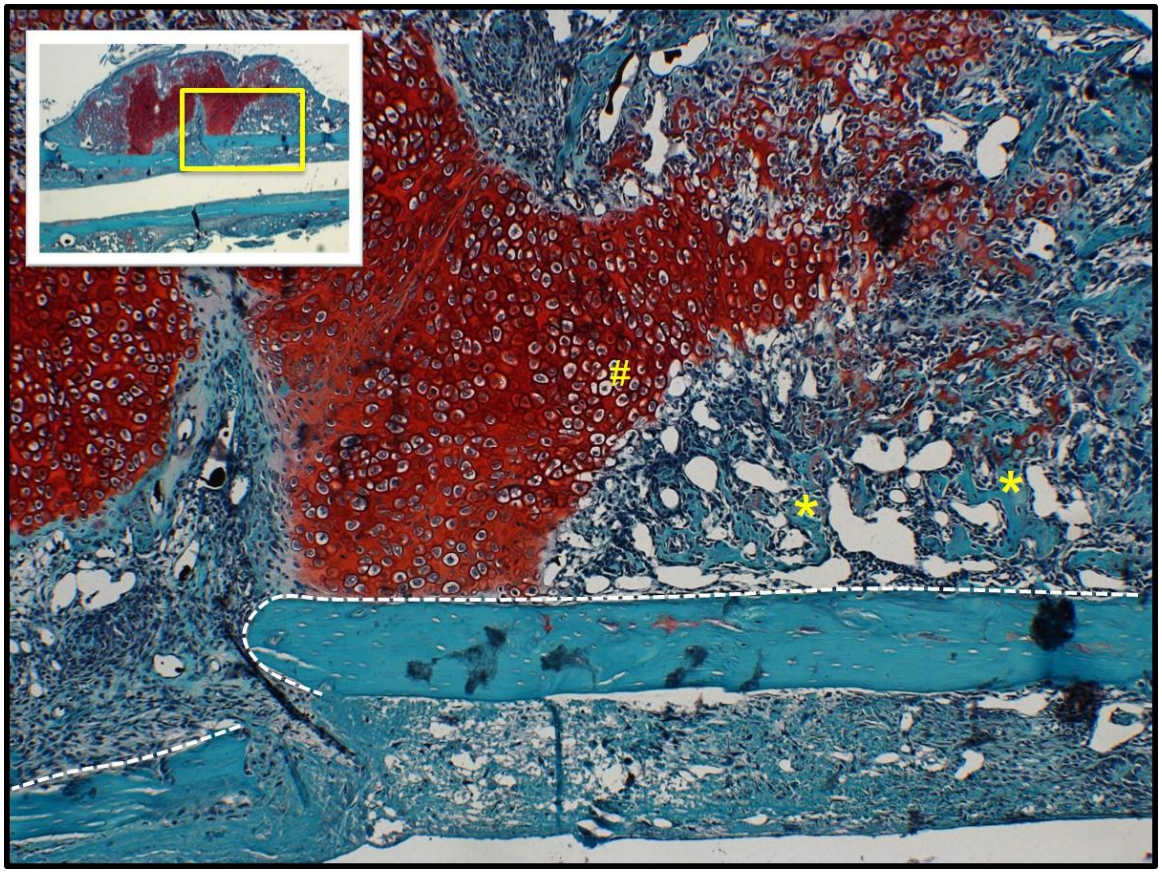

Figure 9: Histological examination of a fractured femur 14 days post fracture. Safranin-o staining of a fractured mouse femur 14 days post fracture reveals newly forming hard tissue callus containing osteoid (blue green staining) (yellow asterisk) invading soft tissue callus (red staining) containing hypertrophic chondrocytes (yellow sharp). Yellow box in the inset image denotes approximate location of image and the white dotted line denotes the border of the cortical bone.

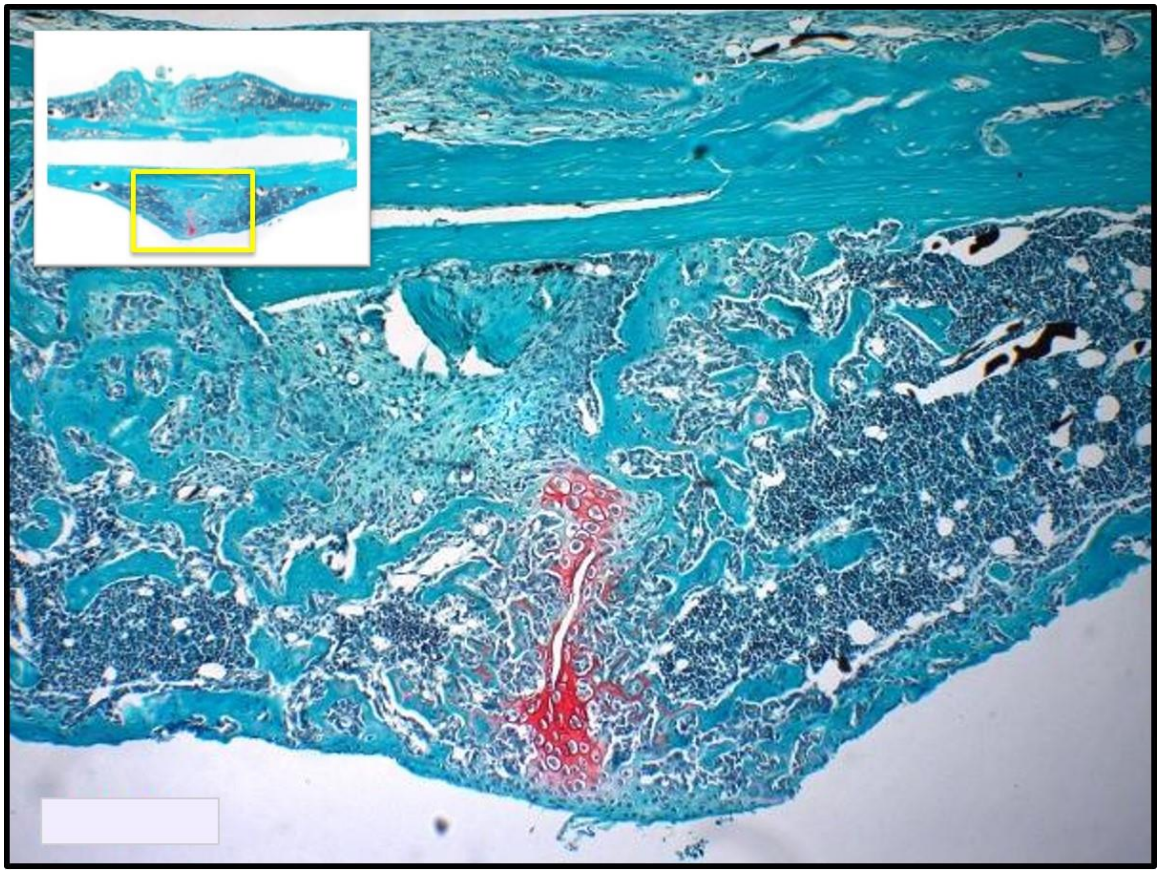

Figure 10: Histological examination of a fractured femur 21 days post fracture. Safranin-o staining of a fractured mouse femur 21 days post fracture reveals newly formed hard tissue callus containing osteoid and bone (Blue green staining) and almost the complete removal of the soft tissue callus (red staining). Yellow box in the inset image denotes approximate location of image and the white dotted line denotes the border of the cortical bone.

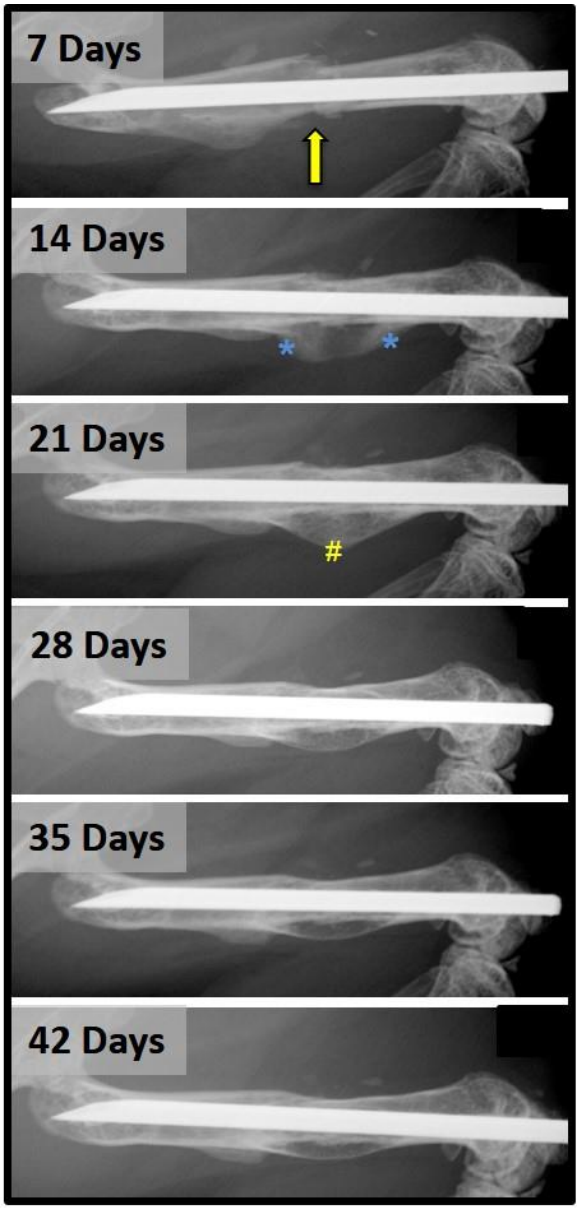

Figure 11: Radiographic examination of a healing fracture.
Serial radiographs taken weekly of a WT mouse fracture demonstrates disruption of the cortical bone at the fracture site (yellow arrow) and formation of the hard tissue callus containing new bone proximal and distal to the fracture site 14 days post fracture (blue asterisk). At 21 days, radiographs reveals that the proximal and distal hard tissue calluses have united over the fracture site (yellow sharp). During 21-42 days post fracture the hard tissue callus remodels back to within the original cortices of the femur.

References

1. Hirose J, Kouro T, Igarashi H, Yokota T, Sakaguchi N, and Kincade PW. A developing picture of lymphopoiesis in bone marrow. *Immunological reviews.* 2002;189(28-40.

2. Taichman RS. Blood and bone: two tissues whose fates are intertwined to create the hematopoietic stem-cell niche. *Blood.* 2005;105(7):2631-9.

3. Franz-Odendaal TA. Induction and patterning of intramembranous bone. *Frontiers in bioscience.* 2011;16(2734-46.

4. Fogelman I, Gnanasegaran G, and Van der Wall H. *Radionuclide and hybrid bone imaging.* Heidelberg: Springer; 2012.

5. Gilbert SF. *Developmental biology.* Sunderland, Mass.: Sinauer Associates; 2000.

6. Mackie EJ, Ahmed YA, Tatarczuch L, Chen KS, and Mirams M. Endochondral ossification: how cartilage is converted into bone in the developing skeleton. *The international journal of biochemistry & cell biology.* 2008;40(1):46-62.

7. van Donkelaar CC, and Wilson W. Mechanics of chondrocyte hypertrophy. *Biomechanics and modeling in mechanobiology.* 2012;11(5):655-64.

8. Kirsch T, Nah HD, Shapiro IM, and Pacifici M. Regulated production of mineralization-competent matrix vesicles in hypertrophic chondrocytes. *The Journal of cell biology.* 1997;137(5):1149-60.

9. Anderson HC, Sipe JB, Hessle L, Dhanyamraju R, Atti E, Camacho NP, and Millan JL. Impaired calcification around matrix vesicles of growth plate and bone in alkaline phosphatase-deficient mice. *The American journal of pathology.* 2004;164(3):841-7.

10. Maes C, Kobayashi T, Selig MK, Torrekens S, Roth SI, Mackem S, Carmeliet G, and Kronenberg HM. Osteoblast precursors, but not mature osteoblasts, move into developing and fractured bones along with invading blood vessels. *Dev Cell.* 2010;19(2):329-44.

11. Rajpurohit R, Koch CJ, Tao Z, Teixeira CM, and Shapiro IM. Adaptation of chondrocytes to low oxygen tension: relationship between hypoxia and cellular metabolism. *Journal of cellular physiology.* 1996;168(2):424-32.

12. Einhorn TA, Simon SR, and American Academy of Orthopaedic Surgeons. *Orthopaedic basic science : biology and biomechanics of the musculoskeletal system.* Rosemont, Ill.: American Academy of Orthopaedic Surgeons; 2000.

13. Gerstenfeld LC, Cullinane DM, Barnes GL, Graves DT, and Einhorn TA. Fracture healing as a post-natal developmental process: molecular, spatial, and temporal aspects of its regulation. *Journal of cellular biochemistry.* 2003;88(5):873-84.

14. Zhang X, Xie C, Lin AS, Ito H, Awad H, Lieberman JR, Rubery PT, Schwarz EM, O'Keefe RJ, and Guldberg RE. Periosteal progenitor cell fate in segmental cortical bone graft transplantations: implications for functional tissue engineering. *Journal of bone and mineral research : the official journal of the American Society for Bone and Mineral Research.* 2005;20(12):2124-37.

15. Nakahara H, Bruder SP, Haynesworth SE, Holecek JJ, Baber MA, Goldberg VM, and Caplan AI. Bone and cartilage formation in diffusion chambers by subcultured cells derived from the periosteum. *Bone.* 1990;11(3):181-8.

16. Liu R, Birke O, Morse A, Peacock L, Mikulec K, Little DG, and Schindeler A. Myogenic progenitors contribute to open but not closed fracture repair. *BMC musculoskeletal disorders.* 2011;12(288.

17. Wosczyna MN, Biswas AA, Cogswell CA, and Goldhamer DJ. Multipotent progenitors resident in the skeletal muscle interstitium exhibit robust BMP-dependent osteogenic activity and mediate heterotopic ossification. *Journal of bone and mineral research : the official journal of the American Society for Bone and Mineral Research.* 2012;27(5):1004-17.

18. Rockwood CA, Green DP, and Bucholz RW. *Rockwood and Green's fractures in adults.* Philadelphia, PA: Wolters Kluwer Health/Lippincott Williams & Wilkins; 2010.

CHAPTER 3

The Fibrinolytic System

During fracture in addition to injury of the bone the blood vessels are disrupted causing hemorrhage. To prevent exsanguination or life threating hemorrhage the bleeding must be stopped by the coagulation system. The coagulation system is composed of cells, platelets and plasma proteins all designed to potentate the conversion of the pro-polymer fibrinogen into polymer fibrin, forming a clot and preventing bleeding. While the some fibrin is deposited at the site of vessel disruption during injury a majority of the fibrin is deposited in the extravascular space (1). Thus the initial steps of fracture healing are thought to initiate around the formation and removal of the fibrin clot. This topic will be explored more in later chapters however to have a better understanding of the physiologic mechanisms involved in the processing of the fibrin matrix during fracture healing it is paramount that we first discuss the fibrinolytic system, which is responsible for the removal of the fibrin clot in a process know as fibrinolysis.

Plasminogen

The principal enzyme responsible for fibrinolysis is plasmin, a serine protease found in both the extravascular compartments and within the blood as the zymogen plasminogen (2). Plasminogen is synthesized by hepatocytes and circulates in plasma

at a concentration of 2.4 μM or 210u μg/ml (2). Plasminogen exists in two distinct glycosylated states known as Plasminogen 1, which has a carbohydrate chain at Asn-289 and Thr-346 and Plasminogen 2, which contains carbohydrate a chain only at Thr-346 (3). In addition to the two glycosylated forms, plasminogen has 3 conformational forms: Glu-plasminogen, Lys-plasminogen and Val plasminogen (Figure 1). Glu-plasminogen is the most abundant and stable conformation with a plasma half-life of 2 days. The stability of Glu-plasminogen is due to is relatively compact structure, that shields 4 out of the 5 lysine binding domains sites within the kringle domains through the interaction of the apple domain with kringle domains 4 and 5 (4). Lys-plasminogen, formed by plasmin cleavage of peptide bond between Lys76 and Lys 77, is considered the "open" form of plasminogen because all 5 lysine binding domains on plasminogen are exposed (2). Finally, Val-plasminogen, which has a markedly reduced affinity for fibrin, is the product of elastase-mediated cleavage of the peptide bond between Val 441 and Val 442 resulting in a much smaller structure containing only the kringle 5 and protease domains (5). Because of its relatively smaller size Val-plasminogen is often referred to as "mini" plasminogen. Regardless of the conformation shape or glycosylation pattern, all forms of plasminogen are converted to plasmin through the cleavage of the peptide bond between Arg 561 and Val 562 by plasminogen activators(2).

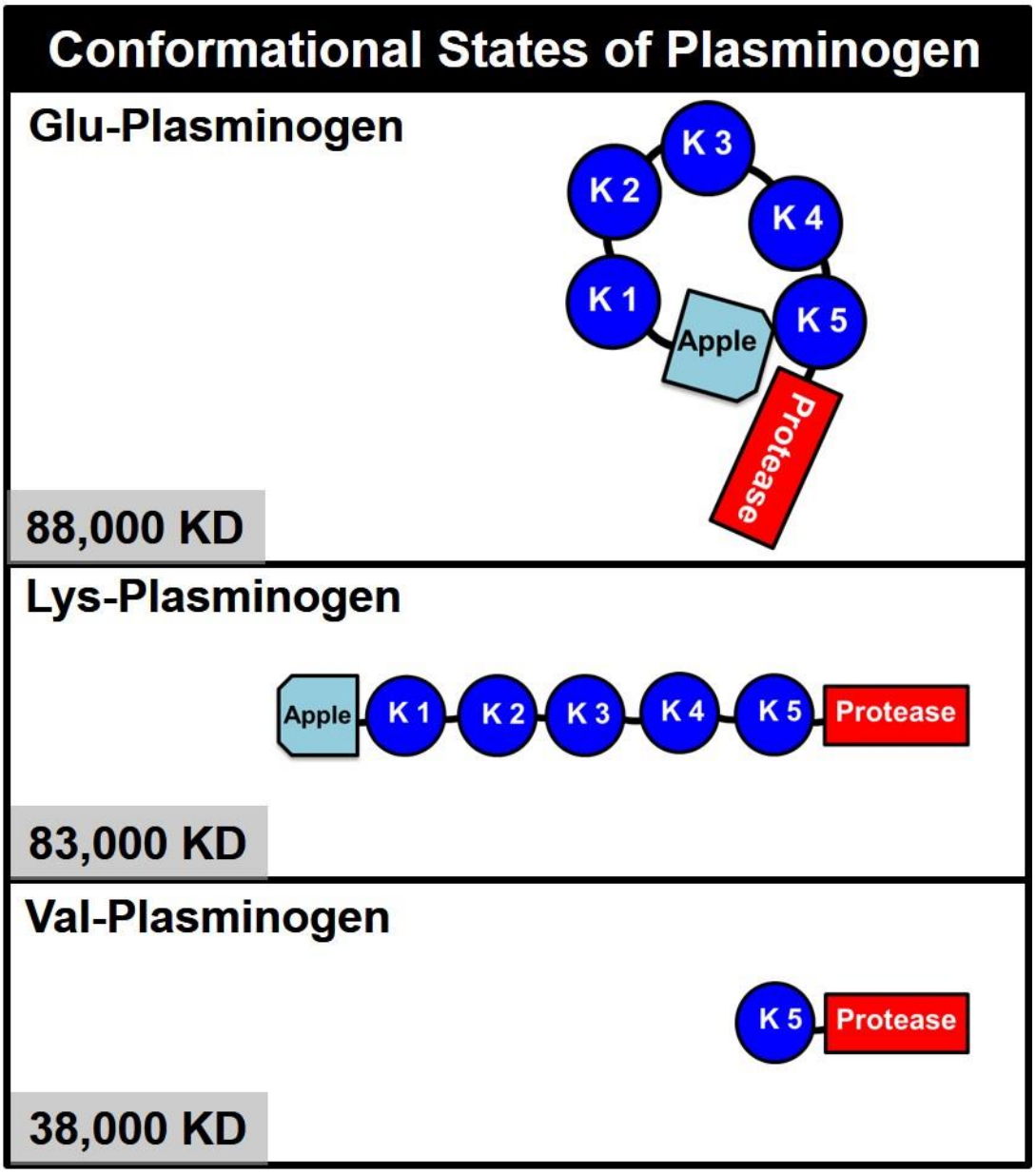

Figure 1: Illustration of the conformational states of plasminogen

Plasminogen Activators

The conversion of plasminogen to plasmin is primarily mediated by tissue plasminogen activator (tPA) and urokinase plasminogen activator (uPA), both of which are serine proteases. While their mechanisms of converting plasminogen to plasmin are identical, these activators have discrete biological applications where they exert their functions. tPA is essential for intravascular fibrinolysis and uPA for extravascular fibrinolysis.

tPA is a 68kd protease that circulates at a plasma concentration of 70 pM and is made by endothelial cells (6). tPA can be found in both single chain and double chain forms (2). In circulating blood, tPA activation of plasminogen is extremely inefficient because of the fibrinolytic system inhibitors (discussed in a later section) and the relatively low plasma concentrations of tPA. Upon formation of a fibrin matrix, both plasminogen and tPA bind to exposed lysine residues on fibrin, bringing plasminogen and tPA into relative close proximity, resulting in an increased efficiency for plasmin of generation (Figure 2) (7). Thus, efficient tPA mediated activation of plasminogen requires an existing fibrin matrix and tPA primarily released from endothelial cells at the site of vascular injury. Therefore, tPA mediated plasmin generation is generally localized to the injured vasculature during thrombosis and trauma. However, the idea that tPA has a limited role in extravascular plasmin generation has recently been called into question with the discovery of the cellular tPA receptors annexin II and S-100A10 (8, 9). These receptors promote tPA and plasminogen binding, allowing for tPA-based cellular plasmin activation in the extravascular space in the absence of fibrin. While the discovery of these receptors certainly expands the role of tPA mediated fibrinolysis, the majority of extravascular plasmin generation is dues to the activity of uPA

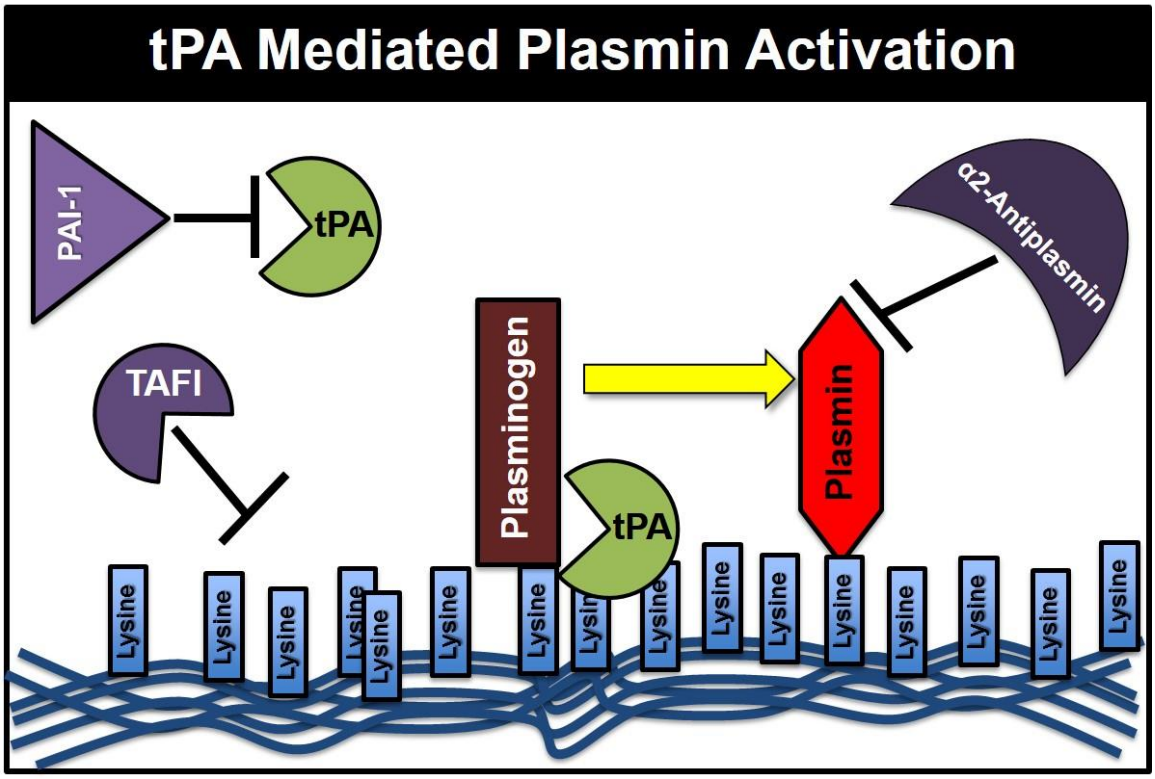

Figure 2: Illustration of tissue plasminogen activator mediated plasmin activation and regulation of fibrinolysis by fibrinolytic inhibitors

.

The zymogen signal chain urokinase plasminogen activator (scuPA) is a 54-kd protease produced by a multitude of cell types, including monocytes and macrophages (2). ScuPA is converted to two chain uPA (tcuPA) by cleavage of the peptide bond between Lys 158 and Ile 159 by several enzymes including plasmin, as well as factor XIIa, and kallikrein. The latter two enzymes, are components of the plasma contact activation system. uPA, tcuPA, unlike tPA, does not have a high affinity for fibrin (10). Instead scuPA and tcuPA primarily bind to the receptor urokinase plasminogen receptor (uPAR) (Figure 3) (2). uPAR is expressed ubiquitously and is required for efficient uPA mediated conversion of plasminogen to plasmin. Given that both uPAR as well as uPA are cellularly derived, the majority of plasmin activation by uPA is cell directed. As such, uPA mediated plasmin generation has been implicated in several biological processes such as tissue repair, cancer cell metastasis, and cellular migration (11-13).

Plasminogen Inhibitors

Regulation of the fibrinolytic system occurs through direct inhibition of plasmin, inhibition of the plasminogen activators, or through inhibition of plasminogen and plasmin activator co-localization (Figure 2). Direct inhibition of plasmin is primarily mediated through interactions with α 2-antiplasmin. α 2-antiplasmin is a serine protease inhibitor (serpin) produced by the liver that circulates in plasma at 1uM or 69ug/ml (14). At this concentration, α 2-antiplasmin circulates at a 2:1 molar ratio to plasminogen suggesting that up to half of generated plasmin can be immediately inactivated by α 2-antiplasmin (15).

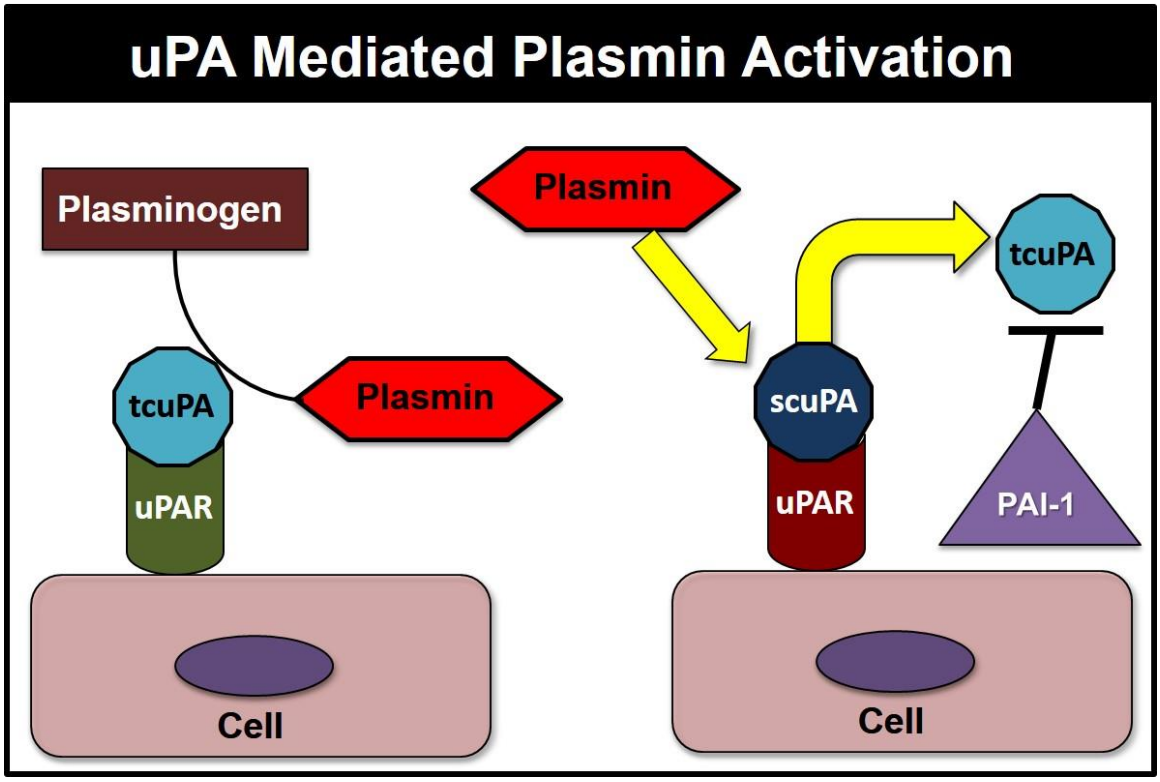

Figure 3: Illustration of urokinase plasminogen activator mediated plasmin activation

Direct inhibition of plasmin activity occurs through a three step process (15). In the first step, α 2-antiplasmin reversibly binds with the kringle 1 domain of plasmin (16). For binding to occur, the active site of plasmin must be unoccupied and plasmin cannot be bound to fibrin. Consequently, α 2-antiplasmin has specificity for fluid phase plasmin rather than plasmin fibrin bound. In the second step, the reactive center loop (RCL) of α 2-antiplasmin interacts with the active site of plasmin, resulting the cleavage of the RCL. In the finally and third step, as a result of this cleavage, an ester-bond is formed between α 2-antiplasmin and the active site of plasmin, irreversibly inhibiting plasmin activity(17).

Inhibition of the fibrinolytic system can also be achieved through inhibition of tPA and uPA by plasminogen activator inhibitors (PAI). There are 5 distinct PAIs: PAI-1 (18), PAI-2 (19), PAI-3 (20), protease nexin-1(21) and neuroserpin (22). All 5 PAI are serpins and have been shown to have irreversible inhibitory effects on uPA and tPA. While the PAIs target one or both plasminogen activators, specific inhibitors appear to be linked to distinct biological processes. For example, PAI-1 is primarily found in circulation and has the greatest impact on intravascular plasmin activity. PAI-2, secreted by cells of monocyte lineage, may have a role in extravascular fibrinolysis (23). Neuroserpin is primarily localized to the nervous system and strongly inhibits tPA. Given that tPA is required for neurite growth and is secreted during neuronal depolarization, it is likely that neuroserpin plays an important role in neuron repair and modulation of neurotransmitters (22, 24). The broad expression and biologic significance of PAI activators and their essential inhibitory functions gives them an important role in the pathogenesis of multiple diseases such diabetes, cardiovascular disease, nerve repair and kidney disease (22, 25-28).

Indirect regulation of fibrinolytic system also occurs by inhibiting co-localization of plasminogen activators with plasminogen. There are two principle inhibitors involved in

indirect inhibition: α2-antiplasmin and thrombin-activatable fibrinolysis inhibitor (TAFI). α2-antiplasmin inhibition occurs when α2-antiplasmin binds to exposed lysine on fibrin. Upon binding, Factor XIII crosslinks α2-antiplasmin thereby stabilizing the fibrin clot and removing a potential binding site for plasminogen, plasmin or tPA. (29). In a mechanism similar to that of α2-antiplasmin and factor XIII, inhibition of fibrinolysis can also occur through the removal of lysine binding sites on fibrin by TAFI, also referred to as carboxypeptidase B2. TAFI is produced in the liver, circulates in the plasma at 2.5ug/m, and is released by platelets upon degranulation (30). Together, both α2-antiplasmin and TAFI add another layer of control for the fibrinolytic system which allows for the precise control of fibrin degradation in both the intravascular and extravascular space.

References

1. Stalker TJ, Traxler EA, Wu J, Wannemacher KM, Cermignano SL, Voronov R, Diamond SL, Brass LF. Hierarchical organization in the hemostatic response and its relationship to the platelet-signaling network. Blood. 2013;121(10):1875-85. doi: 10.1182/blood-2012-09-457739. PubMed PMID: 23303817; PubMed Central PMCID: PMC3591806.

2. Marder VJ. Hemostasis and thrombosis : basic principles and clinical practice. 6th ed. Philadelphia: Wolters Kluwer/Lippincott Williams & Wilkins Health; 2013. xxiv, 1566 p. p.

3. Molgaard L, Ponting CP, Christensen U. Glycosylation at Asn-289 facilitates the ligand-induced conformational changes of human Glu-plasminogen. FEBS letters. 1997;405(3):363-8. PubMed PMID: 9108319.

4. Law RH, Caradoc-Davies T, Cowieson N, Horvath AJ, Quek AJ, Encarnacao JA, Steer D, Cowan A, Zhang Q, Lu BG, Pike RN, Smith AI, Coughlin PB, Whisstock JC. The X-ray crystal structure of full-length human plasminogen. Cell reports. 2012;1(3):185-90. doi: 10.1016/j.celrep.2012.02.012. PubMed PMID: 22832192.

5. Mullertz S, Thorsen S, Sottrup-Jensen L. Identification of molecular forms of plasminogen and plasmin-inhibitor complexes in urokinase-activated human plasma. The Biochemical journal. 1984;223(1):169-77. PubMed PMID: 6208893; PubMed Central PMCID: PMC1144277.

6. Nicoloso G, Hauert J, Kruithof EK, Van Melle G, Bachmann F. Fibrinolysis in normal subjects--comparison between plasminogen activator inhibitor and other components of the fibrinolytic system. Thrombosis and haemostasis. 1988;59(2):299-303. PubMed PMID: 3133812.

7. Ranby M, Bergsdorf N, Nilsson T. Enzymatic properties of the one- and two-chain form of tissue plasminogen activator. Thrombosis research. 1982;27(2):175-83. PubMed PMID: 6890245.

8. Roda O, Valero ML, Peiro S, Andreu D, Real FX, Navarro P. New insights into the tPA-annexin A2 interaction. Is annexin A2 CYS8 the sole requirement for this association? The Journal of biological chemistry. 2003;278(8):5702-9. doi: 10.1074/jbc.M207605200. PubMed PMID: 12468550.

9. O'Connell PA, Surette AP, Liwski RS, Svenningsson P, Waisman DM. S100A10 regulates plasminogen-dependent macrophage invasion. Blood. 2010;116(7):1136-46. doi: 10.1182/blood-2010-01-264754. PubMed PMID: 20424186.

10. Astrup T, Thorsen S. The physiology of fibrinolysis. The Medical clinics of North America. 1972;56(1):153-62. PubMed PMID: 4257246.

11. Dass K, Ahmad A, Azmi AS, Sarkar SH, Sarkar FH. Evolving role of uPA/uPAR system in human cancers. Cancer treatment reviews. 2008;34(2):122-36. doi: 10.1016/j.ctrv.2007.10.005. PubMed PMID: 18162327.

12. Bryer SC, Fantuzzi G, Van Rooijen N, Koh TJ. Urokinase-type plasminogen activator plays essential roles in macrophage chemotaxis and skeletal muscle regeneration. Journal of immunology. 2008;180(2):1179-88. PubMed PMID: 18178858.

13. Murphy G, Gavrilovic J. Proteolysis and cell migration: creating a path? Current opinion in cell biology. 1999;11(5):614-21. PubMed PMID: 10508651.

14. Cederholm-Williams SA. Concentration of plasminogen and antiplasmin in plasma and serum. Journal of clinical pathology. 1981;34(9):979-81. PubMed PMID: 7276224; PubMed Central PMCID: PMC494210.

15. Wiman B, Collen D. On the mechanism of the reaction between human alpha 2-antiplasmin and plasmin. The Journal of biological chemistry. 1979;254(18):9291-7. PubMed PMID: 158022.

16. Wang H, Karlsson A, Sjostrom I, Wiman B. The interaction between plasminogen and antiplasmin variants as studied by surface plasmon resonance. Biochimica et biophysica acta. 2006;1764(11):1730-4. doi: 10.1016/j.bbapap.2006.09.009. PubMed PMID: 17064970.

17. Nilsson T, Wiman B. On the structure of the stable complex between plasmin and alpha-2-antiplasmin. FEBS letters. 1982;142(1):111-4. PubMed PMID: 6213426.

18. Loskutoff DJ, van Mourik JA, Erickson LA, Lawrence D. Detection of an unusually stable fibrinolytic inhibitor produced by bovine endothelial cells. Proceedings of the National Academy of Sciences of the United States of America.

1983;80(10):2956-60. PubMed PMID: 6574465; PubMed Central PMCID: PMC393952.

19. Astedt B, Lindoff C, Lecander I. Significance of the plasminogen activator inhibitor of placental type (PAI-2) in pregnancy. Seminars in thrombosis and hemostasis. 1998;24(5):431-5. PubMed PMID: 9834009.

20. Espana F, Gilabert J, Estelles A, Romeu A, Aznar J, Cabo A. Functionally active protein C inhibitor/plasminogen activator inhibitor-3 (PCI/PAI-3) is secreted in seminal vesicles, occurs at high concentrations in human seminal plasma and complexes with prostate-specific antigen. Thrombosis research. 1991;64(3):309-20. PubMed PMID: 1725227.

21. Scott RW, Bergman BL, Bajpai A, Hersh RT, Rodriguez H, Jones BN, Barreda C, Watts S, Baker JB. Protease nexin. Properties and a modified purification procedure. The Journal of biological chemistry. 1985;260(11):7029-34. PubMed PMID: 3997857.

22. Hastings GA, Coleman TA, Haudenschild CC, Stefansson S, Smith EP, Barthlow R, Cherry S, Sandkvist M, Lawrence DA. Neuroserpin, a brain-associated inhibitor of tissue plasminogen activator is localized primarily in neurons. Implications for the regulation of motor learning and neuronal survival. The Journal of biological chemistry. 1997;272(52):33062-7. PubMed PMID: 9407089.

23. Hu ZY, Liu YX, Liu K, Byrne S, Ny T, Feng Q, Ockleford CD. Expression of tissue type and urokinase type plasminogen activators as well as plasminogen activator inhibitor type-1 and type-2 in human and rhesus monkey placenta. Journal of anatomy. 1999;194 (Pt 2):183-95. PubMed PMID: 10337950; PubMed Central PMCID: PMC1467912.

24. Fernandez-Monreal M, Lopez-Atalaya JP, Benchenane K, Leveille F, Cacquevel M, Plawinski L, MacKenzie ET, Bu G, Buisson A, Vivien D. Is tissue-type plasminogen activator a neuromodulator? Molecular and cellular neurosciences. 2004;25(4):594-601. doi: 10.1016/j.mcn.2003.11.002. PubMed PMID: 15080889.

25. Lyon CJ, Hsueh WA. Effect of plasminogen activator inhibitor-1 in diabetes mellitus and cardiovascular disease. The American journal of medicine. 2003;115 Suppl 8A:62S-8S. PubMed PMID: 14678868.

26. Huber K, Christ G, Wojta J, Gulba D. Plasminogen activator inhibitor type-1 in cardiovascular disease. Status report 2001. Thrombosis research. 2001;103 Suppl 1:S7-19. PubMed PMID: 11567664.

27. Rerolle JP, Hertig A, Nguyen G, Sraer JD, Rondeau EP. Plasminogen activator inhibitor type 1 is a potential target in renal fibrogenesis. Kidney international. 2000;58(5):1841-50. doi: 10.1111/j.1523-1755.2000.00355.x. PubMed PMID: 11044203.

28. Cinelli P, Madani R, Tsuzuki N, Vallet P, Arras M, Zhao CN, Osterwalder T, Rulicke T, Sonderegger P. Neuroserpin, a neuroprotective factor in focal ischemic stroke. Molecular and cellular neurosciences. 2001;18(5):443-57. doi: 10.1006/mcne.2001.1028. PubMed PMID: 11922137.

29. Sakata Y, Aoki N. Significance of cross-linking of alpha 2-plasmin inhibitor to fibrin in inhibition of fibrinolysis and in hemostasis. J Clin Invest. 1982;69(3):536-42. PubMed PMID: 7199538; PubMed Central PMCID: PMC371009.

30. Mosnier LO, Buijtenhuijs P, Marx PF, Meijers JC, Bouma BN. Identification of thrombin activatable fibrinolysis inhibitor (TAFI) in human platelets. Blood. 2003;101(12):4844-6. doi: 10.1182/blood-2002-09-2944. PubMed PMID: 12595308.

CHAPTER 4

Associations Between Hypofibrinolysis, Vascular Disease and Impaired Tissue Regeneration

Determination of the mechanisms leading to impaired fracture healing is essential to improving patient-centered outcomes and controlling health care costs. Numerous studies have demonstrated that the processes of fibrinolysis and angiogenesis at the injury site are independently linked to impaired tissue regeneration. However, few studies have demonstrated the interdependence between fibrinolysis, vascularity and tissue regeneration.

Adequate vascularity at the fracture site has long been recognized as a prerequisite for fracture healing. Much of the seminal work leading to this finding took place in preclinical models. Heppenstall et. al. demonstrated that chronic hypoxia delays fracture healing in dogs (1). Recent investigation into the primary growth factor involved in angiogenesis, vascular endothelial growth factor (VEGF), has demonstrated that, endochondral bone formation in the absence of VEGF and subsequent vascularity is severely impaired (1-3). These findings translate to the clinical setting, where patients with poor vasculature and limited angiogenic potential display poor fracture healing. One of the most profound studies demonstrating the importance of vascularity to fracture healing revealed that in traumatic tibia fracture, if both the proximal and posterior tibial arteries were disrupted, the rate of nonunion reached 75% (4). Furthermore, vascular insufficiency is common in peripheral vascular disease which has been shown to result

in delayed muscle and skin repair (5, 6). Together, these observations, along with data from preclinical models have established the paradigm that poor vascularity is associated with impaired musculoskeletal healing.

In healthy, well-perfused tissue, traumatic injury inevitably causes vascular disruption leading to fibrin deposition and clot formation. As fibrinolysis is biochemically linked to fibrin deposition, and is active at the site of injury, many investigations examine the role of fibrinolysis in the tissue reparative process. Regardless of the organ system studied, the fibrinolytic system has been proven essential for tissue regeneration (7-14). In line with the preclinical models, impaired musculoskeletal healing has been associated with both fibrin accumulation and insufficient fibrinolysis in a multitude of clinical conditions (9, 15-19). Specifically, patients with diabetes in particular, have impaired fibrinolytic activity associated with impaired fracture healing, while patients with muscular dystrophy have both impaired muscle regeneration and fibrin accumulation (9, 20-22).

Impaired fibrinolysis and excessive fibrin accumulation have also been linked impaired vascular patency and ingrowth following Injury. In preclinical models, clearance of fibrin deposited during injury has been shown to be essential for revascularization and angiogenesis following injury (23, 24). Further, fibrin accumulation and micro-vascular obstruction of vessels by fibrin is associated with up regulation of the fibrinolytic inhibitor PAI-1. PAI-1 is commonly elevated in pathological condition associated with hypofibrinolytic states (25). Clinical studies of patients with impaired fibrinolysis and fibrin accumulation reveal that these patients have increased incidence of thrombotic vascular occlusion, vascular disease, and impaired angiogenesis (21, 22, 26, 27). Together these data demonstrate the relationship between impaired fibrinolysis and poor revascularization.

Given that angiogenesis is a perquisite for fracture healing (2, 3, 28-31) and that hypofibrinolysis and vascular dysfunction are common to many comorbid conditions associated with poor fracture healing (32-36), it has been hypothesized that a primary cause of delayed union or non-union is impaired angiogenesis. However, none of these studies have been conducted simultaneously on the same patients. For that reason, and other confounding variables, we cannot conclude that poor fibrinolysis directly causes vascular problems that result in impaired fracture healing. My goal is to use animal models to demonstrate that hypofibrinolysis, impaired vascularization, and impaired fracture healing are mechanistically linked, and not simply associated with each other.

Reference

1. Heppenstall RB, Goodwin CW, Brighton CT. Fracture healing in the presence of chronic hypoxia. The Journal of bone and joint surgery American volume. 1976;58(8):1153-6. PubMed PMID: 1002761.

2. Gerber HP, Vu TH, Ryan AM, Kowalski J, Werb Z, Ferrara N. VEGF couples hypertrophic cartilage remodeling, ossification and angiogenesis during endochondral bone formation. Nature medicine. 1999;5(6):623-8. Epub 1999/06/17. doi: 10.1038/9467. PubMed PMID: 10371499.

3. Beamer B, Hettrich C, Lane J. Vascular endothelial growth factor: an essential component of angiogenesis and fracture healing. HSS journal : the musculoskeletal journal of Hospital for Special Surgery. 2010;6(1):85-94. Epub 2009/09/19. doi: 10.1007/s11420-009-9129-4. PubMed PMID: 19763695; PubMed Central PMCID: PMC2821499.

4. Brinker MR, Bailey DE, Jr. Fracture healing in tibia fractures with an associated vascular injury. The Journal of trauma. 1997;42(1):11-9. PubMed PMID: 9003252.

5. Ting M. Wound healing and peripheral vascular disease. Critical care nursing clinics of North America. 1991;3(3):515-23. PubMed PMID: 1883593.

6. Holm J, Bjorntorp P, Schersten T. Metabolic activity in human skeletal muscle. Effect of peripheral arterial insufficiency. European journal of clinical investigation. 1972;2(5):321-5. PubMed PMID: 5082067.

7. Ploplis VA, Carmeliet P, Vazirzadeh S, Van Vlaenderen I, Moons L, Plow EF, Collen D. Effects of disruption of the plasminogen gene on thrombosis, growth, and health in mice. Circulation. 1995;92(9):2585-93. Epub 1995/11/01. PubMed PMID: 7586361.

8. Suelves M, Lopez-Alemany R, Lluis F, Aniorte G, Serrano E, Parra M, Carmeliet P, Munoz-Canoves P. Plasmin activity is required for myogenesis in vitro and skeletal muscle regeneration in vivo. Blood. 2002;99(8):2835-44. PubMed PMID: 11929773.

9. Vidal B, Ardite E, Suelves M, Ruiz-Bonilla V, Janue A, Flick MJ, Degen JL, Serrano AL, Munoz-Canoves P. Amelioration of Duchenne muscular dystrophy in mdx mice by elimination of matrix-associated fibrin-driven inflammation coupled to the alphaMbeta2 leukocyte integrin receptor. Human molecular genetics. 2012;21(9):1989-2004. doi: 10.1093/hmg/dds012. PubMed PMID: 22381526; PubMed Central PMCID: PMC3315206.

10. Gong Y, Zhao Y, Li Y, Fan Y, Hoover-Plow J. Plasminogen regulates cardiac repair after myocardial infarction through its noncanonical function in stem cell homing to the infarcted heart. Journal of the American College of Cardiology.

2014;63(25 Pt A):2862-72. doi: 10.1016/j.jacc.2013.11.070. PubMed PMID: 24681141; PubMed Central PMCID: PMC4074457.

11. Drixler TA, Vogten JM, Gebbink MF, Carmeliet P, Voest EE, Borel Rinkes IH. Plasminogen mediates liver regeneration and angiogenesis after experimental partial hepatectomy. The British journal of surgery. 2003;90(11):1384-90. doi: 10.1002/bjs.4275. PubMed PMID: 14598419.

12. Romer J, Bugge TH, Pyke C, Lund LR, Flick MJ, Degen JL, Dano K. Impaired wound healing in mice with a disrupted plasminogen gene. Nature medicine. 1996;2(3):287-92. PubMed PMID: 8612226.

13. Kao WW, Kao CW, Kaufman AH, Kombrinck KW, Converse RL, Good WV, Bugge TH, Degen JL. Healing of corneal epithelial defects in plasminogen- and fibrinogen-deficient mice. Investigative ophthalmology & visual science. 1998;39(3):502-8. PubMed PMID: 9501859.

14. Bugge TH, Kombrinck KW, Flick MJ, Daugherty CC, Danton MJ, Degen JL. Loss of fibrinogen rescues mice from the pleiotropic effects of plasminogen deficiency. Cell. 1996;87(4):709-19. PubMed PMID: 8929539.

15. Tavora F, Cresswell N, Li L, Ripple M, Burke A. Immunolocalisation of fibrin in coronary atherosclerosis: implications for necrotic core development. Pathology. 2010;42(1):15-22. doi: 10.3109/00313020903434348. PubMed PMID: 20025475.

16. Aoki K, Aikawa N, Sekine K, Yamazaki M, Mimura T, Urano T, Takada A. Elevation of plasma free PAI-1 levels as an integrated endothelial response to severe burns. Burns : journal of the International Society for Burn Injuries. 2001;27(6):569-75. Epub 2001/08/30. PubMed PMID: 11525850.

17. Huber K, Christ G, Wojta J, Gulba D. Plasminogen activator inhibitor type-1 in cardiovascular disease. Status report 2001. Thrombosis research. 2001;103 Suppl 1:S7-19. PubMed PMID: 11567664.

18. Rerolle JP, Hertig A, Nguyen G, Sraer JD, Rondeau EP. Plasminogen activator inhibitor type 1 is a potential target in renal fibrogenesis. Kidney international. 2000;58(5):1841-50. doi: 10.1111/j.1523-1755.2000.00355.x. PubMed PMID: 11044203.

19. Lijnen HR, Collen D. Impaired fibrinolysis and the risk for coronary heart disease. Circulation. 1996;94(9):2052-4. PubMed PMID: 8901649.

20. Kline AJ, Gruen GS, Pape HC, Tarkin IS, Irrgang JJ, Wukich DK. Early complications following the operative treatment of pilon fractures with and without diabetes. Foot Ankle Int. 2009;30(11):1042-7. Epub 2009/11/17. doi: 10.3113/FAI.2009.1042. PubMed PMID: 19912712.

21. Lemkes BA, Hermanides J, Devries JH, Holleman F, Meijers JC, Hoekstra JB. Hyperglycemia: a prothrombotic factor? Journal of thrombosis and haemostasis : JTH. 2010;8(8):1663-9. doi: 10.1111/j.1538-7836.2010.03910.x. PubMed PMID: 20492456.

22. Pandolfi A, Cetrullo D, Polishuck R, Alberta MM, Calafiore A, Pellegrini G, Vitacolonna E, Capani F, Consoli A. Plasminogen activator inhibitor type 1 is increased in the arterial wall of type II diabetic subjects. Arteriosclerosis, thrombosis, and vascular biology. 2001;21(8):1378-82. PubMed PMID: 11498469.

23. Thompson WD, Harvey JA, Kazmi MA, Stout AJ. Fibrinolysis and angiogenesis in wound healing. The Journal of pathology. 1991;165(4):311-8. doi: 10.1002/path.1711650406. PubMed PMID: 1723752.

24. Ling Q, Jacovina AT, Deora A, Febbraio M, Simantov R, Silverstein RL, Hempstead B, Mark WH, Hajjar KA. Annexin II regulates fibrin homeostasis and neoangiogenesis in vivo. J Clin Invest. 2004;113(1):38-48. doi: 10.1172/JCI19684. PubMed PMID: 14702107; PubMed Central PMCID: PMC300771.

25. Zhang ZG, Chopp M, Goussev A, Lu D, Morris D, Tsang W, Powers C, Ho KL. Cerebral microvascular obstruction by fibrin is associated with upregulation of PAI-1 acutely after onset of focal embolic ischemia in rats. The Journal of neuroscience : the official journal of the Society for Neuroscience. 1999;19(24):10898-907. PubMed PMID: 10594071.

26. Lisman T, de Groot PG, Meijers JC, Rosendaal FR. Reduced plasma fibrinolytic potential is a risk factor for venous thrombosis. Blood. 2005;105(3):1102-5. doi: 10.1182/blood-2004-08-3253. PubMed PMID: 15466929.

27. Meltzer ME, Bol L, Rosendaal FR, Lisman T, Cannegieter SC. Hypofibrinolysis as a risk factor for recurrent venous thrombosis; results of the LETS follow-up study. Journal of thrombosis and haemostasis : JTH. 2010;8(3):605-7. doi: 10.1111/j.1538-7836.2009.03715.x. PubMed PMID: 19995410.

28. Harper J, Klagsbrun M. Cartilage to bone--angiogenesis leads the way. Nature medicine. 1999;5(6):617-8. Epub 1999/06/17. doi: 10.1038/9460. PubMed PMID: 10371495.

29. Brookes M, Landon DN. The Juxta-Epiphysial Vessels in the Long Bones of Foetal Rats. J Bone Joint Surg Br. 1964;46:336-45. Epub 1964/05/01. PubMed PMID: 14167642.

30. Maes C, Kobayashi T, Selig MK, Torrekens S, Roth SI, Mackem S, Carmeliet G, Kronenberg HM. Osteoblast precursors, but not mature osteoblasts, move into developing and fractured bones along with invading blood vessels. Dev Cell.

2010;19(2):329-44. Epub 2010/08/17. doi: 10.1016/j.devcel.2010.07.010. PubMed PMID: 20708594; PubMed Central PMCID: PMC3540406.

31. Hausman MR, Schaffler MB, Majeska RJ. Prevention of fracture healing in rats by an inhibitor of angiogenesis. Bone. 2001;29(6):560-4. Epub 2001/12/01. PubMed PMID: 11728927.

32. Burns DM. Epidemiology of smoking-induced cardiovascular disease. Progress in cardiovascular diseases. 2003;46(1):11-29. Epub 2003/08/16. PubMed PMID: 12920698.

33. Grundy SM, Benjamin IJ, Burke GL, Chait A, Eckel RH, Howard BV, Mitch W, Smith SC, Jr., Sowers JR. Diabetes and cardiovascular disease: a statement for healthcare professionals from the American Heart Association. Circulation. 1999;100(10):1134-46. Epub 1999/09/08. PubMed PMID: 10477542.

34. Meigs JB. Epidemiology of type 2 diabetes and cardiovascular disease: translation from population to prevention: the Kelly West award lecture 2009. Diabetes care. 2010;33(8):1865-71. Epub 2010/07/30. doi: 10.2337/dc10-0641. PubMed PMID: 20668155; PubMed Central PMCID: PMC2909080.

35. Purnell JQ, Zinman B, Brunzell JD, Group DER. The effect of excess weight gain with intensive diabetes mellitus treatment on cardiovascular disease risk factors and atherosclerosis in type 1 diabetes mellitus: results from the Diabetes Control and Complications Trial/Epidemiology of Diabetes Interventions and Complications Study (DCCT/EDIC) study. Circulation. 2013;127(2):180-7. Epub 2012/12/06. doi: 10.1161/CIRCULATIONAHA.111.077487. PubMed PMID: 23212717.

36. Willigendael EM, Teijink JA, Bartelink ML, Kuiken BW, Boiten J, Moll FL, Buller HR, Prins MH. Influence of smoking on incidence and prevalence of peripheral

arterial disease. Journal of vascular surgery. 2004;40(6):1158-65. Epub 2004/12/29. doi: 10.1016/j.jvs.2004.08.049. PubMed PMID: 15622370.

CHAPTER 5

The Temporal and Spatial Development of Vascularity In a Displaced Fractures

In order to demonstrate that impaired fibrinolysis results in impaired vascularity and impaired healing it was necessary to first identify the temporal and spatial development of vascularity following a fracture.

Seminal studies conducted in the last century have investigated the pattern of vascularity in bone following fracture. Investigations by Kolodny (1), Tennef (2) and Gotham (3) suggest a model in which the dominant source of fracture revascularization is the periosteum and other extra-osseous vascular sources such as adjacent skeletal muscle. Conversely, Ladanyi and Trueta discovered patterns of revascularization that apparently contradicted this model by demonstrating the essential nature of the intramedullary vasculature in revascularization of a fracture (4, 5). In a series of papers published in the 1960's, this controversy was revisited by Rhinelander who showed that the mechanism of revascularization was dependent on the type of experimental fracture model employed (6, 7). He made a key observation that in non-displaced fractures, the intramedullary vascularity reunited relatively early, without development of a significant periosteal component (so-called primary bone healing through "trans-medullary revascularization"). However, a different pattern of revascularization was observed in fractures with significant displacement, even with subsequent reduction and stabilization. In the displaced fracture model, initial formation of new periosteal vasculature was followed by intramedullary revascularization (so-called secondary bone healing or "trans-periosteal revascularization"). Thus, Rhinelander's work resolved the apparent discrepancy by showing that different mechanisms of revascularization are employed in

different experimental models (displaced vs. non-displaced fractures). The consensus model of revascularization of a displaced fracture culminating from these classical studies depicts a combination of angiogenesis emanating from both the intact intramedullary and periosteal vasculature.

Subsequent to the plethora of experimental fracture angiography in the early to mid-20th century there has been a paucity of reports describing the pattern of revascularization of a healing fracture. Consequently the classical model of revascularization of a displaced fracture has remained largely unchanged. Determination of the molecular elements responsible for and the pattern of revascularization following fracture are essential for targeting and augmenting discrete events during fracture healing. Importantly, key elements of fracture revascularization were unclear following the development of this model. Specifically, the association of angiogenesis in the intramedullary and periosteal space was unknown. It was hypothesized, that fracture angiogenesis in these anatomically distinct compartments occurred independently and only formed an anastomosis in the later stages of fracture healing (7). It was proposed that intramedullary angiogenesis occurred as a result of direct vascular growth from the remaining intact intramedullary vascularity and periosteal angiogenesis occurred as a result of direct vascular growth from the surrounding musculature. Additionally, the factors directing vascular union were unknown as vascular endothelial growth factor (VEGF) and its receptors (VEGF-R) had yet to be discovered (8). Thus, the molecular patterning leading to vascular union has not been incorporated into this classical model. In addition to these unanswered questions, the principle reason for the lack of advancement in this field has been critical methodological restraints prohibiting high throughput animal studies on fracture vascularity. Specifically, the classical models were performed primarily in relatively cost-inefficient larger animal models without the benefit of axial imaging allowing for detailed evaluation of fracture related angiogenesis.

Here, we have overcome the limitations of animal fracture models performed in the above described classical studies by combining novel techniques of bone angiography and a reproducible murine femur fracture model to demonstrate for the first time the complete temporal and spatial pattern of revascularization in a displaced/stabilized fracture. These studies were designed specifically to i) validate the classical model of fracture revascularization of a displaced/stabilized fracture ii) assess the association between intramedullary and periosteal angiogenesis and iii) elucidate the expression of VEGF/VEGF-R in relation to the classical model.

From the studies, in conjunction with classic studies of angiogenesis during fracture repair (1, 2, 4, 6, 7, 9-19), we propose a novel model that defines the process of bone revascularization subsequent to injury to guide future approaches to enhance fracture healing.

Results

Fracture and/or reaming disrupt diaphyseal intramedullary vascularity. Consistent with previous reports (20), the vasculature of the femoral mid-diaphysis is composed primarily of larger intramedullary vessels with few branching points. In contrast, the proximal and distal metaphysis is composed of multiple intramedullary vessels significantly smaller and with many more branching points than the diaphysis (Figure 1a). Upon fracture the diaphyseal vascularity is disrupted at the fracture site whereas the proximal and distal metaphyseal vascularity remain intact resulting in a segmental loss of intramedullary vascularity approximately 1mm proximal and distal to the insult (Figure 1b) without significant disruption of metaphyseal vascularity. A similar pattern of metaphyseal sparing segmental diaphyseal avascularity occurs following intramedullary

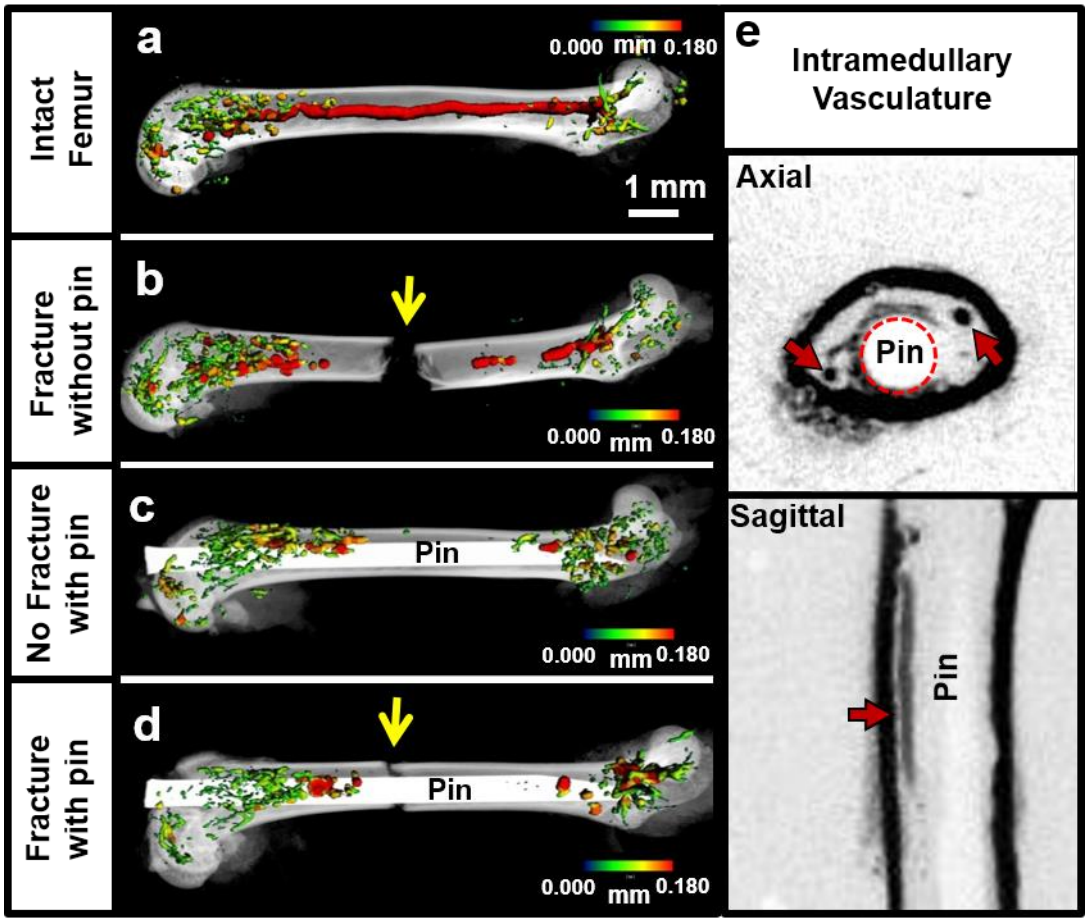

Figure 1: Fracture and/or intramedullary reaming produce a segmental avascular diaphyseal segment. a) Femoral angiography reveals larger unbranched vasculature within the diaphysis and smaller branched vasculature within the proximal and distal metaphysis. **(b)** Immediately following fracture (yellow arrow) angiography demonstrates a segmental diaphyseal avascular segment approximately 1mm proximal and distal to the injury without disruption of the metaphyseal vasculature. **(c)** Reaming and pin placement alone and **(d)** fracture with reaming and pin placement produce a similar diaphyseal avascular segment without disruption of the metaphyseal vasculature. **(e)** Two-dimensional slices from µCT demonstrates that the intramedullary pin does not prevent diaphyseal intramedullary vasculature (red arrows). Vessel diameter demarcated by color (0 and 0.18mm) in all figures.

reaming and pin stabilization without (Figure 1c) or with (Figure 1d) fracture. μCT angiography confirms that the 23G intramedullary pin utilized to stable the fracture permits revascularization through the intramedullary compartment of the diaphysis (Figure 1e).

Vascular development relative to soft tissue and hard tissue callus in a displaced fracture. Safranin-O-staining, radiographs, and angiograms of fractured femurs elucidates the temporal and spatial development of the fracture callus and associated vasculature (Figure 2a). Seven days post-fracture (7-DPF), the diaphyseal intramedullary vasculature remains disrupted, resulting in an avascular femoral segment flanked proximally and distally by intact intramedullary vasculature. Radiographic and histopathologic examination shows formation of a cartilaginous soft tissue callus without evidence of osteoid formation within this avascular zone. The soft tissue callus rapidly enlarges to its maximal size by 10-DPF. Simultaneously, hard tissue callus is initially formed via intramembranous ossification at the extreme proximal and distal aspects of the fracture site, where the periosteum inserts on unaffected adjacent cortical bone. This process occurs in conjunction with the formation of small highly branching extramedullary vessels (10-DPF). As hard tissue callus replaces soft tissue callus (14-DPF), it is accompanied by an expansion of newly formed vasculature. Spatially, the regions of vascular expansion begin at the proximal and distal aspect of the fracture site and migrate centrally toward the soft tissue callus. Vascular ingrowth continues until anastomoses are developed, coinciding with complete dissolution of soft tissue callus and formation of bridging hard tissue callus (21-DPF). Following vascular anastomosis and bridging of hard callus across the fracture site, the fracture callus remodels back to within the original

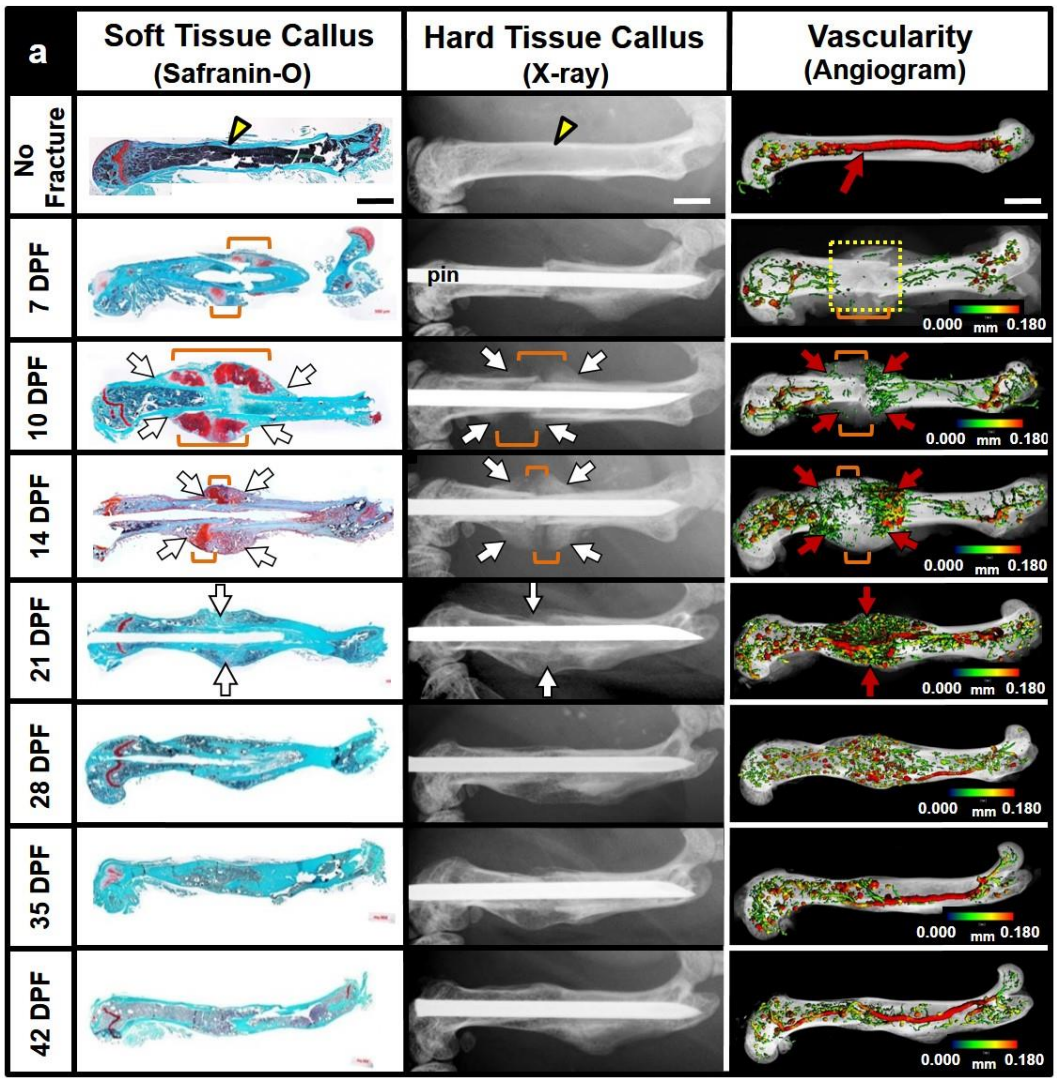

Figure 2A: Vascular development relative to soft tissue and hard tissue callus formation in a displaced, stabilized fracture. (a) Safranin-O-staining, radiographs, and angiograms were performed on fractured femurs at specified intervals following fracture to elucidate the temporal and spatial development of the fracture callus and associated vasculature. (High power images, 2b). Representative images are shown: quantitative measurements of the hard and soft tissue callus and fracture vasculature is provided in Table 1 and Figure 3. Prior to fracture (**No Fracture**) the mid-diaphyseal segment is composed of intact cortical bone (yellow arrowhead on Safranin-O and radiograph) with intact intramedullary vasculature (red arrow on angiogram). 7 days post fracture (**7-DPF**), disruption of the intramedullary vascular system (yellow box on angiogram) is accompanied by the development of chondroid tissue within the avascular zone of the healing fracture (red staining on Safranin-O, orange bracket) without obvious development of hard tissue callus by radiographic examination. By 10 days post fracture, (**10-DPF)** the soft tissue callus has grown to its maximal size (orange bracket on Safranin-O) and is largely limited to the avascular regions of the healing fracture. Small, newly formed vessels are observed (red arrows on angiogram) proximal and distal to the avascular soft tissue callus. These new vessels seem to arise directly from intact intramedullary vessels. Radiographs reveal initial formation of hard tissue callus 10 days post fracture (white arrows X-ray) overlying areas of developing vascularity, but not within avascular soft tissue callus (orange brackets). 14 days post fracture **(14-DPF)**, newly formed extramedullary vasculature rapidly extends from the proximal and distal aspects of the fracture callus towards the center of the fracture callus (red arrows on angiogram). As the vascular network develops, the soft tissue callus is replaced by hard tissue callus (white arrows on Safranin-O and on X-ray). By 21 days post fracture (**21-DPF)** the fracture callus has been completely bridged by vascular anastomosis (red arrows on angiogram) which occurs contemporaneously with complete resorption of the soft tissue callus and union of hard tissue callus (white arrows on Safranin-O and X-ray). Fracture callus undergoes vascular remodeling (angiogram) together with remodeling of the hard tissue callus during the next 14 days (**28-DPF through 42-DPF**), restoring the femoral diaphysis to its original form. Images are representative sections from for each time group (n≥5). Vessel diameter demarcated by color (0 and 0.18mm) in all figures.

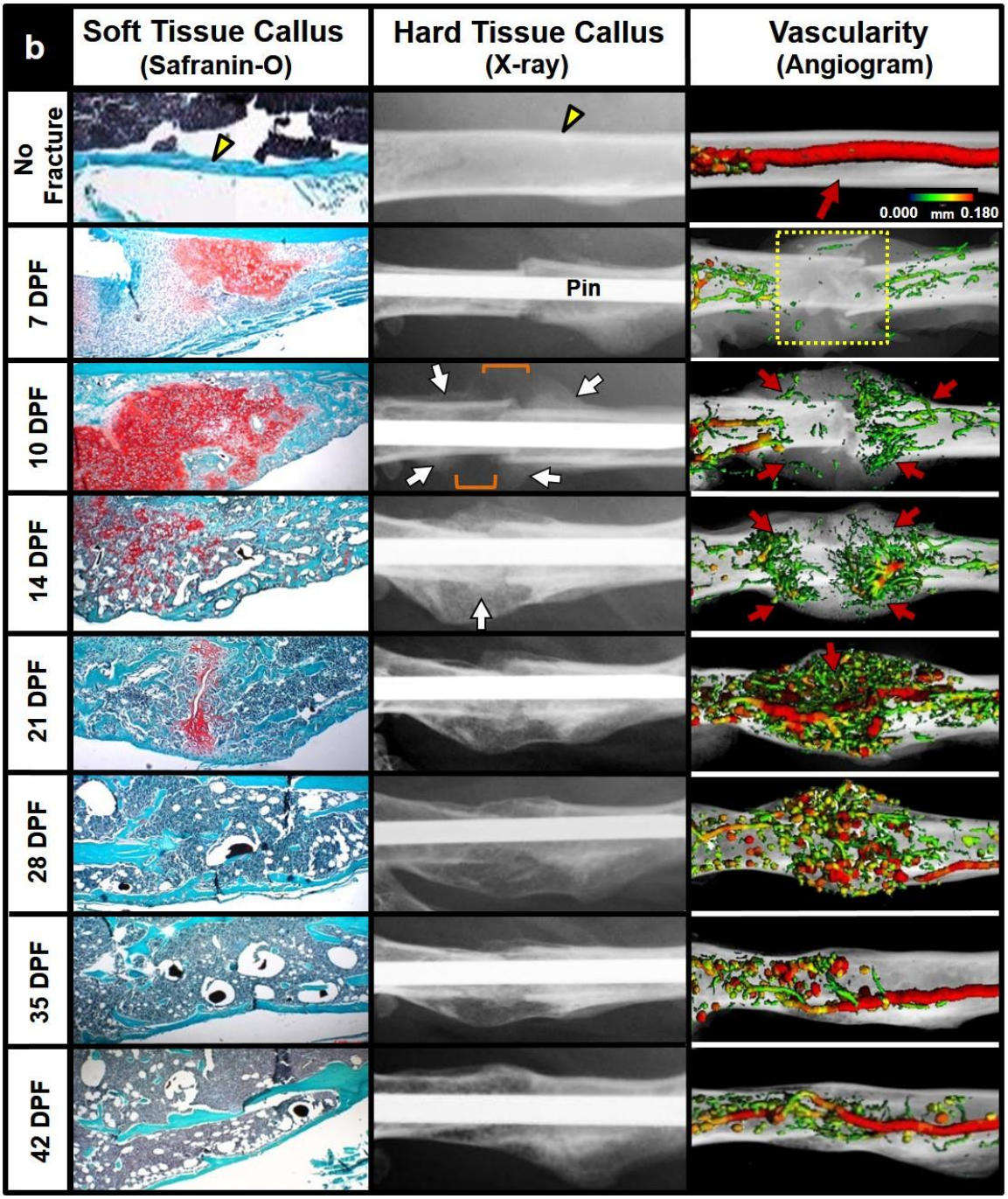

Figure 2B: Vascular development relative to soft tissue and hard tissue callus formation in a displaced, stabilized fracture. b) Higher power magnification of the fracture callus. Images are representative sections from for each time group (n≥5). Vessel diameter demarcated by color (0 and 0.18mm) in all figures.

cortices coinciding with the vasculature returning to larger vessels with reduced branching.(28-42-DPF). Higher power views of the fracture callus are presented in Figure 2b.

Quantitation of angiogenesis relative to soft tissue and hard tissue callus in a displaced fracture. Relative to hard tissue callus and vascularity, the soft tissue callus is the fastest developing matrix following fracture, reaching its maximum size by 10-DPF and decreasing in size until it is undetectable at 28-DPF (Figure 3a). Hard tissue callus develops later than the soft-tissue callus, reaching its maximum size between 14 and 21-DPF, and then steadily returns to its initial size by 42-DPF (Figure 3b). In accordance with our findings that fracture and insertion of an intramedullary device (Figure 1) produce an avascular segment of diaphyseal bone around the fracture site, the average vessel volume initially decreases immediately following fracture (Figure 3c). At the point of maximum soft tissue callus (hashed line) vessel volume begins to increases reaching maximum volume at the same time as maximum hard tissue callus (grey zone). Vessel volume subsequently decreases approaching, but not reaching, the pre-fracture vessel volume by 42-DPF. Data used for generation of the graphs are presented in table 1.

Newly formed subperiosteal vasculature arises from intact intramedullary vasculature. High power magnification of angiograms reveal that by 10-DPF newly formed extramedullary vasculature arises from intact intramedullary blood vessels proximal and distal to the fracture site (Figure 4a). These intramedullary-extramedullary vascular anastomoses are also demonstrated by 2D reconstruction of μCT images and close macroscopic inspection of the cut surfaces of contrast-injected and decalcified femur fracture specimens. These data demonstrate multiple communicating vessels apparently arising from intramedullary vasculature, traversing the cortical bone and branching into numerous small vessels supplying the newly formed hard tissue callus in the subperiosteal

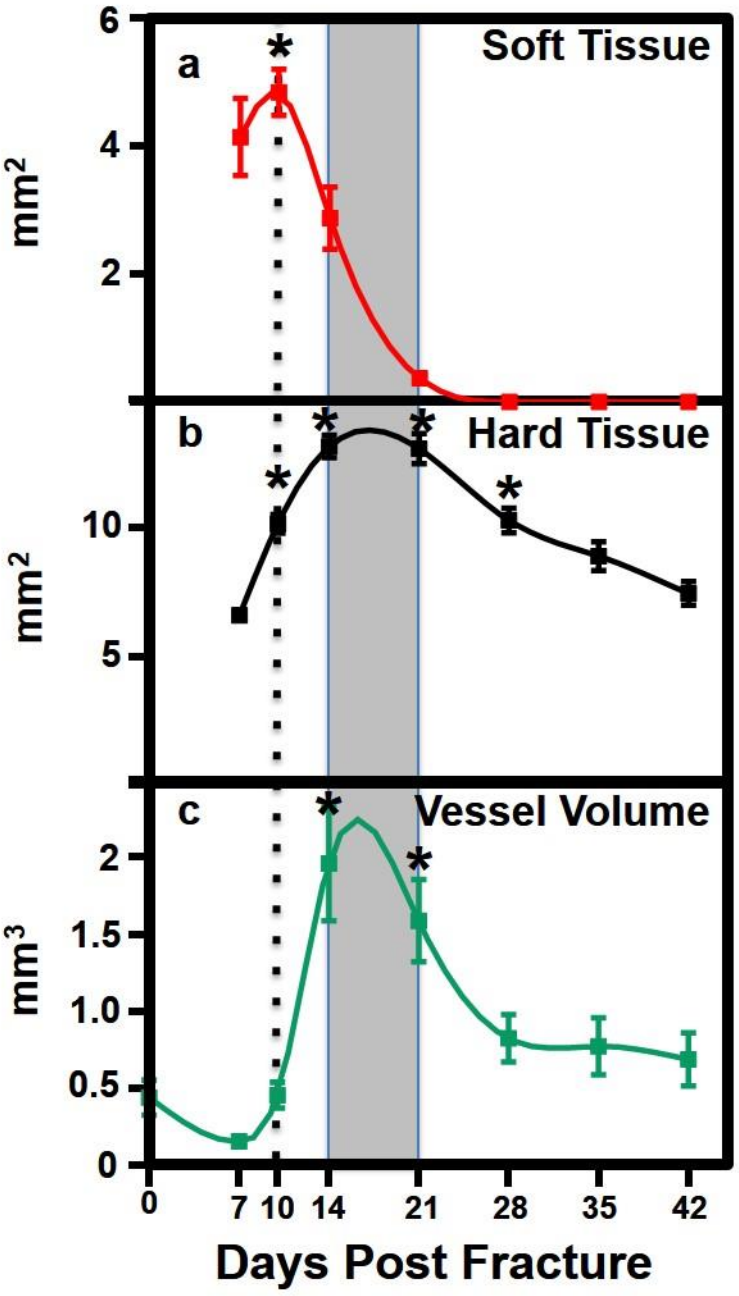

Figure 3: Quantitation of vascular development relative to soft tissue and hard tissue callus in a displaced fracture. (a) Quantification of the soft tissue callus identified by Safranin-O staining reveals significant development of cartilage 7-14-DPF relative to 42-DPF with maximum area 10-DPF (hashed line). Soft tissue callus is last detected 21-DPF. **(b)** Quantification of hard tissue callus identified by X-ray reveals the first significant new bone development occurs at 10-DPF with maximum size between 14-21-DPF (grey zone). Hard tissue callus size subsequently remodels, decreasing in size, to its original pre-fracture size by 42-DPF **(c)** Quantification of vessel volume identified by μCT of decalcified angiograms reveals an initial loss of vascularity with subsequent increase initiating at the time of maximum soft tissue callus and reaching maximum vessel volume between 14 and 21-DPF. Vessel volume then reduces from 21-42-DPF near the pre-fracture diaphyseal vessel volume. All samples were evaluated from 7-42 days following fracture and trend lines were generated using a spline curve fit. Dotted line denotes the maximum soft tissue callus size and gray zone denotes the maximum hard tissue callus size. Statistical analyses of soft tissue callus, hard tissue callus, and vessel volume were performed using non-parametric ANOVA with a Dunn's multiple comparison test. Significance (p value < 0.1) is denoted by asterisk and all error bars represent standard error of the mean. For statistical analysis of the soft tissue callus all values were compared to 21-DPF. For statistical analysis of the hard tissue callus all values were compared to 42-DPF. For statistical analysis of vessel volume all values were compared to un-fractured femora. See

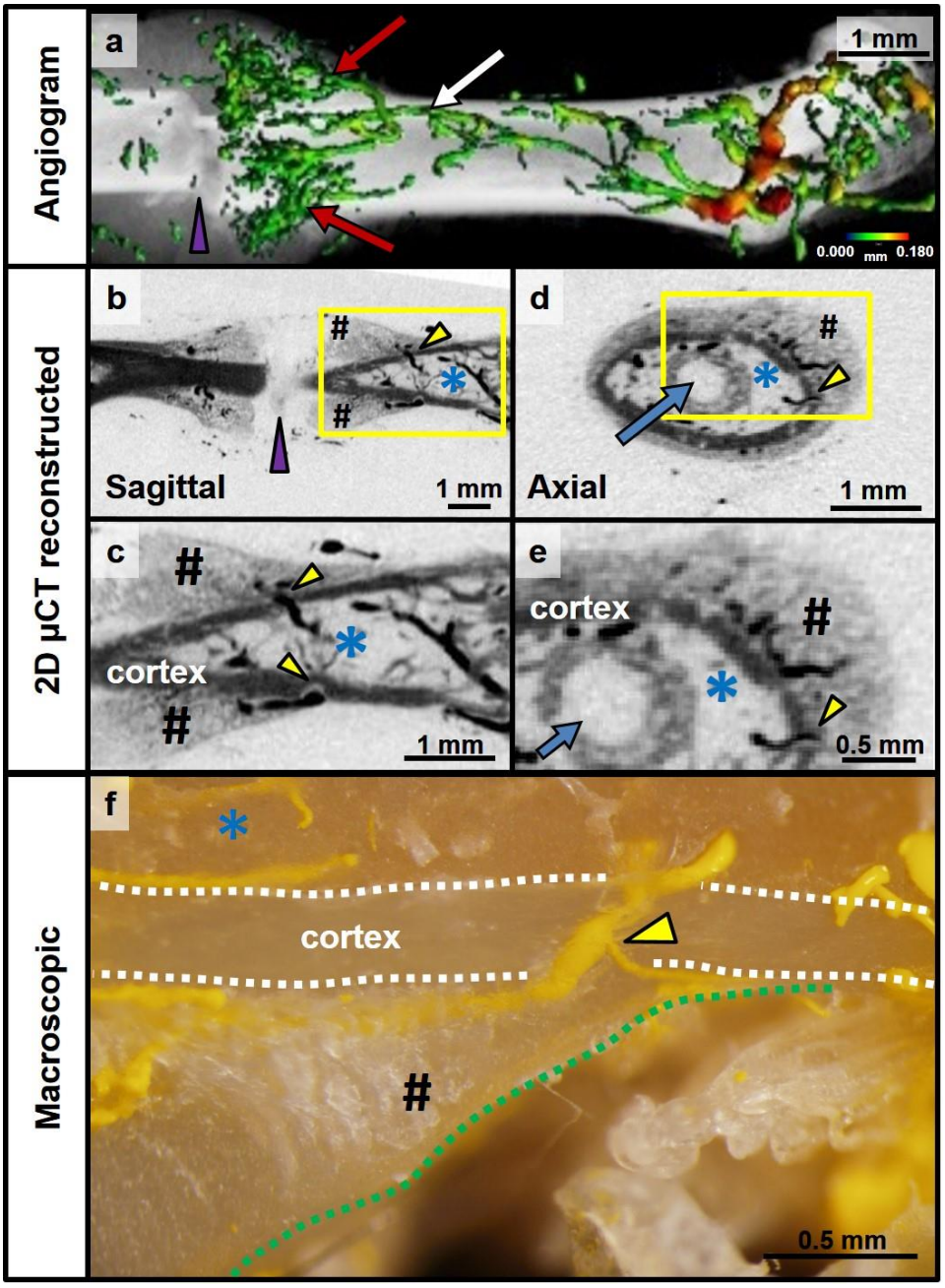

Figure 4: Newly formed vasculature arising from intact intramedullary vasculature adjacent to healing fracture (a) 10 days post fracture, small contrast-filled blood vessels in the extramedullary fracture callus and endosteal areas of the intramedullary cavity (red arrow) appear to arise from intact intramedullary vessels (white arrow) proximal to the fracture callus (purple arrowhead indicates fracture site). **(b-e)** Two dimensional reconstructed sagittal **(b,c)** and axial **(d,e)** µCT images illustrate multiple anastomoses (yellow arrowheads) between the intramedullary (blue asterisks) and extramedullary (#) vasculature (**c** and **e** are magnified regions highlighted in b and d, respectively). The purple arrowhead indicates the fracture site **(b)**. The site of the 23G fixation pin in the axial image is denoted with a blue arrow **(d)**. Notably, the fixation pin does not occupy the entire intramedullary canal. Macroscopic dissection of the proximal end of the fracture callus **(f)** reveals the presence of yellow contrast-filled vessels (yellow arrowhead transgressing the cortical bone (dashed white lines) and communicating between intramedullary space (blue asterisks) and the extramedullary/subperiosteal hard callus (#, outlined by green dashed line)). Scale bars given within the figure. Vessel diameter demarcated by color (0 and 0.18mm) in all figures.

space (Figure 4b-f). Such anastomoses were only observed at the proximal and distal ends of the fracture callus, indicating that they were not native nutrient vessels of the femur. Axial 2D reconstructions confirm that the 23G-pin used to stabilize the fracture did not completely occlude or completely disrupt the intramedullary vasculature.

Fracture angiogenesis co-localizes with the hard tissue callus and invades the soft tissue callus. Multiple lines of evidence illustrate that the extramedullary vasculature is associated with developing hard tissue callus and resorption of soft tissue callus. Sagittal sectioning of vascular contrast-filled fracture callus (10-DPF) reveals robust development of extramedullary vasculature in hard tissue callus at the proximal and distal aspects of the fracture callus (Figure 5a, b) in contrast to the observed avascular fracture callus 7-DPF (data not shown). Histological examination shows a predominance of vascularity at the leading edge of the invading hard tissue callus in the transition zone between the hard and soft tissue calluses as wells as throughout the hard tissue callus. In agreement with macroscopic dissections and 2D-μCT reconstructions, no vessels were found within the avascular cartilaginous soft tissue callus (Figure 5c). These findings were also observed 14-DPF however the soft tissue callus was greatly diminished in size while the hard tissue callus was much more predominate (data not shown).

Spatial patterns of vascular endothelial growth factor and its type 1 and 2 receptors during fracture healing. Vascular endothelial growth factor-A (VEGF-A) and vascular endothelial growth factor receptor 1 (VEGFR1) and 2 (VEGFR2) expression were investigated by immunofluorescence microscopy at distinct foci along the periosteal surface 10-DPF (Figure 6a-b). Compared to unreactive normal periosteum, the immunoreactivity of VEGF-A staining was markedly increased along the periosteum

at its junction with uninvolved cortical bone, which was also the site of initial intramembranous ossification during formation of the hard tissue callus (Figure 6c, boxes 1&4). These areas align anatomically with the sites at which the intramedullary vasculature is disrupted (compare with Figure 3). In contrast, an increase in immunoreactivity of VEGF-A staining was not observed in the periosteum overlying the soft tissue callus and disrupted intramedullary vasculature in the central region of fracture callus (Figure 6c, boxes 2&3).

Evaluations of multiple anatomic locations representing distinct biological activities during fracture healing demonstrate the coordinated spatial expression of VEGFA, VEGFR1 and VEGFR2 in the subperiosteal and extramedullary fracture callus 10-DPF (Figure 7&8a). VEGFR1&2-positive cells are seen only in areas of intramembranous ossification or in hard tissue callus along the interface with soft tissue callus. These VEGFR1&2-positive non-chondrocytic cells are in close proximity to VEGF-A sources, either the periosteum at the proximal and distal aspects of the fracture callus or at the interface with soft tissue callus (Figure 7&8b, box1). Additionally, we observed that immature chondrocytes located deep in the soft tissue callus, and superficial to vascular deficient intramedullary bone did not express either VEGF-A, VEGFR1 or VEGFR2 (Figure 7&8b, box2). However, neighboring hypertrophic chondrocytes as well as chondrocytes situated at the transition between soft tissue and hard tissue callus expressed VEGF-A but not VEGFR1 or 2 (Figure 7&8b, box3). Juxtaposed to hypertrophic chondrocytes in the zone of transition, nondescript mesenchymal cells of the hard tissue callus invading the soft tissue callus were found to demonstrate immunoreactivity for VEGF-A, VEGFR1 and VEGFR2, demonstrating the dichotomous nature of the VEGFR-positive vascularized hard tissue callus from the avascular VEGFR1 & VEGFR2-negative soft tissue callus (Figure 7&8b, box4)

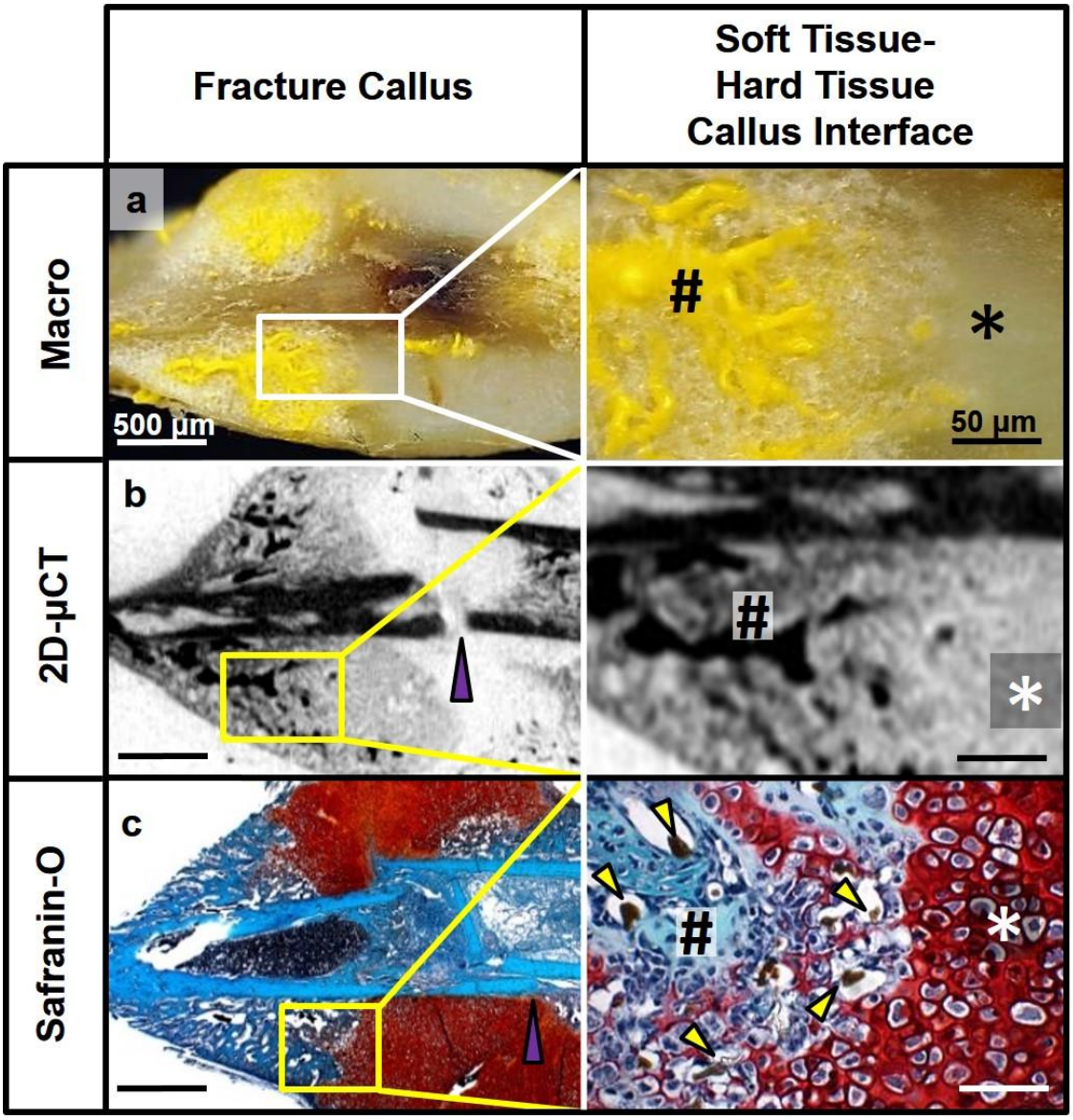

Figure 5: Vascular polarity in hard and soft tissue fracture callus 10 day post fracture. (a) Macroscopic dissection and **(b)** 2D µCT images from Microfil-injected fracture callus both demonstrate contrast agent within the extramedullary hard tissue callus, but not in soft tissue callus (see paired Safranin-O stained sections in (c) for comparison). At higher power magnification, a richly vascularized area with sprouting vessels (#) is seen adjacent to the avascular soft tissue callus (asterisk). **(c)** Paired sections of fracture callus stained with Safranin-O confirm the locations of the hard tissue callus (stained blue/green) and soft tissue callus (stained red). A higher power microscopic view of the interface between the hard tissue callus (#) and the soft tissue callus (asterisk) shows nondescript mesenchymal cells and Microfil-filled small capillaries (yellow arrowheads) replacing areas of soft callus at the interface of the hard tissue and soft tissue callus. Scale bars: 500 µm (left) and 50 µm (right). Images are representative sections from 5 animals 10 days after fracture.

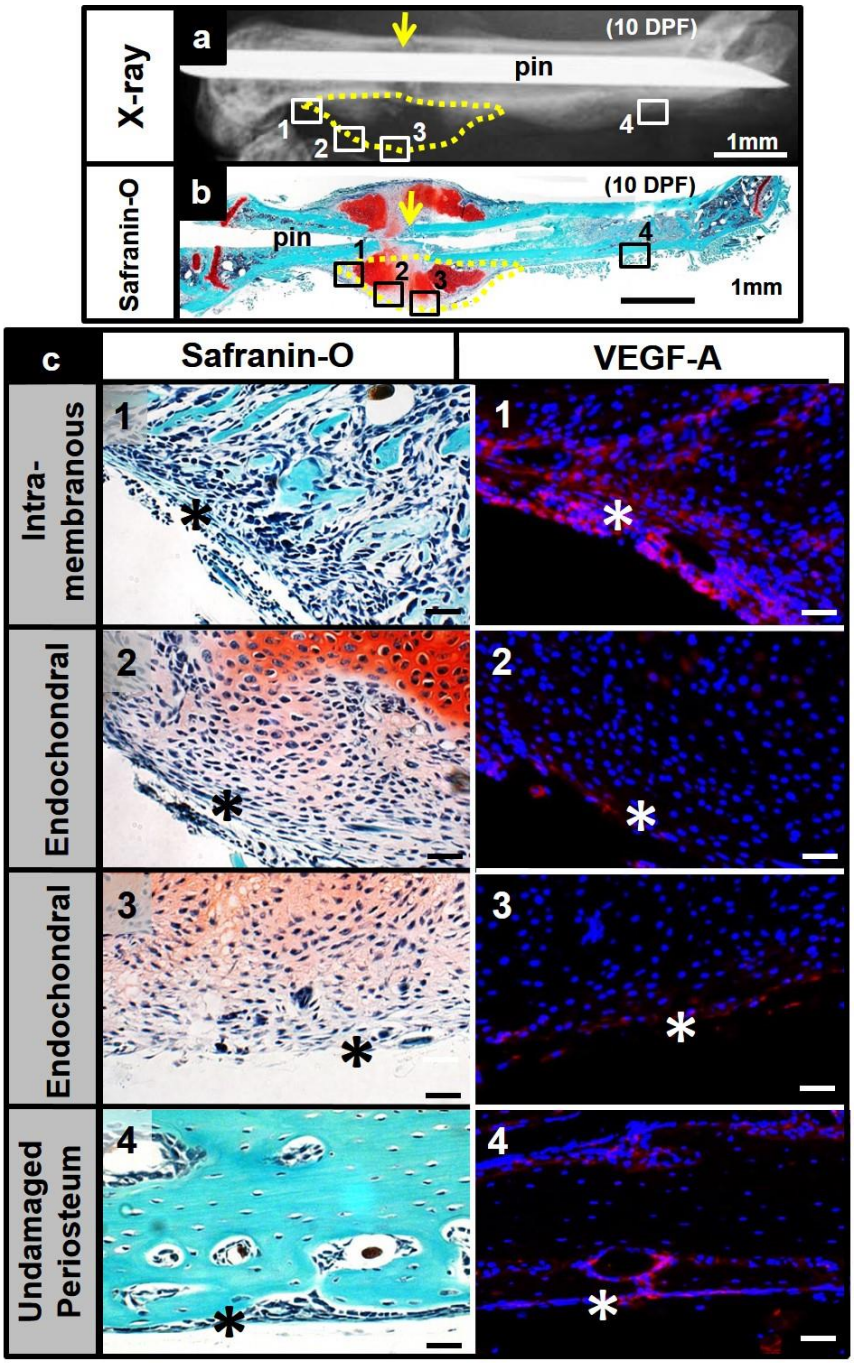

Figure 6: VEGF-A is primarily expressed in periosteum overlying intramembranous bone formation in hard tissue callus. (a, b) Radiograph and Safranin-O-stained section of a 10 days post fracture (10-DPF) transverse femur fracture and its fracture callus (yellow dashed line). VEGF-A staining was examined at various microanatomic periosteal sites, such as the area of initial intramembranous ossification (Box 1), areas overlying the soft chondroid callus (Boxes 2 and 3), and an area of unreactive normal periosteum (Box 4). **(c)** Immunofluorescence demonstrates increased immunoreactivity of VEGF-A (red) in the periosteum (asterisk) overlying the area of hard callus formation (Box 1) compared to minimal levels of immunoreactivity seen in the periosteum overlying the soft callus (Boxes 2 and 3) and normal unreactive periosteum on intact cortical bone (Box 4) Scale bars; 40 μm.

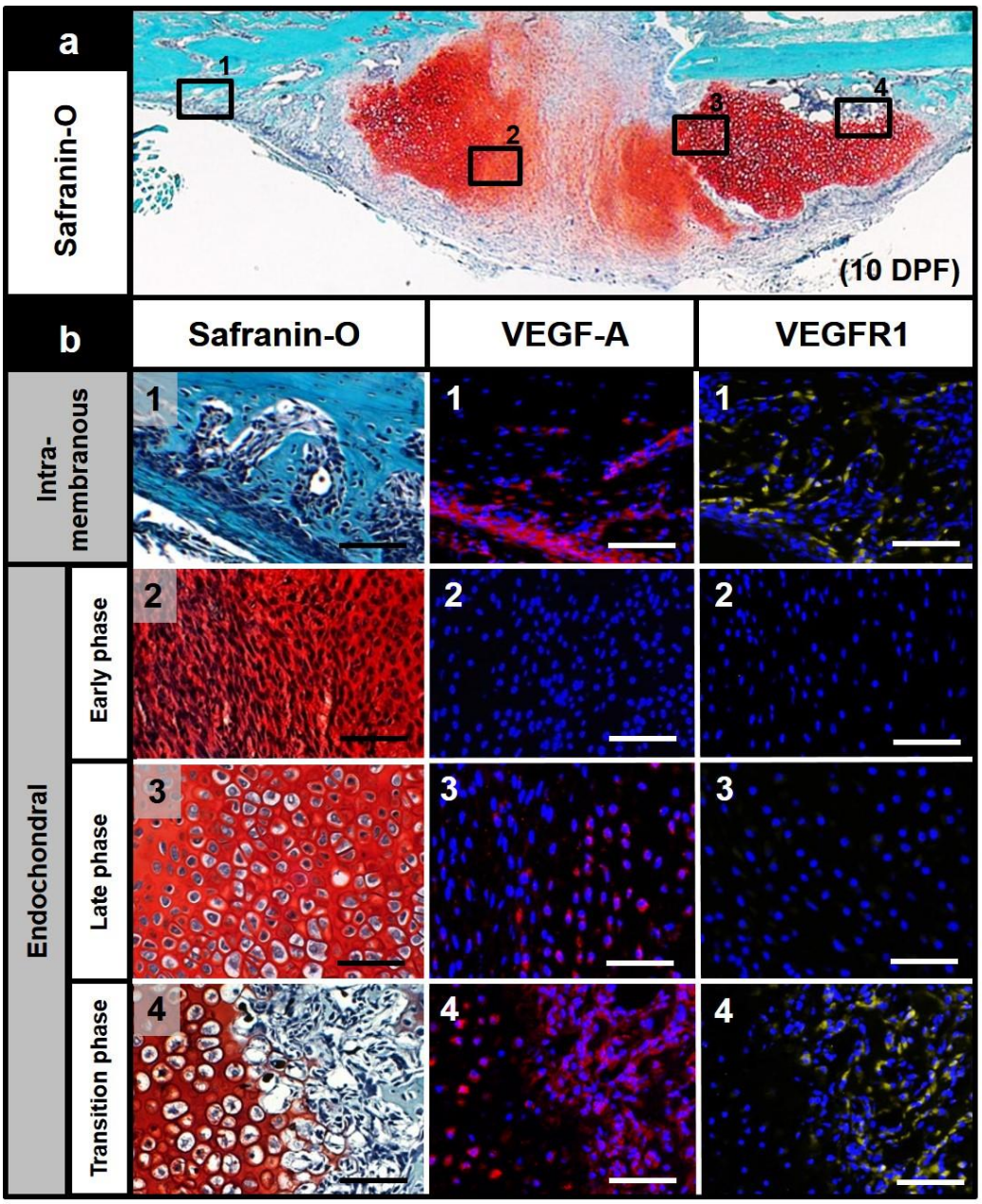

Figure 7: Differential expression of VEGF-A and VEGFR1 in the subperiosteal space in fracture callus. (a) Safranin-O staining of a fracture callus 10 days post fracture (10-DPF) shows a zone of intramembranous bone formation (Box 1), a zone of primitive mesenchymal-appearing cells in the soft tissue callus (Box 2), and an area of mature hyaline-type cartilage in the soft tissue callus (Box 3). The interface between the soft tissue callus and the hard tissue callus is denoted in Box 4. **(b)** High power photomicrographs of the 4 regions of interest stained with Safranin-O and immunofluorescence for VEGF-A (red) or VEGFR1 (yellow). (Box 1) Hard tissue callus consisting of intramembranous ossification shows abundant immunoreactivity of VEGF-A primarily in the overlying periosteum and numerous VEGFR1-positive cells within the sub-periosteal space. (Box 2) Safranin–O staining shows a cellular zone of primitive spindle cells without evidence of matrix deposition, in which VEGF-A or VEGFR1 are not detectable. (Box 3) VEGF-A appears to be limited to occasional enlarged, hypertrophic chondrocytes within this area of hyaline cartilage. No VEGFR1 immunostaining is observed. (Box 4) Abundant VEGF-A immunoreactivity is present in the stromal at the interface of the soft and hard tissue callus, in addition to hypertrophic chondrocytes at the periphery of the avascular soft tissue callus. VEGFR1-positive cells are also present within the hard tissue callus at the transition zone. Scale bars: 20 μm.

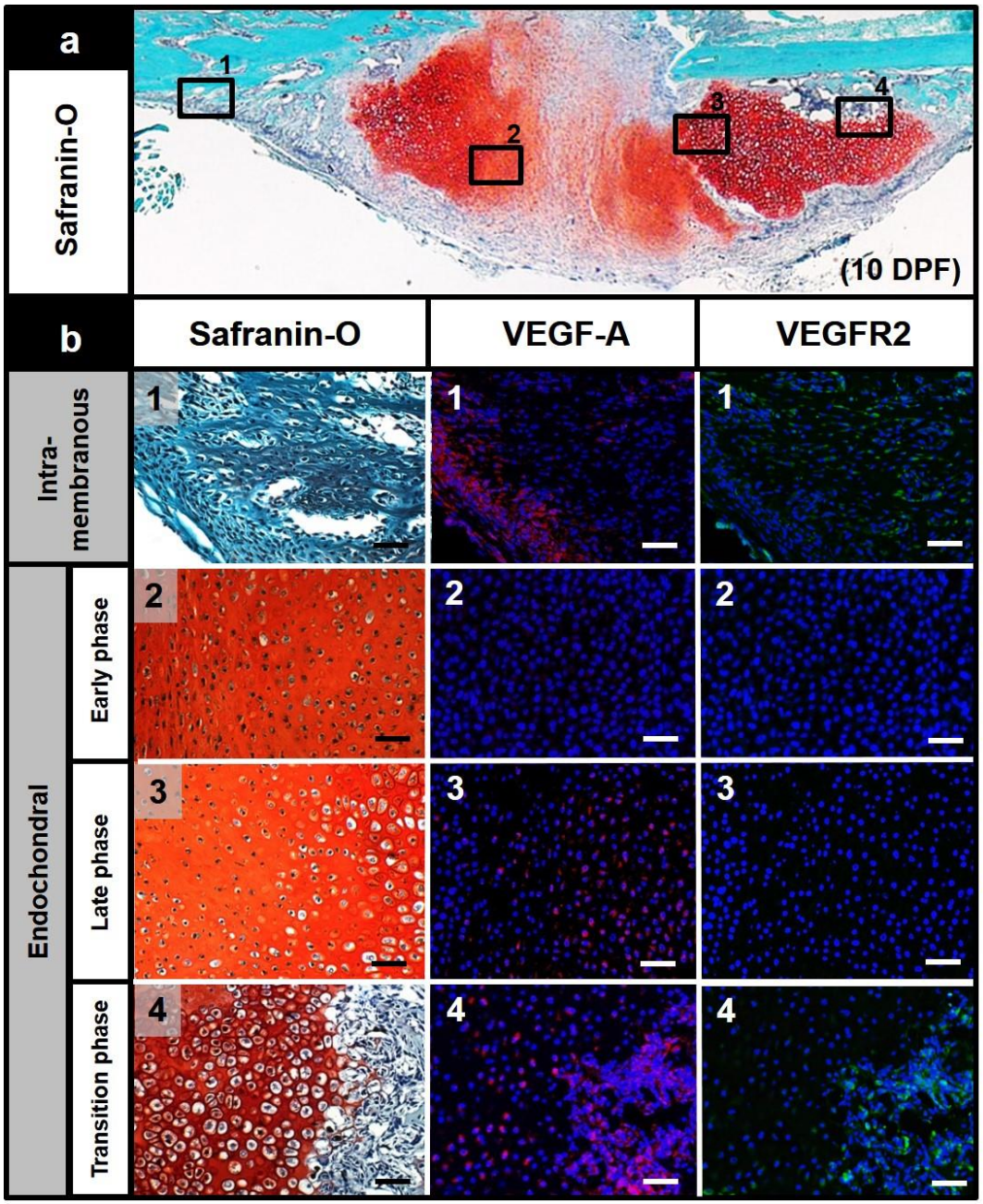

Figure 8: Differential expression of VEGF-A and VEGFR2 in the subperiosteal space in fracture callus. (a) Safranin-O staining of a fracture callus 10 days post fracture (10-DPF) shows a zone of intramembranous bone formation (Box 1), a zone of primitive mesenchymal-appearing cells in the soft tissue callus (Box 2), and an area of mature hyaline-type cartilage in the soft tissue callus (Box 3). The interface between the soft tissue callus and the hard tissue callus is denoted in Box 4. **(b)** High power photomicrographs of the 4 regions of interest stained with Safranin-O and immunofluorescence for VEGF-A (red) or VEGFR2 (green). (Box 1) Hard callus consisting of intramembranous ossification shows abundant VEGF-A immunoreactivity primarily in the overlying periosteum and numerous VEGFR2-positive cells within the sub-periosteal space. (Box 2) Safranin–O staining shows a cellular zone of primitive spindle cells without evidence of matrix deposition, in which VEGF-A or VEGFR2 are not detectable. (Box 3) VEGF-A immunoreactivity appears to be limited to enlarged, hypertrophic chondrocytes within this area of hyaline cartilage. No VEGFR2 immunostaining is observed. (Box 4) Abundant VEGF-A immunoreactivity is present in the stromal at the interface of the soft and hard tissue callus, in addition to hypertrophic chondrocytes at the periphery of the avascular soft tissue callus. VEGFR2-positive cells are also present within the hard tissue callus at the transition zone. Scale bars: 20 μm.

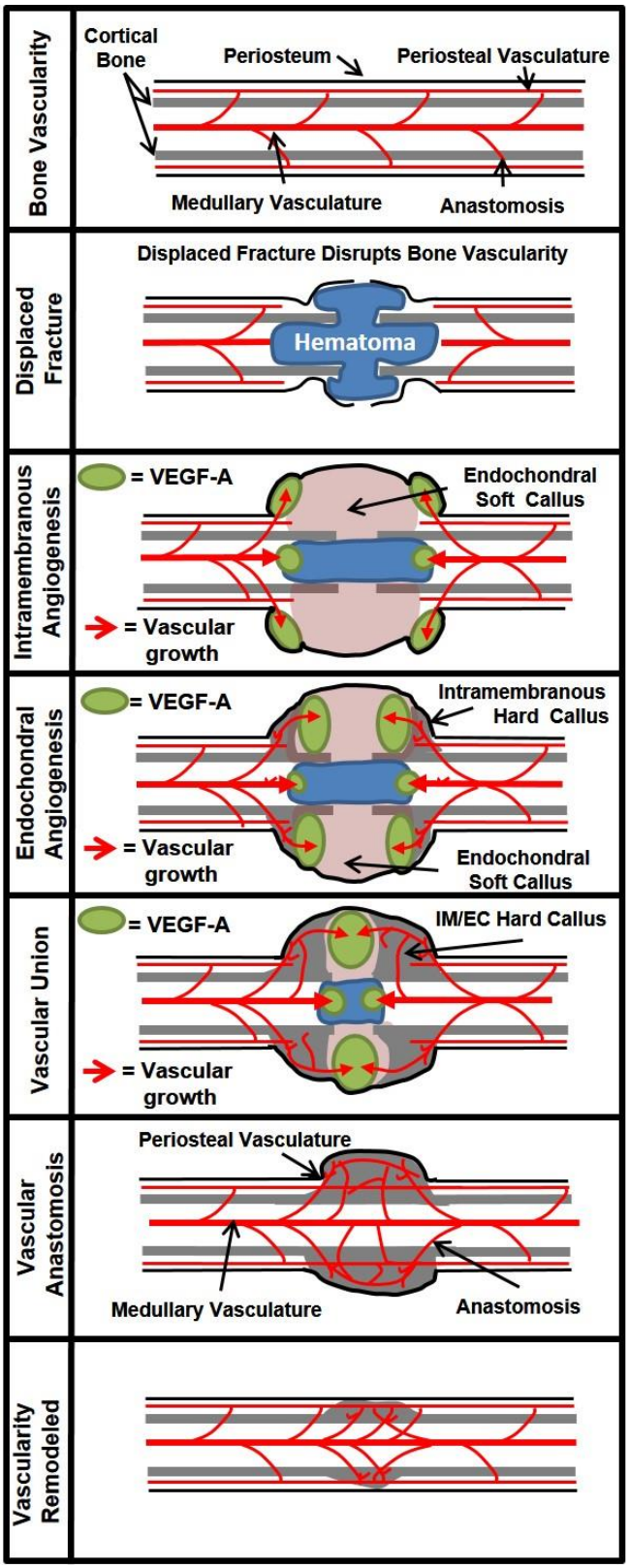

Figure 9: Proposed model of bone revascularization during fracture healing. In a normal long bone, the intramedullary blood supply communicates with periosteal vessels. Trauma and resultant hemorrhage after acute fracture lead to regional hematoma formation, disrupting the intramedullary and periosteal vasculature. As a result of increased centrifugal flow, blood is shunted from the intramedullary vasculature to the periosteal vasculature. Subsequently, cells within the periosteum express VEGF-A and recruit endothelial cells and osteoblasts to the area. This results in the initial hard tissue callus formation through intramembranous ossification. Ordered release of VEGF-A by hypertrophic chondrocytes at the edges of the soft callus directs its replacement by nascent blood vessels and woven bone through endochondral ossification. As the extramedullary vasculature reunites with intramedullary vasculature, the newly formed blood vessels and hard callus are remodeled and resemble the original cortical bone.

Summary and Implications

The indispensable role of angiogenesis in fracture repair has been recognized for over a century (1, 2, 21). However, elements of the temporal and spatial patterns of fracture revascularization have remained elusive. Employing a high-throughout, cost-efficient model of a displaced/stabilized fracture model with advanced imaging techniques; our data clearly supports the unifying theory of revascularization of a displaced fracture requiring both intramedullary and periosteal angiogenesis. These findings provide essential data needed to expand upon the current model of fracture revascularization developed by the pioneers of this field during the early to mid-20th century (Figure 9).

A critical aspect of fracture revascularization unanswered by the classical reports in this field was the association of intramedullary and periosteal angiogenesis. As stated above, it was thought that angiogenesis occurred in these anatomically distinct compartments independently. Trueta and Rhinelander demonstrated that angiogenesis initiated in the intramedullary space directly from the remaining intact vasculature (4, 6, 7). Less was known regarding the originating source of the periosteal vasculature and was conventionally believed to originate from the surrounding musculature as succinctly summarized Kelly (7) in 1968:

> *"….. if the fracture is produced violently or is stabilized by intramedullary fixation, the needed new vessels originate outside the bone and the muscle vessels supply the periosteal system with these necessary new vessels."*

To the contrary, our results suggest that intramedullary and periosteal angiogenesis occur in tandem, not independently. In support of this conclusion, our model is the first to demonstrate a reproducible disruption of the diaphyseal intramedullary vasculature

following fracture and or intramedullary nailing. We further show that the anatomic site of intramedullary vascular disruption corresponds to the region of initial periosteal/subperisoteal intramembranous ossification and revascularization. In 1960, Brookes showed that blood flows in a centrifugal manner from intramedullary vessels to the periosteal vasculature though cortical anastomoses (22). Thus, it is plausible that periosteal elevation results not only from traumatic hemorrhage and hematoma formation, but also from shunting the interrupted intramedullary blood flow to the regional periosteal vasculature. This theory is strongly supported by our application of novel, state of the art molecular and imaging approaches which revealed enhanced vascular anastomosis between the intramedullary vasculature and the areas of periosteal vascular engorgement during the earlier phases of fracture healing. Although these findings do not disprove the conventional hypothesis that periosteal revascularization occurs via ingrowth of vessels from the surrounding soft tissues, it does provide the first evidence that periosteal vasculature is directly connected to the intact intramedullary vasculature. Thus, we posit that shunting blood flow from the intact intramedullary vasculature to the subperiosteal space adjacent to the fracture site is an initial step displaced fracture revascularization in our model.

Formation of new bone during healing of a displaced fracture is achieved through both intramembranous and endochondral ossification. During intramembranous ossification, new bone is produced by direct extension of osteoblasts and endothelial cells (13, 23, 24). Previous investigations have demonstrated that this process is tightly regulated by chemotactic and proliferative responses of endothelial cells and osteoblasts to VEGF-A through VEGF receptors including VEGFR1 (8, 25-27). In our studies, we found that the initial site of intramembranous ossification occurs at the periosteal region with the most robust expression of VEGF-A. Also, at this same location there are numerous VEGFR1 & 2-positive cells morphologically consistent with osteoblasts and

endothelial cells. Based on these observations, we propose the following revisions to the current model of fracture repair: 1) the initial site of intramembranous ossification and revascularization occurs at the proximal and distal aspects of the fracture site, where periosteum inserts on adjacent uninvolved cortical bone because this is the site where intramedullary blood flow is shunted to the periosteum. 2) Although the initiating signal for VEGF release is not clear, the immunolocalization of VEGF-A in the periosteum at this site is likely instrumental for the recruitment and/or activation of VEGFR1 & 2-positive mesenchymal cells, endothelial cells, and osteoblasts to the subperiosteal space to support intramembranous angiogenesis and bone formation.

In contrast to intramembranous ossification, bone is formed on a pre-existing cartilaginous template during endochondral ossification (28). In the central area of the fracture callus that is far from the disrupted regional vasculature, the initial mesenchymal cell proliferation differentiates along the chondrocyte lineage, likely due to the low oxygen tension in this avascular environment. This is supported by our angiographic and histologic data showing that the soft tissue callus is composed of avascular hyaline cartilage and primitive fibrocartilage. In addition, there was minimal detectable periosteal VEGF-A in this location and no VEGF-A positive cells were seen within the central soft callus. Thus, during the initial phases of fracture healing the central, avascular cartilaginous soft tissue callus abuts areas of richly vascular intramembranous ossification composed of VEGFR1-positive osteoblasts and endothelial cells, thereby recapitulating the primary spongiosum of the physis. Therefore, we propose that the fundamental event during fracture repair determining whether bone heals through a vascular intramembranous or an avascular endochondral pathway is its proximity to intact intramedullary vascular system and the presence of VEGFR1-positive cells.

In the active physis, expression of VEGF-A by hypertrophic chondrocytes recruits VEGFR1-positive endothelial cells and osteoblasts to the zone of hypertrophy, where

osteoid deposition on the cartilage matrix results in formation of the primary bone spongiosum. Indeed, the interface between soft and hard tissue callus in a fracture site closely resembles the primary spongiosa of the physis (28-32). In support of this, we have shown that hypertrophic VEGF-A-positive chondrocytes are present in areas of transition from avascular soft tissue callus to vascularized hard tissue callus, which are rich in VEGFR-positive cells. The essential nature of VEGF-A during fracture repair is supported by evidence that inhibiting VEGFR1 & 2 or VEGF-A impairs ossification and results in a persistent avascular soft tissue callus composed of hypertrophic chondrocytes (33-35). Hence, these results indicate that 1) the VEGF-A/VEGFR system is an essential component of the transition from soft-tissue callus to hard tissue callus resulting in vascular and bone union and 2) chondrocyte hypertrophy and release of VEGF-A directs polarized bone formation through the recruitment of the vasculature and mesenchymal osteoprogenitor cells at the periphery of callus.

Our results further suggest that after union of the fracture, angiogenesis and vascular remodeling continue. Specifically, we found that fracture remodeling begins around the time at which the intramedullary vasculature is re-established. From these observations we hypothesize that fracture remodeling occurs as a result of the restoration of intramedullary vascular continuity and as normal intramedullary blood flow is re-established, periosteal shunting is reduced and the periosteal callus becomes relatively hypo-perfused. In support of this theory, Rhinelander observed that when fracture fragments are approximated such that the intramedullary vasculature directly communicates with periosteal vessels, and does not occur until re-establishment of intramedullary blood flow (7, 12).

In conclusion, we have developed a model that indicates that there is an intricate interplay between intramembranous and endochondral ossification during fracture healing in young growing male mice. Periosteal intramembranous bone formation is

critical in providing a richly vascularized network of osteoblastic potential that is necessary for subsequent invasion and replacement of soft tissue callus. Hypertrophic chondrocytes releasing VEGF-A in the avascular soft tissue callus seem to be required for recruiting the developing vascular network and osteoblastic mesenchymal cells to replace the soft tissue callus and form an ossified callus across the fracture site. By quantification of the phases of fracture healing over time (Figure 3 & Table 1), we discovered that fracture revascularization is inversely proportional to the size of the soft tissue callus and directly proportional to the size of the hard tissue callus. Thus, the temporal and spatial development of fracture vascularity is controlled by the precise orchestration of intramembranous and endochondral processes.

The diseases most commonly associated with delayed fracture healing or fracture non-union all share a component of vascular dysfunction. Given this association, several investigations have proposed that addressing vascular dysfunction may significantly reduce fracture healing complications in certain patient populations (36-40). This model of revascularization during healing of displaced/stabilized fractures identifies the specific temporal and spatial events that will provide future insight as to the causes of and potential means to prevent and treat delayed fracture healing and non-union. Additionally, while other investigations have revealed vasculature emanating from muscle surrounding a fracture (41, 42), our model clearly demonstrate communication between the intramedullary vasculature and the fracture callus. Future studies are required to determine the relative significance of the contribution of intramedullary as opposed to muscle derived angiogenesis on fracture revascularization. Additionally, future studies designed to determine if the results regarding the temporal and spatial revascularization of a healing fracture are altered by the mode of fracture or in conditions known to affect bone and vascular biology such as age, sex, and chronic medical conditions such as diabetes or obesity. If so, these findings may provide insight into

novel surgical and medical treatments intended to restore the normal process of bone revascularization following fracture.

Materials & Methods

Murine Fracture Model and X-ray Imaging: Protocols were approved by the Vanderbilt University IACUC. Open femur osteotomies were performed and fixed as previously described using a medial approach to the mid-shaft femur of 8 week old c57/b6 mice. The fracture was fixed through the placement of a 23G (0.6414 mm) retrograde intramedullary pin and the mice were followed from 7-42 days after fracture (43). X-ray was performed as previously described (44). Briefly, mice were placed in the prone position and imaged for 4 seconds at 45KV using a Faxitron LX 60. Mice were sacrificed at various time points (7-42 days) following fracture.

Angiography: Perfusion with Microfil (MV-122 Flow Tech Inc., Carver, MA) vascular contrast was conducted as previously described (45-48). Briefly, mice were euthanized, positioned supine and a thoracotomy extending into a laparotomy was performed. The left ventricle of the heart was cannulated using a 25G butterfly needle. The inferior vena cava (IVC) was transected proximal to the liver and the entire vasculature subsequently perfused with 9ml of warm heparinized saline (100 units/ml in 0.9% saline) through the left ventricle cannula to exsanguinate and anticoagulate thus preventing erythrocyte aggregation and thrombosis thereby promoting consistent perfusion of subsequent infusion materials. Exsanguination and anticoagulation was deemed complete upon widespread hepatic blanching with clear fluid extravasating from the IVC. Mice were then perfused with 9ml of 10% neutral buffered formalin followed by 3ml of Microfil (Flow Tech inc. Carver Massachusetts) vascular contrast polymer. To best verify complete

filling of the vasculature gross images of the liver (Figure 10a), the last organ to be perfused prior to extravasation through the IVC, were examined for extravascular pooling. Mice were excluded from the study if complete hepatic blanching prior to microfil was not achieved, if contrast was not clearly or uniformly visible in the hepatic vasculature or if extravascular pooling occurred. Inspection of hepatic perfusion revealed no differences between manual or infusion pump perfusion set at a constant rate of 0.5ml/min (Figure 10a). Manual filling was conducted at a goal rate approximately equal to the pump rate. Quantitation of liver vasculature also demonstrates no difference in vessel volume, number, or branching (Figure 10b) which in combination our gross observations indicates consistent filling of the vessels with angiogram contrast.

Generation of Angiogram Images: Mice perfused with microfil were then stored overnight at 4 °C to allow the vascular contrast to polymerize. The femurs were dissected and fixed in 4% PFA for another 24hrs. X-rays of the samples were then taken to visualize the femur and the vascular contrast (Supplemental Figure 1b). The femur was placed in 0.5M EDTA pH. 8 for decalcification then imaged via X-ray (Supplemental Figure 1c). The muscles surrounding the femur were removed, and the leg was photographed and X-rayed (Figure 1d&e). Demineralized specimens were imaged by μCT (μCT40, Scanco-Medical-AG, Bassersdorf, Switzerland) with a 20μm isotropic voxel size. A Scanco-Medical evaluation script was applied to render the vasculature with colors corresponding to vessel diameter between 0-0.18mm. These vascular images were integrated into the initial X-rays by matching size and orientation using Adobe Photoshop (San Jose, CA) (Figure 11).

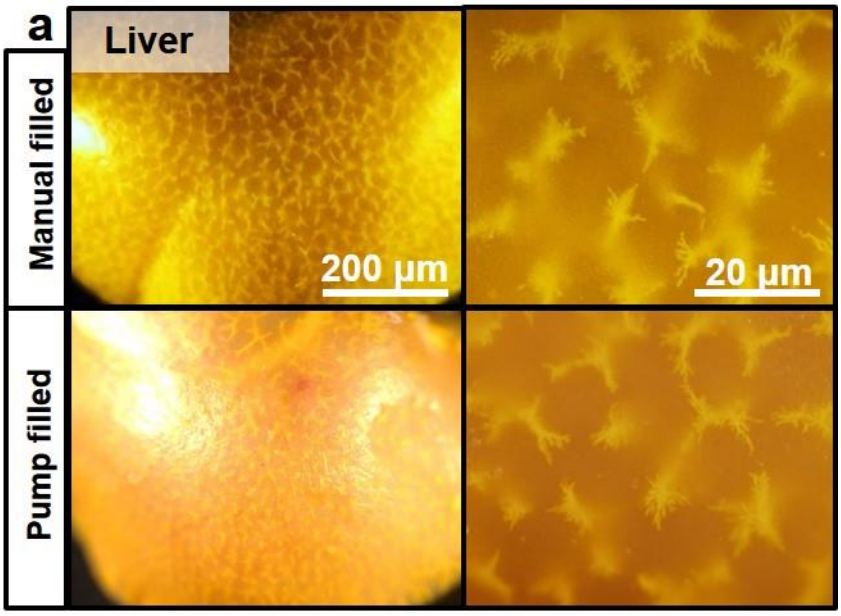

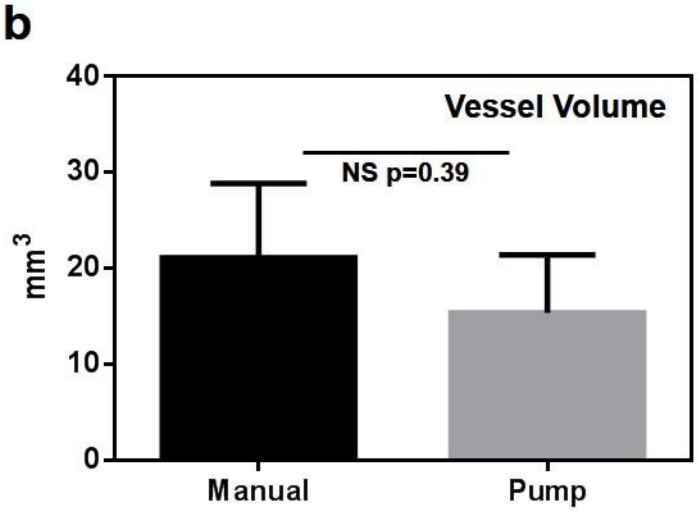

Figure 10: Manual vs Pump filled angiograms (a) Macroscopic view of the liver containing Microfil vascular contrast agent (Yellow) following manual perfusion (top) and perfusion with a constant rate pump injecting a 0.5ml/min**. (b)** Quantitation of the liver vascular volume following perfusion of vascular contrast manually and with a constant rate pump set at 0.5ml/min. Analysis by a non-parametric t-test reveals no significant difference (p value < 0.05) between the manual, and pump perfusion methods. Error bars represent standard error of the mean. N =3 for each value.

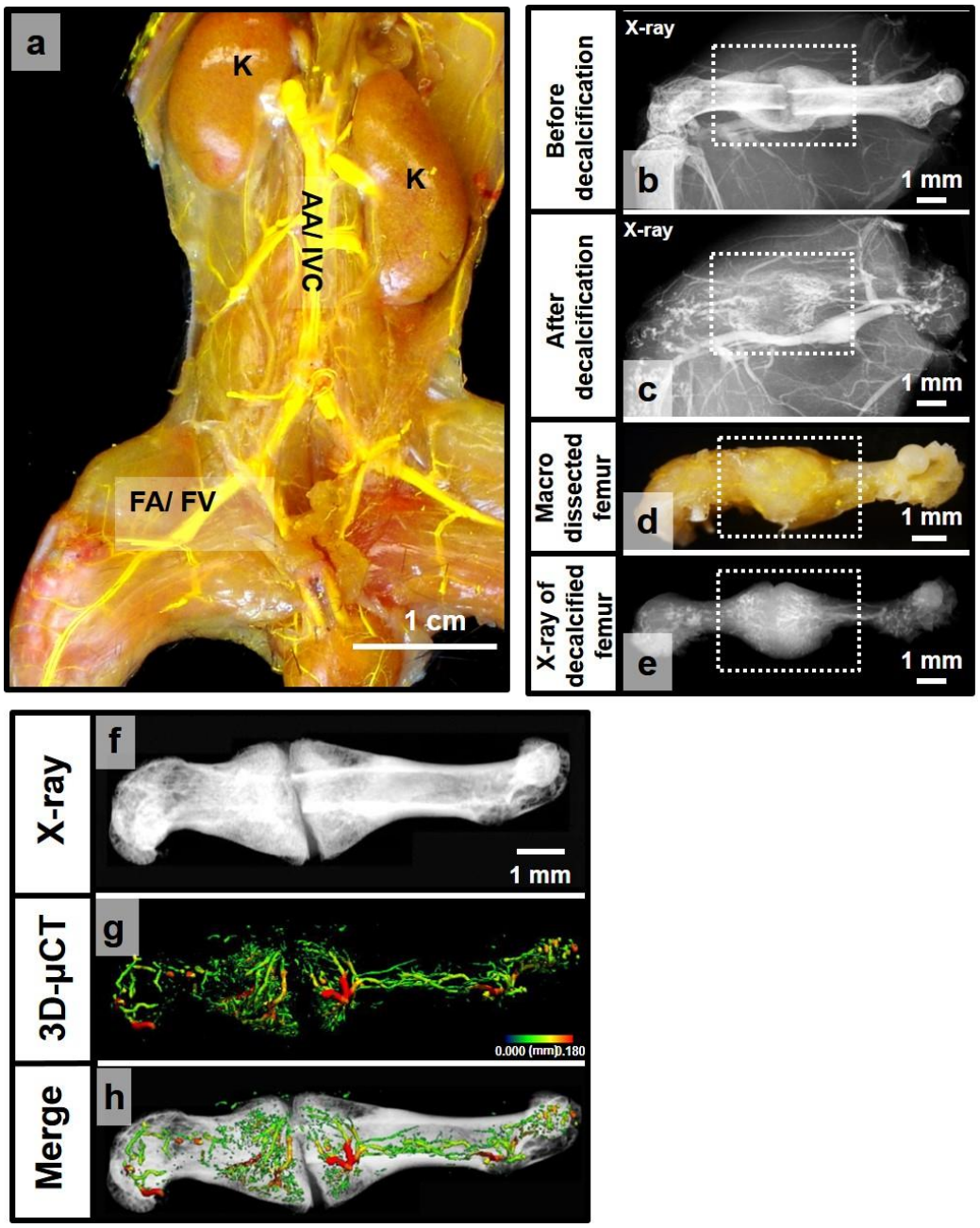

Figure 11: Femoral angiograph methods. (a) Macroscopic photographs of the body cavity after perfusion of Microfil angiograph contrast agent (see Methods; K, kidneys; AA/IVC, abdominal aorta and inferior vena cava; FA/FV, femoral artery and femoral vein). Radiographs of a fractured femur before **(b)** and after decalcification **(c).** Macroscopic examination **(d)** and radiograph **(e)** of a macro-dissected, decalcified, Microfil-perfused femur 2 weeks after fracture demonstrates perfused vessels within and surrounding the fracture site. White dash boxes indicate the site of the fracture callus in c-f. Lateral radiograph of fractured femur prior to EDTA decalcification **(f)**. Microfil contrast-perfused vasculature was visualized in fractured, demineralized femurs by three-dimensional (3D) reconstruction of µCT images. Color of the vasculature denotes the diameter of the vessel **(g)**. Merged 3D µCT images of the vasculature and the fracture site radiograph approximates the location of the vessels in the fractured femur **(h)**. Scale bars are noted within each figure.

Histology: Histologic sections prepared from PFA-fixed, demineralized in 0.5M EDTA (pH7.2) and paraffin-embedded specimens were cut on to slides in 5 micron sections. The slides were then deparaffinized and hydrated for use in Immunohistochemistry or histological staining. (Safranin-O stain) Section were stained with Safranin-O/Fast green (Safranin-O) as previously described (45). Briefly slides were placed in Weigert's hematoxylin for 10 minutes washed in running tap water and then stained with 0.1% fast green solution for 5 minutes. Slides were then rinsed for 5 seconds in 1% acetic acid and placed in 0.1% safranin and orange solution for 5 minutes. The slides were then dehydrated and coverslip for light microscopy.

Immunofluorescence microscopy: After slides were deparaffinized and hydrated. Sodium citrate antigen retrieval was performed using 0.1 M citric acid and 0.1 M sodium citrate. Slides were heated for 2 minutes in the microwave, cooled to room temperature and then washed gently with Tris buffer saline (TBS). Slides were blocked (5% BSA solution containing 10% goat serum) and immunostained with anti-mouse VEGF-A (1:200, Abcam 46154, Cambridge, MA), VEGFR2 goat anti-mouse (1:50, R&D systems AF644) or an rabbit anti-mouse VEGFR1 (1:100, Abcam 32152) antibody overnight at 4°C. Slides were then washed and incubated with 10µg/mL of Alexa Fluor 647-labeled anti-rabbit antibody (Life Technologies 792514, Grand Island, NY) in blocking buffer for 1 hr. Slides were counterstained with DAPI and cover slipped using mounting solution (PolySciences Warrington, PA) and fluorescent images were taken (NIKON AZ100, Upright wide field microscope). Slides incubated without primary antibodies served as negative controls.

Quantification of soft and hard tissue callus size: Soft tissue callus delineated by safranin-O red staining was traced on 5 histological step-sections 200µm apart as previously described with the following changes (49). To determine the

orientation of the 5 slides, the edge of the callus was visualized by identifying the first section with callus on both the medial and lateral femoral cortex and the middle of the callus was determined by the pin space. Each of the specimens 5 sections were measured by 4 blinded reviewers and results were then expressed as mm^2 the soft tissue callus area. Hard tissue callus size was measured from radiographs of fractured femurs as previously described (44). Briefly mice were placed in the prone position and an X-ray was taken. The total area of the mineralized callus was determined each week by tracing the area of the fracture callus on x-rays by 2 reviewers and results were then expressed as mm^2 the hard tissue callus. Image quantification for both the soft and hard tissue callus was performed using the software program ImageJ (NIH, http://rsb.info.nih.gov/ij/). Trend lines were generated between the data points using a Spline curve and GraphPad prism

Quantification of vasculature: Vessel volume was determined by μCT on the fracture callus of the demineralized femurs perfused with angiogram contrast. A cylinder comprised of 250 slices with a 20μm isotropic voxel size was placed over the fracture callus to define the volume of interest. A threshold of 122 (lower) and 1000 (upper) was applied for segmentation with Gauss sigma of 0.8 and a gauss support of 2 to reduce the noise. Vessel Volume (TRI BV) was then evaluated using Scanco μCT standard algorithms and graphed. Spline trend lines were generated between the data points using a spline curve function in GraphPad Prism 6.

References:

1. Kolodny A. Periosteal Blood Supply and Healing Fractures. The Journal of bone and joint surgery American volume. 1923;5:698-711.

2. Teneff S. Experimental studies on vascularization of bony calluses. J Int Coll Surg. 1950;13(2):186-91. Epub 1950/02/01. PubMed PMID: 15403764.

3. Göthman L. Vascular Reactions in Experimental Fractures: Microangiographic and Radioisotope Studies: Acta chirurgica Scandinavica; 1961.

4. Trueta J, Cavadias AX. Vascular changes caused by the Kuntscher type of nailing; an experimental study in the rabbit. J Bone Joint Surg Br. 1955;37-B(3):492-505. Epub 1955/08/01. PubMed PMID: 13252062.

5. Ladanyi J, Hidvegi E. Blood supply of experimental callus formation. Acta morphologica Academiae Scientiarum Hungaricae. 1954;4(1):35-44. Epub 1954/01/01. PubMed PMID: 13147760.

6. Rhinelander FW, Baragry R. Microangiography in bone healing. I. Undisplaced closed fractures. The Journal of bone and joint surgery American volume. 1962;44-A:1273-98. Epub 1962/10/01. PubMed PMID: 19777625.

7. Rhinelander FW, Phillips RS, Steel WM, Beer JC. Microangiography in bone healing. II. Displaced closed fractures. The Journal of bone and joint surgery American volume. 1968;50(4):643-62 passim. Epub 1968/06/01. PubMed PMID: 5658552.

8. Leung DW, Cachianes G, Kuang WJ, Goeddel DV, Ferrara N. Vascular endothelial growth factor is a secreted angiogenic mitogen. Science. 1989;246(4935):1306-9. Epub 1989/12/08. PubMed PMID: 2479986.

9. Barron SE, Robb RA, Taylor WF, Kelly PJ. The effect of fixation with intramedullary rods and plates on fracture-site blood flow and bone remodeling in dogs. The Journal of bone and joint surgery American volume. 1977;59(3):376-85. Epub 1977/04/01. PubMed PMID: 849950.

10. Cavadias AX, Trueta J. An Experimental Study of the Vascular Contribution to the Callus of Fracture. Surg Gynecol Obstet. 1965;120:731-47. Epub 1965/04/01. PubMed PMID: 14271564.

11. Rhinelander FW. The normal microcirculation of diaphyseal cortex and its response to fracture. The Journal of bone and joint surgery American volume. 1968;50(4):784-800. Epub 1968/06/01. PubMed PMID: 5658563.

12. Rhinelander FW. Tibial blood supply in relation to fracture healing. Clin Orthop Relat Res. 1974(105):34-81. Epub 1974/11/01. PubMed PMID: 4609655.

13. Stump CW. The Histogenesis of Bone. Journal of anatomy. 1925;59(Pt 2):136-54. Epub 1925/01/01. PubMed PMID: 17104049 PMCID: PMC1249833.

14. Trueta J. Appraisal of the vascular factor in the healing of fractures of the femoral neck. J Bone Joint Surg Br. 1957;39-B(1):3-5. Epub 1957/02/01. PubMed PMID: 13405943.

15. Trueta J, Amato VP. The vascular contribution to osteogenesis. III. Changes in the growth cartilage caused by experimentally induced ischaemia. J Bone Joint Surg Br. 1960;42-B:571-87. Epub 1960/08/01. PubMed PMID: 17533673.

16. Trueta J, Buhr AJ. The Vascular Contribution to Osteogenesis. V. The Vasculature Supplying the Epiphysial Cartilage in Rachitic Rats. J Bone Joint Surg Br. 1963;45:572-81. Epub 1963/08/01. PubMed PMID: 14058338.

17. Trueta J, Little K. The vascular contribution to osteogenesis. II. Studies with the electron microscope. J Bone Joint Surg Br. 1960;42-B:367-76. Epub 1960/05/01. PubMed PMID: 13855126.

18. Trueta J, Morgan JD. The vascular contribution to osteogenesis. I. Studies by the injection method. J Bone Joint Surg Br. 1960;42-B:97-109. Epub 1960/02/01. PubMed PMID: 13855127.

19. Trueta J, Trias A. The vascular contribution to osteogenesis. IV. The effect of pressure upon the epiphysial cartilage of the rabbit. J Bone Joint Surg Br. 1961;43-B:800-13. Epub 1961/11/01. PubMed PMID: 14039826.

20. Kusumbe AP, Ramasamy SK, Adams RH. Coupling of angiogenesis and osteogenesis by a specific vessel subtype in bone. Nature. 2014;507(7492):323-8. Epub 2014/03/22. doi: 10.1038/nature13145. PubMed PMID: 24646994.

21. Beamer B, Hettrich C, Lane J. Vascular endothelial growth factor: an essential component of angiogenesis and fracture healing. HSS journal : the musculoskeletal journal of Hospital for Special Surgery. 2010;6(1):85-94. Epub 2009/09/19. doi: 10.1007/s11420-009-9129-4. PubMed PMID: 19763695 PMCID: PMC2821499.

22. Brookes M. Sequelae of experimental partial ischaemia in long bones of the rabbit. Journal of anatomy. 1960;94(Pt 4):552-61. Epub 1960/10/01. PubMed PMID: 17105117 PMCID: PMC1244354.

23. Brighton CT, Hunt RM. Early histologic and ultrastructural changes in microvessels of periosteal callus. Journal of orthopaedic trauma. 1997;11(4):244-53. Epub 1997/05/01. PubMed PMID: 9258821.

24. Percival CJ, Richtsmeier JT. Angiogenesis and intramembranous osteogenesis. Developmental dynamics : an official publication of the American Association of Anatomists. 2013;242(8):909-22. Epub 2013/06/06. doi: 10.1002/dvdy.23992. PubMed PMID: 23737393.

25. Mayr-Wohlfart U, Waltenberger J, Hausser H, Kessler S, Gunther KP, Dehio C, Puhl W, Brenner RE. Vascular endothelial growth factor stimulates chemotactic migration of primary human osteoblasts. Bone. 2002;30(3):472-7. Epub 2002/03/08. PubMed PMID: 11882460.

26. Deckers MM, Karperien M, van der Bent C, Yamashita T, Papapoulos SE, Lowik CW. Expression of vascular endothelial growth factors and their receptors during osteoblast differentiation. Endocrinology. 2000;141(5):1667-74. Epub 2000/05/10. PubMed PMID: 10803575.

27. Ferrara N, Henzel WJ. Pituitary follicular cells secrete a novel heparin-binding growth factor specific for vascular endothelial cells. Biochemical and biophysical research communications. 1989;161(2):851-8. Epub 1989/06/15. PubMed PMID: 2735925.

28. Gerstenfeld LC, Cullinane DM, Barnes GL, Graves DT, Einhorn TA. Fracture healing as a post-natal developmental process: molecular, spatial, and temporal aspects of its regulation. Journal of cellular biochemistry. 2003;88(5):873-84. Epub 2003/03/05. doi: 10.1002/jcb.10435. PubMed PMID: 12616527.

29. Maes C, Kobayashi T, Selig MK, Torrekens S, Roth SI, Mackem S, Carmeliet G, Kronenberg HM. Osteoblast precursors, but not mature osteoblasts, move into

developing and fractured bones along with invading blood vessels. Dev Cell. 2010;19(2):329-44. Epub 2010/08/17. doi: 10.1016/j.devcel.2010.07.010. PubMed PMID: 20708594 PMCID: PMC3540406.

30. Brookes M, Landon DN. The Juxta-Epiphysial Vessels in the Long Bones of Foetal Rats. J Bone Joint Surg Br. 1964;46:336-45. Epub 1964/05/01. PubMed PMID: 14167642.

31. Lee FY, Choi YW, Behrens FF, DeFouw DO, Einhorn TA. Programmed removal of chondrocytes during endochondral fracture healing. Journal of orthopaedic research : official publication of the Orthopaedic Research Society. 1998;16(1):144-50. Epub 1998/05/09. doi: 10.1002/jor.1100160124. PubMed PMID: 9565087.

32. Zuscik MJ, Hilton MJ, Zhang X, Chen D, O'Keefe RJ. Regulation of chondrogenesis and chondrocyte differentiation by stress. J Clin Invest. 2008;118(2):429-38. Epub 2008/02/05. doi: 10.1172/JCI34174. PubMed PMID: 18246193 PMCID: PMC2214711.

33. Gerber HP, Vu TH, Ryan AM, Kowalski J, Werb Z, Ferrara N. VEGF couples hypertrophic cartilage remodeling, ossification and angiogenesis during endochondral bone formation. Nature medicine. 1999;5(6):623-8. Epub 1999/06/17. doi: 10.1038/9467. PubMed PMID: 10371499.

34. Hausman MR, Schaffler MB, Majeska RJ. Prevention of fracture healing in rats by an inhibitor of angiogenesis. Bone. 2001;29(6):560-4. Epub 2001/12/01. PubMed PMID: 11728927.

35. Jacobsen KA, Al-Aql ZS, Wan C, Fitch JL, Stapleton SN, Mason ZD, Cole RM, Gilbert SR, Clemens TL, Morgan EF, Einhorn TA, Gerstenfeld LC. Bone formation during distraction osteogenesis is dependent on both VEGFR1 and VEGFR2 signaling. Journal of bone and mineral research : the official journal of the American

Society for Bone and Mineral Research. 2008;23(5):596-609. Epub 2008/04/25. doi: 10.1359/jbmr.080103. PubMed PMID: 18433297 PMCID: PMC2674537.

36. Groothuis A, Duda GN, Wilson CJ, Thompson MS, Hunter MR, Simon P, Bail HJ, van Scherpenzeel KM, Kasper G. Mechanical stimulation of the pro-angiogenic capacity of human fracture haematoma: involvement of VEGF mechano-regulation. Bone. 2010;47(2):438-44. Epub 2010/06/29. doi: 10.1016/j.bone.2010.05.026. PubMed PMID: 20580871.

37. Paglia DN, Wey A, Breitbart EA, Faiwiszewski J, Mehta SK, Al-Zube L, Vaidya S, Cottrell JA, Graves D, Benevenia J, O'Connor JP, Lin SS. Effects of local insulin delivery on subperiosteal angiogenesis and mineralized tissue formation during fracture healing. Journal of orthopaedic research : official publication of the Orthopaedic Research Society. 2013;31(5):783-91. Epub 2012/12/15. doi: 10.1002/jor.22288. PubMed PMID: 23238777.

38. Athanasopoulos AN, Schneider D, Keiper T, Alt V, Pendurthi UR, Liegibel UM, Sommer U, Nawroth PP, Kasperk C, Chavakis T. Vascular endothelial growth factor (VEGF)-induced up-regulation of CCN1 in osteoblasts mediates proangiogenic activities in endothelial cells and promotes fracture healing. The Journal of biological chemistry. 2007;282(37):26746-53. Epub 2007/07/13. doi: 10.1074/jbc.M705200200. PubMed PMID: 17626014 PMCID: PMC2831223.

39. Matsumoto T, Kawamoto A, Kuroda R, Ishikawa M, Mifune Y, Iwasaki H, Miwa M, Horii M, Hayashi S, Oyamada A, Nishimura H, Murasawa S, Doita M, Kurosaka M, Asahara T. Therapeutic potential of vasculogenesis and osteogenesis promoted by peripheral blood CD34-positive cells for functional bone healing. The American journal of pathology. 2006;169(4):1440-57. Epub 2006/09/28. doi: 10.2353/ajpath.2006.060064. PubMed PMID: 17003498 PMCID: PMC1698844.

40. Park AG, Paglia DN, Al-Zube L, Hreha J, Vaidya S, Breitbart E, Benevenia J, O'Connor JP, Lin SS. Local insulin therapy affects fracture healing in a rat model. Journal of orthopaedic research : official publication of the Orthopaedic Research Society. 2013;31(5):776-82. Epub 2012/12/15. doi: 10.1002/jor.22287. PubMed PMID: 23238765.

41. Morgan EF, Hussein AI, Al-Awadhi BA, Hogan DE, Matsubara H, Al-Alq Z, Fitch J, Andre B, Hosur K, Gerstenfeld LC. Vascular development during distraction osteogenesis proceeds by sequential intramuscular arteriogenesis followed by intraosteal angiogenesis. Bone. 2012;51(3):535-45. Epub 2012/05/24. doi: 10.1016/j.bone.2012.05.008. PubMed PMID: 22617817 PMCID: PMC3412922.

42. Uhrig BA, Boerckel JD, Willett NJ, Li MT, Huebsch N, Guldberg RE. Recovery from hind limb ischemia enhances rhBMP-2-mediated segmental bone defect repair in a rat composite injury model. Bone. 2013;55(2):410-7. Epub 2013/05/15. doi: 10.1016/j.bone.2013.04.027. PubMed PMID: 23664918.

43. Doyon AR, Ferries IK, Li J. Glucocorticoid attenuates the anabolic effects of parathyroid hormone on fracture repair. Calcified tissue international. 2010;87(1):68-76. Epub 2010/05/07. doi: 10.1007/s00223-010-9370-3. PubMed PMID: 20445968.

44. O'Neill KR, Stutz CM, Mignemi NA, Burns MC, Murry MR, Nyman JS, Schoenecker JG. Micro-computed tomography assessment of the progression of fracture healing in mice. Bone. 2012;50(6):1357-67. Epub 2012/03/29. doi: 10.1016/j.bone.2012.03.008. PubMed PMID: 22453081.

45. Cole HA, Yuasa M, Hawley G, Cates JM, Nyman JS, Schoenecker JG. Differential development of the distal and proximal femoral epiphysis and physis in mice. Bone. 2013;52(1):337-46. Epub 2012/10/20. doi: 10.1016/j.bone.2012.10.011. PubMed PMID: 23079139.

46. Duvall CL, Taylor WR, Weiss D, Guldberg RE. Quantitative microcomputed tomography analysis of collateral vessel development after ischemic injury. American journal of physiology Heart and circulatory physiology. 2004;287(1):H302-10. Epub 2004/03/16. doi: 10.1152/ajpheart.00928.2003. PubMed PMID: 15016633.

47. Duvall CL, Taylor WR, Weiss D, Wojtowicz AM, Guldberg RE. Impaired angiogenesis, early callus formation, and late stage remodeling in fracture healing of osteopontin-deficient mice. Journal of bone and mineral research : the official journal of the American Society for Bone and Mineral Research. 2007;22(2):286-97. Epub 2006/11/08. doi: 10.1359/jbmr.061103. PubMed PMID: 17087627.

48. Dhillon RS, Xie C, Tyler W, Calvi LM, Awad HA, Zuscik MJ, O'Keefe RJ, Schwarz EM. PTH-enhanced structural allograft healing is associated with decreased angiopoietin-2-mediated arteriogenesis, mast cell accumulation, and fibrosis. Journal of bone and mineral research : the official journal of the American Society for Bone and Mineral Research. 2013;28(3):586-97. Epub 2012/09/20. doi: 10.1002/jbmr.1765. PubMed PMID: 22991274 PMCID: PMC3540116.

49. Gerstenfeld LC, Cho TJ, Kon T, Aizawa T, Tsay A, Fitch J, Barnes GL, Graves DT, Einhorn TA. Impaired fracture healing in the absence of TNF-alpha signaling: the role of TNF-alpha in endochondral cartilage resorption. Journal of bone and mineral research : the official journal of the American Society for Bone and Mineral Research. 2003;18(9):1584-92. Epub 2003/09/13. doi: 10.1359/jbmr.2003.18.9.1584. PubMed PMID: 12968667.

CHAPTER 6

Fibrin is Dispensable for Fracture Healing and Fibrinolysis is Essential for Fracture Repair and Prevention of Heterotopic Ossification

Mechanistically, fractures heal via intramembranous and endochondral ossification, which are the same biological processes present during bone development (1, 2). However, in contrast to bone development, bone formation during fracture repair initiates within a vastly different micro-environment, which is secondary to tissue injury and hemorrhage. As a result, fracture healing inevitably initiates within, or around, extravascular fibrin deposits that are distributed throughout the injury. Previous studies have suggested that intrinsic elements of the fibrin matrix are essential for initiating bone formation. The proposed molecular mechanisms include: 1) acting as a reservoir for growth factors and vasoactive molecules from platelets (3-5), 2) by promoting an influx of inflammatory and mesenchymal progenitor cells through specific integrin/receptor interactions, and 3) providing the structural framework for the initial phase of tissue repair (6, 7). Thus, the fibrin matrices that form after fracture are considered a vital component of fracture repair. Indeed, most fracture care protocols emphasize the importance of preserving the fracture hematoma, specifically the fibrin matrix (6, 8). Conversely, a failure of efficient fibrin clearance from wound fields, either due to pathologic hemostasis and/or impaired clearance of fibrin, can also be detrimental to normal tissue repair (9-11). Additionally, we recently determined that fibrin is a driver of pathologic bone disease (12). Thus, the contribution of fibrin to fracture repair could be both supportive and detrimental.

Over 16 million fractures are treated in the United States annually (13). Of these, between 2.5% and 10% of cases suffer from impaired healing (14-16), resulting in pain, loss of function and a significant cost burden on the health care system (13). The most common comorbid conditions associated with impaired fracture healing are obesity, diabetes, smoking and advanced age (17-23). Considering that these comorbid conditions are each associated with a prothrombotic state, characterized in part by the increased and persistence of fibrin within damaged tissue, we hypothesize that although the extravascular fibrin matrices may exert beneficial effects on fracture healing, exuberant or delayed fibrin deposition may have deleterious effects on fracture healing. In this study, we investigated if fibrin is essential for, and capable of impeding, efficient fracture repair.

Results

Fibrin deposition is essential for hemostasis following bone fracture but is not essential for fracture healing. In order to identify the potential roles of fibrin in fracture repair, we first defined the temporal and spatial patterns of fibrin deposition relative to angiogenesis and the development of soft- and hard-tissue callus (1); each are key biologic events during fracture repair. Histological analyses indicated that fibrin is formed at the site of fracture shortly after injury, but is rapidly cleared during the process of intramembranous and endochondral bone formation, and is no longer present at the fracture site by the time of vascular and osseous union (Figure 1). To determine if fibrin is essential for fracture repair, we examined mice lacking fibrinogen (Fbg-/-), the precursor of fibrin, during healing of a femoral fracture. As expected, Fbg-/- mice excessively hemorrhaged after fracture of the femur, whereas no overt evidence of

hemorrhage was observed in WT mice (Figure 2A). Serial weekly x-rays of fractured femurs were performed to monitor the temporal development and subsequent remodeling of the hard-tissue callus (Figure 2B). Hard-tissue callus was clearly evident proximal and distal to the fracture site

in WT mice at 14 days post fracture (DPF). During 14 to 21-DPF, the proximal and distal hard-tissue calluses converge toward the fracture site and eventually form a bridging callus that represents the maximum size of the hard tissue callus. Over the following 3 weeks, the hard-tissue callus was remodeled and becomes hardly discernable by 42-DPF (Figure 2B). Fbg-/- mice show no temporal or quantitative differences in the development or remodeling of the hard tissue callus, demonstrating that fibrin, although required to prevent hemorrhage, is dispensable for fracture repair (Figure 2 & Table 1).

Given that the presence of fibrin is not required for fracture healing, we asked if critical biological steps during the process of fracture healing were altered in the absence of fibrin. Histological evaluation of the soft-tissue callus at 14-DPF reveals a centrally located avascular chondroid matrix flanked by reactive woven bone in both WT and Fbg-/- mice (Figure 3A). Quantitative assessment of soft- and hard-tissue callus shows no significant differences between genotypes (Table 1). To determine if fibrin is essential for vascularization of fracture callus, angiography and immunohistochemistry for CD31 were performed. Angiography of fracture calluses 14-DPF reveals exuberant endochondral-mediated vascularization both proximal and distal to the fractures in both WT and Fbg-/- mice (Figure 3B). CD31 staining reveals numerous vessels at the interface of the hard and soft tissue callus in both genotypes (Figure 3B), and quantitation of vascularity shows no difference in either the vascular area or the number of vessels within the facture callus of WT or Fbg-/- mice at 14-DPF (Figure 3C). Collectively, these data demonstrate that fibrin is not required for either endochondral bone formation or vascularization of the fracture callus.

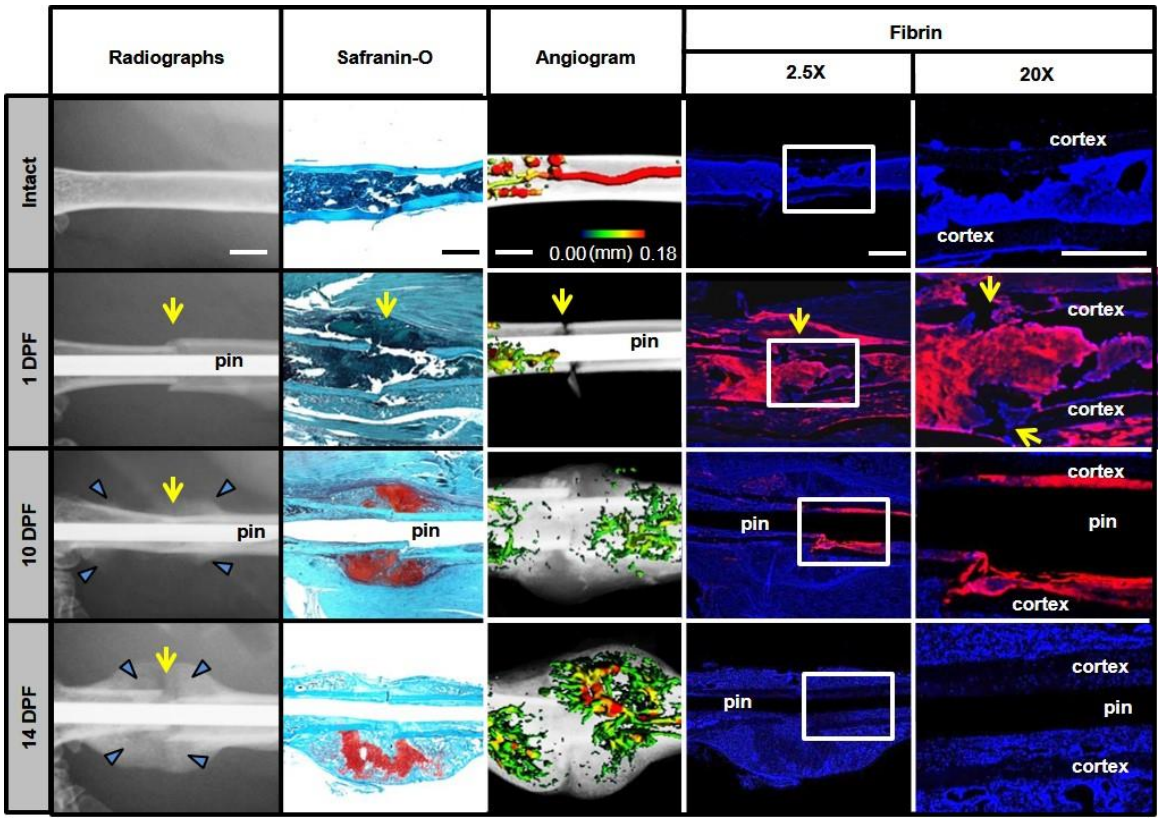

Figure 1: Temporal and spatial deposition and removal of fibrin during fracture repair. Displaced transverse femur fractures we examine by radiography, angiography, and conventional light and immunofluorescence microscopy. One day post fracture (1-DPF) the vasculature is disrupted resulting in an avascular segment of bone proximal and distal to the fracture site (yellow arrows). Fibrin is seen in the intramedullary space and soft tissues adjacent to the fracture site. By 10-DPF, an avascular soft-tissue callus forms directly around the fracture site and an ossified hard-tissue callus develops at the proximal and distal aspects of the soft tissue callus (blue arrowheads). There is a marked reduction in fibrin deposition in the soft-tissues surrounding the fracture site, while intramedullary fibrin persists (10-DPF). As hard-tissue callus replaces the soft-tissue callus beginning from the periphery of the fracture callus (14-DPF), this conversion is accompanied by both endochondral-mediated vascular expansion and the absence (removal) of fibrin from the fracture callus and intramedullary space. White box denotes area of 20x fibrin. Scale bars = 1mm. (DPF= days post fracture).

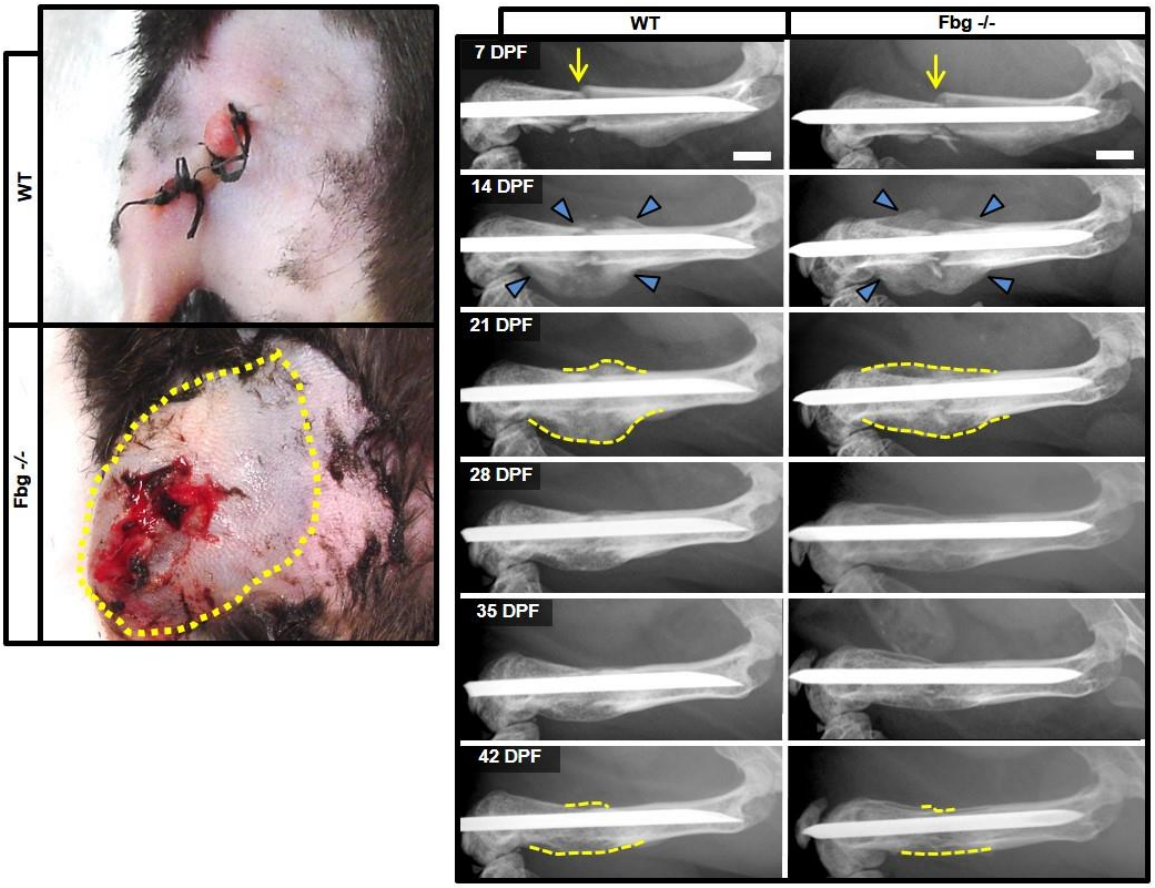

Figure 2: Fibrin is essential to prevent hemorrhage, but not for fracture callus formation. (A) Gross photographs of control (WT) and fibrinogen-deficient (Fbg-/-) mice extremities one day post-fracture (1-DPF) show hematoma formation in (Fbg-/-) mice (outlined by yellow dashes). **(B)** Serial radiographic analysis of fractured femurs (yellow arrows) shows no apparent differences in the formation (blue arrowheads) of and remodeling (dashed yellow lines) of fracture callus in WT and Fbg-/- mice. Scale bars, 1mm. (DPF= days post fracture).

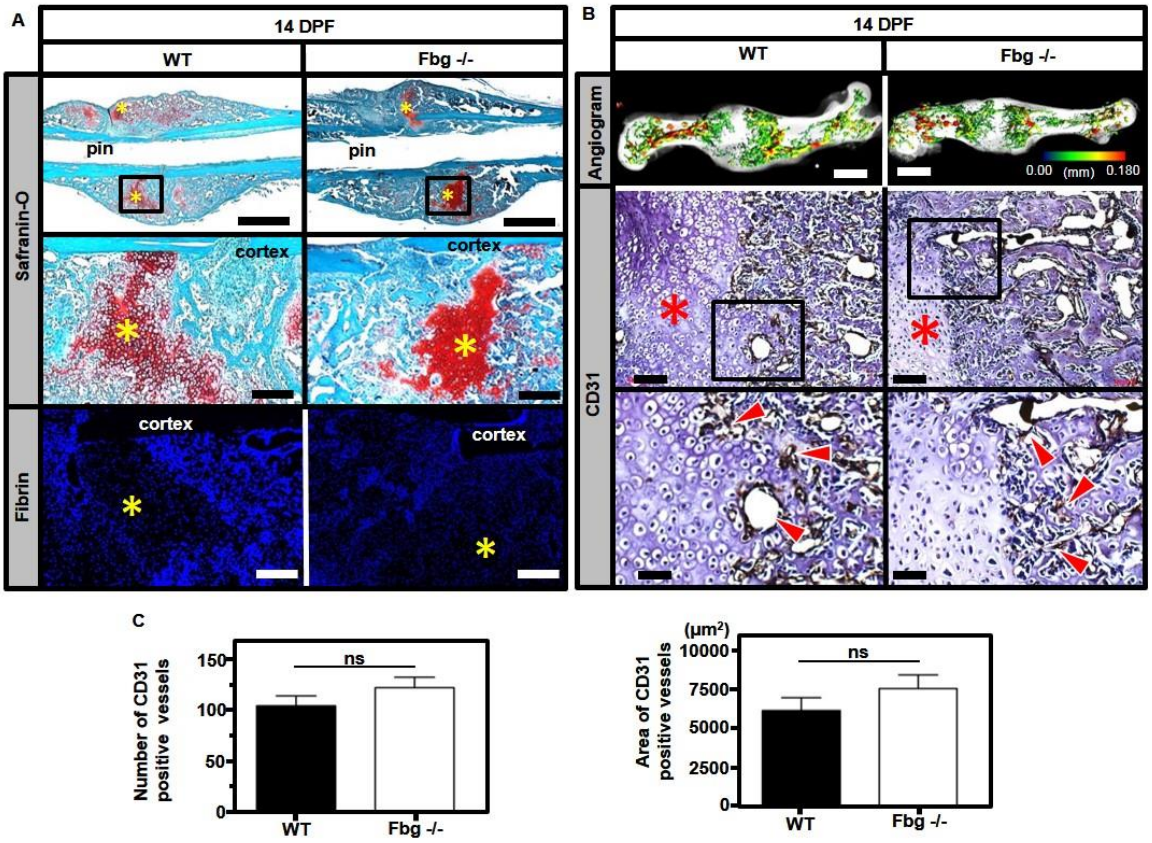

Figure 3: Fibrin is not essential for soft tissue callus formation and vascularization of fracture callus. (A) Representative histologic sections of fracture callus stained with Safranin-O or immunofluorescence for fibrin 14 days post fracture (14-DPF). No clear differences in fracture callus formation (chondroid soft tissue callus, yellow asterisks) or fibrin deposition is seen between WT and Fbg-/- mice. Scale bars, 1000 μm (top) and 100 μm (middle and bottom panels). **(B)** 3-dimensional μCT reconstructions of angiogram contrast-perfused femurs and immunofluorescence for CD31 demonstrate no clear differences in the macro- and microvasculature of the fracture callus 14-DPF between WT and Fbg-/- mice (soft tissue callus, red asterisks; CD31-positive vessels, red arrowheads) Scale bars, 1 mm (top) 100 μm (middle) and 50 μm (bottom). In the angiographic images, the color scale bar denotes vessel size: black (0.00mm), red (0.18mm). Black boxes denote areas shown at higher magnification. **(C)** Quantitation of number of CD31-positive blood vessels in the callus (top) and total area of CD31-positive blood vessels (bottom). (DPF= days post fracture; ns= not significant; Error bars = SEM).

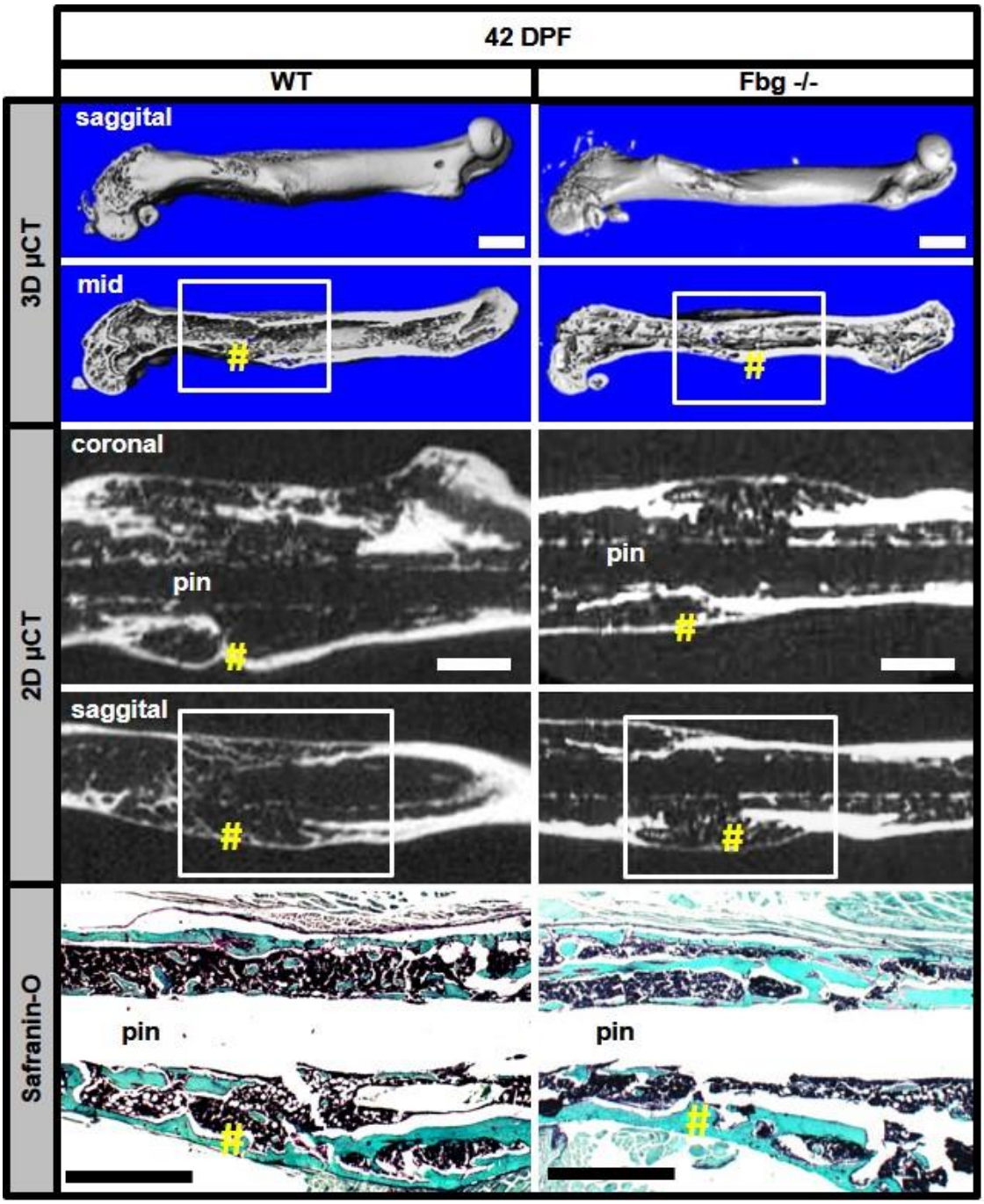

Figure 4: Fibrin is not essential for hard tissue callus union or remodeling. (Top Rows) 3-dimensional µCT reconstructions of femurs from of WT and Fbg-/- mice 42-DPF show no clear differences (white squares denote site of fracture; yellow sharps denote areas of cortical bridging). **(Middle Rows)** Coronal and sagittal 2D µCT images further demonstrates cortical bridging by hard tissue callus in both WT and Fbg-/- mice (yellow sharps). **(Bottom Row)** Safranin-O confirms complete bone union in both WT and Fbg-/- mice (yellow sharps). Scale bars, 1 mm. (DPF= days post fracture).

To determine whether fibrin has an effect on the union of the hard callus or subsequent remodeling, microcomputed tomography (μCT) of each fracture callus at 42-DPF was performed in WT and Fbg-/- mice. Consistent with radiographic data 3-dimensional (3D) (Figure 4-top), and 2-dimensional (2D) (Figure 4- middle) μCT reconstructions demonstrate cortical bridging at fracture sites in both genotypes. Quantitative assessments of each fracture callus by μCT (Table 2) disclosed no significant differences in geometric properties (polar moment of inertia, pMOI), structural properties (anisotropy), or tissue mineral density of fracture calluses when comparing genotypes. Histological sections verified the complete transition of soft-tissue callus composed of a chondroid matrix into hard-tissue callus containing woven bone, as well as documenting cortical bridging over the fracture site (Figure 4-bottom & Table 1). Together, these data demonstrate that fibrin is not required for the formation of the hard-tissue callus union or the subsequent remodeling of fracture callus.

Plasmin is required for fracture healing. Since fibrin was dispensable for fracture healing we next set out to determine if *removal* of fibrin matrix is important during fracture healing. In our first test of this hypothesis we used mice with a genetically imposed plasminogen deficiency (Plg-/-), the precursor of plasmin that allows degradation of the fibrin matrices. In Plg-/- mice, but not in WT mice, we observed extensive mineralization surrounding the fracture site at 7-DPF (Figure 5). At 14-DPF, the area of mineralization in Plg-/- is much larger than in WT mice. Union of the proximal and distal hard tissue calluses was difficult to determine radiographically because of the presence of diffuse mineralization around the fracture site. WT mice achieved hard-tissue callus union at 21–DPF that was subsequently remodeled between 21 and 42-DPF. In contrast, Plg-/- mice at 42-DPF display no apparent signs of hard tissue remodeling and exhibit persistence diffuse mineralization surrounding the fracture site.

The early aberrant mineralization surrounding the fracture site noted in Plg-/- mice was suggestive of heterotopic ossification (Figure 5). Further analysis of the hard callus formation at the site of fracture in Plg-/- mice show foci of mineralization within soft tissues distant from the fracture site in sagittal and axial μCT images acquired at 14-DPF and 42-DPF (Figure 6 A&B). Von Kossa staining of tissue sections demonstrated that the soft tissue mineralization seen on μCT represents calcium deposition within skeletal muscle fibers (Figure 6C). These findings are characteristic of heterotopic ossification and suggest impaired plasmin activity as a mechanism for this pathological response to tissue injury. Therefore, loss of plasmin was associated with impaired hard tissue callus formation and heterotopic ossification.

In order to better understand the role of plasmin during fracture repair, we next examined in detail both callus formation and vascularization during the healing process. Histologic examination of fracture callus at 14-DPF in Plg-/- mice reveals a large non-centrally located soft tissue callus composed of avascular chondroid matrix with limited reactive woven bone (Figure 6 A-top). At this time, VEGF expression was observed within the hypertrophic chondrocytes contained within the chondroid matrix from both WT and Plg-/- mice, consistent with endochondral mediated angiogenesis (Figure 7A-middle). Abundant fibrin within the fracture callus of Plg -/- mice is interposed between the separating femoral cortices and within the newly formed hard tissue callus at the periphery of the fracture callus (Figure 7A-bottom). In contrast, WT mice possess no detectable fibrin at the fracture site 14-DPF. Since endochondral hard tissue callus formation requires vascular invasion of soft tissue callus, we next determined if fibrin clearance is essential for vascularization of the fracture callus. Angiograms of the fracture callus in WT mice demonstrated robust revascularization within the hard tissue callus proximal and distal to the fracture site (Figure 7B-top). In contrast, Plg-/- mice show a pronounced lack of vascularization characterized by the absence of identifiable

blood vessels, as illustrated by reduced CD31 staining in the central region of the fracture site (Figure 6 B-bottom) and significant reductions in both the number and total area of blood vessels in the fracture callus (Figure 8). These data suggest that plasmin is required for the proper endochondral-mediated vascularization of the fracture callus as well as the timely conversion of the soft tissue callus to newly formed woven bone.

To determine if a plasminogen deficiency affects cortical bridging of the fracture callus, and to elucidate the structure and remodeling of hard tissue callus in the absence of plasmin, μCT was performed on WT and Plg-/- mice at 42-DPF. Consistent with radiologic data, representative images of 3D μCT reconstructions of a fractured femur from a Plg-/- mice show a markedly disorganized fracture callus (Figure 9). In addition, while 2D μCT reconstructions of fracture sites in WT mice show evidence of cortical bridging over the fracture site, the hard tissue callus in Plg-/- mice fail to unite across the fracture site (Figure 9 & Table 1). This failure to unite was associated with an absence of remodeling in Plg-/- mice. Quantitative evaluations of fracture callus by μCT at 42–DPF demonstrate that Plg-/- mice have alterations in composition and structure including an elevated pMOI, bone volume, and bone area (Table 2). Together these data independently validate radiograph evidence suggesting impaired callus formation and remodeling in Plg-/- mice. Histological examination of the fracture gap in Plg-/- mice confirms that absence of cortical bridging and a persistent soft tissue callus surrounding a central area of fibrosis at the fracture site demonstrating that there is a delay in replacing avascular soft tissue callus with vascularized hard tissue callus (Figure 8). Immunohistochemistry reveals that fibrin is centrally located over the fracture site and within the area of fibrosis opposing the ends of the fracture callus (Figure 9-bottom). Together, these data confirm that plasmin is essential for the removal of fibrin from the fracture callus, endochondral-mediated vascularization of the fracture callus, as well as the appropriate formation and union of new bone over the fracture site.

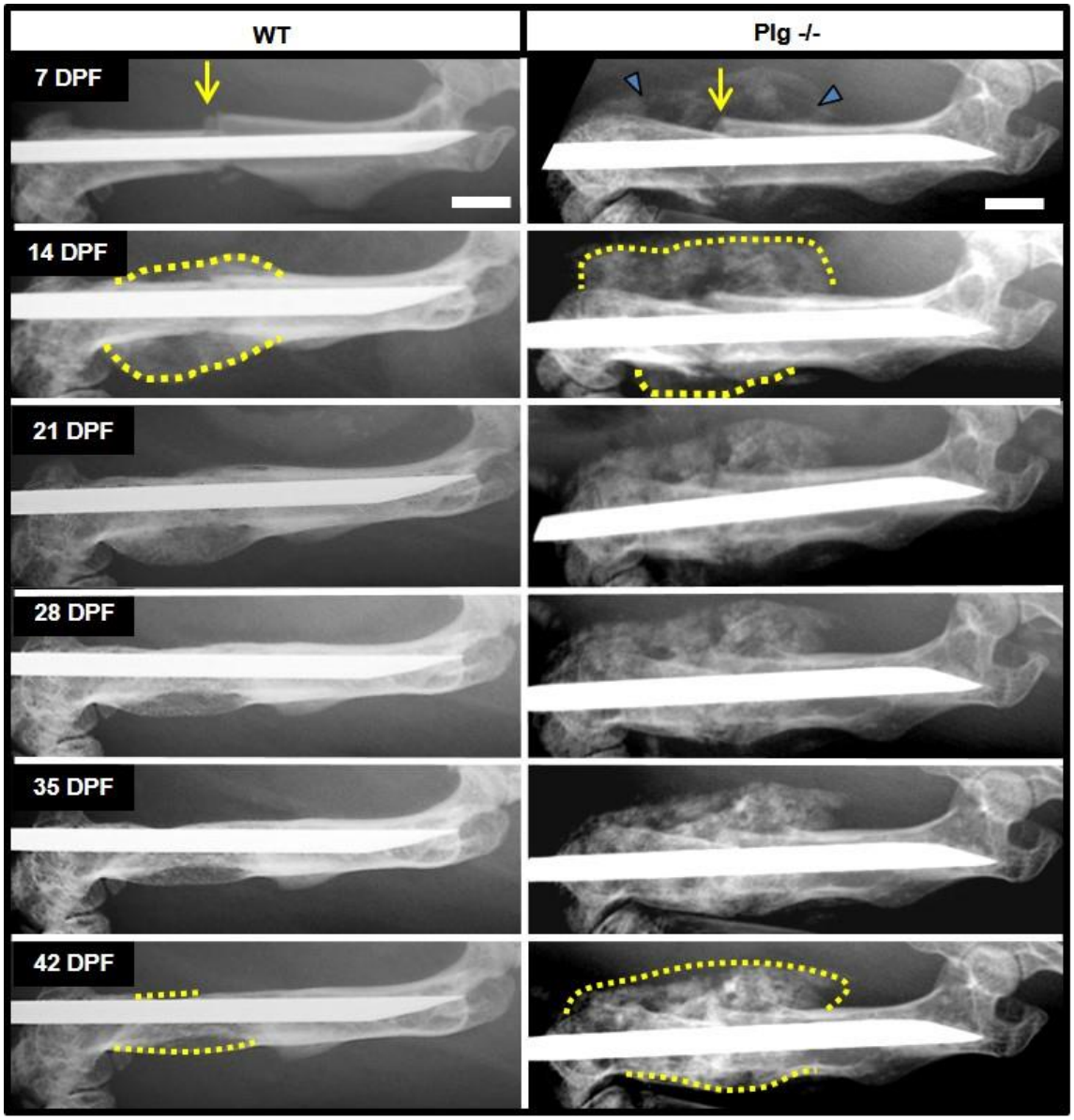

Figure 5: Plasminogen-deficient mice show abnormal hard tissue callus formation. Serial radiographic analysis of fractured femurs (yellow arrows) shows marked differences in the formation (blue arrowheads) of and remodeling (dashed yellow lines) of fracture callus in WT and plasminogen deficient (Plg-/- mice). In comparison to WT mice, the fracture callus in Plg-/- mice is hypertrophic and fails to undergo remodeling over the first 6 weeks post-fracture. In addition, sites of soft tissue mineralization are noted adjacent to the injury site (blue triangles). Yellow dashed lines delineate fracture callus, scale bars, 1 mm. (DPF= days post fracture)

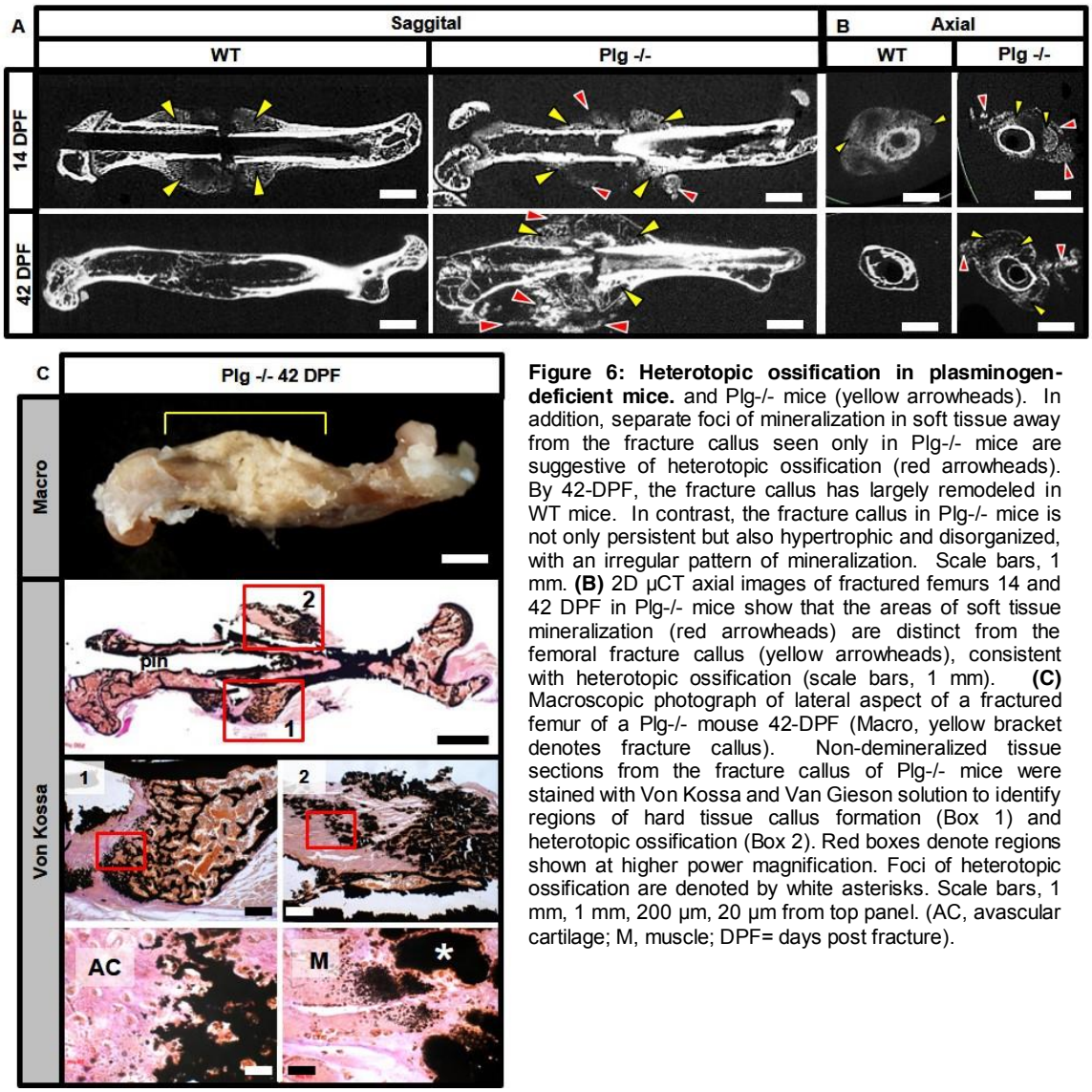

Figure 6: Heterotopic ossification in plasminogen-deficient mice. and Plg-/- mice (yellow arrowheads). In addition, separate foci of mineralization in soft tissue away from the fracture callus seen only in Plg-/- mice are suggestive of heterotopic ossification (red arrowheads). By 42-DPF, the fracture callus has largely remodeled in WT mice. In contrast, the fracture callus in Plg-/- mice is not only persistent but also hypertrophic and disorganized, with an irregular pattern of mineralization. Scale bars, 1 mm. **(B)** 2D μCT axial images of fractured femurs 14 and 42 DPF in Plg-/- mice show that the areas of soft tissue mineralization (red arrowheads) are distinct from the femoral fracture callus (yellow arrowheads), consistent with heterotopic ossification (scale bars, 1 mm). **(C)** Macroscopic photograph of lateral aspect of a fractured femur of a Plg-/- mouse 42-DPF (Macro, yellow bracket denotes fracture callus). Non-demineralized tissue sections from the fracture callus of Plg-/- mice were stained with Von Kossa and Van Gieson solution to identify regions of hard tissue callus formation (Box 1) and heterotopic ossification (Box 2). Red boxes denote regions shown at higher power magnification. Foci of heterotopic ossification are denoted by white asterisks. Scale bars, 1 mm, 1 mm, 200 μm, 20 μm from top panel. (AC, avascular cartilage; M, muscle; DPF= days post fracture).

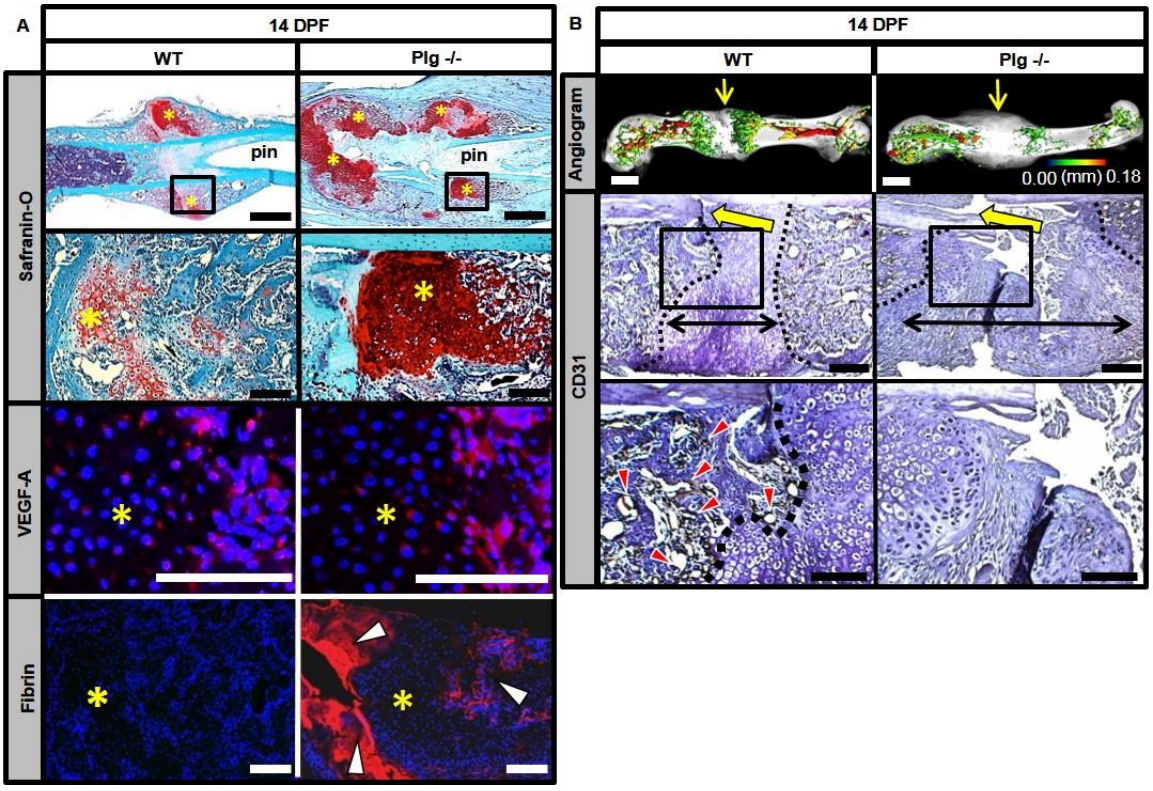

Figure 7: Plasmin is not required for soft tissue callus formation but is essential for vascularization of fracture callus. (A) Safranin-O-stained sections and immunofluorescence for VEGF-A and fibrin in the fracture callus 14-DPF. VEGF immunofluorescence staining reveals VEGF expression within the hypertrophic chondrocytes (avascular soft tissue callus, yellow asterisks) of both WT and Plg -/- mice. Fibrin immunofluorescence reveals excessive fibrin deposition (white arrowheads) at the fracture site and with the hard tissue callus of Plg-/- mice 14-DPF compared to WT mice. Scale bar, 1 mm, 100 µm, 100 µm, 100 µm from top panel. **(B)** Representative 3D µCT reconstructions of angiogram contrast-perfused femurs show reduced revascularization of the fracture callus in Plg-/- mice 14-DPF (color scale bar indicates vessel size range: black= 0.00mm red= 0.18mm. Immunohistochemistry for CD31-positive vessels (red arrowheads) in the fracture site (yellow arrows). The interface of avascular soft tissue callus and vascularized hard tissue callus is marked by a black dashed line. The fracture gap is defined as the region between hard tissue calluses (black double arrows). Scale bar, 1 mm, 100 µm, 100 µm from top panel

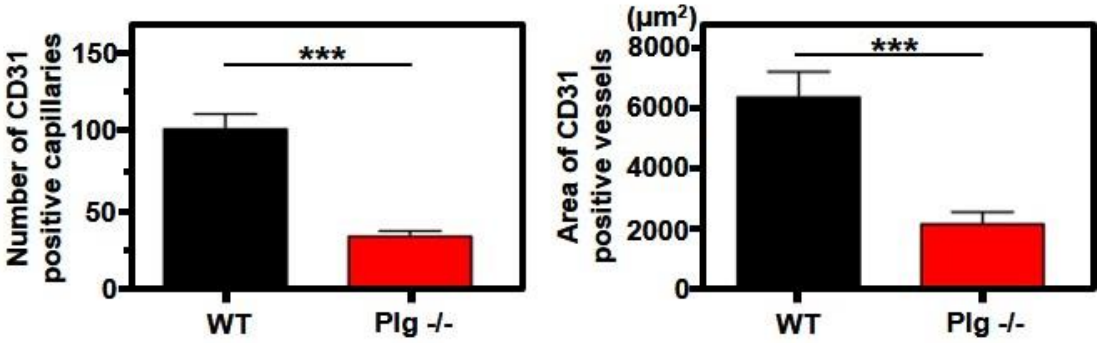

Figure 8: Plasminogen is essential for vascularization of the fracture callus. Quantitation of Cd-31 staining Quantitation of number (left) and total area (right) of CD31-positive blood vessels in the callus ($n \geq 5$ for each group; *** $P < 0.01$, Student's t-test, Error bars = SEM). (DPF= days post fracture).

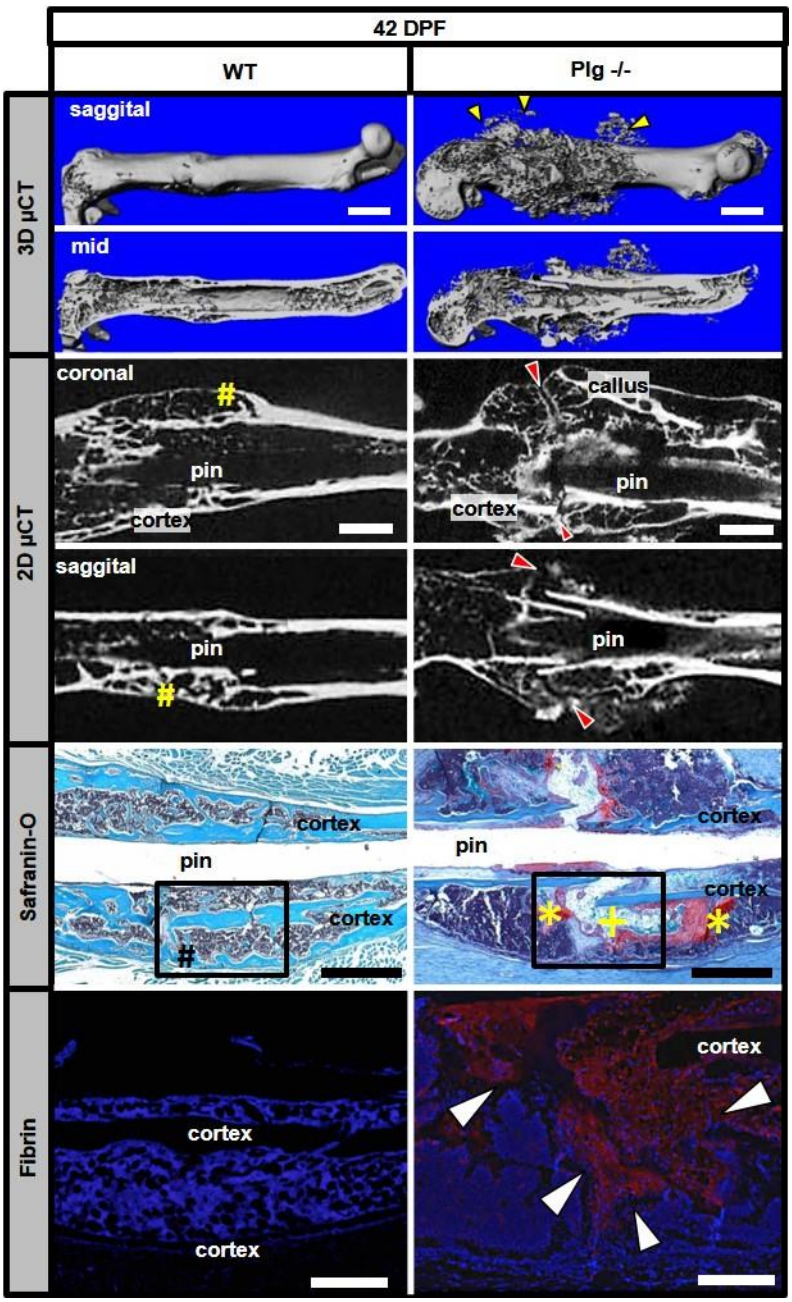

Figure 9: Plasmin is required for hard tissue callus union and remodeling.
3D µCT reconstruction of a displaced fracture 42 days post-fracture (42-DPF) shows evidence of soft tissue mineralization away from the fracture callus in Plg-/- mice (yellow arrowheads). Coronal and sagittal 2D µCT slices of WT and Plg-/- mice femurs show cortical bridging by hard fracture callus (yellow sharps) in WT mice. In contrast, a failure to unite the proximal and distal hard tissue callus was observed in Plg-/- mice (red arrowheads). White scale bars, 1 mm. Safranin-O-stained sections confirm complete cortical bridging in WT mice (black sharp), whereas the fracture gap in Plg-/- mice remains composed on chondroid soft tissue callus (yellow asterisks) and fibrous tissue (yellow Plus), without evidence of cortical bridging. (Black scale bars, 1mm). Immunofluorescence microscopy for fibrin shows abundant fibrin deposition at the fracture site in Plg-/- mice (red stain with DAPI-blue counterstain, white arrowheads). Black boxes in Safranin-O sections indicate region displayed for fibrin Immunofluorescence. White scale bars, 500µm.

Knock down of the fibrin precursor, fibrinogen, restores fracture healing and limits heterotopic ossification in plasminogen-deficient mice. Since both plasminogen and plasmin have biologic functions other than fibrin removal, we next determined if a failure to remove fibrin was responsible for impaired fracture repair and heterotopic ossification. Fibrinogen levels were reduced using an antisense oligonucleotide (ASO) designed to inhibit fibrinogen protein production in Plg-/- mice (Figure 10), resulting in Plg-/- Fbg^{low} mice. Serial radiographs of Plg-/- mice and Plg-/- Fbg^{low} mice demonstrated a well-formed hard tissue callus emanating from the periphery of the fracture callus at 14-DPF in Plg-/- Fbg^{low} mice (Figure 11). Conversely, similar to results described above, in Plg-/- mice the hard tissue callus was disorganized and difficult to discern due to the presence of heterotopic ossification. As previously described (Figure 6), Plg -/- mice show little radiographic evidence of fracture callus remodeling or organization over the next 4 weeks (14-DPF to 42-DPF). In contrast, Plg-/- Fbg^{low} mice show a significant reduction in size of the initial fracture callus by 42-DPF consistent with remodeling. This apparent rescue of callus formation and remodeling was accompanied by a marked reduction in soft tissue mineralization or heterotopic ossification. These findings show that reduction of fibrinogen in Plg-/- mice at least partially rescues aberrant fracture callus formation through the formation of organized hard tissue callus proximal and distal to the fracture site (Figure 11). Histologic evaluation of fracture callus in Plg-/- Fbg^{low} mice at 14-DPF demonstrates a well-formed and organized soft tissue callus flanked by hard tissue callus that is similar to that seen in WT mice (Figure 12 Top). In contrast, the soft tissue callus in Plg-/- mice is poorly formed and disorganized. Immunofluorescence staining for fibrin at 14-DPF confirmed persistent fibrin at the fracture site in Plg-/- mice, but a marked reduction of fibrin was observed in Plg-/- Fbg^{low} mice (Figure 12 & Figure 13a). Fracture sites were examined for CD31 immunostaining to determine if fibrinogen knockdown resulted in

increased vascularity of the fracture callus. Increases in the numbers of CD31-postive cells and the percentage of total tissue area defined by CD31 positive vessels at the periphery of the fracture callus were noted (red arrow heads Figure12 & 13B). These data demonstrate that impaired fibrinolysis results in persistent fibrin which compromises soft tissue callus formation and the normal vascularization of the fracture callus in Plg-/- mice.

To further define the structure of the hard tissue callus and timing of fracture callus union in Plg-/- Fbg^{low} mice, µCT was performed at 42-DPF. In Plg-/- Fbg^{low} mice 3D µCT reconstructions demonstrate a more organized hard tissue callus with evidence of remodeling (Figure 14-3D µCT). Cortical bridging of the fracture site by hard tissue callus is better defined on 2D µCT reconstructions, which show that in contrast to Plg-/- mice, which fail to form a complete hard callus bridge over the fracture gap by 42-DPF (Figure 14- 2D µCT), the gap in most Plg-/- Fbg^{low} mice (10 of 13 mice- Table 1) is overlaid with a well-formed hard tissue callus (Figure 14-2D µCT). Histological sections and histomorphometric analysis also demonstrated an improved, organized, and mature fracture calluses as evidenced by a lack of residual soft tissue callus and robust cortical bridging in Plg-/- Fbg^{low} mice when compared to Plg-/- mice (Figure 14 & Table 1). Quantitative µCT evaluation confirmed that the fracture calluses of Plg-/- Fbg^{low} mice had significantly improved geometric and structural properties compared to those of Plg-/- mice (Table 2). In contrast to Plg -/- mice, Plg-/- Fbg^{low} mice showed significant increases in tissue mineral density and decreases in bone volume, bone area, and polar moment of inertia,; all indicative of a well-formed remodeled callus. To confirm that fibrinogen knockdown was successful in preventing fibrin deposition within the fracture callus, we histologically investigated for the presence of fibrin at the fracture site (Figure 14-Bottom). Immunostaining confirmed a marked reduction in fibrin deposition in both the fracture callus and within the intramedullary space of Plg-/- Fbg^{low}

mice. These results demonstrate that depletion of fibrin in Plg-/- mice partially rescues impaired endochondral-mediated vascularization of the facture callus as well as the aberrant hard tissue callus formation, union, and remodeling seen in Plg-/- mice.

Fibrin deposits at the interface between the avascular soft tissue callus and the vascularized hard tissue callus impede migration of osteoblasts and endothelial cells. Since Plg-/- mice had a persistent fibrin matrix associated with both impaired bone formation and vascularization, we next examined whether fibrin is present at the interface of the avascular soft tissue callus and vascularized hard tissue callus (Figure 15-Top) where it might serve as a barrier to cell migration. We observed angiogram contrast material at the interface between soft and hard tissue callus indicative of chondrocyte-mediated recruitment of vascularity, which supports transport of mesenchymal progenitors and newly forming bone into the soft tissue callus. Consistent with previous findings (1, 24), CD31 immunostaining revealed endothelial cells surrounding patient vessels located at the leading edge of the hard tissue callus (Figure 15-Middle). Immunohistochemistry for fibrin performed on serial sections show fibrin deposits interposed between the soft and hard tissue callus and surrounding patent vessels. Fibrin localized near the sites of active vascularization, suggesting that persistent fibrin deposition at these sites may impede the remodeling of the soft tissue callus into a vascularized hard tissue callus (Figure 15-bottom). Comparison of the number of CD31-positive vessels, as a measure of the degree of vascularization, and the percentage of total mineralized area of hard tissue callus at 14-DPF reveals that removal of fibrin is associated with both increased blood vessel area and hard tissue callus area. These results suggest that the persistence of fibrin within the fracture site inhibits vascularization and formation of hard tissue callus (Figure 16A). This conclusion is further substantiated by our *in vitro* investigations, in which a trans-well migration

assay was employed to investigate fibrin's ability to impede osteoblast and endothelial cell migration. Through this work we identified that, in a concentration dependent manner, increasing density of a fibrin matrix leads to both impeded osteoblast and endothelial cell migration (Figure 16B). In total, this data supports the concept that persistent fibrin acts as a physical barrier to revascularization of the fracture callus, by inhibiting osteoblast and endothelial cell migration, resulting in the subsequent conversion of the soft tissue callus into newly formed vascularized woven bone.

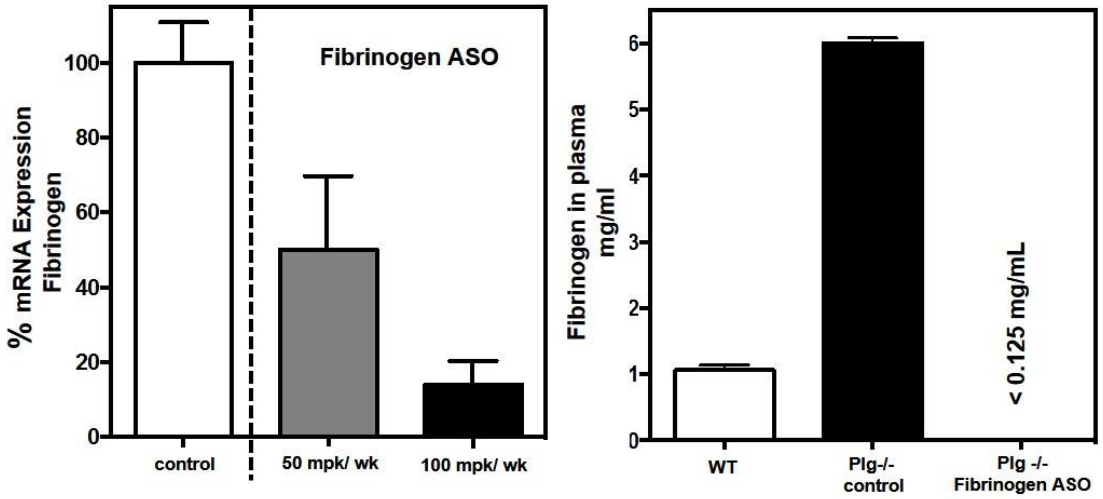

Figure 10: Antisense Oligonucleotide Knocks down of Fibrinogen. To ensure knockdown of fibrinogen in Plg -/- mice prior to fracture we conducted a pilot study. Plg -/- mice were treated with fibrinogen ASO for 2 weeks and then sacrificed. mRNA data demonstrates a dose dependent knock down of fibrinogen (Right). Values shown are standardized by control as 100%. An ELISA was performed on their plasma to determine fibrinogen levels demonstrate that upon administration of 100mg/kg per week (mpk/wk) Fibrinogen ASO, no fibrinogen was detectable in Plg -/- mice (Left). These data demonstrate that treatment with fibrinogen ASO 2 weeks prior to fracture is sufficient to knock down fibrinogen levels in blood. Error bars = SEM.

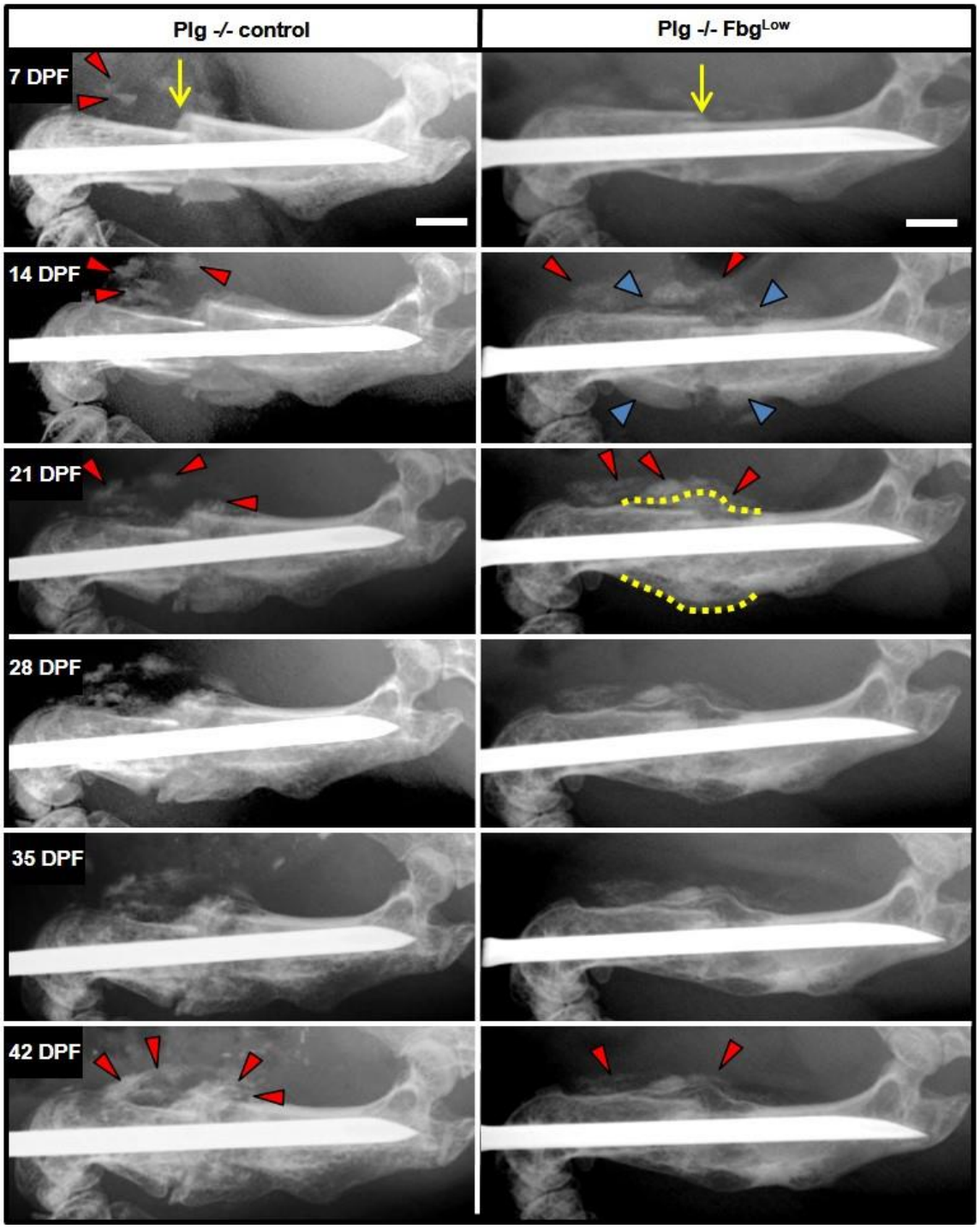

Figure 11: Fibrinogen knock down rescues plasmin-deficient mice from impaired callus formation. Serial radiographs of fractured femurs in Plg-/- mice treated with antisense oligonucleotide directed against fibrinogen (Plg-/- Fbg^{Low}) show improvement in fracture callus remodeling compared to Plg-/- mice (red arrowheads, heterotopic ossification; blue arrowheads, hard tissue callus; yellow dotted line, delineation of hard tissue callus from the adjacent heterotopic ossification in skeletal muscle). Scale bars, 1 mm. (DPF= days post fracture).

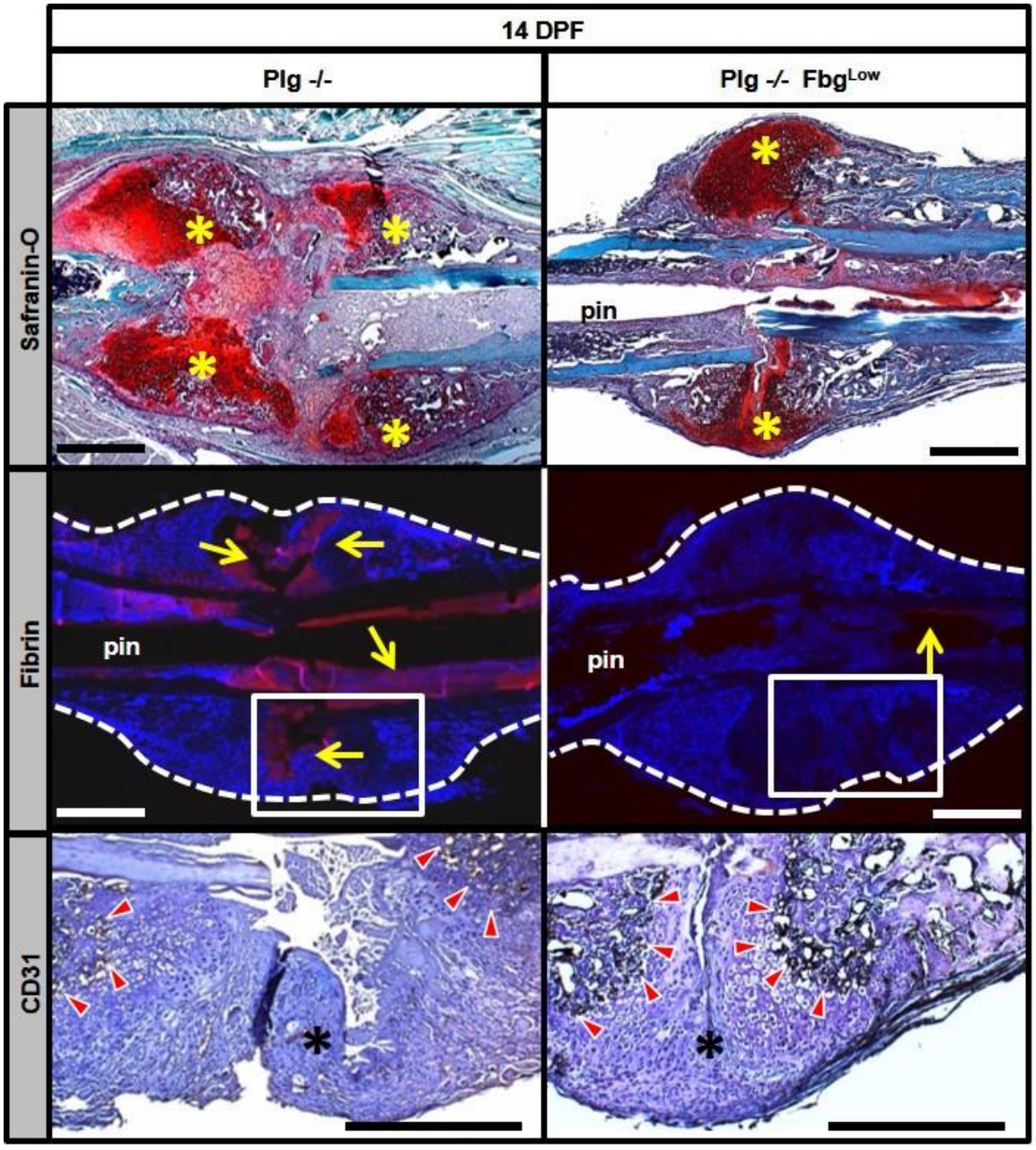

Figure 12: Fibrinogen knockdown rescues impaired callus formation and revascularization. Representative histological sections of femoral fracture sites from Plg-/- mice and Plg-/- mice treated with an antisense oligonucleotide against fibrinogen (Plg-/- Fbg^{Low}) 14 days post-fracture (14-DPF) stained with Safranin-O, by immunofluorescence for fibrin, and by immunohistochemistry for CD31. Whereas the fracture callus of Plg-/- mice is somewhat disorganized, with multiple foci of chondroid soft tissue callus (Safranin-O, yellow asterisks), the callus in Plg-/- Fbg^{Low} mice is more organized with a central soft tissue callus bordered proximally and distally by hard callus. There is markedly reduced fibrin deposition in the fracture callus of Plg-/- Fbg^{Low} mice compared to Plg-/- mice (yellow arrows); (white box denotes area shown for CD31 staining). CD31 highlights numerous CD31-positive cells lining blood vessels in the hard tissue callus of Plg-/- Fbg^{Low} mice (red arrowheads), with fewer vessels in Plg-/- mice (black asterisks denote areas of soft tissue callus in fracture gap). Scale bars, 1mm (DPF= days post fracture).

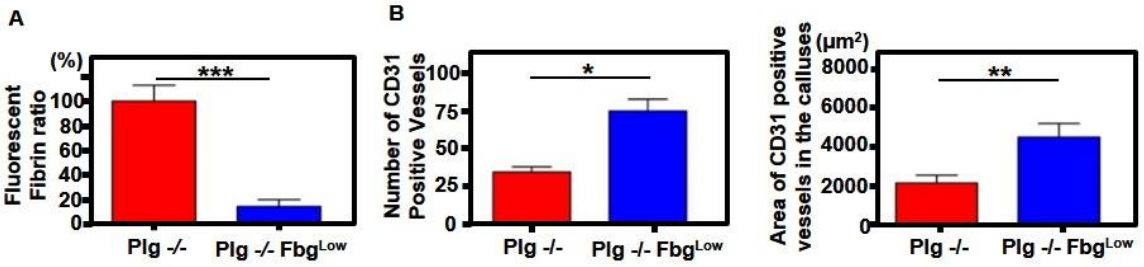

Figure 13: Fibrinogen knockdown rescues impaired revascularization. (A) Quantitation of fibrin deposition at fracture site (*n*=5 for each group). **(B)** Quantitation of number of CD31-positive vessels in the callus (left) and total area of CD31-positive vessels (right) (*n*≥5 for each group). *** *P*<0.001, ** *P*<0.01 * *P*<0.05; Student's t-test, Error bars = SEM.

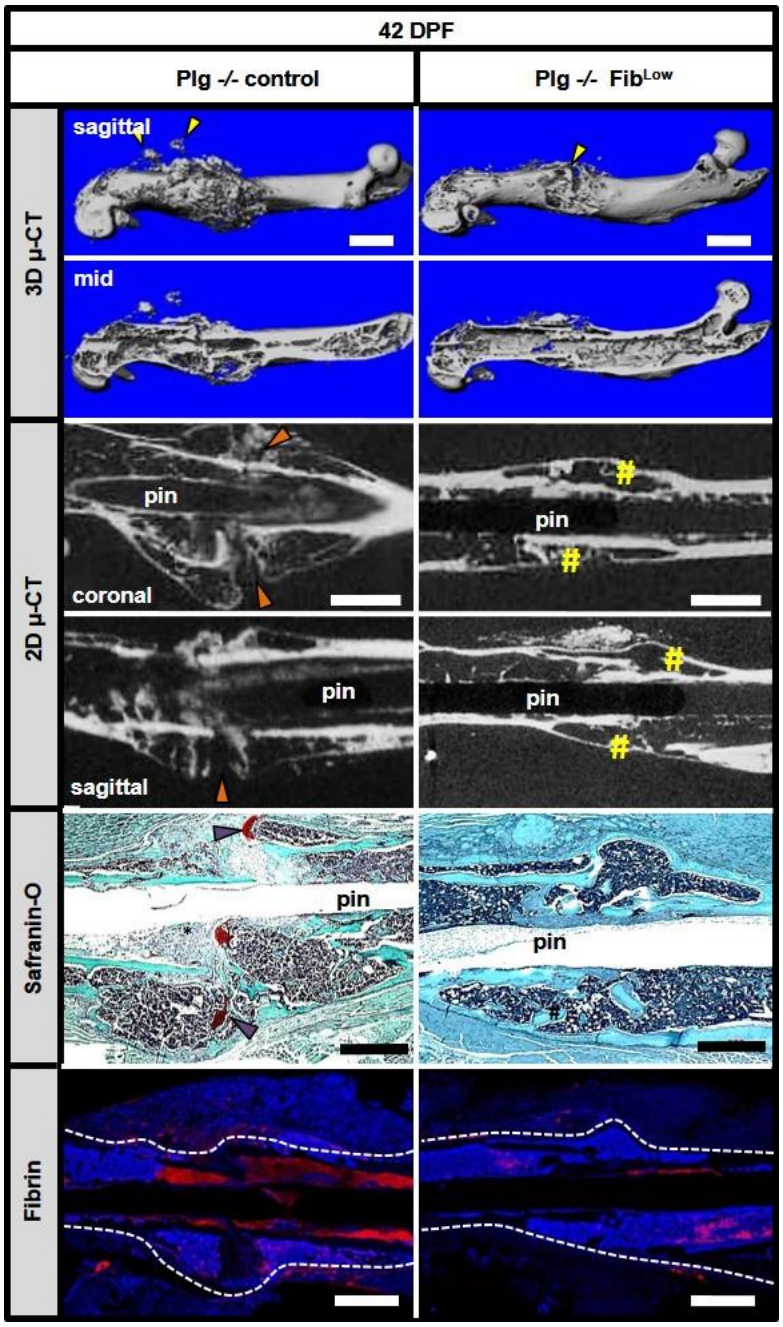

Figure 14: Fibrinogen knockdown rescues hard tissue callus union and fracture callus remodeling. Representative 3D and 2D µCT images, Safranin-O-stained sections, and immunofluorescence microscopy for fibrin in Plg-/- and Plg-/- Fbg^{Low} mice. 3D µCT images demonstrate heterotopic ossification (yellow arrowheads) and poorly remodeled fracture callus in Plg-/- mice 42-DPF formation. 2D µCT of the fracture sites in Plg-/- Fbg^{Low} mice show cortical bridging by hard tissue callus (yellow sharps) whereas Plg-/- mice do not (orange arrowheads) Scale bars, 1mm. Histological sections confirmed well remodeled fracture sites in Plg-/- Fbg^{Low} mice, in contrast to the disorganized callus with residual soft tissue callus in Plg-/- mice (purple arrowheads). Immunofluoresence for fibrin confirms markedly less fibrin in the fracture site in Plg-/- Fbg^{Low} mice (red stain, fibrin, with DAPI-blue counterstain). White dotted line denotes border of the femur and fracture callus. Scale bars, 1mm.

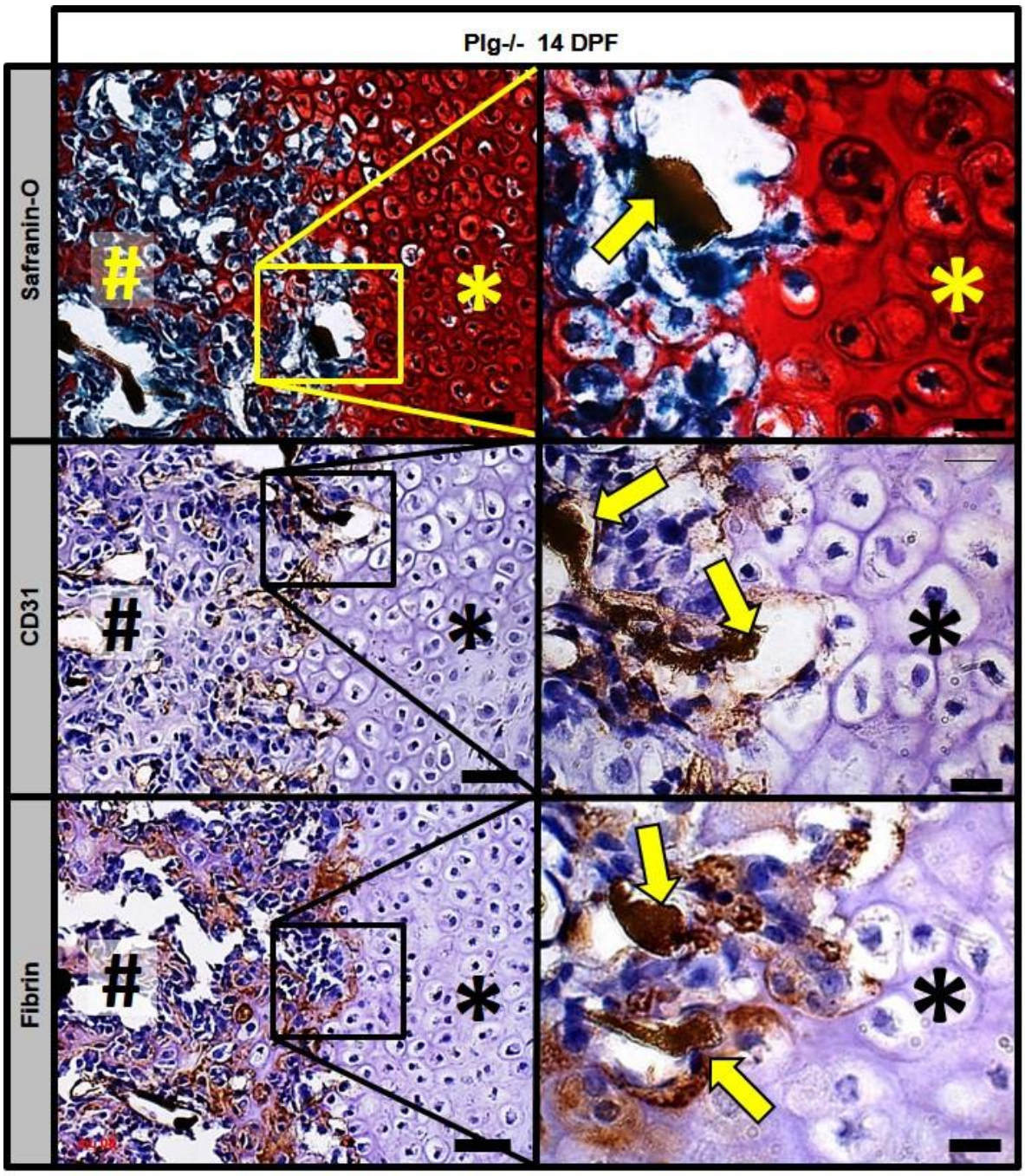

Figure 15: Fibrin is deposited at the interface between avascular soft tissue callus and vascularized hard tissue callus. Histological evaluation of the fracture callus of Plg-/- mice 14-DPF discloses angiogram contrast-perfused blood vessels (Safranin-O, yellow arrow) at the interface of the soft tissue callus (asterisks) and hard tissue callus (sharps). Immunohistochemical stains for CD31(brown staining) highlights thin-walled blood vessels filled with angiogram contrast material (CD31, yellow arrows) at the interface of soft and hard tissue callus. Immunohistochemistry also identifies fibrin (brown staining) at this interface surrounding angiogram contrast-perfused blood vessels (Fibrin, yellow arrows). Immunohistochemistry slides were counterstained with hematoxylin. Scale bars, 50 μm (left column); 20 μm (right column).

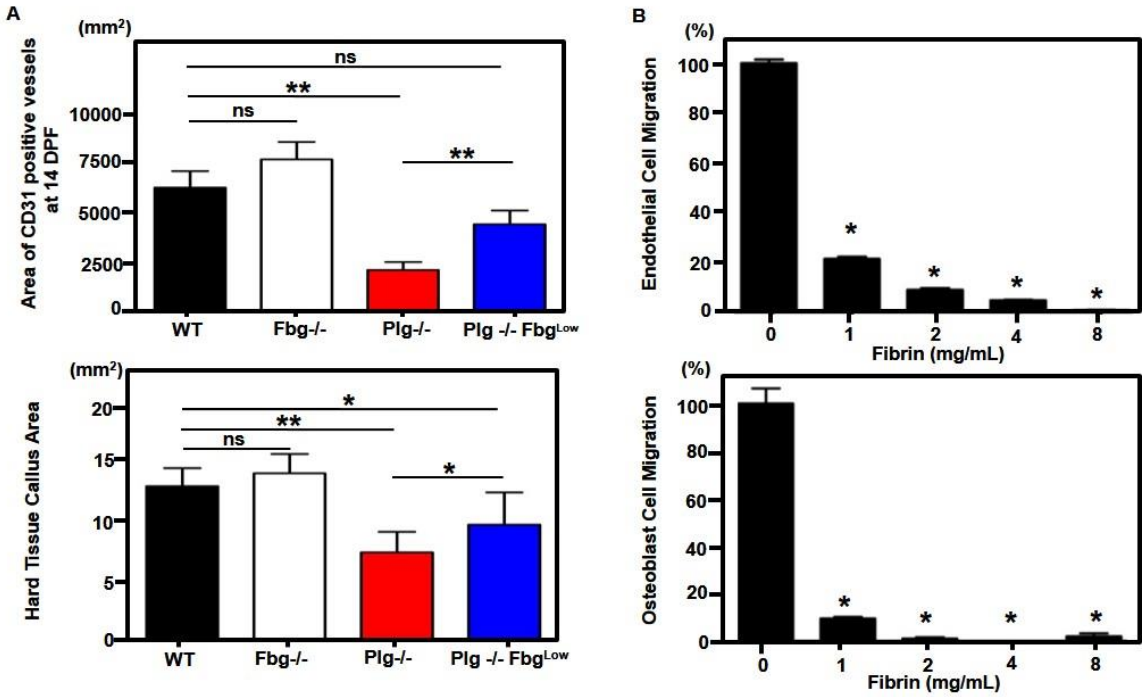

Figure 16: Quantitative assessment of fracture healing in mice with impaired fibrinolysis. (A) Quantitation of CD31-positive vessel area ($n \geq 5$ for each group). Quantitation of hard tissue callus area ($n \geq 5$ for each group). **(B)** *In vitro* transwell migration of EAhy.926 endothelial cells and Mc3T3 osteoblasts through a fibrin clot made with increasing concentrations of fibrinogen ($n=3$ for each fibrin concentration) * $P < 0.05$, ** $P < 0.01$, ns= not significant; Error bars = SEM.

V

Properties	Soft Tissue Callus (mm^2)							
genotype	14 DPF				42 DPF			
	n	Mean±SEM	*p-value*		n	Mean±SEM	*p-value*	
			vs WT	vs Plg-/-			vs WT	vs Plg-/-
WT	13	8.33±3.43	-	*0.05*	15	0.00±0.00	-	*0.001*
Fbg-/-	4	8.94±2.50	*n.s.*	*0.05*	10	0.00±0.00	*n.s.*	*0.001*
Plg-/-	8	14.49±6.63	*0.05*	-	15	0.26±0.14	*0.001*	-
Plg-/- Fbg^{Low}	5	13.22±4.26	*n.s.*	*n.s*	13	0.00±0.01	*n.s.*	*0.001*
Properties	**X-ray Grading (points)**							
genotype	14 DPF				42 DPF			
	n	Mean±SEM	*p-value*		n	Mean±SEM	*p-value*	
			vs WT	vs Plg-/-			vs WT	vs Plg-/-
WT	15	4.44±0.98	-	*0.001*	15	7.92±0.26	-	*0.001*
Fbg-/-	10	4.23±1.33	*n.s.*	*0.001*	10	7.90±0.43	*n.s.*	*0.001*
Plg-/-	15	2.07±0.51	*0.001*	-	15	4.14±1.52	*0.001*	-
Plg-/- Fbg^{Low}	13	2.70±0.79	*0.001*	*n.s.*	13	6.26±1.77	*0.001*	*0.001*
Properties	**Heterotopic Ossification (mm^2)**				**Cortical Bridging**			
genotype	42 DPF				42 DPF			
	n	Mean±SEM	*p-value*		n	Ratio (%)	*p-value*	
			vs WT	vs Plg-/-			vs WT	vs Plg-/-
WT	15	0.00±0.00	-	*0.001*	15	100 (15/15)	-	*0.0001*
Fbg-/-	10	0.00±0.00	*n.s.*	*0.001*	10	100 (10/10)	*n.s.*	*0.0001*
Plg-/-	15	7.27±2.57	*0.001*	-	15	26 (4/15)	*0.0001*	-
Plg-/- Fbg^{Low}	13	4.14±3.01	*0.001*	*0.001*	13	77 (10/13)	*n.s.*	*0.05*

Table 1: Histomorphometry and radiographic analysis at 14 and 42 days post fracture (14 and 42 DPF) in wild type (WT), fibrinogen deficient (Fbg-/-), plasminogen defiecient (Plg-/-) and plasminogen deficient mice treated with an antisense oligonucleotide against fibrinogen (Plg-/- Fbg^{Low}) mice. Soft tissue callus area at 14 and 42 DPF was analyzed using Safranin-O staining sections. X-ray grading was determined using lateral radiographs. Heterotopic ossification area was analyzed using 42 DPF radiographs. Cortical bridging analysis was examined using 2D microCT images. A One-Way ANOVA test was used for the comparisons of soft tissue callus formation, x-ray grading and heterotopic ossification area. Fisher's exact test was used for the comparison about cortical bridging rate. Values represent mean± SEM. *** $P<0.001$, ** $P<0.01$, * $P<0.05$, ns= not significant. Sample number used in each group is shown in the table.

Properties	pMOI (mm^4)			Tb. TMD (mg HA/cm^3)		
genotype	Mean±SEM	*p-value*		Mean±SEM	*p-value*	
		vs WT	vs Plg-/-		vs WT	vs Plg-/-
WT	0.77±0.30	-	*0.001*	1075±38	-	*0.001*
Fbg -/-	0.77±0.19	*n.s.*	*0.001*	1044±25	*n.s.*	*0.001*
Plg -/-	1.79±0.62	*0.001*	-	973±37	*0.001*	-
Plg -/- Fbg^{Low}	0.88±0.28	*n.s.*	*0.001*	1049±29	*n.s.*	*0.001*
Properties	**Bone Volume (mm^3)**			**Anisotropy (1)**		
genotype	Mean±SEM	*p-value*		Mean±SEM	*p-value*	
		vs WT	vs Plg-/-		vs WT	vs Plg-/-
WT	4.02±0.81	-	*0.001*	2.32±0.41	-	*0.001*
Fbg-/-	4.20±1.07	*n.s*	*0.001*	2.28±0.31	*n.s.*	*0.001*
Plg-/-	6.36±0.93	*0.001*	-	1.40±0.11	*0.001*	-
Plg -/- Fbg^{Low}	5.23±0.70	*0.05*	*n.s*	1.74±0.37	*n.s.*	*0.01*
Properties	**Bone Area (mm^2)**					
genotype	Mean±SEM	*p-value*				
		vs WT	vs Plg-/-			
WT	1.01±0.20	-	*0.001*			
Fbg-/-	1.05±0.27	*n.s.*	*0.001*			
Plg-/-	1.59±0.23	*0.001*	-			
Plg -/- Fbg^{Low}	1.22±0.35	*n.s.*	*0.01*			

Table 2: Bone properties of fractured femur at 42 days post fracture were analyzed using the Scanco microCT software. Polar moment of inertia (pMOI), trabecular tissue mineral density (Tb. TMD), bone volume, bone area and anisotropy were analyzed. A One-Way ANOVA test was used for this comparison. Values represent mean± SEM. *** $P<0.001$, ** $P<0.01$ * $P<0.05$, ns= not significant. WT ($n=15$), Fbg-/- ($n=10$), Plg-/- ($n=15$) and Plg-/- Fbg^{Low} ($n=13$) mice were used for this analysis.

Summary and Interpretation

Our findings reveal surprisingly that the coagulation matrix protein fibrin is not essential for fracture repair. To date, the prevailing theory regarding the role of fibrin during fracture repair has been that the fibrin matrix serves as the initial scaffold for healing as it promotes inflammatory and mesenchymal progenitor cell migration into the damaged bone. The discovery of multiple integrin binding motifs capable of promoting cellular migration on fibrin strongly supports this theory (25). However, our data refutes the current paradigm as we clearly demonstrate that fibrin is not essential for fracture repair in mice, since we did not observe any detectable deficiency in fracture repair in the absence of fibrin. Not surprisingly, we found that fibrin prevents excessive hemorrhage from the injured zone following long-bone fracture. These findings indicate that following fracture, fibrin is essential for hemostasis, and although it can support inflammatory and mesenchymal cell recruitment, activation and differentiation in many physiological and pathological processes, these biological functions appear to not be essential for efficient bone repair. Unexpectedly, we further show that it is the timely and efficient removal of fibrin that is essential for fracture repair as it is the removal of fibrin, which allows vascularization of the soft-tissue callus and the subsequent formation and remodeling of the hard-tissue callus. Our results direct a re-evaluation of the role of fibrin in fracture repair specifically in tissue response to injury and repair in general.

In addition to determining that fibrin is dispensable for fracture repair, we found that prolonged deposition of fibrin at the site of fracture could impair fracture healing. Given that angiogenesis is requisite for the formation of osteoblast-mediated matrix mineralization during fracture repair (24, 26-30), and that vascular dysfunction and poor fibrinolysis are common to many comorbid conditions associated with delayed fracture healing (17-20, 23, 31-35), we postulated that impaired fracture healing in Plg -/- mice is

the result of impaired angiogenesis. Endochondral angiogenesis in fracture healing is regulated by hypertrophic chondrocytes. Just as in the growth plate, hypertrophic chondrocytes release VEGF-A, calcium and phosphate, which direct endothelial and osteoprogenitor cells to form new blood vessels and bone. The absence of plasmin(ogen) did not impair development of the chondroid soft tissue callus or expression of VEGF-A in hypertrophic chondrocytes. Instead, reduction of fibrinolytic activity resulted in persistent fibrin deposition at the interface between hypertrophic chondrocytes in soft tissue callus and invading endothelial and osteoblastic cells in the leading edge of the hard tissue callus. Both the specific location of fibrin and the paucity of extramedullary vasculature that typically develops from the shunting of blood flow from the intramedullary vasculature after fracture (1), support the notion that a the persistence of fibrin secondary to impaired fibrinolysis is a physical barrier preventing required cellular trafficking and movement. Indeed, such a mechanism is strongly supported by our finding that reducing fibrinogen prior to fracture in plasminogen-deficient mice partially rescues endochondral angiogenesis and fracture union consistent with an inhibitory role for fibrin. Thus, these studies highlight the strict requirement for plasmin-mediated fibrinolysis for the recruitment of endothelial and osteoblast precursors by hypertrophic chondrocytes, thereby inhibiting endochondral angiogenesis and ossification.

Importantly, targeting fibrinogen, and hence fibrin, at least partially rescues fracture repair. Fibrinogen depletion was confirmed by the absence of fibrinogen in the serum and the finding that fibrin deposition was significantly reduced in the fracture callus at 42 DPF. The partial rescue of fracture repair may be due to this residual fibrin or a role for plasminogen that is independent of fibrinolysis. While the principal role of plasmin in fracture repair is to digest the fibrin matrix, and subsequently promote fracture callus vascularity and bone formation, we concede that it may have other physiologic

roles in this setting. Plasmin activity increases migration of monocytes and macrophages (36), which phagocytose necrotic debris from the site of injury and inhibit the acute inflammatory response (37). Thus, plasmin deficiency can impede fracture repair by prolonging the necroinflammatory phase. Plasmin activity also releases growth factors important for wound healing, such as TGFβ(38, 39) and VEGF(40), from both cells and matrices. Finally, plasmin may have direct effects on the osteoblast within the fracture callus. Inhibition of plasmin delays mineralization and differentiation of *in vitro* osteoblast cultures grown in the absence of fibrin (41), suggestive that plasmin may directly promote maturation of osteoblast precursors to mature osteoblast during fracture repair. While future studies are required to further explore the non-fibrinolytic roles of plasmin during fracture repair, our data indicate that plasmin activity is at least in part essential for fracture repair by removing fibrin.

Although our data implicate persistent fibrin deposition or impaired fibrinolysis as a principal cause of delayed fracture repair in plasminogen-deficient mice, the fracture healing process was not completely restored to normal. One possible explanation is that although our method to deplete fibrinogen reduced serum levels below the sensitivity level of ELISA, fibrin deposition, albeit significantly reduced, was still present within 42-day-old fracture callus. Interestingly, Kawao et al., have suggested that although plasminogen is essential for bone repair, its role is independent of its fibrinolytic activity (42). Possible explanations for these contradictory conclusions include the differences in the bone injury models, a drill hole bone defect, and the methods to reduce and confirm circulating fibrinogen levels.

Development of heterotopic ossification in skeletal muscle adjacent to the fracture was an unexpected finding in our model. Heterotopic ossification often occurs following musculoskeletal trauma associated with electrocution, burn/blast injuries, or with neurological injury (43-46). Although these conditions have been anecdotally

associated with diminished fibrinolytic activity (47-49) there are no reports that suggest that plasmin(ogen) is directly involved in preventing heterotopic ossification. It has been determined that absence of urokinase-type plasminogen activator results in spontaneous heterotopic ossification in mice with Duschenne's Muscular Dystrophy, although it was not determined whether this was secondary to a deficiency of downstream plasmin activity (50). Moreover, fibrin can bind calcium phosphate and promote mineralization (and in fact has been used in bone graft substitutes for this property) (51). Heterotopic ossification was significantly reduced when fibrinogen levels were reduced in plasminogen-deficient mice. Therefore, we posit that fibrin and plasminogen (or the active enzyme plasmin) play a role in the etiology of traumatic heterotopic ossification. Future studies are required to determine the precise mechanism by which plasminogen and fibrinogen contribute to heterotopic ossification following fracture.

Our results suggest a new paradigm for the roles of fibrin and plasmin during fracture repair. Fibrin is not essential for fracture repair, and indeed, fibrin must be timely and effectively removed to allow fracture vascularization and repair. Given that vascular dysfunction is seen in comorbid conditions associated with poor fracture healing, (17-20, 23, 31-35), and since it has been hypothesized that impaired angiogenesis is a primary cause of delayed union or non-union, our findings suggest that persistent or excessive fibrin deposition at the fracture site is the molecular mechanism of impaired fracture angiogenesis and subsequent delayed or non-union in these conditions.

Materials and Methods

Animals: Homozygous breeding pairs of plasminogen deficient mice (Plg -/-) and fibrinogen deficient mice(Fbg -/-) of C57BL/6 genetic background were kindly given by

Dr. Degen (Cincinnati, Ohio) and bred in the animal facility of Vanderbilt University with a 12 hour light cycle. At the time of study both fibrinogen and plasminogen deficient mice were 11 generations from the founding pair of mice provide by Dr. Degen. The C57BL/6 mouse wild type (WT) strain, recommended by Jackson Laboratory as the control strain for comparison to Plg -/- and Fbg -/- mice, was obtained from Jackson Laboratory (Bar Harbor, Maine). To avoid sex-related confounding effects on developmental bone growth and fracture repair, only male mice were used in this study. All mice were used for fracture study at 8 weeks of age.

Murine Femur Fracture Model: Mice were placed under anesthesia using 60mg/kg ketamine and 4mg/kg xylazine. The fur overlying the medial of the thigh was shaved and the skin prepped with betadine prior to making an incision. A 10-12 mm long medial incision of mid to distal femur was made, and mid-shaft femur was exposed by blunt dissection of muscle. After patella moved laterally, fracture was created by cutting the midshaft of the femur with fine scissors. A 23- gauge needle (0.6414 mm) was inserted into the intercondylar notch through a trephine technique and advanced through the intramedullary canal to the sub- or inter-trochanteric femur. Before closure, we confirmed that the fracture has been created in neither comminuted nor partially fractured. The incision was closed by silk suture. Fracture healing was followed radiographically using a Faxitron X-ray system (Lincolnshire, IL) (4 seconds at 35kV) weekly. Mice were sacrificed at 14 and 42 days after surgery and samples processed for micro-CT, Microfil, and histology.

Gross Pictures: The fractured femora were dissected after we sacrificed the mice. We removed the surrounding muscle around the femora. We carefully removed muscle not to damage any mineralized tissues around the fracture site using micro forceps. After fixing the specimens in 4% paraformaldehyde, we took pictures with Olympus dissecting microscope.

X-ray: X-ray was performed as previously described (52). Briefly, mice were placed in the prone position and imaged for 4 seconds at 45KV using a Faxitron LX 60. Mice were sacrificed at various time points (7-42 days) following fracture.

Angiography: Perfusion with Microfil (MV-122 Flow Tech Inc., Carver, MA) vascular contrast was conducted as previously described (53-56). Briefly, mice were euthanized, positioned supine and a thoracotomy extending into a laparotomy was performed. The left ventricle of the heart was cannulated using a 25- gauge butterfly needle. The inferior vena cava (IVC) was transected proximal to the liver and the entire vasculature subsequently perfused with 9mL of warm heparinized saline (100 units/ml in 0.9% saline) through the left ventricle cannula to prevent erythrocyte aggregation and thrombosis using perfusion pump (Braintree Scientific, Inc) to achieve consistent perfusion at the ratio of 2 mL/ min. Exsanguination and anticoagulation was deemed complete upon widespread hepatic blanching with clear fluid extravasating from the IVC. Mice were then perfused with 9mL of 10% neutral buffered formalin at 2 mL/min followed by 3ml of Microfil (Flow Tech inc. Carver Massachusetts) vascular contrast polymer at 0.5 mL/ min. To best verify complete filling of the vasculature gross images of the liver, the last organ to be perfused prior to extravasation through the IVC, were examined for extravascular pooling. Mice were excluded from the study if complete hepatic blanching prior to microfil was not achieved, if contrast was not clearly or uniformly visible in the hepatic vasculature or if extravascular pooling occurred. Due to the similarities in the density of bone and Microfil contrast, all fracture samples that were already taken by X-ray were then decalcified in 0.5M EDTA, pH 8 prior to X-ray and micro- CT imaging.

Micro- Computed Tomography (µCT): µCT images were acquired (µCT40, Scanco medical AG, Bassersdorf, Switzerland) following specimen harvest for the fractured femurs. at 55kVp, 145uA, 200ms integration, 500 projections per 180^{o} rotation, with a 20µm isotropic voxel size. After reconstruction, a volume of interest was selected

comprising the medullary space starting at the center of fracture site and extending an 0.5mm additional distally and proximally. The bone tissue within the VOI was segmented from soft tissue using a threshold of 220 per thousand (or 450.7mgHA/cm^3), a Gaussian noise filter of 0.2, and support of 1. Bone volume, and bone area were calculated using the Scanco evaluation software. A combination of uCT parameters was chosen to describe the material and geometrical properties of the callus. Tissue mineral density (TMD) was used for description of fracture healing. TMD is the average of attenuation value of all voxels above the threshold and within the total volume. This value has the units of mgHA/cm^3 because a hydroxyapatite phantom is scanned weekly providing the conversion of attenuation to equivalent density of HA. Polar moment of inertia (pMOI) and anisotropy describes the geometrical distribution of this material and is associated with torsional distribution strength. These parameters were determined by including all mineralized tissue within the outer perimeter of the fracture callus from uCT images by the Scanco script for midshaft evaluation.

Histological Analysis: Specimens removed for histology were fixed in 4% paraformaldehyde, decalcified in 0.5M EDTA (pH8.0) for approximately 5 days. Subsequently, they were dehydrated in graded series of ethanol, cleared and embedded in paraffin. Each sample was sectioned saggitally at 6 μm and used for each staining.

Safranin Orange/ Fast green stains (Safranin- O): Paraffin-embedded tissue was sectioned onto slides and deparaffinized and rehydrated as for H&E, above. Slides were placed in freshly filtered working Weigert's hematoxylin for 10 minutes and immediately washed in running tap water for 10 minutes. Slides were then placed in working 0.1% Fast green solution for 5 minutes and rinsed quickly in 1% acetic acid for no more than 10-15 seconds. Slides were then placed in 0.1% Safranin O solution for 5 minutes. Finally, slides were dehydrated through two changes of 95% EtOH and 100% EtOH for 3

minutes each and cleared in two changes of xylene for 5 minutes. Slides were then cover slipped with Permount.

Immunohistochemistry: Paraffin was removed from the slides using two xylene washes for 10 minutes each. The slides were then rehydrated in the following series of solutions: 100% EtOH twice for 2 minutes each, 90% EtOH for 2 minutes, 80% EtOH for 2 minutes, 70% EtOH for 2 minutes, dH2O for 2 minutes). Antigen retrieval was performed using 0.1 M citric acid and 0.1 M sodium citrate. Slides are heated for about 2 minutes in the microwave. Subsequently, the endogenous peroxide was then quenched with the 3% H_2O_2 for 15 *minutes.* After washing the slide gently with Phosphate buffer saline for 3 times, the sections were then blocked for 30 minutes using blocking solution (TSA kit Perkin Elmer) to minimize nonspecific staining. The slides were immunostained for rabbit anti mouse fibrin using a 1:1000 dilution of the primary antibody (Fibrin) in the blocking solution and incubated overnight at 4 C. Slides incubated without primary antibody served as negative controls. The slides were washed 3 times in TNT wash buffer for 5 minutes each. We applied Biotin Goat Anti-Rabbit Ig antibody (BD Pharmigen, 550338) for secondary antibody. After amplification by TSA amplification, the Dako Envision+ HRP/DAB System (Catalog # K4007, Dako) was used to produce localized, visible staining. All slides were incubated for equal amounts of time. They were then rinsed in dH_20 for 2 minutes, counterstained with Mayer's hematoxylin, and cover slipped. The slides were immunostained for rat anti mouse CD31 using a 1:50 dilution of the primary antibody (CD31) in the blocking solution and incubated overnight at 4 C. Slides incubated without primary antibody served as negative controls. The slides were washed 3 times in TNT wash buffer for 5 minutes each. We applied Biotin Goat Anti-Rat Ig antibody (BD Pharmigen, 559286) for secondary antibody. After amplification by TSA amplification, the Dako Envision+ HRP/DAB System (Catalog # K4007, Dako) was used to produce localized, visible staining. All slides were incubated for equal

amounts of time. They were then rinsed in dH_20 for 2 minutes, counterstained with Mayer's hematoxylin, and cover slipped.

Immunofluorescence microscopy: After slides were deparaffinized and hydrated, sodium citrate antigen retrieval was performed using 0.1 M citric acid and 0.1 M sodium citrate. Slides were heated for 2 minutes in the microwave, cooled to room temperature and then washed gently with Tris buffer saline (TBS). Slides were blocked (5% BSA solution containing 10% goat serum) and immunostained with rabbit anti-mouse Fibrin(ogen) (1:1000, provided by Dr. Degen) antibody overnight at 4°C. Slides were then washed and incubated with 10µg/mL of Alexa Fluor 647-labeled anti-rabbit antibody (Life Technologies 792514, Grand Island, NY) in blocking buffer for 1 hr. Slides were counterstained with DAPI and cover slipped using mounting solution (PolySciences Warrington, PA) and fluorescent images were taken (NIKON AZ100, Upright wide field microscope). Slides incubated without primary antibodies served as negative controls.

Van Gieson/ von Kossa staining in Plastic Section: Undecalcified femur of each mouse were fixed in PFA and dehydrated in ascending alcohol concentrations and then embedded in methylmetacrylate as previously described [16]. Sections of 7-µm thickness were cut on a Microtec rotation microtome (Techno-Med GmbH, Munich, Germany). Sections were stained by van Gieson/ von Kossa procedures as described [16] Undecalcified sections of 4 µm were cut in the sagittal plane on a Microtec rotation microtome (Techno-Med GmbH, Munich, Germany).

Quantification of soft tissue callus size: Hard and soft tissue callus delineated by Safranin-O red staining was traced on 5 histological step-sections 200µm apart as previously described with the following changes (57). To determine the orientation of the 5 slides, the edge of the callus was visualized by identifying the first section with callus on both the medial and lateral femoral cortex and the middle of the callus was determined by the pin space. Each of the specimens 5 sections were measured by 3

blinded reviewers and results were then expressed as mm^2 the soft tissue callus area. Image quantification for the soft tissue callus was performed using the software program Image J (NIH, http://rsb.info.nih.gov/ij/).

Quantification of fracture callus Vascularity: To assess vascularity of the fracture callus Immunohistochemical staining for CD31 was performed 14 DPF. Photographs of distal the proximal ends fracture callus were taken under low magnification (20X) so that the entirety of fracture calluses was collected. CD31 area was determined by using Photoshop (threshold 40) to select all CD31 positive staining from the background. The CD31 positive staining was then imported into Image J and the area of CD31 positive staining was calculated. To determine the number of CD31 positive vessels, two blinded observers counted CD31 positive vessels with in the fracture callus. A vessel was defined as a structure, which has CD31 cells lining a lumen.

Anti-sense Oligonucleotide treatment: Antisense oligonucleotide (ASO) for fibrinogen (ISIS, CA) was administered to Plg -/- mice 2 weeks prior to fracture and throughout the course of this study at a concentration of 100mg/Kg subcutaneously weekly. Fibrinogen ASO targets hepatic translation of gamma chain of fibrinogen and has been shown to have no toxicity at this dose.

Fibrinogen ELISA: To determine the effect of ASO for fibrinogen, we performed Fibrinogen ELISA. For collecting the plasma, we collected blood from mice using one-tenth volume of 0.1 M sodium citrate as an anticoagulant. After the collection of the blood in the centrifuge tubes, the blood was centrifuged at 1,500g for 15minutes at room temperature. Supernatant was collected and centrifuged again at 13,000g for 15minutes at room temperature. Plasma in the supernatant was stored at -80 degree until use. We measured the circulating fibrinogen level by following the manufacturer's instruction. (Immunology Consultants Laboratory, INC).

Transwell chamber migration assay: The cell migration assay was performed in a 12 well plate using cell culture insert (8 μm pore size, Falcon, 353182). Prior to seeding cells, the upper surface of the filter was coated with 100 μL of different doses of fibrin gel (1, 2, 4, 8, 16 μM). Fibrin gel was prepared as follows. 80 μL of different doses of human fibrinogen (Fib1, plasminogen depleted, Enzyme Research) and 10μL of 50 mM of $CaCl_2$ were mixed and added onto the insert. 10 μL of 20 U/ mL of thrombin (bovine origin, King Pharmaceuticals, 60793-215-05) was added to each fibrinogen solution to convert from fibrinogen to fibrin. Chambers were then gently shaken. Each insert was left for about 3 hours at 37℃ until gelled. 5x 10^4 of bEnd.3 cells were seeded onto the upper chamber with 500μL of 1% fetal calf serum (FCS) in Dulbecco Modified Eagle Medium (DMEM; Invitrogen Life Technologies, Carlsbad, CA). 1500 μL of 10% FCS in DMEM was added in the lower chamber. Cells were incubated for 24 hours at 37℃ in a humidified normoxic atmosphere in the presence of 5% of CO_2. After 24 hours incubation, non-migrating cells and fibrin gels on the upper surface of the filter were removed using a cotton swab and migrated cells adherent to the lower surface of filter were fixed in 10% formalin and then stained with 0.1% of crystal violet solution for 10 minutes. After each filter was taken photograph under the microscope. The transwell was then submerged in 0.2% Triton X-100 for 10 mins and the color metric measurement was conducted at 590 nm with a microplate reader (Biotek, Winooski, VT).

Radiographic Quantification of fracture healing: We quantified the fracture healing by measuring the 4 criteria. 1. mineralization 2. organization 3. union 4. remodeling. Samples were scored in a binary fashion with 0 meaning does not meet the criteria and 1 means meet the criteria. Both the upper side of femur and bottom of the femur were scored allowing for each radiograph to have the possibility of 8 total points. All the x-rays are assessed in a blinded manner by three orthopaedic clinicians from 1 to 6 weeks post fracture.

Statistics: Comparisons among the groups were performed using the one-way analysis of variance with the least significant difference procedure was used for analyzing 2 or multiple groups, respectively. A level of $p < 0.05$ was considered significant for the differences between mean values (*)

References

1. Yuasa M, Mignemi NA, Barnett JV, Cates JM, Nyman JS, Okawa A, Yoshii T, Schwartz HS, Stutz CM, Schoenecker JG. The temporal and spatial development of vascularity in a healing displaced fracture. Bone. 2014;67:208-21. Epub 2014/07/16. doi: 10.1016/j.bone.2014.07.002. PubMed PMID: 25016962.

2. Gerstenfeld LC, Cullinane DM, Barnes GL, Graves DT, Einhorn TA. Fracture healing as a post-natal developmental process: molecular, spatial, and temporal aspects of its regulation. Journal of cellular biochemistry. 2003;88(5):873-84. Epub 2003/03/05. doi: 10.1002/jcb.10435. PubMed PMID: 12616527.

3. Anitua E, Andia I, Ardanza B, Nurden P, Nurden AT. Autologous platelets as a source of proteins for healing and tissue regeneration. Thrombosis and haemostasis. 2004;91(1):4-15. Epub 2003/12/24. doi: 10.1267/THRO04010004. PubMed PMID: 14691563.

4. Martino MM, Briquez PS, Ranga A, Lutolf MP, Hubbell JA. Heparin-binding domain of fibrin(ogen) binds growth factors and promotes tissue repair when

incorporated within a synthetic matrix. Proceedings of the National Academy of Sciences of the United States of America. 2013;110(12):4563-8. Epub 2013/03/15. doi: 10.1073/pnas.1221602110. PubMed PMID: 23487783; PubMed Central PMCID: PMC3607046.

5. Sahni A, Francis CW. Vascular endothelial growth factor binds to fibrinogen and fibrin and stimulates endothelial cell proliferation. Blood. 2000;96(12):3772-8. Epub 2000/11/23. PubMed PMID: 11090059.

6. Rockwood CA, Green DP, Bucholz RW. Rockwood and Green's fractures in adults. 7th ed. Philadelphia, PA: Wolters Kluwer Health/Lippincott Williams & Wilkins; 2010.

7. Kolar P, Schmidt-Bleek K, Schell H, Gaber T, Toben D, Schmidmaier G, Perka C, Buttgereit F, Duda GN. The early fracture hematoma and its potential role in fracture healing. Tissue Eng Part B Rev. 2010;16(4):427-34. Epub 2010/03/04. doi: 10.1089/ten.TEB.2009.0687. PubMed PMID: 20196645.

8. Key JA, Conwell HE. The management of fractures, dislocations, and sprains. 4th ed. St. Louis,: The C. V. Mosby Company; 1946. 3 p. l., 9-1322 p. p.

9. Bugge TH, Flick MJ, Danton MJ, Daugherty CC, Romer J, Dano K, Carmeliet P, Collen D, Degen JL. Urokinase-type plasminogen activator is effective in fibrin clearance in the absence of its receptor or tissue-type plasminogen activator. Proceedings of the National Academy of Sciences of the United States of America. 1996;93(12):5899-904. PubMed PMID: 8650190; PubMed Central PMCID: PMC39159.

10. Romer J, Bugge TH, Pyke C, Lund LR, Flick MJ, Degen JL, Dano K. Impaired wound healing in mice with a disrupted plasminogen gene. Nature medicine. 1996;2(3):287-92. PubMed PMID: 8612226.

11. Bugge TH, Kombrinck KW, Flick MJ, Daugherty CC, Danton MJ, Degen JL. Loss of fibrinogen rescues mice from the pleiotropic effects of plasminogen deficiency. Cell. 1996;87(4):709-19. PubMed PMID: 8929539.

12. Cole HA, Ohba T, Nyman JS, Hirotaka H, Cates JM, Flick MJ, Degen JL, Schoenecker JG. Fibrin accumulation secondary to loss of plasmin-mediated fibrinolysis drives inflammatory osteoporosis in mice. Arthritis & rheumatology. 2014;66(8):2222-33. doi: 10.1002/art.38639. PubMed PMID: 24664548.

13. Gunnar B. J. Andersson M, PhD, Bouchard J, Kevin J. Bozic M, MBA, Robert M. Campbell J, MD, Miriam G. Cisternas M, Adolfo Correa M, MPH, PhD, Felicia Cosman M, Janet D. Cragan M, MPH, Kristen D'Andrea B, Doernberg N, John P. Dormans M, FACS, Ann L. Elderkin P, Zarina Fershteyn M, Aimee J. Foreman M, Steven Gitelis M, Steve M. Gnatz M, MHA, Robert H. Haralson I, MD, MBA, Charles G. (Chad) Helmick M, Marc C. Hochberg M, MPH, Serena Hu M, Jeffrey N. Katz M, Toby King C, Ron Kirk M, DC, Steven M. Kurtz P, Nancy Lane M, Ann Looker P, Joan McGowan P, Assia Miller M, MPH, Reba L. Novich M, Richard Olney M, MPH, Peter Panopalis M, David J. Pasta M, Andrew N. Pollak M, J. Edward Puzas P, B. Stephens Richards I, MD, John P. Sestito J, MS, Csaba Siffel M, PhD, Paul D. Sponseller M, E. William St. Clair M, Andrew Stuart M, Kimberly J. Templeton M, George Thompson M, Laura Tosi M, Anna N.A. Tosteson S, William G. Ward S, MD, Sylvia I. Watkins-Castillo P, Stuart L. Weinstein M, Mark W.

Wieting M, James G. Wright M, MPH, FRCSC, Edward H. Yelin P. United States Bone and Joint Initiative: The Burden of Musculoskeletal Diseases in the United States, Second Edition. 1st ed. Park Ridge, Ill.: American Academy of Orthopaedic Surgeons; 2011. vii, 199 p. p.

14. Einhorn TA. Enhancement of fracture-healing. The Journal of bone and joint surgery American volume. 1995;77(6):940-56. Epub 1995/06/01. PubMed PMID: 7782368.

15. Ebraheim NA, Martin A, Sochacki KR, Liu J. Nonunion of distal femoral fractures: a systematic review. Orthop Surg. 2013;5(1):46-50. Epub 2013/02/20. doi: 10.1111/os.12017. PubMed PMID: 23420747.

16. Robinson CM, Court-Brown CM, McQueen MM, Wakefield AE. Estimating the risk of nonunion following nonoperative treatment of a clavicular fracture. The Journal of bone and joint surgery American volume. 2004;86-A(7):1359-65. Epub 2004/07/15. PubMed PMID: 15252081.

17. Cobb TK, Gabrielsen TA, Campbell DC, 2nd, Wallrichs SL, Ilstrup DM. Cigarette smoking and nonunion after ankle arthrodesis. Foot Ankle Int. 1994;15(2):64-7. Epub 1994/02/01. PubMed PMID: 7981802.

18. Macey LR, Kana SM, Jingushi S, Terek RM, Borretos J, Bolander ME. Defects of early fracture-healing in experimental diabetes. The Journal of bone and joint surgery American volume. 1989;71(5):722-33. Epub 1989/06/01. PubMed PMID: 2659600.

19. Gruber R, Koch H, Doll BA, Tegtmeier F, Einhorn TA, Hollinger JO. Fracture healing in the elderly patient. Experimental gerontology. 2006;41(11):1080-93. Epub 2006/11/10. doi: 10.1016/j.exger.2006.09.008. PubMed PMID: 17092679.

20. Kline AJ, Gruen GS, Pape HC, Tarkin IS, Irrgang JJ, Wukich DK. Early complications following the operative treatment of pilon fractures with and without diabetes. Foot Ankle Int. 2009;30(11):1042-7. Epub 2009/11/17. doi: 10.3113/FAI.2009.1042. PubMed PMID: 19912712.

21. Rodriguez EK, Boulton C, Weaver MJ, Herder LM, Morgan JH, Chacko AT, Appleton PT, Zurakowski D, Vrahas MS. Predictive factors of distal femoral fracture nonunion after lateral locked plating: a retrospective multicenter case-control study of 283 fractures. Injury. 2014;45(3):554-9. doi: 10.1016/j.injury.2013.10.042. PubMed PMID: 24275357.

22. Foulk DA, Szabo RM. Diaphyseal humerus fractures: natural history and occurrence of nonunion. Orthopedics. 1995;18(4):333-5. PubMed PMID: 7603916.

23. Castillo RC, Bosse MJ, MacKenzie EJ, Patterson BM, Group LS. Impact of smoking on fracture healing and risk of complications in limb-threatening open tibia fractures. Journal of orthopaedic trauma. 2005;19(3):151-7. PubMed PMID: 15758667.

24. Maes C, Kobayashi T, Selig MK, Torrekens S, Roth SI, Mackem S, Carmeliet G, Kronenberg HM. Osteoblast precursors, but not mature osteoblasts, move into developing and fractured bones along with invading blood vessels. Dev Cell.

2010;19(2):329-44. Epub 2010/08/17. doi: 10.1016/j.devcel.2010.07.010. PubMed PMID: 20708594; PubMed Central PMCID: PMC3540406.

25. Gailit J, Clarke C, Newman D, Tonnesen MG, Mosesson MW, Clark RA. Human fibroblasts bind directly to fibrinogen at RGD sites through integrin alpha(v)beta3. Experimental cell research. 1997;232(1):118-26. doi: 10.1006/excr.1997.3512. PubMed PMID: 9141628.

26. Beamer B, Hettrich C, Lane J. Vascular endothelial growth factor: an essential component of angiogenesis and fracture healing. HSS journal : the musculoskeletal journal of Hospital for Special Surgery. 2010;6(1):85-94. Epub 2009/09/19. doi: 10.1007/s11420-009-9129-4. PubMed PMID: 19763695; PubMed Central PMCID: PMC2821499.

27. Gerber HP, Vu TH, Ryan AM, Kowalski J, Werb Z, Ferrara N. VEGF couples hypertrophic cartilage remodeling, ossification and angiogenesis during endochondral bone formation. Nature medicine. 1999;5(6):623-8. Epub 1999/06/17. doi: 10.1038/9467. PubMed PMID: 10371499.

28. Harper J, Klagsbrun M. Cartilage to bone--angiogenesis leads the way. Nature medicine. 1999;5(6):617-8. Epub 1999/06/17. doi: 10.1038/9460. PubMed PMID: 10371495.

29. Brookes M, Landon DN. The Juxta-Epiphysial Vessels in the Long Bones of Foetal Rats. J Bone Joint Surg Br. 1964;46:336-45. Epub 1964/05/01. PubMed PMID: 14167642.

30. Hausman MR, Schaffler MB, Majeska RJ. Prevention of fracture healing in rats by an inhibitor of angiogenesis. Bone. 2001;29(6):560-4. Epub 2001/12/01. PubMed PMID: 11728927.

31. Burns DM. Epidemiology of smoking-induced cardiovascular disease. Progress in cardiovascular diseases. 2003;46(1):11-29. Epub 2003/08/16. PubMed PMID: 12920698.

32. Grundy SM, Benjamin IJ, Burke GL, Chait A, Eckel RH, Howard BV, Mitch W, Smith SC, Jr., Sowers JR. Diabetes and cardiovascular disease: a statement for healthcare professionals from the American Heart Association. Circulation. 1999;100(10):1134-46. Epub 1999/09/08. PubMed PMID: 10477542.

33. Meigs JB. Epidemiology of type 2 diabetes and cardiovascular disease: translation from population to prevention: the Kelly West award lecture 2009. Diabetes care. 2010;33(8):1865-71. Epub 2010/07/30. doi: 10.2337/dc10-0641. PubMed PMID: 20668155; PubMed Central PMCID: PMC2909080.

34. Purnell JQ, Zinman B, Brunzell JD, Group DER. The effect of excess weight gain with intensive diabetes mellitus treatment on cardiovascular disease risk factors and atherosclerosis in type 1 diabetes mellitus: results from the Diabetes Control and Complications Trial/Epidemiology of Diabetes Interventions and Complications Study (DCCT/EDIC) study. Circulation. 2013;127(2):180-7. Epub 2012/12/06. doi: 10.1161/CIRCULATIONAHA.111.077487. PubMed PMID: 23212717.

35. Willigendael EM, Teijink JA, Bartelink ML, Kuiken BW, Boiten J, Moll FL, Buller HR, Prins MH. Influence of smoking on incidence and prevalence of peripheral arterial disease. Journal of vascular surgery. 2004;40(6):1158-65. Epub 2004/12/29. doi: 10.1016/j.jvs.2004.08.049. PubMed PMID: 15622370.

36. Ploplis VA, French EL, Carmeliet P, Collen D, Plow EF. Plasminogen deficiency differentially affects recruitment of inflammatory cell populations in mice. Blood. 1998;91(6):2005-9. PubMed PMID: 9490683.

37. Wu AC, Raggatt LJ, Alexander KA, Pettit AR. Unraveling macrophage contributions to bone repair. BoneKEy reports. 2013;2:373. doi: 10.1038/bonekey.2013.107. PubMed PMID: 25035807; PubMed Central PMCID: PMC4098570.

38. Khalil N, Corne S, Whitman C, Yacyshyn H. Plasmin regulates the activation of cell-associated latent TGF-beta 1 secreted by rat alveolar macrophages after in vivo bleomycin injury. American journal of respiratory cell and molecular biology. 1996;15(2):252-9. doi: 10.1165/ajrcmb.15.2.8703482. PubMed PMID: 8703482.

39. Yee JA, Yan L, Dominguez JC, Allan EH, Martin TJ. Plasminogen-dependent activation of latent transforming growth factor beta (TGF beta) by growing cultures of osteoblast-like cells. Journal of cellular physiology. 1993;157(3):528-34. doi: 10.1002/jcp.1041570312. PubMed PMID: 8253864.

40. Roth D, Piekarek M, Paulsson M, Christ H, Bloch W, Krieg T, Davidson JM, Eming SA. Plasmin modulates vascular endothelial growth factor-A-mediated

angiogenesis during wound repair. The American journal of pathology. 2006;168(2):670-84. doi: 10.2353/ajpath.2006.050372. PubMed PMID: 16436680; PubMed Central PMCID: PMC1606492.

41. Schoenecker J, Mignemi N, Stutz C, Liu Q, Edwards J, Lynch C, Holt G, Schwartz H, Mencio G, Hamm H. 2010 Young Investigator Award winner: Therapeutic aprotinin stimulates osteoblast proliferation but inhibits differentiation and bone matrix mineralization. Spine. 2010;35(9):1008-16. doi: 10.1097/BRS.0b013e3181d3cffe. PubMed PMID: 20407341.

42. Kawao N, Tamura Y, Okumoto K, Yano M, Okada K, Matsuo O, Kaji H. Plasminogen plays a crucial role in bone repair. Journal of bone and mineral research : the official journal of the American Society for Bone and Mineral Research. 2013;28(7):1561-74. doi: 10.1002/jbmr.1921. PubMed PMID: 23456978.

43. Potter BK, Forsberg JA, Davis TA, Evans KN, Hawksworth JS, Tadaki D, Brown TS, Crane NJ, Burns TC, O'Brien FP, Elster EA. Heterotopic ossification following combat-related trauma. The Journal of bone and joint surgery American volume. 2010;92 Suppl 2:74-89. Epub 2010/12/09. doi: 10.2106/JBJS.J.00776. PubMed PMID: 21123594.

44. Forsberg JA, Davis TA, Elster EA, Gimble JM. Burned to the bone. Science translational medicine. 2014;6(255):255fs37. doi: 10.1126/scitranslmed.3010168. PubMed PMID: 25253672.

45. Sakellariou VI, Grigoriou E, Mavrogenis AF, Soucacos PN, Papagelopoulos PJ. Heterotopic ossification following traumatic brain injury and spinal cord injury: insight into the etiology and pathophysiology. Journal of musculoskeletal & neuronal interactions. 2012;12(4):230-40. PubMed PMID: 23196266.

46. Cipriano CA, Pill SG, Keenan MA. Heterotopic ossification following traumatic brain injury and spinal cord injury. The Journal of the American Academy of Orthopaedic Surgeons. 2009;17(11):689-97. PubMed PMID: 19880679.

47. Aoki K, Aikawa N, Sekine K, Yamazaki M, Mimura T, Urano T, Takada A. Elevation of plasma free PAI-1 levels as an integrated endothelial response to severe burns. Burns : journal of the International Society for Burn Injuries. 2001;27(6):569-75. Epub 2001/08/30. PubMed PMID: 11525850.

48. Hofstra JJ, Vlaar AP, Knape P, Mackie DP, Determann RM, Choi G, van der Poll T, Levi M, Schultz MJ. Pulmonary activation of coagulation and inhibition of fibrinolysis after burn injuries and inhalation trauma. The Journal of trauma. 2011;70(6):1389-97. doi: 10.1097/TA.0b013e31820f85a7. PubMed PMID: 21460745.

49. Winther K, Gleerup G, Snorrason K, Biering-Sorensen F. Platelet function and fibrinolytic activity in cervical spinal cord injured patients. Thrombosis research. 1992;65(3):469-74. PubMed PMID: 1321515.

50. Suelves M, Vidal B, Serrano AL, Tjwa M, Roma J, Lopez-Alemany R, Luttun A, de Lagran MM, Diaz-Ramos A, Jardi M, Roig M, Dierssen M, Dewerchin M, Carmeliet P, Munoz-Canoves P. uPA deficiency exacerbates muscular dystrophy in MDX mice. The

Journal of cell biology. 2007;178(6):1039-51. doi: 10.1083/jcb.200705127. PubMed PMID: 17785520; PubMed Central PMCID: PMC2064626.

51. Douglas TE, Gassling V, Declercq HA, Purcz N, Pamula E, Haugen HJ, Chasan S, de Mulder EL, Jansen JA, Leeuwenburgh SC. Enzymatically induced mineralization of platelet-rich fibrin. J Biomed Mater Res A. 2012;100(5):1335-46. Epub 2012/03/01. doi: 10.1002/jbm.a.34073. PubMed PMID: 22374736.

52. O'Neill KR, Stutz CM, Mignemi NA, Burns MC, Murry MR, Nyman JS, Schoenecker JG. Micro-computed tomography assessment of the progression of fracture healing in mice. Bone. 2012;50(6):1357-67. Epub 2012/03/29. doi: 10.1016/j.bone.2012.03.008. PubMed PMID: 22453081.

53. Cole HA, Yuasa M, Hawley G, Cates JM, Nyman JS, Schoenecker JG. Differential development of the distal and proximal femoral epiphysis and physis in mice. Bone. 2013;52(1):337-46. Epub 2012/10/20. doi: 10.1016/j.bone.2012.10.011. PubMed PMID: 23079139.

54. Duvall CL, Taylor WR, Weiss D, Guldberg RE. Quantitative microcomputed tomography analysis of collateral vessel development after ischemic injury. American journal of physiology Heart and circulatory physiology. 2004;287(1):H302-10. Epub 2004/03/16. doi: 10.1152/ajpheart.00928.2003. PubMed PMID: 15016633.

55. Duvall CL, Taylor WR, Weiss D, Wojtowicz AM, Guldberg RE. Impaired angiogenesis, early callus formation, and late stage remodeling in fracture healing of osteopontin-deficient mice. Journal of bone and mineral research : the official journal of

the American Society for Bone and Mineral Research. 2007;22(2):286-97. Epub 2006/11/08. doi: 10.1359/jbmr.061103. PubMed PMID: 17087627.

56. Dhillon RS, Xie C, Tyler W, Calvi LM, Awad HA, Zuscik MJ, O'Keefe RJ, Schwarz EM. PTH-enhanced structural allograft healing is associated with decreased angiopoietin-2-mediated arteriogenesis, mast cell accumulation, and fibrosis. Journal of bone and mineral research : the official journal of the American Society for Bone and Mineral Research. 2013;28(3):586-97. Epub 2012/09/20. doi: 10.1002/jbmr.1765. PubMed PMID: 22991274; PubMed Central PMCID: PMC3540116.

57. Gerstenfeld LC, Cho TJ, Kon T, Aizawa T, Tsay A, Fitch J, Barnes GL, Graves DT, Einhorn TA. Impaired fracture healing in the absence of TNF-alpha signaling: the role of TNF-alpha in endochondral cartilage resorption. Journal of bone and mineral research : the official journal of the American Society for Bone and Mineral Research. 2003;18(9):1584-92. Epub 2003/09/13. doi: 10.1359/jbmr.2003.18.9.1584. PubMed PMID: 12968667.

CHAPTER 7

Methylglyoxal Modifies Plasminogen Binding and Activation

Type 2 diabetes mellitus (DM2) is a pathologic condition that affects 6.5 percent of the world's population and nearly 10% of the US population (1). One of the most common complications of DM2 is impaired regeneration of injured musculoskeletal tissue and increased thrombosis after surgery or trauma. This deficiency causes substantial morbidity and mortality resulting in a loss of function and increased rates of infection, often resulting in amputation of the afflicted limb (2, 3). Consequently, diabetic patients often require skilled nursing assistance and/or prolonged hospitalization for the treatment of healing complications. As a result, treatment for these complications represents a substantial portion of the nearly $245 billion spent on health care for diabetics annually (4). Improving the regeneration of musculoskeletal tissue in diabetics would therefore reduce the morbidity, mortality, and cost associated with diabetes care. Although a multitude of studies conducted in both animal models and patients have attempted to identify the pathophysiology of deficient musculoskeletal healing in diabetics, a significant knowledge gap remains. As a result, other than medically controlling hyperglycemia, there is a lack of pharmacological treatments to improve regeneration of musculoskeletal tissue in diabetics after injury or surgery.

Effective fibrinolysis mediated by plasmin after activation by tissue plasminogen activator (tPA) prevents intravascular thrombosis by degrading fibrin thrombi (6). Recently, it has been shown that plasmin has numerous other functions essential for tissue regeneration in the extravascular compartment where it is primarily activated by urokinase plasminogen activator (uPA) (7-11). Along these lines we, in addition to other groups, have determined that extravascular plasmin-mediated proteolysis is essential for regeneration of muscle, bone and

skin (12-14). As the clinical phenotype of patients with DM2 includes insufficient intravascular and extravascular fibrinolysis (resulting in thrombosis and impaired wound healing, respectively), global hypofibrinolysis is thought to be associated with hyperglycemia (15). It has been suggested that hypofibrinolysis in this setting results from an increased expression of plasminogen activator inhibitor (PAI-1) (15-17); however, the exact mechanism remains unclear.

Reactive oxidative species (ROS), commonly produced during cellular respiration as well as other metabolic reactions, were first discovered in mammals during the 1960's and 70's as part of the body's microbial defense system (18, 19). While playing an important role in immunology, ROS are also capable of post-translational modification of proteins through adduction of exposed amino acids which results in dysregulation of protein function (20). Recent investigation into diabetes has revealed that these patients have elevated circulating ROS levels in their blood and furthermore, the level of ROS positively correlates with the severity of diabetes (21). Methylglyoxal is an ROS generated through glycolysis, oxidation of acetone, catabolism of threonine or through degradation of glycosylated proteins (26). Several studies have identified elevated levels of the ROS methylglyoxal in the plasma of patients with diabetes, Plasma concentration in these patients has been reported as high as 6μm, while intracellular concentrations methylglyoxal have been shown be theoretical possible as high as 32μm (22-24). Methylglyoxal may play a role in thrombosis in diabetes through the adduction and inactivation of the thrombin inhibitor anti-thrombin (25). Methylglyoxal is an ROS generated through glycolysis, oxidation of acetone, catabolism of threonine and through the degradation of glycosylated proteins (26). Methylglyoxal is of particular importance because it adducts lysine and arginine residues, which are essential for plasminogen binding and activation (27). Thus, considering that the severity of diabetes correlates with both ROS burden and impairment of tissue regeneration, we hypothesize that methylglyoxal adducts amino acids in regions of plasminogen responsible for binding and activation, resulting in an acquired hypo-fibrinolytic state.

Results

Structural Adduction of Plasminogen. Plasminogen contains 47 lysine residues and 40 arginine residues, which are susceptible to methylglyoxal adduction. In order to determine the specific arginine and lysine residues adducted by methylglyoxal, we treated plasminogen with methylglyoxal at a molar ratio of 16:1 (see methods) and performed LC-coupled tandem mass spectrometry looking for two specific adducts of plasminogen. After manual examination and validation of peptide fragments, these data revealed adduction of Arg-504 located in a kringle domain of plasminogen that is critical for binding fibrin and receptors (Figure 1A). Interestingly, modification of these amino acid is also know to result in a genetic mutation in plasminogen that causes a state of hypo-plasminogenima (5). In addition to modifications of Arg-504, we also observed adduction of Arg-561, the cleavage site used by plasminogen activators to convert plasminogen into its active form, plasmin (Figure 1B). Together these data suggest that methylglyoxal adduction of plasminogen may impact both the cleavage of plasminogen to its active form and impair plasminogen binding.

Functional Evaluation of Adducted Plasminogen. To determine the functional effect of adductions to plasminogen by methylglyoxal, we developed a novel assay that simultaneously measures fibrin clot formation, fibrin clot lysis, and plasmin activity in a 96-well plate (Figure 2 A&B). In our initial validation of this assay, we observed that plasmin activation occurred following formation of the fibrin clot, which suggests that plasmin activation was dependent on fibrin clot formation at the concentrations of plasminogen and tPA used in our assay (Figure 2C). We then optimized the concentration of plasminogen, fibrinogen and tPA for detection of changes in turbidity and plasmin generation with our assay (Figure 3). Confirming our previous observations, we noted that the presence of fibrin greatly reduced the amount of tPA required to

maximally activate plasminogen as evident in the tPA concentration dependent curves in the presence and absence of fibrin (Figure 3 Bottom).

To validate that simultaneous turbidity and plasmin generation assays were sensitive in detecting inhibition of plasminogen activation and fibrinolysis experiments were performed in the presence of increasing concentrations of aminocaproic acid, a known inhibitor of plasmin activation. The results confirms that our assay was sensitive to changes in fibrinolysis and plasmin activation, with a half maximal inhibitory concentration (IC_{50}) of 41uM of aminocaproic acid for clot lysis, and an IC_{50} of 73uM of aminocaproic acid for plasmin activity (Figure 4). Having established the ability of our simultaneous turbidity plasmin generation assay to detect changes in plasmin activity and fibrinolysis, we next determined if adduction of plasminogen by ROS, such as methylglyoxal, inhibits fibrinolysis and plasminogen activation.

Plasminogen was treated with increasing molar ratios of methylglyoxal for 24 hours and then used in for our simultaneous turbidity plasmin generation assays to assess the effects on fibrinolysis and plasminogen activation. Treating plasminogen with methylglyoxal resulted in a concentration-dependent decrease in fibrinolysis (Figure 5A), as well as a concentration-dependent decrease in plasmin activity (Figure 5B). Having determined that methylglyoxal treated with plasminogen is functionally inhibited, we next investigated the mechanism of methylglyoxal inhibition by performing simultaneous turbidity plasmin generation assays in concentrations with tPA that do not require fibrin for plasminogen activation (>100pM) (Figure 5C). We found that increased concentrations of tPA were capable of activating methylglyoxal-treated plasminogen. However, the maximal amount of plasmin activity was reduced compared to control treated plasminogen, indicating that a population of the plasminogen was incapable of being activated. Paired with our mass spectrometry findings, the concentration-dependent decrease in plasmin activity in the presence of fibrin and tPA, and the decreased total plasminogen activation even at maximal doses of tPA (10nM), suggest that functional

impairment of plasminogen is likely the result of both an inability to bind fibrin as well as an inability to be convert to active plasmin by tPA.

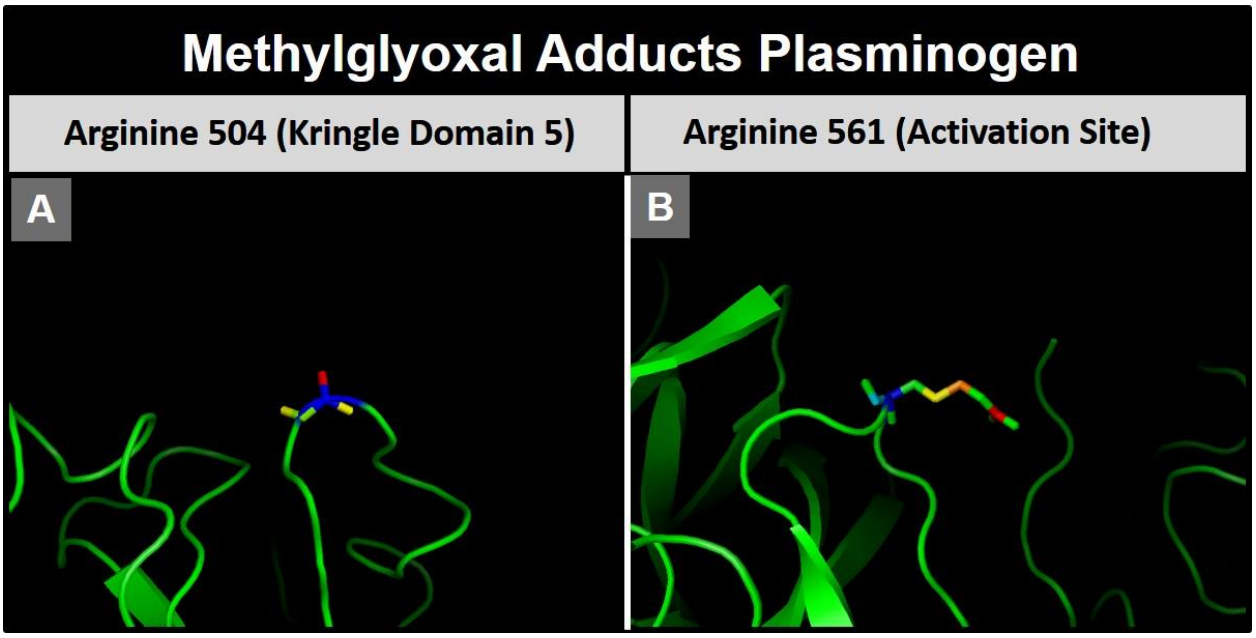

Figure 1: Methylglyoxal Adducts Plasminogen. Plasminogen incubated with methylglyoxal at a molar ratio of 16:1 reveals modification of Arg 504 (A) and Arg 561 (B).

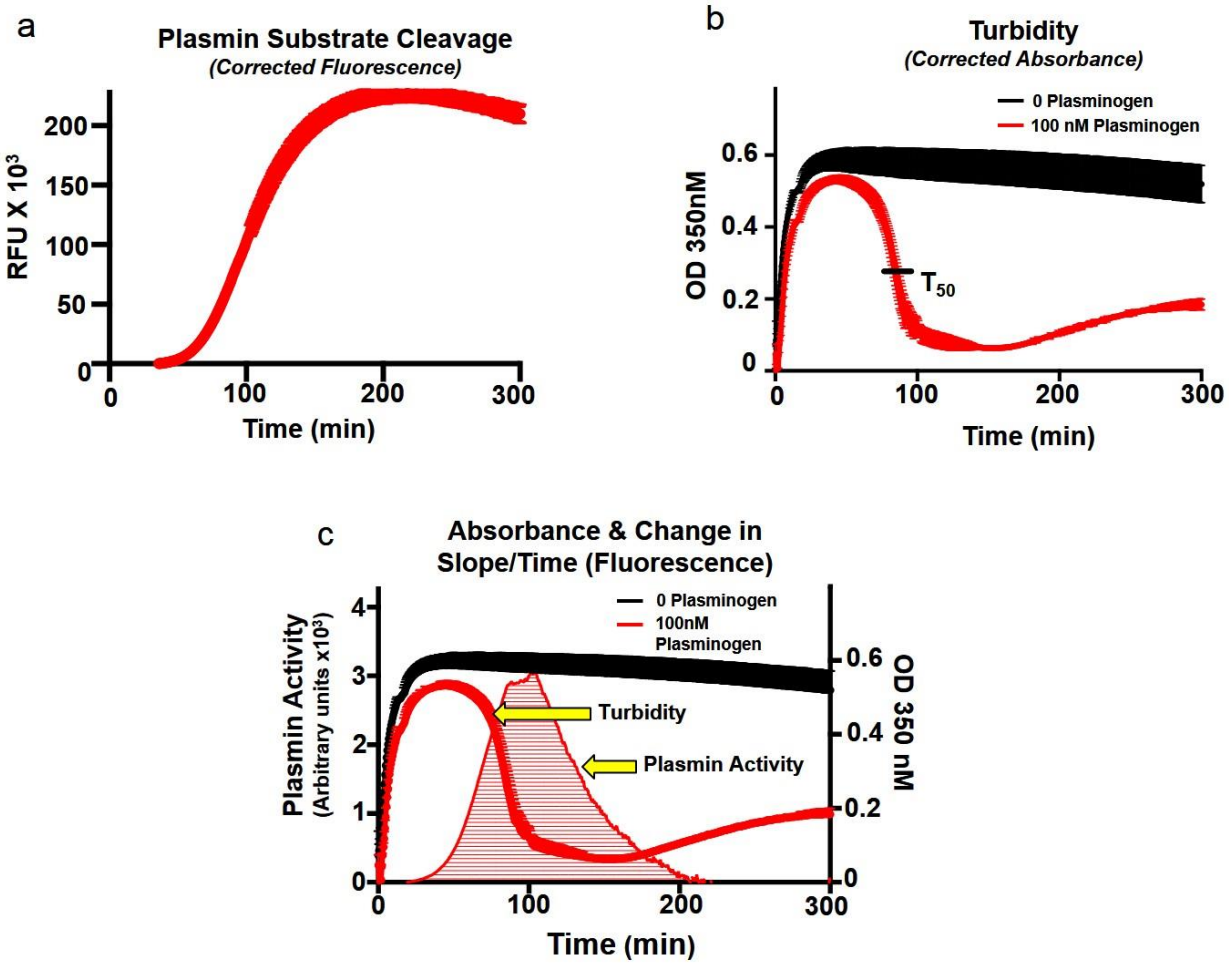

Figure 2: Simultaneous Turbidity and Plasmin Generation Assay (a) Using a fluorescent substrate for plasmin, plasmin activity is quantified by measuring plasmin substrate relative fluorescence units (RFU). **(b)** Thrombin-induced fibrin clot formation is represented by a rapid increase in turbidity. Subsequent clot lysis occurs in the presence of functioning plasmin, and is represented by a decrease in turbidity. Time to reach half maximal OD (T_{50}) is marked on the 100nm plasminogen well and is used to quantify clot lysis time. **(c)** The first derivative (change in slope/time) of the RFU curve was used to calculate the velocity of plasmin generation and graphed alongside the turbidity. The area under the curve (shaded) of the velocity curve was then determined and used to express plasmin activity units.

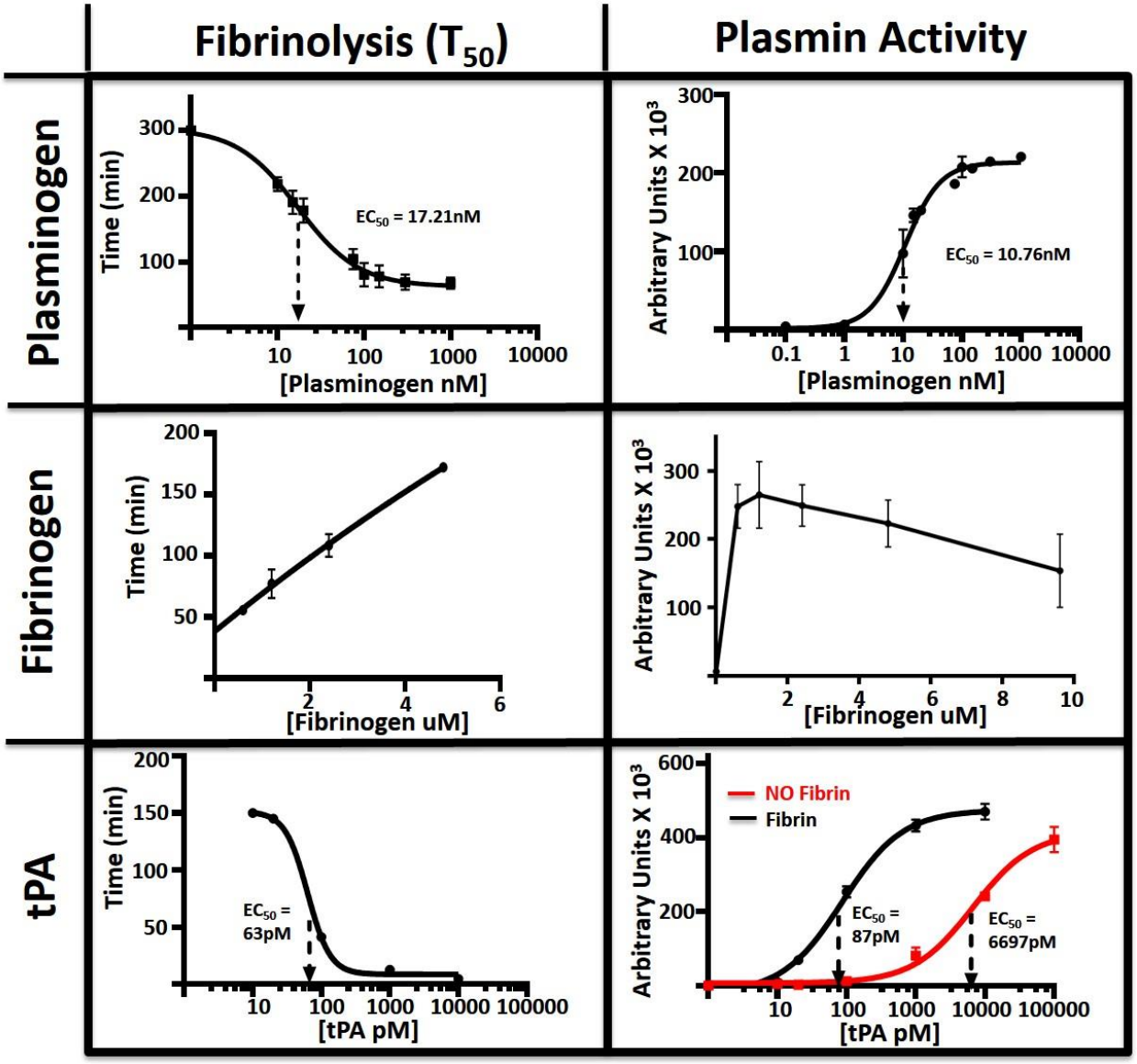

Figure 3: Fibrinolysis is dependent on the concentration of plasminogen, fibrinogen, and tPA in the simultaneous turbidity and plasmin generation assay. Optimal concentrations were determined to yield high sensitivity in physiologically relevant ranges. a) Increasing concentrations of plasminogen in the presence of 2.4uM fibrinogen, and 70pM tPA increases the amount of plasmin activity and enhances fibrinolysis (T_{50}). b) In the presence of 100nM plasminogen and 70pM tPA, fibrinogen catalyzes the conversion of plasminogen to plasmin in a biphasic manner with maximum plasmin generation occurring at 1.2uM fibrinogen. Fibrinolysis (T_{50}) is delayed as the fibrinogen concentration increases. c) Increasing concentrations of tPA in the presence of 100nM plasminogen and 2.4 uM fibrinogen increases plasminogen activation and enhances fibrinolysis (T_{50}). Additionally, in the absence of fibrinogen (and thus no fibrin clot) (red line), tPA concentrations greater than 100pM were capable of converting plasminogen to plasmin in a concentration dependent manner.

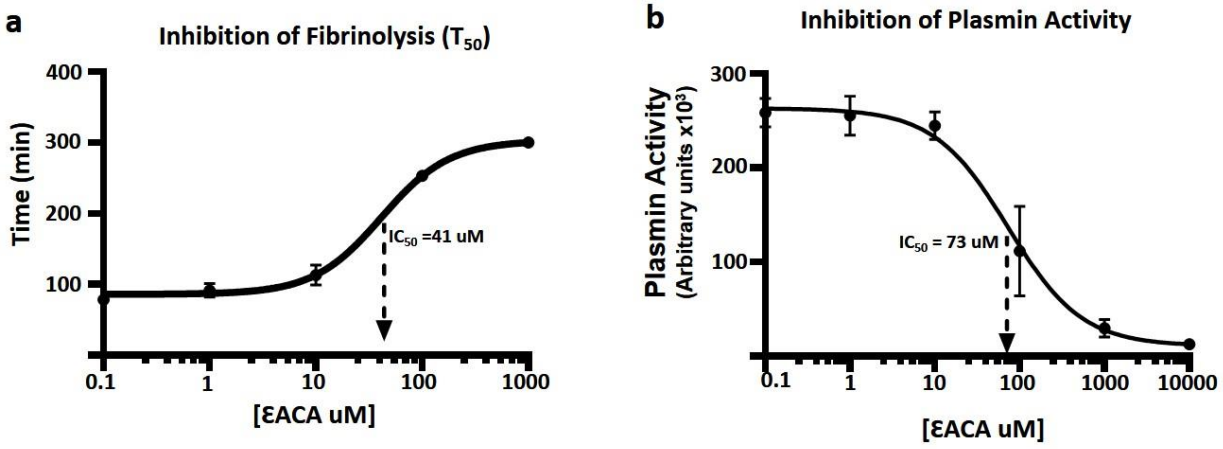

Figure 4: Plasmin inhibition and delayed fibrinolysis is detected. Aminocaproic acid exhibits a concentration-dependent inhibition of **(a)** fibrinolysis (T_{50}) and **(b)** plasmin activity in the presence of 2.4uM fibrinogen, 100nM Plasminogen and 70pM tPA. Error bars represent the standard error of the mean of n=2 experiments.

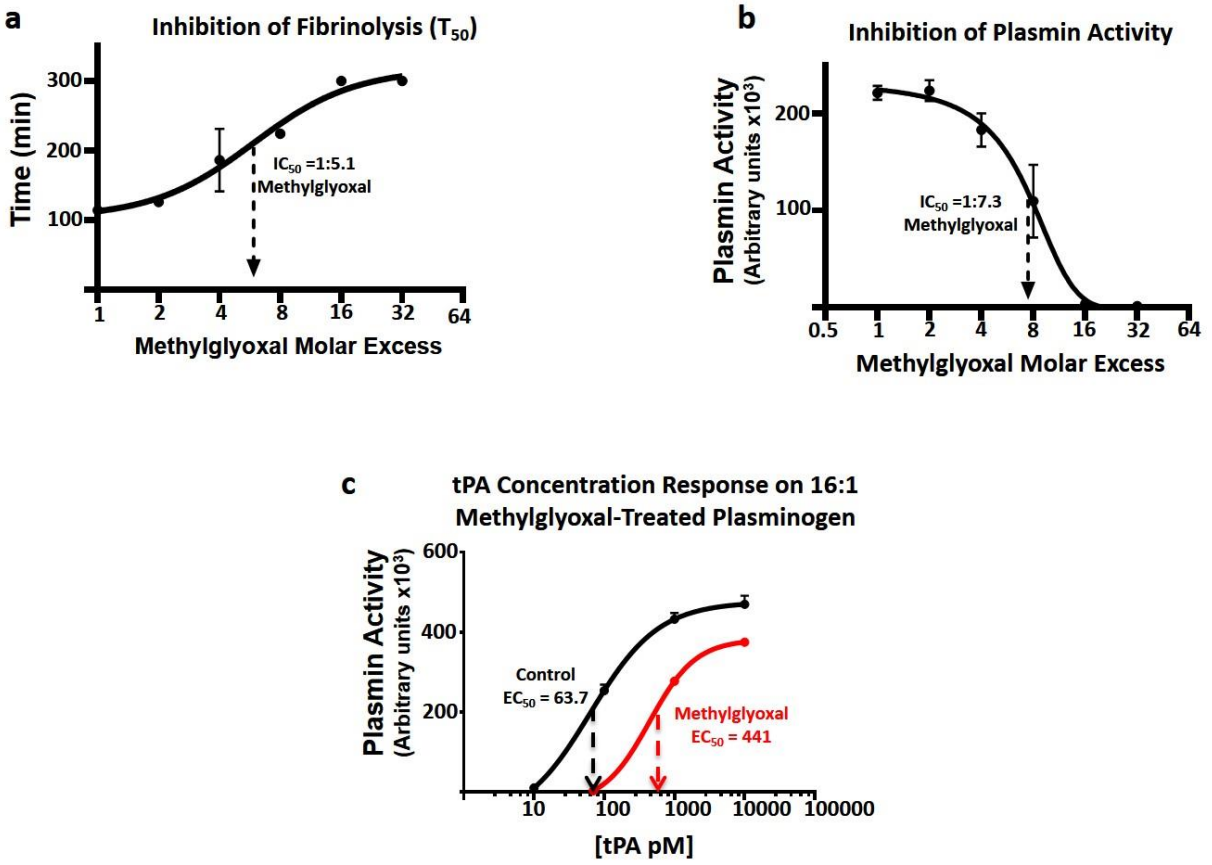

Figure 5: Methylglyoxal inhibits fibrinolysis, inhibits plasmin activity, and impairs fibrin-dependent tPA-mediated activation of plasminogen. a) After treating plasminogen with methylglyoxal for 24 hrs, fibrinolysis is inhibited in a concentration-dependent manner. b) After treating plasminogen with methylglyoxal for 24 hurs, plasmin activity is inhibited in a concentration-dependent manner. c). Methylglyoxal-treated plasminogen (at molar ratio of 16:1) is activated when tPA concentrations are at levels that do not require fibrin for plasminogen activation (>100pM tPA), but the maximal plasmin activity is still reduced in methylglyoxal-treated plasminogen compared to control plasminogen.

Methylglyoxal Impairs Plasminogen Activation. To confirm that plasminogen treatment with methylglyoxal at a 16:1 molar ratio modified plasminogen in a manner that impaired its activation, we performed a gel shift assay in which methylglyoxal-treated plasminogen and untreated control plasminogen were incubated with 1uM of tPA. After 24 hours in the presence of tPA, methylglyoxal-treated plasminogen showed bands at molecular weights of both plasminogen and plasmin, indicating that a population of plasminogen was not activated. In contrast, the untreated control plasminogen incubated with tPA resulted in single band at the molecular weight of plasmin, indicating that all plasminogen had been converted to the active form, plasmin (Figure 6). These results demonstrate that methylglyoxal can render plasminogen incapable of being activated.

Methylglyoxal Impairs Plasminogen Binding. Physiologic activation of plasminogen by tPA requires that both plasminogen and tPA bind to lysine residues on a fibrin matrix, allowing for plasminogen and tPA to be co-localized, resulting in plasminogen activation. Using a lysine-sepharose affinity column to simulate lysine residues on a fibrin matrix, we examined whether the ability of plasminogen to bind lysine residues was impaired by methylglyoxal treatment. These data demonstrate that during loading of methylglyoxal-treated plasminogen onto the lysine column an increase in absorbance was detected in fractions 5-10, indicating that a population of the methylglyoxal-treated plasminogen was unable to bind the column (Figure 7). The remaining methylglyoxal-treated plasminogen and control untreated plasminogen were eluted from the column in fractions 32-50.

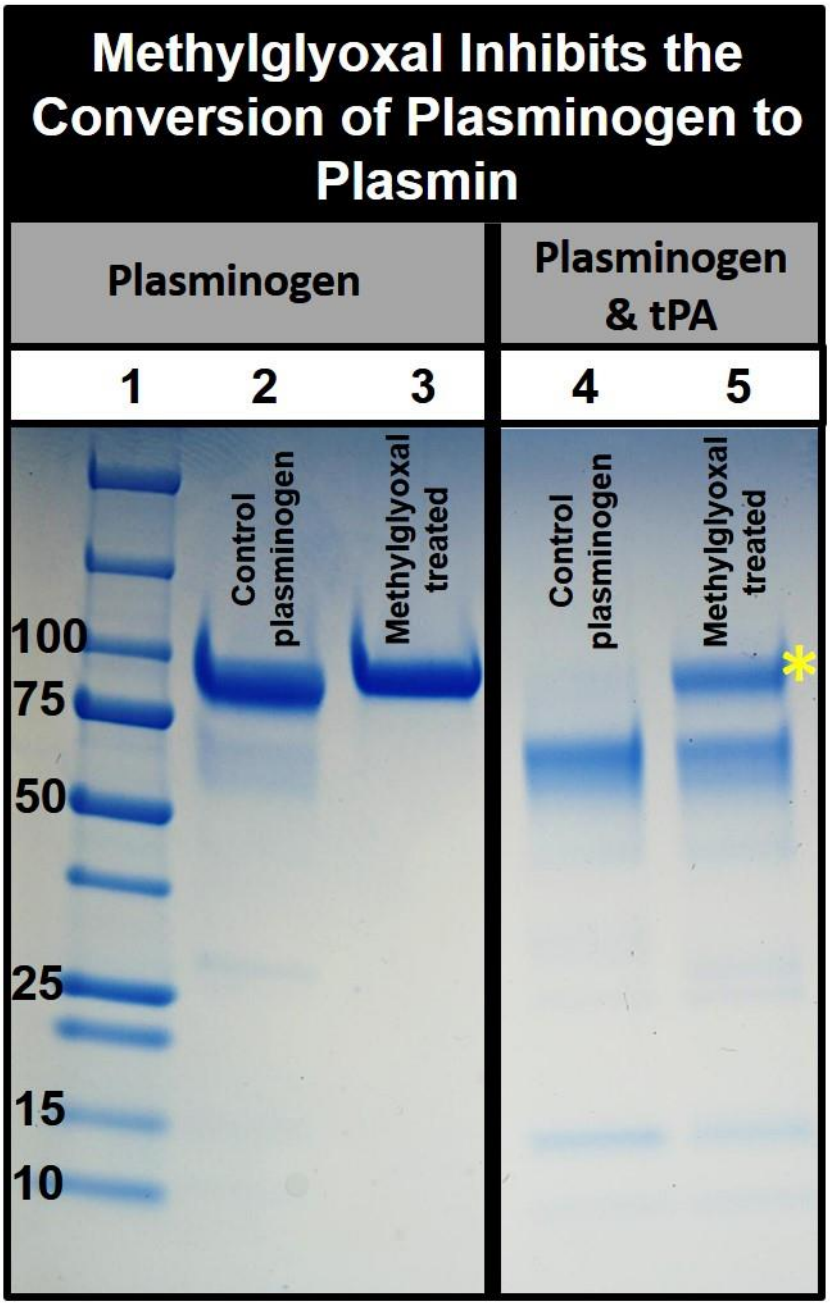

Figure 6: Methylglyoxal Inhibits the Conversion of Plasminogen to Plasmin. Control plasminogen (lanes 2 & 4) and methylglyoxal-treated plasminogen (at molar ratio of 16:1; lanes 3 & 5) were incubated in the presence and absence of 1uM tPA for 24 hours and samples were run on a 6% acrylamide gel under reducing conditions stained with simple blue to identify the presence of plasminogen and plasmin bands. When incubated with tPA, a large band is still evident at that molecular weight of plasminogen in the methylglyoxal-treated plasminogen (yellow asterisk, lane 5), representing a population of methylglyoxal-treated plasminogen that could not be converted to plasmin. In the untreated control plasminogen (lane 4), a single band is evident, indicating that all plasminogen was converted to plasmin in the presence of tPA. Lane 1 contains Precision Plus Protein Standard (molecular weights are noted next to the bands in KD).

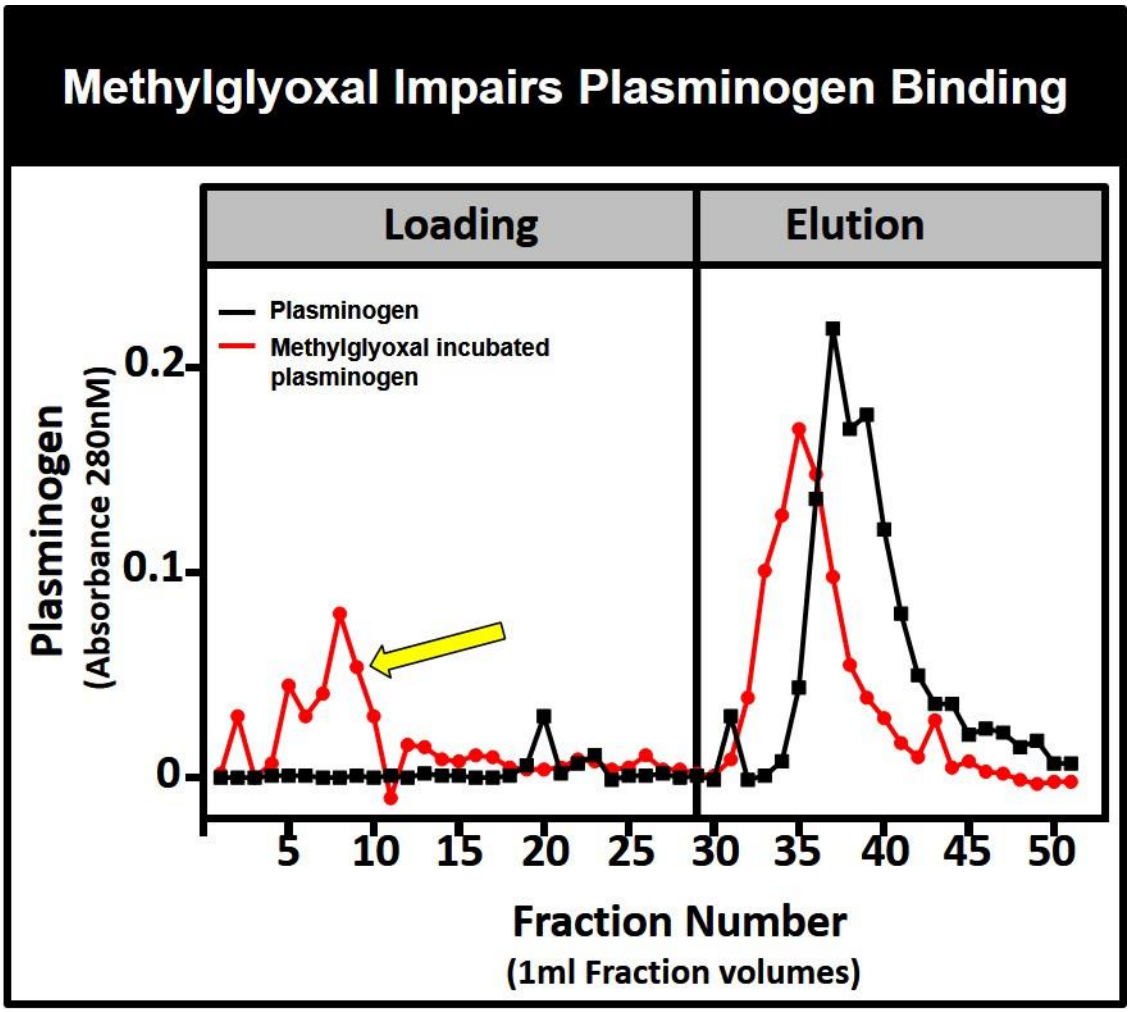

Figure 7: Methylglyoxal Impairs Plasminogen Binding. 280nm absorbance of 1ml fractions from control plasminogen and methylglyoxal-treated plasminogen (at a molar ratio of 16:1 for 24hrs) were loaded (fractions 1-29) onto a lysine sepharose column and eluted (fractions 29-51). The yellow arrow denotes a population of methylglyoxal-treated plasminogen that was unable to bind to column.

Summary and Interpretation

Our findings reveal that methylglyoxal, an ROS previously reported to be elevated in diabetics, is capable of modifying plasminogen results in decreased activation and impaired fibrinolytic activity (24, 28-30). These functional changes occur primarily through two mechanisms: adduction to amino acids critical for binding fibrin and adduction to amino acids at the plasminogen activation/cleavage. Though other investigations have demonstrated that plasminogen can be adducted by ROS such as methylglyoxal (31), this is the first study to confirm that methylglyoxal's inhibitory action on plasminogen occurs in a concentration-dependent manner, not only through adduction of plasminogen binding domains, but also through adduction of Arg-561, an essential residue for plasmin activation. Together, along with other investigations of impaired fibrinolysis in diabetic patients, our data supports the hypothesis that elevated ROS in diabetics can modify plasminogen, resulting in an acquired hypofibrinolytic state.

Previous investigations have shown that diabetics have elevated levels of reactive oxidative species (ROS) that correlate with levels hyperglycemia, which are capable of modifying proteins through adduction of exposed amino acids (20, 19). Additionally, studies have reported an acquired hypofibrinolytic state in diabetics associated with hyperglycemia. Given these associations and that fibrinolysis and plasminogen have been shown to be essential for the reparative process in a variety of injury systems (12-14, 32-34), much investigation is now focused on the etiology of the acquired hypofibrinolytic state in diabetic patients. Plasma analysis of DM2 patients has demonstrated a significant elevation in the fibrinolytic activation inhibitor PAI-1. Therefore, it has been postulated that hypofibrinolysis is the result of this elevation (17). Our data demonstrates as a proof of concept that an impaired fibrinolytic system may also occur in patients with DM2 through ROS modification. This hypothesis is further supported by investigations demonstrating that: 1) in poorly controlled type

1 diabetics, plasminogen is indeed post-translationally modified resulting in decreased plasmin activity and these modifications are associated with glycemic control (30) and 2) increased ROS levels, specifically methylglyoxal, have been demonstrated to occur in patients with DM2 (22, 23, 28). However, future studies are needed to determine if ROS adduction of plasminogen imposes an acquired hypofibrinolytic state that impairs tissue regeneration and is associated with clinical manifestations in patients with DM2. The execution of these studies poses some significant technical challenges. Specifically, our finding that a portion of adducted plasminogen does not bind lysine sepharose columns used during affinity chromatography, a common technique used to isolate plasminogen from plasma, is likely to miss a portion of the adducted plasminogen. To overcome this limitation, antibodies either specific to methylglyoxal adductions or antibodies capable of binding adducted plasminogen must be used in the purification of plasminogen from plasma.

Plasminogen is not the only component of the fibrinolytic system that could be affected by ROS adduction and thus capable of contributing to in an acquired deficiency in fibrinolysis. Fibrinogen, which circulates in adults at a concentration of 4 mg/ml, the second highest protein concentration in our blood, contains many lysine and arginine residues susceptible to ROS adduction (35). Supporting this hypothesis, *in vivo* investigations have demonstrated that fibrinogen is susceptible to methylglyoxal adduction (36). Given its long half-life in plasma, it is likely that fibrinogen is exposed to ROS in plasma and that once adducted, fibrinogen would remain in the circulation. However, future investigations are needed to examine the functional impact of ROS adducted fibrinogen on fibrinolysis in patients with DM2.

In addition to the clinical implications of our findings, this study also demonstrates that both fibrinolysis and plasmin generation can be measured simultaneously. Using near physiologic concentrations of activators, we were able to initiate the conversion of plasminogen to plasmin. The use of these concentrations more closely replicates *in vivo* fibrinolysis and made our assay dependent upon the co-localization of tPA and plasminogen on exposed lysine

residues generated during the formation of the fibrin clot. This interdependence of both the activator and plasminogen on fibrin for co-localization may prove invaluable for screening of new anti-fibrinolytic drugs designed to control bleeding, or may be used to assess the utility of new pharmacological strategies aimed at preventing the formation of or modulating the stability of a fibrin clot.

The results presented in this investigation demonstrate that ROS, such as methylglyoxal, are capable of modifying plasminogen in a concentration dependent manner that decreases plasminogen binding, activation, and function. Future studies will have to determine if an association exists between ROS modified plasminogen and the impaired musculoskeletal regeneration phenotype observed in DM2 patients and if this plasminogen modification has a functional impact on musculoskeletal healing.

Materials and Methods

Glu-plasminogen-1 was purified from human plasma by lysine-sepharose column and provided by the Bock Lab (Vanderbilt University). Human fibrinogen depleted of plasminogen was purchased from Enzyme Research Laboratories (South Bend, IN). Recombinant human tissue-type Plasminogen Activator (tPA) was purchased from Merck KGaA (Darmstadt, Germany). Bovine thrombin was purchased from King Pharmaceuticals (Bristol, TN). The fluorescent plasmin substrate (H-D-Val-Leu-Lys-AFC) was purchased from AnaSpec, Inc (Fremont, CA). ε-Aminocraproic acid (εACA) was purchased from American Regent, Inc. (Shirley, NY). Methylglyoxal solution was purchased from Sigma-Aldrich (St. Louis, MO). $CaCl_2$ was purchased from Sigma-Aldrich (St. Louis, MO). All experiments were carried out on 96-well

plates purchased from Corning Inc. (Corning, New York). Experiments were read using a BioTek Synergy2 Luminescence Micro-plate Reader (Winooski, VT). All data analysis, calculations, and statistics were performed Graphpad Prism 5.

Plasminogen Purification: 25 units of human plasma were added to an 8L flask and warmed to 30 Celsius. H-D-Phe-Phe-Arg-chloromethylketone 1μM (FFR-CK), H-D-Phe-Pro-Arg-chloromethylketone (FPR-CK) 1μM, and phenylmethylsulfonyl fluoride (PMSF) 144μM were added to the plasma and allowed to stir in for 20 mins. Plasma was then centrifuged at 2796 RFC for 20 mins to remove any clots or precipitants and then loaded onto a Lysine sepharose column at room temperature followed by 2L of start buffer (0.15M NaH_2PO_4, 3mM EDTA, 0.02% NaN_3 pH 7.4) until the absorbance at 280nm was stable below 0.05. The column was then eluted with 1L of step buffer (0.3M NaH_2PO_4, 200 mM εACA, 3mM EDTA, 0.02% NaN_3 pH 7.4) collecting 15 ml fractions. Fraction absorbance was measured at 280 nm and all samples with a large amount of protein were pooled. Again, 1 μM FFR-CK, 1 μM FPR-CK, and 144 μM PMSF were added to the plasma and the pooled samples were dialyzed vs. 24L of start buffer with 4 changes. After dialysis the sample was again loaded onto a lysine sepharose column equilibrated at 4^0C followed by the addition of 2L of start buffer until the absorbance at 280 nm of the fractions was zero or stable. Plasminogen was eluted off the column using a 2 liter gradient consisting of 1liter of start buffer and 1 liter of limit buffer (0.3M NaH_2PO_4, 3mM εACA, 3mM EDTA, 0.02% NaN_3 pH 7.4). Fractions were again read at 280nm with the first peak of protein being Glu plasminogen-1 and the second peak being Glu Plasminogen-2. The plasminogen was concreted down using a centrifugal filter with a molecular weight cut off of 10,000 Daltons (Amicon). The sample was then dialyzed vs 12L of storage buffer storage buffer (50mM HEPES, 0.125M NaCl, pH 7.4) with 3 changes.

Inhibition of Plasminogen Activation by Reactive Oxygen Species: Methylglyoxal treatments were carried out in 50 mM Hepes, 125mM NaCl, pH 7.4 buffer. 20 uM Glu-plasminogen 1 treated with Methylglyoxal at physiologic and supraphysiologic molar ratios of:

1:1, 2:1, 4:1, 8:1, 16:1, and 32:1 corresponding to 20uM, 40uM, 80uM, 160uM, 320uM, 640uM for 24 hours at 37°C. Plasminogen that was treated with phosphate buffered saline under the same conditions served as control plasminogen for all experiments.

LC-Coupled Tandem Mass Spectrometry: 20 uM Plasminogen and 20 uM of methylglyoxal treated Plasminogen (16:1 molar ratio) was diluted with 100 mM ammonium bicarbonate, treated with 1 µL of 50 mM TCEP for 30 min, followed by 1 µL of 100 mM iodoacetamide to carbamidomethylate Cys residues. Plasminogen was then digested with 200ng of trypsin overnight at 37 °C. Plasminogen digestions were then acidified to 0.1% formic acid. For analysis of each protein digest by LC-coupled tandem mass spectrometry (LC-MS/MS), peptides were loaded onto a capillary reverse-phase analytical column (360 µm o.d. × 100 µm i.d.) using an Eksigent NanoLC Ultra HPLC and autosampler. The analytical column was packed with 20 cm of C18 reversed-phase material (Jupiter, 3 µm beads, 300 Å, Phenomenex), directly into a laser-pulled emitter tip. Peptides were gradient-eluted over a 90-minute gradient at a flow rate of 500 nL/min. The mobile phase solvents consisted of water containing 0.1% formic acid (solvent A) and acetonitrile containing 0.1% formic acid (solvent B). Gradient-eluted peptides were mass analyzed on anmass spectrometer (Thermo Scientific), equipped with a nanoelectrospray ionization source. The instrument was operated using a data-dependent method with dynamic exclusion enabled. Full-scan spectra were acquired with the Orbitrap (resolution 60,000), and the top 16 most abundant ions in each MS scan were selected for fragmentation by collision-induced dissociation (CID) in the LTQ Velos ion trap in a data-dependent fashion, with dynamic exclusion enabled. For identification of plasminogen peptides, tandem mass spectra were searched with Sequest (Thermo Fisher Scientific) against a human subset database created from the UniprotKB protein database (www.uniprot.org). Variable modifications of + 57.0214 on Cys (carba-midomethylation), + 15.9949 on Met (oxidation), and + 54.010565 and +72.021129 on Arg (corresponding to Methylglyoxal adducts MG-HI and MG-DH, respectively) were included for database searching. Search results were assembled using Scaffold 3.0 (Proteome

Software), and spectra acquired of plasminogen peptides of interest were inspected using Xcalibur 2.2 Qual Browser software (Thermo Scientific). Tandem mass spectra were examined by manual interrogation to validate MG-derived adducts on Arg-504 and Arg-561. Accurate mass measurements acquired in the Orbitrap were used to generate extracted ion chromatograms (XICs) for adducted peptides of plasminogen. Using a 10 ppm tolerance, the theoretical monoisotopic m/z values of the observed $[M + 3H]^{+3}$ precursor ions were used for generating XICs.

Simultaneous Turbidity Plasmin Generation Assay: A simultaneous turbidity plasmin generation assay was performed in a 96-well culture plate with black sides and a clear bottom. Each well contained Glu-plasminogen-1 100nM, tPA 70pM, fibrinogen 2.4μM, $CaCl_2$ 5mM, and fluorescent plasmin substrate 210 μM are added to a buffer composed of 50mM Hepes and 125 mM NaCl, at pH 7.4. Thrombin (0.2units/mL) was injected automatically by the Synergy 2 Microplate reader for a final volume of 200 uL. Reactions were read every 30 seconds for 5 hours. Clot generation and clot lysis was measured by absorbance (OD) at 350 nM every 30 seconds. Plasmin activity was directly monitored via fluorescent (RFU) excitation wavelength of 400 nM and emission wavelength of 508 nM. All experiments included two wells that were run in the absence of fibrin (210μM fluorescent substrate, 5 mM $CaCl^2$, 0.2units/ml thrombin, Glu-plasminogen-1 100 nM, tPA 70 pM and buffer). Additionally, another two wells served as our zero fibrinolysis control and were run in absence of plasminogen (2.4μM Fibrinogen, 70pM tissue plasmin activator, 5mM $CaCl_2$, 210 uM fluorescent substrate and buffer). As a control to ensure that the presence of in well methylglyoxal did not have an effect on the assay, methylglyoxal was added to control wells containing 2.4 μM Fibrinogen 210 μM fluorescent substrate, 5mM $CaCl_2$, 0.2units/ml thrombin, Glu-plasminogen-1 100 nM, tPA 70 pM and buffer. These data demonstrated what methylglyoxal has no effect on the assay (data now shown). All data calculations were performed in GraphPad Prism 5.

Analysis of Simultaneous Turbidity & Plasmin Generation Assay: Because the fluorescent plasmin substrate has absorbance capacity at 350 nM , which is also the absorbance wavelength, used to measure turbidity, the first 2 wells of the assay plate contained no fibrinogen to determine the effect of the fluorescent substrate on absorbance at 350 nM. These background values were subtracted from all conditions to correct for this. Wells 3-4 for each assay plate contained no plasminogen and thus, the fluorescent values (RFU) obtained from these wells are used as baseline fluorescence and subtracted from each corresponding time point to account for background fluorescence in the absence of plasmin.

To determine if fibrinolysis was inhibited in the simultaneous turbidity and plasmin generation assay, clot lysis time was calculated as the T_{50} or the time to reach half-maximal OD. To determine if plasmin generation was inhibited in the simultaneous turbidity plasmin generation assay, we measured the RFU emitted from the plasmin substrate. These values were then used to calculate the rate of plasmin generation as the change in slope of RFU over time (first order derivative). The area under the curve of the plasmin generation rate (first order derivative) was then calculated and expressed as plasmin activity units.

Determination of Plasminogen, Fibrinogen, and tPA concentration dependencies and fibrin-dependent [tPA] range: Concentration response curves for plasmin activity were generated by adjusting the concentration of plasminogen, fibrinogen, and tPA in the assay. The simultaneous turbidity and plasmin generation assay was performed for a range of plasminogen (10 nM – 1 uM) plasmin activity and T_{50} were calculated. Using a log(stimulator) vs. response – variable slope curve within prism, the EC_{50} was calculated. Fibrinogen concentration response was generated with [Fibrinogen] ranging from 0.6 uM – 9.6 uM. A T_{50} was calculated for each condition in which fibrinolysis was observed. A t-PA concentration response was generated in the range from 1pM – 100nM both in the presence and absence of fibrinogen in order to determine the range of t-PA that was fibrin-dependent for plasminogen activation. Non-linear

regression curves were fit using the log(stimulator) vs. response – variable slope within Prism to determine EC50.

Inhibition of Plasminogen Activation by εACA: The sensitivity of the assay to plasminogen inhibition was validated using the known therapeutic plasminogen inhibitor εACA. The reaction was prepared as described above and final concentrations of εACA (0.1 uM -10 mM) were added just prior to starting the reaction. A log(inhibitor) vs. response curve was used to fit the inhibition response on plasmin activity and determine IC50 in Prism. T_{50} was calculated for those concentrations in which fibrinolysis occurred.

Plasminogen binding studies on methylglyoxal-treated plasminogen: Plasminogen binding studies were conducted using a 5 ml lysine sepharose column. 2 mg of control plasminogen or plasminogen treated with methylglyoxal (molar ratio of 16

;1) were loaded on to the column and 1 ml fractions were collected at a flow rate of 1 ml/min continuously adding a phosphate buffer (0.15 M NaH_2PO_4, 3 mM EDTA, 0.02% NaN_3 pH 7.4) continually. Fractions 1-28 were collected during loading and fractions 29-51 were collected after the addition of limit buffer to elute the plasminogen. Protein levels were determined by absorbance at 280 nM on a Synergy 2 Microplate reader. The background absorbance of the both the phosphate buffer and the limit buffer were subtracted from their respected fractions.

Plasminogen Gel Shift assays: Plasminogen gel shift assays were performed on control plasminogen and plasminogen treated with methylglyoxal (molar ratio of 16:1). Samples were incubated in the presence and absence of 1 uM tPA for 24 hours. Samples were then run on a 4-20% gradient gel under reducing conditions and stained with simple blue for identification of protein bands.

References:

1. Ginter E, Simko V. Global prevalence and future of diabetes mellitus. Advances in experimental medicine and biology. 2012;771:35-41. Epub 2013/02/09. PubMed PMID: 23393669.

2. Martins-Mendes D, Monteiro-Soares M, Boyko EJ, Ribeiro M, Barata P, Lima J, Soares R. The independent contribution of diabetic foot ulcer on lower extremity amputation and mortality risk. Journal of diabetes and its complications. 2014;28(5):632-8. doi: 10.1016/j.jdiacomp.2014.04.011. PubMed PMID: 24877985; PubMed Central PMCID: PMC4240944.

3. Reiber GE, Lipsky BA, Gibbons GW. The burden of diabetic foot ulcers. Am J Surg. 1998;176(2A Suppl):5S-10S. PubMed PMID: 9777967.

4. Rice JB, Desai U, Cummings AK, Birnbaum HG, Skornicki M, Parsons NB. Burden of diabetic foot ulcers for medicare and private insurers. Diabetes care. 2014;37(3):651-8. doi: 10.2337/dc13-2176. PubMed PMID: 24186882.

5. Marder VJ. Hemostasis and thrombosis : basic principles and clinical practice. 6th ed. Philadelphia: Wolters Kluwer/Lippincott Williams & Wilkins Health; 2013. xxiv, 1566 p. p.

6. Van de Werf F, Ludbrook PA, Bergmann SR, Tiefenbrunn AJ, Fox KA, de Geest H, Verstraete M, Collen D, Sobel BE. Coronary thrombolysis with tissue-type plasminogen activator in patients with evolving myocardial infarction. The New England journal of medicine. 1984;310(10):609-13. doi: 10.1056/NEJM198403083101001. PubMed PMID: 6537987.

7. Bugge TH, Flick MJ, Danton MJ, Daugherty CC, Romer J, Dano K, Carmeliet P, Collen D, Degen JL. Urokinase-type plasminogen activator is effective in fibrin clearance in the absence of its receptor or tissue-type plasminogen activator. Proceedings of the National Academy of Sciences of the United States of America. 1996;93(12):5899-904. PubMed PMID: 8650190; PubMed Central PMCID: PMC39159.

8. Khalil N, Corne S, Whitman C, Yacyshyn H. Plasmin regulates the activation of cell-associated latent TGF-beta 1 secreted by rat alveolar macrophages after in vivo bleomycin injury. American journal of respiratory cell and molecular biology. 1996;15(2):252-9. doi: 10.1165/ajrcmb.15.2.8703482. PubMed PMID: 8703482.

9. Roth D, Piekarek M, Paulsson M, Christ H, Bloch W, Krieg T, Davidson JM, Eming SA. Plasmin modulates vascular endothelial growth factor-A-mediated angiogenesis during wound repair. The American journal of pathology. 2006;168(2):670-84. doi: 10.2353/ajpath.2006.050372. PubMed PMID: 16436680; PubMed Central PMCID: PMC1606492.

10. Schoenecker J, Mignemi N, Stutz C, Liu Q, Edwards J, Lynch C, Holt G, Schwartz H, Mencio G, Hamm H. 2010 Young Investigator Award winner: Therapeutic aprotinin stimulates osteoblast proliferation but inhibits differentiation and bone matrix mineralization. Spine. 2010;35(9):1008-16. doi: 10.1097/BRS.0b013e3181d3cffe. PubMed PMID: 20407341.

11. Yee JA, Yan L, Dominguez JC, Allan EH, Martin TJ. Plasminogen-dependent activation of latent transforming growth factor beta (TGF beta) by growing cultures of osteoblast-like cells. Journal of cellular physiology. 1993;157(3):528-34. doi: 10.1002/jcp.1041570312. PubMed PMID: 8253864.

12. Suelves M, Lopez-Alemany R, Lluis F, Aniorte G, Serrano E, Parra M, Carmeliet P, Munoz-Canoves P. Plasmin activity is required for myogenesis in vitro and skeletal muscle regeneration in vivo. Blood. 2002;99(8):2835-44. PubMed PMID: 11929773.

13. Kawao N, Tamura Y, Okumoto K, Yano M, Okada K, Matsuo O, Kaji H. Plasminogen plays a crucial role in bone repair. Journal of bone and mineral research : the official journal of the American Society for Bone and Mineral Research. 2013;28(7):1561-74. Epub 2013/03/05. doi: 10.1002/jbmr.1921. PubMed PMID: 23456978.

14. Romer J, Bugge TH, Pyke C, Lund LR, Flick MJ, Degen JL, Dano K. Impaired wound healing in mice with a disrupted plasminogen gene. Nature medicine. 1996;2(3):287-92. PubMed PMID: 8612226.

15. Lemkes BA, Hermanides J, Devries JH, Holleman F, Meijers JC, Hoekstra JB. Hyperglycemia: a prothrombotic factor? Journal of thrombosis and haemostasis : JTH. 2010;8(8):1663-9. doi: 10.1111/j.1538-7836.2010.03910.x. PubMed PMID: 20492456.

16. Pandolfi A, Cetrullo D, Polishuck R, Alberta MM, Calafiore A, Pellegrini G, Vitacolonna E, Capani F, Consoli A. Plasminogen activator inhibitor type 1 is increased in the arterial wall of type II diabetic subjects. Arteriosclerosis, thrombosis, and vascular biology. 2001;21(8):1378-82. PubMed PMID: 11498469.

17. Schneider DJ, Sobel BE. PAI-1 and diabetes: a journey from the bench to the bedside. Diabetes care. 2012;35(10):1961-7. doi: 10.2337/dc12-0638. PubMed PMID: 22996180; PubMed Central PMCID: PMC3447837.

18. Iyer G.Y.N IDMF, Quastel J.H. Bioechemical Aspects of Phagocytosis. Nature. 1961;192:535-41. doi: 10.1038/192535a0.

19. McCord JM, Fridovich I. Superoxide dismutase. An enzymic function for erythrocuprein (hemocuprein). The Journal of biological chemistry. 1969;244(22):6049-55. PubMed PMID: 5389100.

20. Stadtman ER, Berlett BS. Reactive oxygen-mediated protein oxidation in aging and disease. Chemical research in toxicology. 1997;10(5):485-94. doi: 10.1021/tx960133r. PubMed PMID: 9168245.

21. Vincent AM, Russell JW, Low P, Feldman EL. Oxidative stress in the pathogenesis of diabetic neuropathy. Endocrine reviews. 2004;25(4):612-28. doi: 10.1210/er.2003-0019. PubMed PMID: 15294884.

22. Thornalley PJ, Hooper NI, Jennings PE, Florkowski CM, Jones AF, Lunec J, Barnett AH. The human red blood cell glyoxalase system in diabetes mellitus. Diabetes research and clinical practice. 1989;7(2):115-20. PubMed PMID: 2776650.

23. Lu J, Randell E, Han Y, Adeli K, Krahn J, Meng QH. Increased plasma methylglyoxal level, inflammation, and vascular endothelial dysfunction in diabetic nephropathy. Clinical

biochemistry. 2011;44(4):307-11. doi: 10.1016/j.clinbiochem.2010.11.004. PubMed PMID: 21126514.

24. Chaplen FW, Fahl WE, Cameron DC. Evidence of high levels of methylglyoxal in cultured Chinese hamster ovary cells. Proceedings of the National Academy of Sciences of the United States of America. 1998;95(10):5533-8. PubMed PMID: 9576917; PubMed Central PMCID: PMC20412.

25. Jacobson R, Mignemi N, Rose K, O'Rear L, Sarilla S, Hamm HE, Barnett JV, Verhamme IM, Schoenecker J. The hyperglycemic byproduct methylglyoxal impairs anticoagulant activity through covalent adduction of antithrombin III. Thrombosis research. 2014;134(6):1350-7. doi: 10.1016/j.thromres.2014.09.038. PubMed PMID: 25307422.

26. Rabbani N, Thornalley PJ. The critical role of methylglyoxal and glyoxalase 1 in diabetic nephropathy. Diabetes. 2014;63(1):50-2. doi: 10.2337/db13-1606. PubMed PMID: 24357696.

27. Oya T, Hattori N, Mizuno Y, Miyata S, Maeda S, Osawa T, Uchida K. Methylglyoxal modification of protein. Chemical and immunochemical characterization of methylglyoxal-arginine adducts. The Journal of biological chemistry. 1999;274(26):18492-502. PubMed PMID: 10373458.

28. Matafome P, Sena C, Seica R. Methylglyoxal, obesity, and diabetes. Endocrine. 2013;43(3):472-84. doi: 10.1007/s12020-012-9795-8. PubMed PMID: 22983866.

29. Han Y, Randell E, Vasdev S, Gill V, Curran M, Newhook LA, Grant M, Hagerty D, Schneider C. Plasma advanced glycation endproduct, methylglyoxal-derived hydroimidazolone is elevated in young, complication-free patients with Type 1 diabetes. Clinical biochemistry. 2009;42(7-8):562-9. doi: 10.1016/j.clinbiochem.2008.12.016. PubMed PMID: 19154730.

30. Ajjan RA, Gamlen T, Standeven KF, Mughal S, Hess K, Smith KA, Dunn EJ, Anwar MM, Rabbani N, Thornalley PJ, Philippou H, Grant PJ. Diabetes is associated with posttranslational modifications in plasminogen resulting in reduced plasmin generation and enzyme-specific activity. Blood. 2013;122(1):134-42. doi: 10.1182/blood-2013-04-494641. PubMed PMID: 23699598.

31. Lerant I, Kolev K, Gombas J, Machovich R. Modulation of plasminogen activation and plasmin activity by methylglyoxal modification of the zymogen. Biochimica et biophysica acta. 2000;1480(1-2):311-20. PubMed PMID: 10899632.

32. Ploplis VA, Carmeliet P, Vazirzadeh S, Van Vlaenderen I, Moons L, Plow EF, Collen D. Effects of disruption of the plasminogen gene on thrombosis, growth, and health in mice. Circulation. 1995;92(9):2585-93. Epub 1995/11/01. PubMed PMID: 7586361.

33. Gong Y, Zhao Y, Li Y, Fan Y, Hoover-Plow J. Plasminogen regulates cardiac repair after myocardial infarction through its noncanonical function in stem cell homing to the infarcted heart. Journal of the American College of Cardiology. 2014;63(25 Pt A):2862-72. doi: 10.1016/j.jacc.2013.11.070. PubMed PMID: 24681141; PubMed Central PMCID: PMC4074457.

34. Drixler TA, Vogten JM, Gebbink MF, Carmeliet P, Voest EE, Borel Rinkes IH. Plasminogen mediates liver regeneration and angiogenesis after experimental partial hepatectomy. The British journal of surgery. 2003;90(11):1384-90. doi: 10.1002/bjs.4275. PubMed PMID: 14598419.

35. Mosesson MW. Fibrinogen and fibrin structure and functions. Journal of thrombosis and haemostasis : JTH. 2005;3(8):1894-904. doi: 10.1111/j.1538-7836.2005.01365.x. PubMed PMID: 16102057.

36. Lund T, Svindland A, Pepaj M, Jensen AB, Berg JP, Kilhovd B, Hanssen KF. Fibrin(ogen) may be an important target for methylglyoxal-derived AGE modification in elastic arteries of humans. Diabetes & vascular disease research : official journal of the International Society of Diabetes and Vascular Disease. 2011;8(4):284-94. doi: 10.1177/1479164111416831. PubMed PMID: 21844128.

CHAPTER 8

Future Directions

The Role of Intramedullary Vascularity in Displaced Fracture Healing

My investigation into the temporal and spatial development of vascularity in a displaced fracture model has revealed for the first time that intramedullary vascularity is in direct communication with the newly forming callus. This finding was surprising given that until now, the extraosseous component of fracture callus vascularization was thought to be the primary source of new vessels to the fracture callus (1, 2). This finding raises the possibility that there is a previously unappreciated role of the intramedullary vasculature during fracture healing, as the relative contributions of the extraosseous or intraosseous vascularity have been determined. While extraosseous vascularity and the surrounding musculature likely contribute to the vascular ingrowth of the healing fracture, it would be prudent to further examine the role of intraosseous vascularity. In preliminary studies of model development, I proposed that I could occlude the intramedullary vascularity of the murine femur by filling the medullary cannel with bone wax following fracture. Radiographs taken 4 weeks post fracture demonstrated a delay in hard tissue callus formation and bridging at the fracture site (Figure 1). While these results are promising, there are confounding variables that may be affecting the development of the hard tissue callus and thus making interpretation of these results difficult. Our displaced open fracture model uses an intramedullary nail that that leaves space between the pin and cortical bone. However, the presence of bone wax surrounding the nail likely provides additional fixation to the fracture callus. This is problematic, as our laboratory has demonstrated that

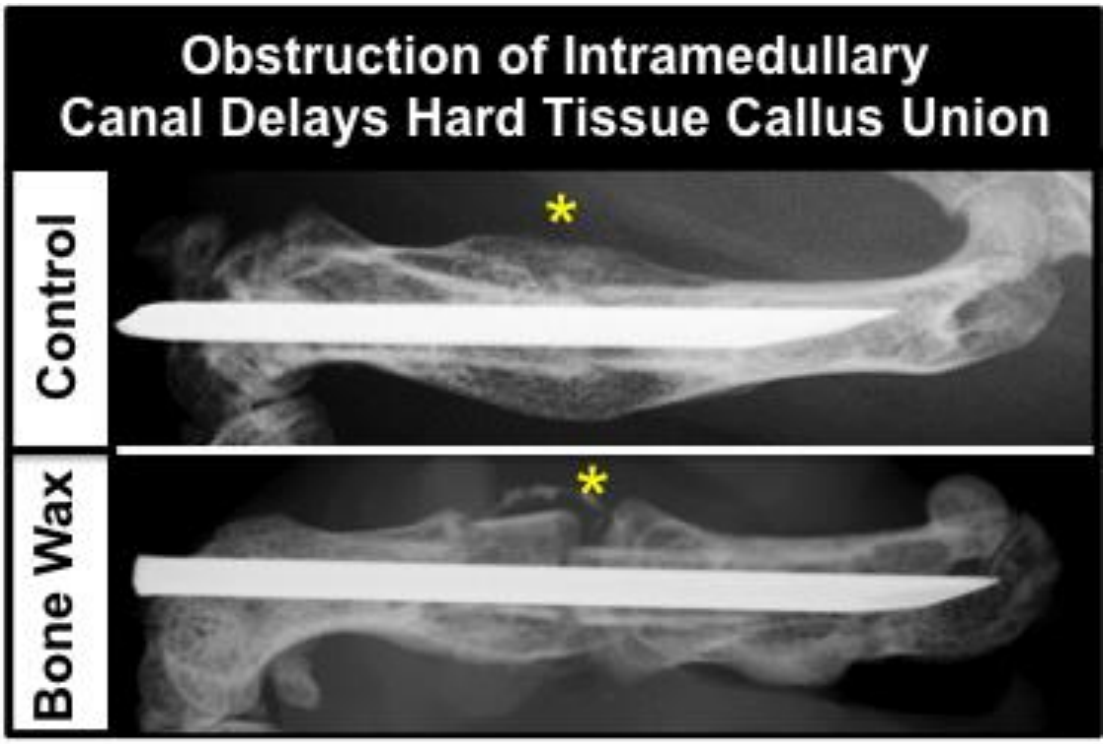

Figure 1: Obstruction of the Intramedullary Canal Impairs Hard Tissue Formation Following Fracture. Radiographs of wild type c57bl6 mice 4 weeks following the generation of a displace femur stabilized with intramedullary fixation. These data reveals while control mice have established hard tissue callus union of the fracture site (yellow asterisk) mice with bone wax placed within the intramedullary canal have delayed hard tissue callus union.

changes in fracture fixation can affect the size of the fracture callus (data not shown). To overcome this technical limitation, a different model of fracture must be used that does not rely on internal fixation. Still, it is unknown if changing the method of fixation has an impact on the temporal and spatial development of vascularity and callus formation. Preliminary studies will need to be done in order to validate our new model of fracture healing with external fixation.

In addition to being useful for determining the role of intramedullary vascularity upon fracture callus formation, the external fixation model will also be useful in evaluating the re-establishment of intramedullary vascularity following fracture. Our finding that fracture remodeling begins around the time when intramedullary vasculature is re-established leads us to postulate that fracture remodeling occurs as a result of the restoration of intramedullary vascular continuity. We propose that as normal intramedullary blood flow is re-established, periosteal shunting of the blood is reduced resulting in hypoperfusion of the fracture callus and that this is the signal for initiation of remodeling. To test this hypothesis, I would propose to prevent intramedullary vascular anastomosis by injecting bone wax into the bone proximal and distal to the fracture site after formation of the soft tissue callus but before intramedullary vascular anastomosis and evaluate the remodeling.

Mechanism and Prevention of Heterotopic Ossification

My studies examining the role of the firbinolytic system in fracture healing demonstrated that the development of heterotopic ossification (HO) in the skeletal muscle occurs adjacent to the fracture site. Discovering HO development in this model is truly novel, as this is the first time HO as been induced in preclinical models without biochemical manipulation through the addition of BMP or supraphysiologic doses of

phosphate and calcium in the presence of muscle injury (3, 4). The observation of HO in the muscle of plasminogen-deficient mice spurred me to examine whether fracture was required for HO development in muscle. For these studies, I mechanically injured the quadriceps of the mice, exposing the femur in a manner identical to our approach used to expose the femur during open fracture. Three weeks following injury, radiographic analysis of the injured muscle revealed the presence of HO (Figure 2). Further, to validate that a plasminogen deficiency resulted in the formation of HO following skeletal muscle I crossed our plasminogen-deficient mice with mice that undergo continuous, chronic muscle injury, dystrophin deficient mice (MDX) (Figure 3). These data revealed diffuse mineralization present throughout the skeletal muscles, supporting our previous results from both the mechanically and toxin-induced models of muscle injury that plasminogen is essential for preventing HO formation. Through investigations by others in our lab, we have gone on to describe in detail both the immature and mature phases of HO development during a skeletal muscle injury.

Evaluations of our HO model also led to an interesting observation: that the development of HO was associated with impairment in the invasion of F4/80 positive cells. Furthermore, previous investigations have demonstrated that plasminogen is essential for macrophage migration, that macrophages support plasmin activation (5), and that macrophages are essential for muscle healing (6-8). These findings, coupled with our own, have led me to hypothesize that deficiency in macrophage migration is a contributing factor in the development of HO. To test this hypothesis, I would deplete macrophages and monocytes from wild type mice then acutely injure the skeletal muscle and investigate the formation of immature HO. If this hypothesis were supported, I would then examine the phenotypes and function of the macrophages in the skeletal muscle of wild type mice following injury. Together, these pilot studies would provide

valuable information not only on how to prevent the formation of HO but how to possibly promote the regression of immature HO.

While fracture is not necessary for the formation of HO, bone may have a role in development of immature HO. Calcium (Ca) and Phosphate (P_i) are ubiquitous throughout or bodies, and are the principal components of cell signaling and energy transfer reactions. Additionally, Ca and P_i crystalize, forming various biological minerals such as hydroxyapatite, the principal mineral in mammalian bone. To meet metabolic demand, Ca and P_i circulate at concentrations optimal for biological function, resulting in circulating levels of these ions roughly at 10,000 times intracellular concentrations. Bone is the main reservoir for these ions, accounting for 99% of total body Ca and 85% of total body P_i (9, 10). Ca and P_i levels in blood and interstitial fluid are tightly regulated by multiple physiologic mechanisms involving the endocrine, renal, gastrointestinal, and musculoskeletal systems. These systems are integrated to maintain the ideal bioavailability of Ca and P_i necessary for physiologic function. Nonetheless, physiologic extracellular Ca and P_i concentrations are close to their solubility coefficient and can readily crystallize in soft tissue compartments (11). Such spontaneous CaP_i mineralization causes profound loss of function in tissues other than bone and teeth. Since Ca and P_i crystallize at near physiological concentrations (12), there must exist mechanisms of preventing dystrophic calcification in muscle while simultaneously allowing calcification in bone. The principal systemic mediator of muscular dystrophic calcification during homeostasis is pyrophosphate (PPi) (13, 14). Following injury, there is an increase in the bioavailability of Ca and P_i in the microenvironment of the damaged tissue from cell death and from an increased need for Ca and P_i in tissue regeneration, potentially overwhelming the PP_i system. Given that injuries associated with the development of HO, such as burn, blast and spinal cord injury, all stimulate robust bone turnover (15, 16) we hypothesize that metabolic bone activity contributes to the

formation of HO by increasing the local bioavailability of Ca and P_i, thus overwhelming local and systemic protective mechanisms against calcification. In preliminary tests of this hypothesis, I injected the bisphosphonate zoledronic acid in mice with a deficiency in plasminogen and injured their muscle. I found that mice with a plasminogen deficiency treated with zoledronic acid had reduced osteoclast activity and did not develop HO, suggesting that inhibition of bone turnover may prevent the formation of HO (Figure 4). While promising, these preliminary results do not however perfectly support the hypothesis as zoledronic acid can also directly inhibit CaPi crystal formation (17). To overcome this limitation, I would injure the skeletal muscle of mice in the presence and absence of a RANKL blocking antibody, to prevent osteoclast formation and bone turnover while preserving potential crystal formation, and evaluate of the development of HO. In addition to elucidating the mechanism of action, this preliminary discovery mimics clinical observations that bisphosphonates may be useful in the prevention and spread of HO (18).

While determining the precise biochemical mechanism of how plasmin results in impaired muscle healing and HO is important, there is also the need to further investigate the potential clinical impact of these findings. I would next like to investigate the role of enhanced plasmin activity in disease models of impaired musculoskeletal skeletal healing and fibrin accumulation. Specifically, it would be prudent to investigate the effect of enhancing plasmin activity in a mouse model of diabetes, such as the leptin receptor deficient mice. These mice are ideal for investigating if modulation of plasmin activity rescues impaired healing as they have been shown to have extravascular fibrin accumulation (19), impaired muscle healing, and impaired fracture healing (20, 21) phenocopying the diabetic state. To investigate whether the enhancement of plasmin activity rescues impaired musculoskeletal healing I would take two approaches. First, I would inhibit α2 anti-plasmin, the main physiologic inhibitor of plasmin, then evaluate

muscle and fracture healing. Second, I would augment endogenous plasminogen made by the mice via IP injections of plasminogen, then investigate muscle and fracture healing. Together, these studies would provide evidence supporting the pharmacological approach that enhancement of plasmin activity can support tissue healing in conditions of chronic disease and pathologic wound healing.

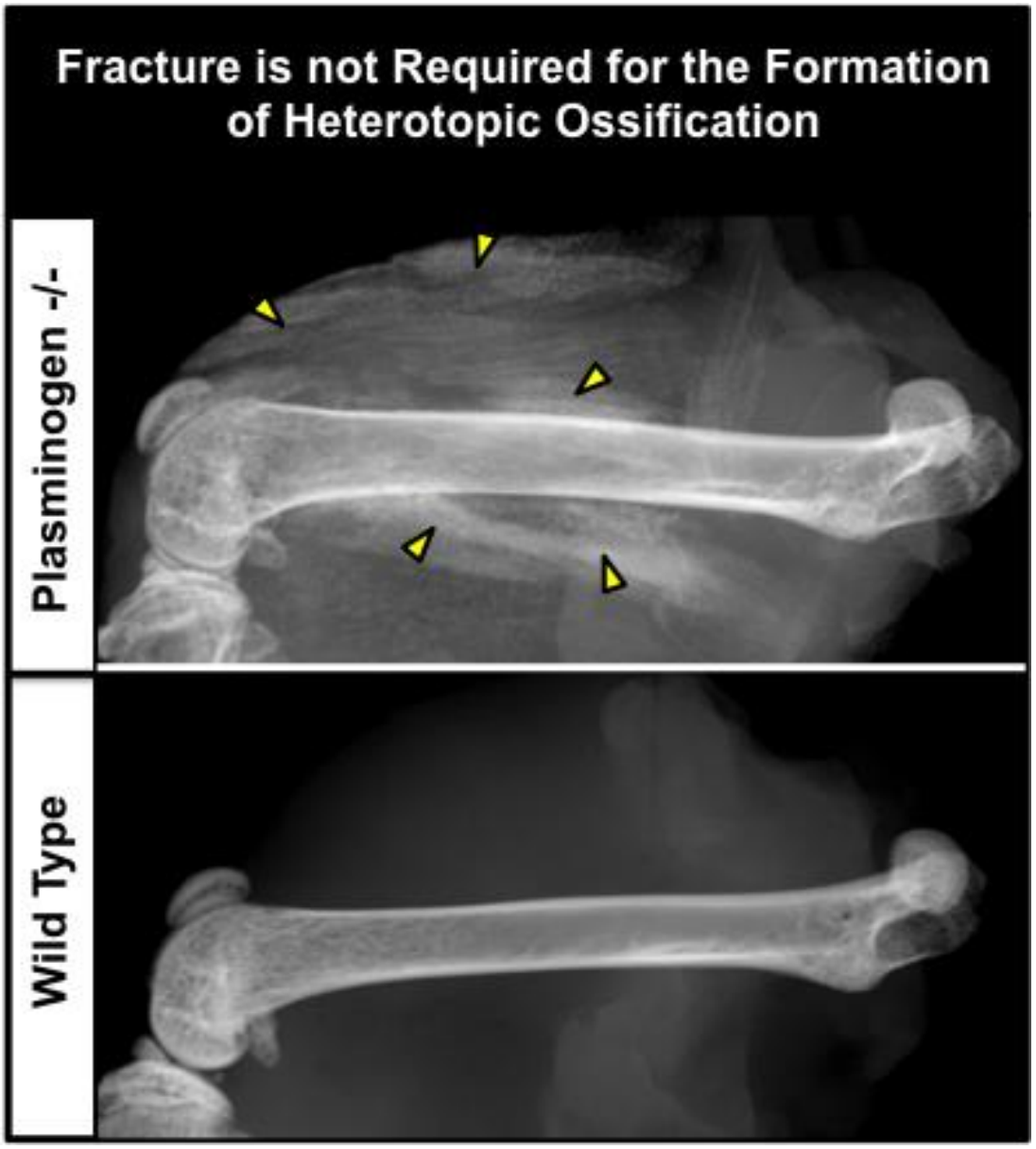

Figure 2: Fracture is not required for the development of heterotopic ossification in plasminogen deficient mice. Radiographs of plasminogen deficient mice (plasminogen -/-) and wild type mice 4 weeks following mechanically induced damage to skeletal muscle. Diffuse mineralization (yellow triangles) is clearly evident in the Plg -/- mice following injury while wild type mice show not apparent muscle mineralization

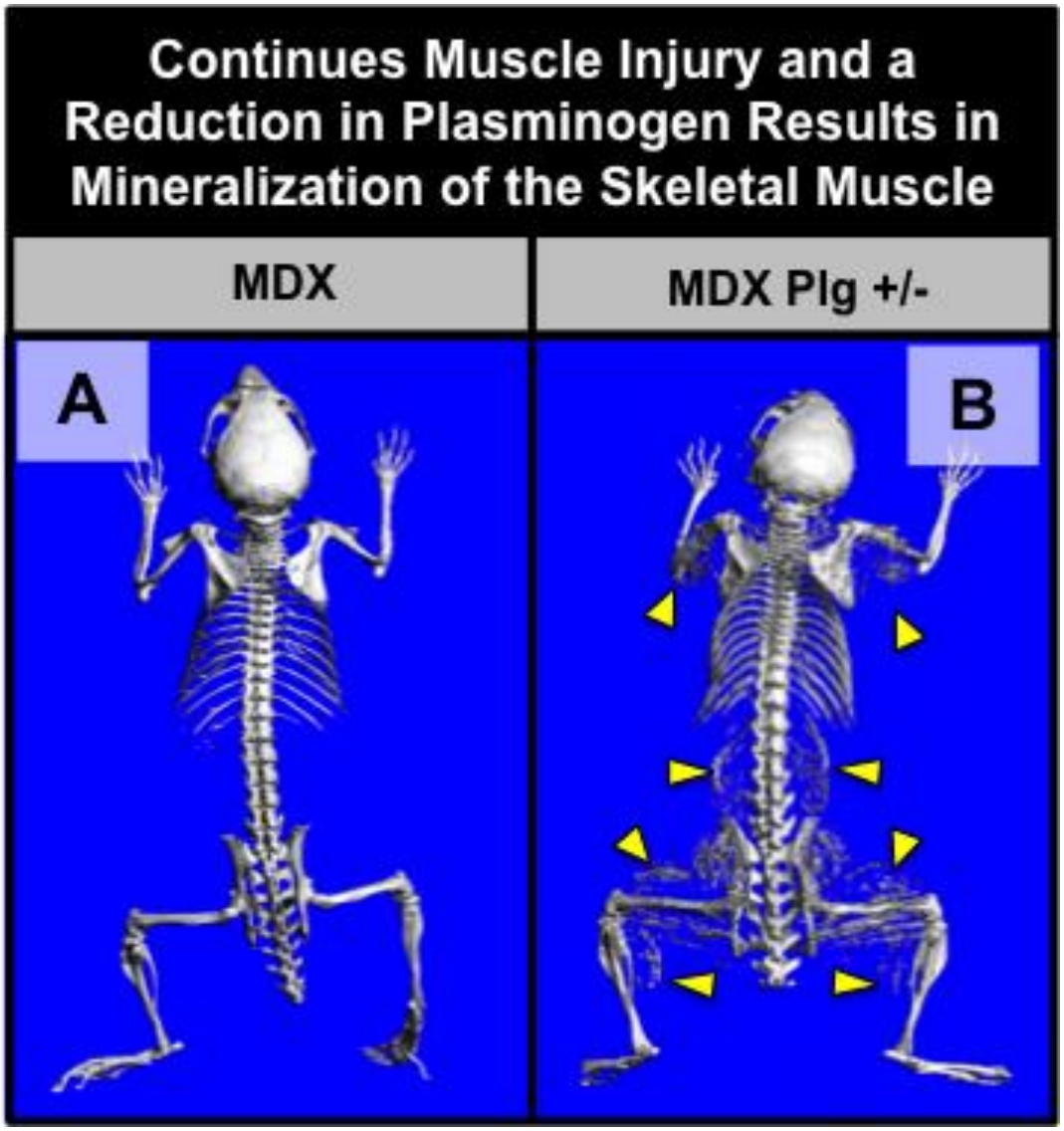

Figure 3: Continuous Muscle Injury and a Reduction in Plasminogen Results in Mineralization of the Skeletal Muscle. u-CT reconstruction of MDX mice, a model of Duchene's Muscular Dystrophy, and MDX plasminogen heterozygous (plasminogen +/-) mice which have genetic reduction in circulating plasminogen. These data demonstrate that MDX mice (A) have no apparent heterotopic ossification within their skeletal muscle. In contrast MDX plasminogen +/- mice (B) demonstrate abundant HO formation (yellow triangles) within the muscle of the mice 8 weeks after birth.

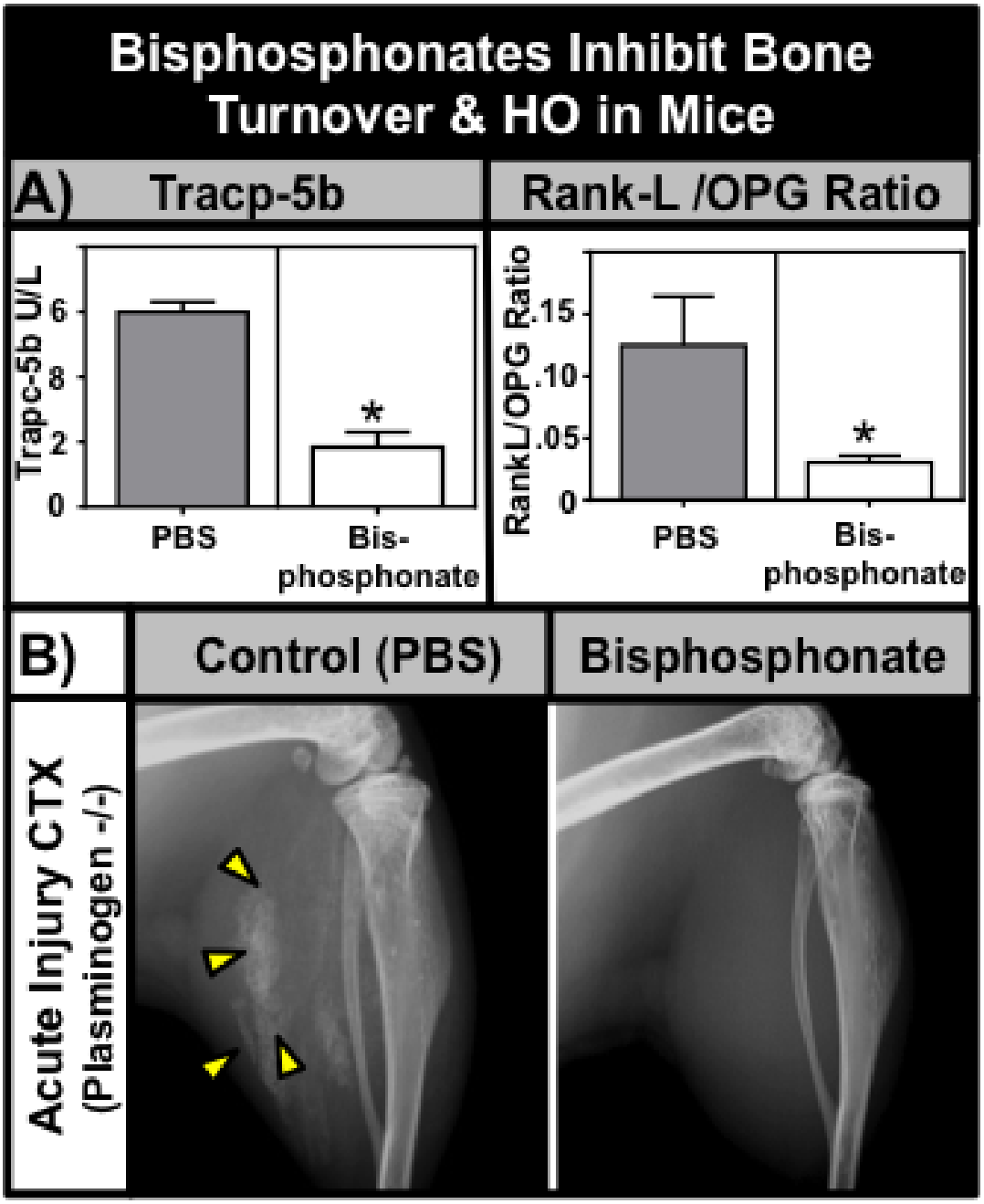

Figure 4: Bisphosphonates Inhibit Bone Turnover and Development of Heterotopic Ossification in Plasminogen Deficient Mice. Mice susceptible to developing HO (deficient in plasminogen) were treated with bisphosphonate immediately prior to muscle injury. A) Multiplex ELISA analysis 4 weeks after injury demonstrates that bisphosphonate treatment reduces bone turnover (as measured by TRACP-5b and RANKL/OPG ratio). **B)** Radiographs at 4 weeks reveal that mice injected with saline develop abundant HO (yellow triangles) whereas, despite their predisposition, mice treated with bisphosphonates do not develop HO after skeletal muscle injury.

References

1. Uhrig BA, Boerckel JD, Willett NJ, Li MT, Huebsch N, Guldberg RE. Recovery from hind limb ischemia enhances rhBMP-2-mediated segmental bone defect repair in a rat composite injury model. Bone. 2013;55(2):410-7. Epub 2013/05/15. doi: 10.1016/j.bone.2013.04.027. PubMed PMID: 23664918.

2. Morgan EF, Hussein AI, Al-Awadhi BA, Hogan DE, Matsubara H, Al-Alq Z, Fitch J, Andre B, Hosur K, Gerstenfeld LC. Vascular development during distraction osteogenesis proceeds by sequential intramuscular arteriogenesis followed by intraosteal angiogenesis. Bone. 2012;51(3):535-45. doi: 10.1016/j.bone.2012.05.008. PubMed PMID: 22617817; PubMed Central PMCID: PMC3412922.

3. Leblanc E, Trensz F, Haroun S, Drouin G, Bergeron E, Penton CM, Montanaro F, Roux S, Faucheux N, Grenier G. BMP-9-induced muscle heterotopic ossification requires changes to the skeletal muscle microenvironment. Journal of bone and mineral research : the official journal of the American Society for Bone and Mineral Research. 2011;26(6):1166-77. Epub 2011/05/26. doi: 10.1002/jbmr.311. PubMed PMID: 21611960.

4. Kikkawa N, Ohno T, Nagata Y, Shiozuka M, Kogure T, Matsuda R. Ectopic calcification is caused by elevated levels of serum inorganic phosphate in mdx mice. Cell structure and function. 2009;34(2):77-88. Epub 2009/07/23. PubMed PMID: 19622873.

5. Bryer SC, Fantuzzi G, Van Rooijen N, Koh TJ. Urokinase-type plasminogen activator plays essential roles in macrophage chemotaxis and skeletal muscle regeneration. Journal of immunology. 2008;180(2):1179-88. PubMed PMID: 18178858.

6. Segawa M, Fukada S, Yamamoto Y, Yahagi H, Kanematsu M, Sato M, Ito T, Uezumi A, Hayashi S, Miyagoe-Suzuki Y, Takeda S, Tsujikawa K, Yamamoto H. Suppression of macrophage functions impairs skeletal muscle regeneration with severe fibrosis. Experimental cell research. 2008;314(17):3232-44. doi: 10.1016/j.yexcr.2008.08.008. PubMed PMID: 18775697.

7. Wang H, Melton DW, Porter L, Sarwar ZU, McManus LM, Shireman PK. Altered macrophage phenotype transition impairs skeletal muscle regeneration. The American journal of pathology. 2014;184(4):1167-84. doi: 10.1016/j.ajpath.2013.12.020. PubMed PMID: 24525152; PubMed Central PMCID: PMC3969996.

8. Summan M, Warren GL, Mercer RR, Chapman R, Hulderman T, Van Rooijen N, Simeonova PP. Macrophages and skeletal muscle regeneration: a clodronate-containing liposome depletion study. American journal of physiology Regulatory, integrative and comparative physiology. 2006;290(6):R1488-95. doi: 10.1152/ajpregu.00465.2005. PubMed PMID: 16424086.

9. Fogelman I, Gnanasegaran G, Van der Wall H. Radionuclide and hybrid bone imaging. xiv, 1046 pages p.

10. Pozzan T, Rizzuto R, Volpe P, Meldolesi J. Molecular and cellular physiology of intracellular calcium stores. Physiological reviews. 1994;74(3):595-636. Epub 1994/07/01. PubMed PMID: 8036248.

11. Eidelman N, Chow LC, Brown WE. Calcium phosphate saturation levels in ultrafiltered serum. Calcified tissue international. 1987;40(2):71-8. PubMed PMID: 3105836.

12. Driessens FC, Verbeeck RM, van Dijk JW, Borggreven JM. Degree of saturation of blood plasma in vertebrates with octocalcium phosphate. Zeitschrift fur Naturforschung C, Journal of biosciences. 1988;43(1-2):74-6. PubMed PMID: 3376518.

13. Fleisch H, Russell RG, Straumann F. Effect of pyrophosphate on hydroxyapatite and its implications in calcium homeostasis. Nature. 1966;212(5065):901-3. Epub 1966/11/26. PubMed PMID: 4306793.

14. Fleisch H, Maerki J, Russell RG. Effect of pyrophosphate on dissolution of hydroxyapatite and its possible importance in calcium homeostasis. Proceedings of the Society for Experimental Biology and Medicine Society for Experimental Biology and Medicine. 1966;122(2):317-20. Epub 1966/06/01. PubMed PMID: 4292457.

15. Cipriano CA, Pill SG, Keenan MA. Heterotopic ossification following traumatic brain injury and spinal cord injury. The Journal of the American Academy of Orthopaedic Surgeons. 2009;17(11):689-97. PubMed PMID: 19880679.

16. Forsberg JA, Davis TA, Elster EA, Gimble JM. Burned to the bone. Science translational medicine. 2014;6(255):255fs37. doi: 10.1126/scitranslmed.3010168. PubMed PMID: 25253672.

17. Russell RG. Bisphosphonates: the first 40 years. Bone. 2011;49(1):2-19. doi: 10.1016/j.bone.2011.04.022. PubMed PMID: 21555003.

18. Schuetz P, Mueller B, Christ-Crain M, Dick W, Haas H. Amino-bisphosphonates in heterotopic ossification: first experience in five consecutive cases. Spinal cord. 2005;43(10):604-10. doi: 10.1038/sj.sc.3101761. PubMed PMID: 15867938.

19. Sumi A, Yamanaka-Hanada N, Bai F, Makino T, Mizukami H, Ono T. Roles of coagulation pathway and factor Xa in the progression of diabetic nephropathy in db/db mice. Biological & pharmaceutical bulletin. 2011;34(6):824-30. PubMed PMID: 21628879.

20. Macey LR, Kana SM, Jingushi S, Terek RM, Borretos J, Bolander ME. Defects of early fracture-healing in experimental diabetes. The Journal of bone and joint surgery American volume. 1989;71(5):722-33. Epub 1989/06/01. PubMed PMID: 2659600.

21. Nguyen MH, Cheng M, Koh TJ. Impaired muscle regeneration in ob/ob and db/db mice. TheScientificWorldJournal. 2011;11:1525-35. doi: 10.1100/tsw.2011.137. PubMed PMID: 21805021.

CHAPTER 9

Therapeutic Implication

Clinical Hypofibrinolysis

The results of these investigations clearly demonstrate the essential nature of fibrinolysis in musculoskeletal healing, as well as reveal new questions regarding the role of the fibrinolysis and vascularity in musculoskeletal repair. Given these findings, it is important to also understand the implications and underlying causes of clinical deficiencies of fibrinolysis. Patients become deficient in fibrinolysis through two main mechanisms: 1) they are born with a genetic deficiency in plasminogen, or 2) they acquire a deficiency in fibrinolysis in disease states or trauma.

Genetic mutations in plasminogen are classified into two categories: 1) those with no detectable antigen levels for plasminogen but may have limited plasmin activity, called hypoplasminogenmia; and 2) those with normal antigen levels but little to no plasmin activity, called dysplasminogenemia (1-3). Genetic deficiencies in plasminogen and the resulting hypofibrinolytic state are associated with development of ligneous conjunctivitis, periodontal diseases such as ligneous gingivitis, and impaired skin wound healing (2-4). Additionally, patients with a genetic deficiency in plasminogen have been shown to accumulate fibrin at the site of injury as in our investigations (3, 5). However while fibrin accumulation has been noted in their extravascular tissue, neither patients with hypoplasminogenmia or dysplasminogenemia have an elevated risk for thrombosis

(6, 7). However, it remains difficult to study hypoplasminogenmia and dysplasminogenemia because of it is exceedingly rare (1.6 in every 100,000,000 births) (8). As a result of the low prevalence of plasminogen deficiency in the population it is likely that additional associated phenotypes are yet to be determined. Further, there is also an incomplete understanding of the impact of heterozygous plasminogen deficiency, which has a much higher prevalence (2.9 per every 1000). These patients are asymptomatic under physiologic conditions, but during times of injury may manifest complications due to reduced plasminogen activity (7). Further studies are warranted to determine if and how genetic deficiencies in plasminogen and their resulting impairment of the fibrinolytic system contribute to the pathogenesis of disease and impaired healing following injury.

An acquired deficiency in fibrinolysis can also occur in disease states. As discussed in chapter 7, patients with diabetes are known to be hypofibrinolytic (9, 10). Impairment in fibrinolysis has also been linked to various common pathologies such as: muscular dystrophy, cardiovascular disease, renal disease, and pre-eclampsia (11-14). Additionally, deficiencies in fibrinolysis also occur in critically ill patients and those whom have undergone trauma (15-18). These deficiencies occur through a multitude of mechanisms including: overexpression of plasminogen activator inhibitors (12), consumption and or decreased expression of fibrinolytic factors (19), and modification of plasminogen (20). Given our findings of the crucial nature of fibrinolytic system in musculoskeletal repair (Chapter 6) and numerous other supportive investigations demonstrating the essential nature of fibrinolysis in injuries of other organ systems (21-28), enhancement of the fibrinolytic system presents itself as a novel therapeutic target for promoting healing through the promotion of extravascular fibrinolysis.

Pharmacological Approaches Designed To Rescue Impaired Fibrinolysis

Pharmacological strategies designed to enhance fibrinolysis can be employed at many points throughout the fibrinolytic system. Currently, the only approved therapy designed to increase plasmin activity is the administration of intravascular tPA (29). A bolus of recombinant tPA is given in ischemic injuries such as stroke, pulmonary embolism, as well as myocardial infraction to promote plasminogen activation and removal of the thrombus occluding the vessels (30). While bolus administration of tPA has been shown to be beneficial, it is also associated with a high incidence of uncontrolled hemorrhage following administration and 1 of every 18 patients either dies or suffers a long term disability as a result of its administration. These adverse effects are due to the systemic, nonselective activation of plasminogen, rather than activation solely at the site of injury. Given the high incidence of complications associated with tPA there is a need for alternative pharmacological approaches.

An alternative strategy is to target the coagulation system's ability to deposit fibrin through inhibition of its precursor, fibrinogen. Given that many of the conditions associated with impaired fibrinolysis are also associated with fibrin accumulation, and that fibrin is inflammatory, the targeted depletion of fibrinogen has the potential to be efficacious in attenuating impaired musculoskeletal healing. However, targeting fibrinogen is likely to also result in uncontrolled bleeding similar or worse than that seen from tPA administration, making the depletion of fibrin an unappealing approach to promoting fibrinolysis and healing. Owing to the perceived deleterious effects of fibrinogen depletion, an alternative approach to targeted fibrin therapy may be to inhibit its ability to promote an inflammatory response while retaining its hemostatic function. Fibrin-mediated inflammation is thought to promote the progression of many chronic diseases. However, this approach could lead to increased risk of infection, as the pro-

inflammatory response of fibrin is crucial for host defense following injury (31). Further, this pharmacological strategy: 1) only addresses fibrin's role in inflammation and not fibrin's role as a physical barrier to healing and/or 2) does not address the non-fibrinolytic functions of plasmin such as activation or release of growth factors (32, 33). Given the severity of these complications, neither bolus administration of tPA or fibrinogen ablation are ideal targets for manipulation of the fibrinolytic system.

Administration of purified factors has proven to be a highly successful strategy in repletion of the coagulation system in hemophiliacs and following trauma. (34, 35). Given the success of this pharmacological strategy, another possible approach to rescuing impaired fibrinolysis could be through the administration of purified plasminogen. This approach would address both fibrin accumulation and supplementation of plasmin's functions outside of fibrinolysis, and would likely only be activated in areas that express the plasminogen activators. However, this potential benefit may be offset if deficiency in fibrinolysis is the result of overexpression of plasminogen activator inhibitors.

To overcome a deficiency in fibrinolysis as a result of increased expression of plasminogen inhibitors, targeted inhibition of these inhibitors may be beneficial in rescuing hypofibrinolytic states. Inhibition of plasminogen activator inhibitors would increase the concentrations of available plasminogen activators. Along similar lines, targeted inhibition of α2-antiplasmin is also a promising pharmacological approach for rescuing impaired fibrinolysis. α2-antiplasmin is a highly specific serpin with little known physiological activity outside of the inhibition of plasmin. Supporting this approach was our data demonstrating that impaired muscle healing can be rescued in plasminogen heterozygous mice through the administration of an anti-sense oligonucleotide designed to inhibit α2-antiplasmin activity. It is important to note that inhibition of plasminogen activator inhibitor and of α2-antiplasmin would also put patients at risk for bleeding

complications as patients with either a genetic deficiency of plasminogen activator inhibitor or α2-antiplasmin have known bleeding phenotypes (36, 37). Given these observations, dosing, timing and frequency studies will be critical and likely different for each pathology and musculoskeletal injury. Thus future studies are warranted to determine the temporal spatial activation of fibrinolytic system following injury and rapid methods to functionally measure fibrinolysis in patients.

References

1. Robbins KC. Classification of abnormal plasminogens: dysplasminogenemias. Seminars in thrombosis and hemostasis. 1990;16(3):217-20. doi: 10.1055/s-2007-1002672. PubMed PMID: 2146745.

2. Schuster V, Hugle B, Tefs K. Plasminogen deficiency. Journal of thrombosis and haemostasis : JTH. 2007;5(12):2315-22. doi: 10.1111/j.1538-7836.2007.02776.x. PubMed PMID: 17900274.

3. Kurtulus I, Gokbuget A, Efeoglu A, Cintan S, Tefs K, Schuster V, Scully C. Hypoplasminogenemia with ligneous periodontitis: a failed local therapeutic approach. Journal of periodontology. 2007;78(6):1164-75. doi: 10.1902/jop.2007.060422. PubMed PMID: 17539733.

4. Schuster V, Zeitler P, Seregard S, Ozcelik U, Anadol D, Luchtman-Jones L, Meire F, Mingers AM, Schambeck C, Kreth HW. Homozygous and compound-heterozygous type I plasminogen deficiency is a common cause of ligneous conjunctivitis. Thrombosis and haemostasis. 2001;85(6):1004-10. PubMed PMID: 11434676.

5. Scully C, Gokbuget AY, Allen C, Bagan JV, Efeoglu A, Erseven G, Flaitz C, Cintan S, Hodgson T, Porter SR, Speight P. Oral lesions indicative of plasminogen deficiency (hypoplasminogenemia). Oral surgery, oral medicine, oral pathology, oral radiology, and endodontics. 2001;91(3):334-7. doi: 10.1067/moe.2001.112158. PubMed PMID: 11250632.

6. Demarmels Biasiutti F, Sulzer I, Stucki B, Wuillemin WA, Furlan M, Lammle B. Is plasminogen deficiency a thrombotic risk factor? A study on 23 thrombophilic patients and their family members. Thrombosis and haemostasis. 1998;80(1):167-70. PubMed PMID: 9684804.

7. Tait RC, Walker ID, Conkie JA, Islam SI, McCall F. Isolated familial plasminogen deficiency may not be a risk factor for thrombosis. Thrombosis and haemostasis. 1996;76(6):1004-8. PubMed PMID: 8972025.

8. Schuster V, Seregard S. Ligneous conjunctivitis. Survey of ophthalmology. 2003;48(4):369-88. PubMed PMID: 12850227.

9. Pandolfi A, Cetrullo D, Polishuck R, Alberta MM, Calafiore A, Pellegrini G, Vitacolonna E, Capani F, Consoli A. Plasminogen activator inhibitor type 1 is increased in the arterial wall of type II diabetic subjects. Arteriosclerosis, thrombosis, and vascular biology. 2001;21(8):1378-82. PubMed PMID: 11498469.

10. Schneider DJ, Sobel BE. PAI-1 and diabetes: a journey from the bench to the bedside. Diabetes care. 2012;35(10):1961-7. doi: 10.2337/dc12-0638. PubMed PMID: 22996180; PubMed Central PMCID: PMC3447837.

11. Rerolle JP, Hertig A, Nguyen G, Sraer JD, Rondeau EP. Plasminogen activator inhibitor type 1 is a potential target in renal fibrogenesis. Kidney international. 2000;58(5):1841-50. doi: 10.1111/j.1523-1755.2000.00355.x. PubMed PMID: 11044203.

12. Huber K, Christ G, Wojta J, Gulba D. Plasminogen activator inhibitor type-1 in cardiovascular disease. Status report 2001. Thrombosis research. 2001;103 Suppl 1:S7-19. PubMed PMID: 11567664.

13. Reith A, Booth NA, Moore NR, Cruickshank DJ, Bennett B. Plasminogen activator inhibitors (PAI-1 and PAI-2) in normal pregnancies, pre-eclampsia and hydatidiform mole. British journal of obstetrics and gynaecology. 1993;100(4):370-4. PubMed PMID: 8494839.

14. Vidal B, Ardite E, Suelves M, Ruiz-Bonilla V, Janue A, Flick MJ, Degen JL, Serrano AL, Munoz-Canoves P. Amelioration of Duchenne muscular dystrophy in mdx mice by elimination of matrix-associated fibrin-driven inflammation coupled to the alphaMbeta2 leukocyte integrin receptor. Human molecular genetics. 2012;21(9):1989-2004. doi: 10.1093/hmg/dds012. PubMed PMID: 22381526; PubMed Central PMCID: PMC3315206.

15. Zouaoui Boudjeltia K, Piagnerelli M, Brohee D, Guillaume M, Cauchie P, Vincent JL, Remacle C, Bouckaert Y, Vanhaeverbeek M. Relationship between CRP and hypofibrinolysis: Is this a possible mechanism to explain the association between CRP and outcome in critically ill patients? Thrombosis journal. 2004;2(1):7. doi: 10.1186/1477-9560-2-7. PubMed PMID: 15456513; PubMed Central PMCID: PMC524363.

16. Kimoto T, Kohno H, Uchida M, Yamanoi A, Yamamoto A, Nagasue N, Ando S, Suemitsu K, Ohtani M. Inferior vena caval thrombosis after traumatic liver injury. HPB surgery : a world journal of hepatic, pancreatic and biliary surgery. 1998;11(2):111-6. PubMed PMID: 9893241; PubMed Central PMCID: PMC2423952.

17. Enderson BL, Chen JP, Robinson R, Maull KI. Fibrinolysis in multisystem trauma patients. The Journal of trauma. 1991;31(9):1240-6. PubMed PMID: 1920554.

18. Sorensen JV. Levels of fibrinolytic activators and inhibitors in plasma after severe trauma. Blood coagulation & fibrinolysis : an international journal in haemostasis and thrombosis. 1994;5(1):43-9. PubMed PMID: 7514044.

19. Evans TW, Fink MP. Mechanisms of organ dysfunction in critical illness. Berlin ; New York: Springer; 2002. xvi, 410 p. p.

20. Rabbani N, Thornalley PJ. The critical role of methylglyoxal and glyoxalase 1 in diabetic nephropathy. Diabetes. 2014;63(1):50-2. doi: 10.2337/db13-1606. PubMed PMID: 24357696.

21. Bugge TH, Kombrinck KW, Flick MJ, Daugherty CC, Danton MJ, Degen JL. Loss of fibrinogen rescues mice from the pleiotropic effects of plasminogen deficiency. Cell. 1996;87(4):709-19. PubMed PMID: 8929539.

22. Drixler TA, Vogten JM, Gebbink MF, Carmeliet P, Voest EE, Borel Rinkes IH. Plasminogen mediates liver regeneration and angiogenesis after experimental partial hepatectomy. The British journal of surgery. 2003;90(11):1384-90. doi: 10.1002/bjs.4275. PubMed PMID: 14598419.

23. Gong Y, Zhao Y, Li Y, Fan Y, Hoover-Plow J. Plasminogen regulates cardiac repair after myocardial infarction through its noncanonical function in stem cell homing to the infarcted heart. Journal of the American College of Cardiology. 2014;63(25 Pt A):2862-72. doi: 10.1016/j.jacc.2013.11.070. PubMed PMID: 24681141; PubMed Central PMCID: PMC4074457.

24. Kao WW, Kao CW, Kaufman AH, Kombrinck KW, Converse RL, Good WV, Bugge TH, Degen JL. Healing of corneal epithelial defects in plasminogen- and fibrinogen-deficient mice. Investigative ophthalmology & visual science. 1998;39(3):502-8. PubMed PMID: 9501859.

25. Lisman T, de Groot PG, Meijers JC, Rosendaal FR. Reduced plasma fibrinolytic potential is a risk factor for venous thrombosis. Blood. 2005;105(3):1102-5. doi: 10.1182/blood-2004-08-3253. PubMed PMID: 15466929.

26. Meltzer ME, Bol L, Rosendaal FR, Lisman T, Cannegieter SC. Hypofibrinolysis as a risk factor for recurrent venous thrombosis; results of the LETS follow-up study. Journal of thrombosis and haemostasis : JTH. 2010;8(3):605-7. doi: 10.1111/j.1538-7836.2009.03715.x. PubMed PMID: 19995410.

27. Romer J, Bugge TH, Pyke C, Lund LR, Flick MJ, Degen JL, Dano K. Impaired wound healing in mice with a disrupted plasminogen gene. Nature medicine. 1996;2(3):287-92. PubMed PMID: 8612226.

28. Zhang ZG, Chopp M, Goussev A, Lu D, Morris D, Tsang W, Powers C, Ho KL. Cerebral microvascular obstruction by fibrin is associated with upregulation of PAI-1 acutely after onset of focal embolic ischemia in rats. The Journal of neuroscience : the official journal of the Society for Neuroscience. 1999;19(24):10898-907. PubMed PMID: 10594071.

29. Adams HP, Jr., del Zoppo G, Alberts MJ, Bhatt DL, Brass L, Furlan A, Grubb RL, Higashida RT, Jauch EC, Kidwell C, Lyden PD, Morgenstern LB, Qureshi AI, Rosenwasser RH, Scott PA, Wijdicks EF, American Heart Association/American Stroke Association Stroke C, American Heart Association/American Stroke Association Clinical Cardiology C, American Heart Association/American Stroke Association Cardiovascular R, Intervention C, Atherosclerotic Peripheral Vascular Disease Working G, Quality of Care Outcomes in Research Interdisciplinary Working G. Guidelines for the early management of adults with ischemic stroke: a guideline from the American Heart Association/American Stroke Association Stroke Council, Clinical Cardiology Council, Cardiovascular Radiology and Intervention Council, and the Atherosclerotic Peripheral Vascular Disease and Quality of Care Outcomes in Research Interdisciplinary Working Groups: The American Academy of Neurology affirms the value of this guideline as an educational tool for neurologists. Circulation. 2007;115(20):e478-534. doi: 10.1161/CIRCULATIONAHA.107.181486. PubMed PMID: 17515473.

30. Stangl K, Laule M, Tenckhoff B, Stangl V, Gliech V, Dubel P, Grohmann A, Melzer C, Langel J, Wernecke KD, Baumann G, Ziemer S. Fibrinogen breakdown, long-lasting systemic fibrinolysis, and procoagulant activation during alteplase double-bolus regimen in acute myocardial infarction. The American journal of cardiology. 1998;81(7):841-7. PubMed PMID: 9555772.

31. Degen JL, Bugge TH, Goguen JD. Fibrin and fibrinolysis in infection and host defense. Journal of thrombosis and haemostasis : JTH. 2007;5 Suppl 1:24-31. doi: 10.1111/j.1538-7836.2007.02519.x. PubMed PMID: 17635705.

32. Khalil N, Corne S, Whitman C, Yacyshyn H. Plasmin regulates the activation of cell-associated latent TGF-beta 1 secreted by rat alveolar macrophages after in vivo bleomycin injury. American journal of respiratory cell and molecular biology. 1996;15(2):252-9. doi: 10.1165/ajrcmb.15.2.8703482. PubMed PMID: 8703482.

33. Yee JA, Yan L, Dominguez JC, Allan EH, Martin TJ. Plasminogen-dependent activation of latent transforming growth factor beta (TGF beta) by growing cultures of osteoblast-like cells. Journal of cellular physiology. 1993;157(3):528-34. doi: 10.1002/jcp.1041570312. PubMed PMID: 8253864.

34. Kutcher ME, Kornblith LZ, Vilardi RF, Redick BJ, Nelson MF, Cohen MJ. The natural history and effect of resuscitation ratio on coagulation after trauma: a prospective cohort study. Ann Surg. 2014;260(6):1103-11. doi: 10.1097/SLA.0000000000000366. PubMed PMID: 24846092.

35. Ledgerwood AM, Blaisdell W. Coagulation challenges after severe injury with hemorrhagic shock. The journal of trauma and acute care surgery. 2012;72(6):1714-8. doi: 10.1097/TA.0b013e318245225c. PubMed PMID: 22695446.

36. Carpenter SL, Mathew P. Alpha2-antiplasmin and its deficiency: fibrinolysis out of balance. Haemophilia : the official journal of the World Federation of Hemophilia. 2008;14(6):1250-4. doi: 10.1111/j.1365-2516.2008.01766.x. PubMed PMID: 19141165.

37. Fay WP, Parker AC, Condrey LR, Shapiro AD. Human plasminogen activator inhibitor-1 (PAI-1) deficiency: characterization of a large kindred with a null mutation in the PAI-1 gene. Blood. 1997;90(1):204-8. PubMed PMID: 9207454.